DESIGN OF BIOMIMETICALLY INSPIRED HYDROXYAPATITE-GELATIN BASED COMPOSITE FOR BONE SCAFFOLD APPLICATION

Huamin Hu

A dissertation submitted to the faculty at the University of North Carolina at Chapel Hill in partial fulfillment of the requirements for the degree of Doctor of Philosophy in the Department of Chemistry

Chapel Hill
2018

Approved by:

Wei You

Ching-Chang Ko

Matthew Lockett

Sergei Sheiko

Frank Leibfarth

ABSTRACT

Huamin Hu: Design of Biomimetically Inspired Hydroxyapatite-Gelatin Based Composite for Bone Scaffold Application
(Under the direction of Wei You)

Bone tissue engineering (BTE) requires a sturdy biomimetic scaffold for restoration of large bone defects. This dissertation describes the progress made in improving our previously developed Gemosil composite consisting of Hydroxyapatite-Gelatin (HAp-Gel) with silane cross-linker as a potential scaffold. Our initial goal was to further improve the mechanical strength of the composite. We first successfully doubled the mechanical strength of the composite through adding selected co-solvent during the sol-gel process. We further experimentally confirmed that the improvement of the mechanical strength is due to the improved morphology of both the silane network and the Gemosil composite. Unfortunately, the scaffold fabricated from this composite (even with the newly optimized processing condition) underwent rapid degradation in water, and rapidly lost its mechanical strength.

To mitigate this degradation issue, we attempted to incorporate a cross-linkable polymer into the Gemosil composite, aiming to further increase mechanical strength of the Gemosil composite with an additional polymeric network (i.e., reinforcing network). Specifically, we synthesized a new biocompatible and biodegradable copolymer, poly(L-lactide-*co*-propargyl carbonate) with pendent catechol functional groups. These catechol functional groups served as "liaison" molecules to help to improve the interfacial adhesion between the polymer network and the various components of the Gemosil. We demonstrated that through incorporating this

copolymer together with mussel-inspired dopamine into Gemosil system, the compressive strength of the scaffold could be improved by 20% under aqueous condition.

Finally, despite the impressive adhesive and coating property of dopamine/polydopamine demonstrated by us and others, polydopamine (PDA) has its own limitations. For instance, PDA's black color is not favored for clinical applications and its polymerization mechanism is still elusive. We synthesized a series of dopamine analogues with different alkyl chain lengths between the catechol and the amine. We found all of these new dopamine analogues were able to polymerize. Through studying the adhesive and coating ability of these new dopamine analogues, together with systems having catechol and selected alkyl amines (unbound to catechol), we showed that the covalent linkage between the catechol and the amine via an alkyl chain is not required to show the adhesive property; however, this covalent link is crucial to achieve the impressive coating property of dopamine and its analogs. Our findings offer new insights in designing mussel-inspired materials for future BTE application, and further mechanistic understanding of the polymerization of dopamine and these new dopamine analogues.

ACKNOWLEDGEMENTS

First, I would like to express my deep and sincere gratitude to my advisor Prof. Wei You for his guidance, encouragement, patience and support during the last five years. Research has not always been easy. Most of time, the experiment results didn't meet our expectations. However, Wei has always been there to help with his knowledge and understanding. As an international student, presentation and writing were difficult for me at the beginning. I really appreciate Wei's assistance in helping me to improve my presentation and writing skills step by step. Most importantly, Wei has taught me to always keep a positive attitude, which already has and will still have a positive impact on my life. I would also like to thank my co-advisor, Dr. Ching-Chang Ko in UNC Dental School, for his valuable suggestions during the three years of working together on the bone scaffold project. With Dr. Ko's support, I have made a smooth transition from knowing just polymer synthetic chemistry to understanding and practicing biomaterials science and engineering. I really enjoyed our collaboration in this new field.

Second, I want to thank the members in both the You Group and the Ko Groups, who have helped to build a friendly and supportive working environment. Without the support and help of my partners in these two groups, this dissertation would never happen. In particular, I would like to thank Dr. Jason Dyke for his guidance and help during my first year in the You group. I would also like to express my thanks to Mr. John Whitley in the Ko group for teaching me how to use Instron machine. At the same time, I want to thank Dr. Dong Joon Lee, Dr. Bo-Wen Huang, Mr. Yan-ting Lee and Mr. Sing-Wong Wang in the Ko group for their invaluable help with experiment discussion and cell study experiments design during our collaboration.

Moreover, I would like to acknowledge Professors Matthew Lockett, Sergei Sheiko and Frank Leibfarth for serving my committee. I thank them for taking the time out of their busy schedule. In particular, I want to express my sincere thanks to Professor Lockett for his kind help in improving my presentation skills. Thank you for your time and invaluable advice.

Finally, I would like to thank my friends and family. Without them, this journey would not have been possible. I would like to thank my friends for listening and kindly sharing their valuable life experience with me. I would like to thank my parents and my younger brother for supporting me all the time. Your trust has helped me to get through the hard time in my life. I would like to thank my husband for his love. You have taught me how to love and motivated me to become a better person. Many thanks to all of you!

TABLE OF CONTENTS

LIST OF FIGURES x

LIST OF TABLES xii

LIST OF SCHEMES xiii

LIST OF ABBREVIATIONS xiv

Chapter 1 INTRODUCTION TO BONE TISSUE ENGINEERING 1

1.1 Needs for Developing Bone Repair Methods 1

1.2 Characteristics of Bone 1

1.3 Current Treatments and Emerging Bone Tissue Engineering Field 3

1.4 Bone Tissue Engineering: General Principles and Challenges 5

1.5 Bone Scaffold Design Rules 7

1.6 Current Materials Options and Limitations 9

1.7 Biomimetic Hydroxyapatite-Gelatin Composite Materials 11

Chapter 2 DRAMATIC IMPROVEMENT OF MECHANICAL STRENGTH OF SILANE-MODIFIED HYDROXYAPATITE-GELATIN COMPOSITES VIA PROCESSING WITH CO-SOLVENT 14

2.1 Introduction 14

2.2 Co-Solvent Effect: Observation 16

2.3 Hypothesis for Co-solvent Effect 19

2.4 FT-IR Study 20

2.5 Morphology Study 21

2.6 Biocompatibility Study 24

2.7 3D Porous Scaffold Fabrication and Mechanical Properties 25

2.8 Conclusion 26

2.9 Experimental Section 27

Chapter 3 CATECHOL-FUNCTIONALIZED ADHESIVE POLYMER FOR ENHANCING MECHANICAL STRENGTH OF SILANE-MODIFIED HYDROXYAPATITE-GELATIN COMPOSITE IN WET CONDITION 32

3.1 Introduction 32

3.2 Synthesis of Monomer and Cross-linker 37

3.3 Synthesis of P(LLA-*co*-PC) Copolymers and Post-functionalization with Catechol 38

3.4 Optimization of Catechol Amount 40

3.5 Optimization of the Molecular Weight of Copolymer 43

3.6 Optimization of Relative Amount of Catechol Functionalized Copolymer and Dopamine 45

3.7 Compressive Strength of Scaffold Under Wet Condition 47

3.8 Conclusion 48

3.9 Experimental Section 49

Chapter 4 INVESTIGATION OF DOPAMINE ANALOGUES: SYNTHESIS, MECHANISTIC UNDERSTANDING, AND STRUCTURE-PROPERTY RELATIONSHIP 55

4.1 Introduction 55

4.2 Synthesis of Dopamine Analogues 60

4.3 Polymerization Behavior Studied by UV-Vis Spectra 62

4.4 Adhesive Property Studied by Lap-shear Testing 69

4.5 Coating Property Studied by XPS 72

4.6 Conclusion 75

4.7 Experimental Section 76

Chapter 5 CONCLUSION AND FUTURE DIRECTION 86
5.1 Conclusion 86
5.2 Future Direction 87
5.2.1 Exploring new polymers with better processability 87
5.2.2 Replacing dopamine with other catecholamines 88
5.2.3 Exploring new materials: graphene oxide (GO) 89
5.3 Concluding Remarks 90
APPENDIX 91
Appendix for Chapter 2 91
Appendix for Chapter 3 95
Appendix for Chapter 4 102
REFERENCES 129

LIST OF FIGURES

Figure 1.1. Hierarchical structure of human cortical bone. (Reprinted from reference 7b with permission. Copyright nature publishing group) 2

Figure 1.2. Bone remodeling process for bone self-repair. (Reprinted from https://www.york.ac.uk/res/bonefromblood/background/boneremodelling.html. Copyright by Biomedical Tissue Research, University of York. Reprinted with permission).....3

Figure 1.3. Bone tissue engineering concept. (Reprinted from https://goo.gl/images/CtzKJF. Reprinted with permission).....5

Figure 1.4. The paradigm of bone tissue engineering. (Reprinted from reference 27 with permission. Copyright Royal Society of Chemistry).....6

Figure 1.5. The evolution of different generations of HAp-Gel based composites. 13

Figure 2.1. FT-IR spectra of (a) enTMOS gels and (b) Gemosil composites prepared from different solvent systems.....21

Figure 2.2. SEM images of composites made from (a) MeOH only; (b) CH_3CN/MeOH; (c) THF/MeOH; (d) THF only. Inset: the physical appearance of the composite under that condition. 23

Figure 2.3. Cell viability test by RealTime-GloTM MT cell viability assay (two way ANOVA analysis, P=0.0012). 25

Figure 2.4. (a) Picture of the porous scaffold (pore size: 400 μm, porosity: 50%) and (b) compressive strength of porous scaffold processed with different co-solvents (student *t*-test, P=0.0001).....26

Figure 3.1. The ^1H NMR spectra of homopolymers, copolymer and catechol functionalized copolymer.....40

Figure 3.2. Mechanical strength of composite processed with different molecular weight of P(LLA-*co*-PC)(Catechol). 45

Figure 3.3. Contour plot for (a) compressive strength and (b) biaxial flexural strength of composite with various amount of copolymer/dopamine.....47

Figure 3.4. Compressive strength of scaffold under wet condition. 48

Figure 4.1. Time dependent UV-Vis spectroscopy for the polymerization of dopamine analogues in aqueous solution after adding 1M NaOH. 64

Figure 4.2. Time dependent UV-Vis spectroscopy for dopamine analogues in MeOH (1mM) after adding 1M NaOH (MeOH:water=125:1, v/v).....66

Figure 4.3. (a) Image of test sample (left) and main part of Instron machine (right) for lap-shear testing; (b) results for adhesive strength for PDA, poly(3C-DA), poly(4C-DA), poly(5C-DA) and catechol/propylamine in water at 6.7 mg/mL; (c) results for adhesive strength for PDA, poly(3C-DA), poly(4C-DA), poly(5C-DA), catechol/propylamine and catechol/dodecylamine in IPA: H_2O at 6.7 mg/mL (IPA:H_2O=1:2, v/v); (d) results for adhesive strength for PDA, poly(3C-DA), poly(4C-DA), poly(5C-DA), catechol/propylamine and catechol/dodecylamine in IPA: H_2O at 33.3 mM (IPA:H_2O=1:2, v/v). 70

Figure 4.4. (a) XPS spectra of bare PTFE substrates, PDA coated PTFE and poly(3C-DA) coated PTFE, poly(4C-DA) coated PTFE, and poly(5C-DA) coated PTFE; (b) the quantitative analysis of nitrogen/carbon (N/C) ratio of different substrates coated with PDA and poly(3C-DA) as indicated by the black bar and red bar, respectively. Blue bar and green bar represent the N/C ratio of PTFE substrate coated with poly(4C-DA) and poly(5C-DA), respectively.....74

Figure 5.1. Polymer design (a) old copolymer, and (b) new copolymer. 88

Figure 5.2. Replace dopamine with (a) catechol/propylamine, and (b) 3C-DA. 89

Figure 5.3. Silane or catechol functionalized GO as new materials for enhancing composite mechanical property. 90

LIST OF TABLES

Table 1.1. Current material options and related properties 11

Table 2.1. Biaxial flexural strength of composite with different co-solvents 17

Table 3.1. Summarized polymerization data for P(LLA-*co*-PC) copolymers 38

Table 3.2. P(LLA-*co*-PC) copolymers with different amount of catechol 42

Table 3.3. P(LLA-*co*-PC)(Catechol) with different polymer molecular weight 44

Table 3.4. Mechanical strength of bulk composite with different amount of copolymer and dopamine 46

LIST OF SCHEMES

Scheme 2.1. enTMOS network formed in different solvent system 16

Scheme 3.1. Proposed polymer network formed through the catechol oxidative coupling between polymer and dopamine 36

Scheme 3.2. Synthesis route of PC monomer 37

Scheme 3.3. Synthesis route of Catechol-4C-SH.....38

Scheme 3.4. Synthesis of PLLA-*co*-PC copolymer functionalized with catechol through “thiol-yne” click chemistry.....39

Scheme 4.1. Overview of mussel-inspired materials and proposed polymer structure.....59

Scheme 4.2. Synthesis route of 3C-DA Analogue 61

Scheme 4.3. Synthesis route of 4C-DA, 5C-DA and 12C-DA Analogues 61

Scheme 4.4. Proposed reaction intermediates during polymerization 68

LIST OF ABBREVIATIONS

BTE	bone tissue engineering
HAp-Gel	hydroxyapatite-gelatin
PDA	polydopamine
M.W.	molecular weight
HAp	hydroxyapatite
3D	three-dimensional
ECM	extracellular matrix
MSCs	mesenchymal stem cells
BMP	bone morphogenetic protein
Col	collagen
Gel	gelatin
PLA	polylactic acids
PGA	poly(glycolic acid)
PLGA	poly(lactic-*co*-glycolic acid)
CTD	computational topology design
HAp-Col	hydroxyapatite-collagen
enTMOS	bis[3-(trimethoxysilyl) propyl] ethylenediamine
$Ca(OH)_2$	calcium hydroxide
MeOH	methanol
EtOH	ethanol
CH_3CN	acetonitrile
THF	tetrahydrofuran

THP	tetrahydropyran
DMSO	dimethyl sulfoxide
DME	dimethoxyethane
CHX	chlorhexidine
APS	ammonium persulfate
ATR	attenuated total reflection
Q8M8	octakis(trimethylsiloxy) silsequioxane
FT-IR	fourier-transform infrared spectroscopy
SEM	scanning electron microscopy
EDS	energy-dispersive X-ray spectroscopy
TEM	transmission electron microscopy
rMSCs	rat mesenchymal stem cells
H_2O	water
PLLA	poly(L-lactide acid)
PCL	polycaprolactone
PTMC	poly(trimethylene carbonate)
T_g	glass transition temperature
PC	propargyl carbonate
GPC	gel permeation chromatography
ROP	ring-opening polymerization
M_n	number average molecule weight
M_w	weight average molecule weight
THME	1,1,1-tris(hydroxyl methyl) ethane

TEA	triethylamine
DMPA	2,2-dimethoxy-2-phenylacetophenone
TsOH	p-toluene sulfonic acid
$SnOCt_2$	tin (II) 2-ethyl hexanoate
DCM	dichloromethane
EtOAc	ethyl acetate
$MgSO_4$	magnesium sulfate
L-DOPA	L-3,4-dihydroxyphenylalanine
2C-DA	dopamine
XPS	X-ray photoelectron spectroscopy
PTFE	polytetrafluoroethylene
ITO	indium tin oxide
PET	poly(ethylene terephthalate)
PEO	polyethylene oxide
GO	graphene oxide

Chapter 1 INTRODUCTION TO BONE TISSUE ENGINEERING

1.1 Needs for Developing Bone Repair Methods

Bone is a rigid organ in our body, which has many important physiological functions. First, it provides a rigid skeletal framework, which supports and protects other body tissues. Second, it can form a system of rigid levers, which allow body to move with attached muscles. However, large bone defects, which can't heal by bone self-repair mechanisms alone, frequently occur due to injuries, diseases and aging.[1] It has been reported that the total number of bone surgeries has increased from 700,000 in 1998 to over 1.1 million in 2005 in the US alone,[2] accompanied with the rapidly increase in medical expenses. The prevalence of bone defects highlights the needs for exploring effective and affordable bone treatments.

1.2 Characteristics of Bone

To find an ideal treatment for large bone defects, it is necessary to understand the chemical composition, structure and biology of natural bone. Macroscopically, bone consists of two types of tissues, cortical bone (dense out shell) which is mainly responsible for mechanical support, and cancellous bone (inner porous core) which provides space for nutrition exchange and metabolic activities.[3] Despite differences in the macro-scale structure of these two tissues, they have similar chemical compositions. It was found that bone is actually a composite material with two main components. One is a strong and brittle inorganic component (mainly hydroxyapatite (HAp), $Ca_{10}(PO_4)_6(OH)_2$), which gives bone strength. The other is a soft and flexible organic component (mainly protein collagen), which endows bone with toughness.[4] However, HAp and collagen are not just physically blended with each other in natural bone. It

has been demonstrated that cortical bone consists of a hierarchical structure in which HAp and collagen are highly organized at different length scales.[5] As shown in **Figure 1.1**, at nanoscale, HAp and collagen are presented in the form of mineralized collagen fibril, in which HAp nucleates along collagen fibers.[6,7] This mineralized collagen fibril will function as the "building block" to further form different microarchitecture in bone, such as extrafibrillar matrix, lamellae and finally osteons.[8] The composite nature and the complex hierarchical structure of cortical bone explain why bone has such impressive mechanical properties.[9,10] It has been reported that the compressive strength of cortical bone is around 200 MPa.[11] In contrast, due to the porous macrostructure and irregular microstructure of cancellous bone,[12] it demonstrates a much lower compressive strength compared to cortical bone, ranges from 1-13 MPa.[13]

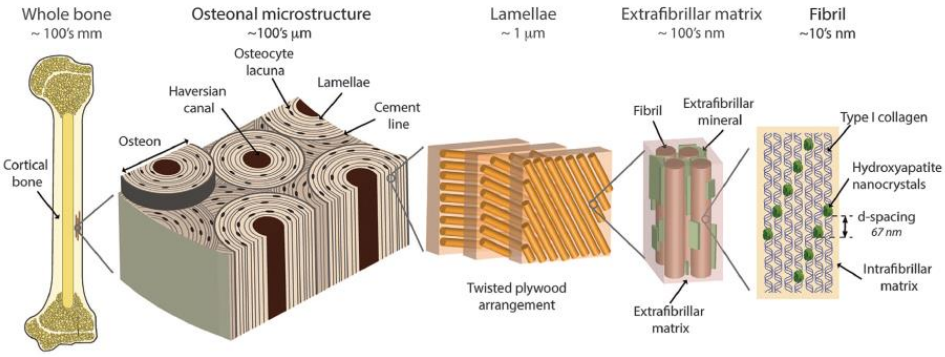

Figure 1.1. Hierarchical structure of human cortical bone. (Reprinted from reference 7b with permission. Copyright nature publishing group)

Furthermore, bone has been regarded as a "smart material" due to its self-repair ability when the damage is small.[14] The self-repair ability is realized by a process known as bone remodeling, during which older or damaged bone is gradually replaced by new bone cells.[3] **Figure 1.2** has shown a simplified bone remodeling cycle with three major stages: starting with bone resorption which is accomplished with osteoclasts, followed by a reversal/transition period and finally new bone formation through osteoblasts.[15] Additionally, it has been recognized that

bone remodeling follows “Wolff’s Law”, which states that bone will accommodate itself to become denser/looser to the change of external load.[16] In summary, considering the complexity of natural bone, it is a grand challenge to find a treatment for large bone defects, which could structurally, mechanically and functionally replicate our natural bone.

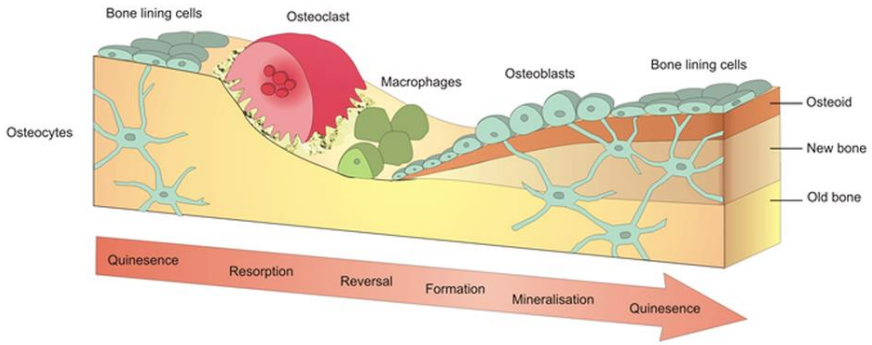

Figure 1.2. Bone remodeling process for bone self-repair. (Reprinted from https://www.york.ac.uk/res/bonefromblood/background/boneremodelling.html. Copyright by Biomedical Tissue Research, University of York. Reprinted with permission)

1.3 Current Treatments and Emerging Bone Tissue Engineering Field

To date, the majority of treatments for large bone defects have focused on developing bone graft to fill bone defects and stimulating new bone formation. Despite the fact that various bone grafts have been developed, they all have significant drawbacks. Autograft, which involves the use of host bone (usually from the pelvis iliac crest of the patient) to fill bone defect, has been regarded as the gold standard for bone grafts.[17] However, its clinical application has been greatly impeded due to the limited supply and risk of donor site morbidity.[18] To mitigate this issue, allograft[19] and xenograft,[20] which replace patients own bone tissue with bone tissue from other humans and non-humans, respectively, have been actively explored for bone treatment. Nevertheless, they are now considered to be inappropriate for bone treatment due to the risk of infection, disease transmission and most importantly, host immune rejection.[21-24]

Considering the pitfalls in using natural bone grafts (i.e. autograft, allograft and xenograft) discussed above, synthetic biomaterials with good biocompatibility and mechanical properties have been extensively investigated as an alternative bone substitutes for treatment. These synthetic alternatives have demonstrated several advantages over natural bone grafts, such as availability, reduced infection, and mitigated host rejection.[25] Initial attempts were focused on the utilization of inert, nonporous materials with physical properties (such as mechanical strength) similar to natural bone to permanently undertake the function of damaged bone. Implants including metals (such as stainless steel, titanium, and alloys),[26] ceramics (such as alumina-oxide),[27] and polymers (such as polymethylmethacrylate)[28] have become the well-established bone grafts for decades.[29] However, the inert property of such materials will cause a non-specific immune response from our body, which results in the formation of a soft fibrous tissue at the biomaterial-tissue interface.[30] This indirect contact between the implant and the bone would likely induce mechanical instability and dislocation over time. To overcome this problem, materials with bioactive surfaces were developed to promote bone formation at the material-bone interface, thereby inducing a stronger bonding between the bone and the implant. This bioactive surface can be easily obtained through coating material with bioactive ceramics such as HAp, bioactive glass, and β-tricalcium phosphate.[31] While there has been significant progress in developing synthetic bone grafts, there are still challenges to be addressed. For example, the mismatch of mechanical strength between synthetic bone grafts and natural bone often results in stress-shielding to surrounding bone[32] and fatigue failure of the implant under cyclic loading.[33]

Recently, bone tissue engineering (BTE) has emerged as a promising approach to overcome these aforementioned issues. The fundamental concept behind BTE is to utilize a temporary three-dimensional (3D) porous scaffold at the bone defect site, which will provide

microenvironment for cell transplantation and proliferation. As the new bone starts to regenerate, the 3D scaffold will gradually degrade in *vivo*. Eventually, the synthetic scaffold will be totally replaced by the newly regenerated bone (**Figure 1.3**).[34] It is envisioned that BTE will avoid the disadvantages of current treatments and be the ideal treatment for bone defects in the near future.

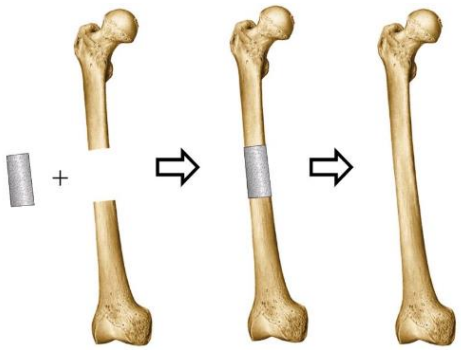

Figure 1.3. Bone tissue engineering concept. (Reprinted from https://goo.gl/images/CtzKJF. Reprinted with permission)

1.4 Bone Tissue Engineering: General Principles and Challenges

As shown in **Figure 1.4**, BTE relies on three main components: (1) a temporary 3D porous scaffold made from natural and/or synthetic degradable biomaterials to provide mechanical support and proper environment for bone regeneration; (2) biochemical factors such as signals and growth factors to induce cells to the implant site and promote cells to regenerate new bone tissue; and (3) cells (usually stem cells) to produce bone matrix.[35] Typically, the BTE surgical procedure starts with obtaining cells from patients, followed by seeds cells to scaffold to allow the production of extracellular matrix (ECM) inside the scaffold *in vitro*, and finally implants the scaffold with ECM at bone defect site in patients.[36] After years of efforts, it was found that each of the individual components presents its unique challenges.

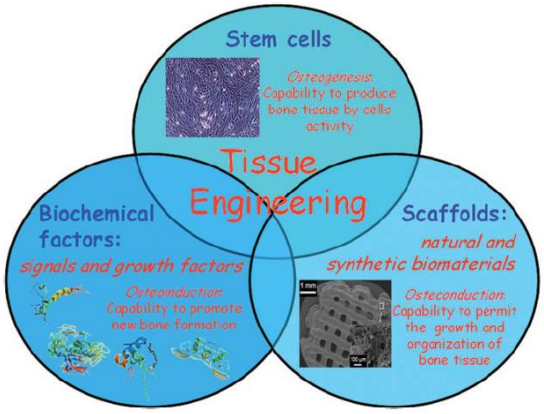

Figure 1.4. The paradigm of bone tissue engineering. (Reprinted from reference 27 with permission. Copyright Royal Society of Chemistry)

Cells: Until now, multiple cell sources have been explored for BTE application. To name a few, bone marrow aspirates,[37] bone marrow mesenchymal stem cells,[38] embryonic stem cells, etc.[39] Among these, mesenchymal stem cells (MSCs) obtained from bone marrow have been widely studied due to their capability to differentiate into various tissues, including bone. Moreover, from a technical perspective, it's relatively easy to collect MSCs from bone marrow. Preliminary clinical trials have indicated that implanted scaffolds seeded with MSCs promote faster bone tissue regeneration compared to scaffolds without cells.[40] Nevertheless, in many cases, the number of collected stem cells is not sufficient for clinical application. As a result, the biggest challenge is to increase the number of MSCs. In practice, we can expand the MSCs by cell culture *in vitro*, however, this process not only increases the surgery time and cost but also demonstrates complexity. For instance, it has been observed that stem cells will gradually lose their proliferation and differentiation ability during expanding (i.e., increase the number of MSCs) *in vitro*.[41,42]

3D porous scaffold: The scaffold has been regarded as a crucial component for BTE since it provides the mechanical support for cell growth and following bone regeneration

process. There are several key considerations in designing a scaffold, including biocompatibility, biodegradability, proper mechanical properties, scaffold architecture, fabrication technique, among others.[43] A detailed review of scaffold design rules is provided in the following section.

Biochemical factors: Proteins that play a key role in cell proliferation and differentiation are called biochemical factors.[44] Recently, various studies have been focused on exploring bone-related growth factors and applied them to BTE. It's generally agreed that growth factors would stimulate cell growth in bone scaffold.[2] For instance, bone morphogenetic protein (BMP)[45] (a type of growth factor) alone (i.e. without scaffold and cells) can induce bone regeneration, which indicates their impressive capability in promoting cell growth. However, the biggest challenge in utilizing growth factors is targeted delivery to the repair site. Currently, various carriers for growth factors have been examined, such as hydrogels and stimuli-responsive polymers.[46] Unfortunately, they could not afford a steady, controllable and sustained release profile.[42] Another significant challenge is the identification of the effective dose of growth factors for bone regeneration, preferably with minimal/tolerable side effects, which needs further study.[47]

1.5 Bone Scaffold Design Rules

Based on the discussions above, an ideal scaffold is essential for successful BTE applications. In principle, the scaffold should allow and/or promote cell attachment, proliferation, and differentiation, and most importantly, provide sufficient strength for load bearing. As a result, an ideal scaffold should satisfy following requirements: biocompatibility, good mechanical properties, proper pore size, bioresorbability, growth factor delivery, and easy fabrication.

Good biocompatibility: First, the scaffold needs to ensure all normal cell activities during bone regeneration, and secondly, the scaffold should not cause any side/toxic effects to the

body.[48] More recently, “osteoinductive biomaterials” have been demonstrated to have great promise for BTE due to their ability to stimulate MSCs to develop into preosteoblasts, which will promote bone regeneration.[49]

Good mechanical properties: Ideally, the scaffold should have mechanical strength comparable to natural bone in the implanted site, which helps load transfer during bone regeneration process.[50,51]

Proper pore size: The scaffold should possess a minimal pore size of 50 μm for effective cell seeding. Larger pores are preferred as they provide better cell seeding and essential nutrients exchange for cell survival. Recently, research has suggested that the scaffold should have inter-connected pore structure with pore size ranging from 200-350 μm.[52] Moreover, it was demonstrated that the combination of micro and macro pores would enhances bone regeneration.[53] It should be mentioned that the scaffold porosity is also closely related to its mechanical strength and is largely determined by the fabrication technique.[54] As a consequence, designing the porosity of scaffold should also consider the balance of these factors.

Bioresorbability: An ideal scaffold should be able to degrade with time *in vivo*, preferably at a controlled resorption rate, produce non-toxic degradation products and create space for the new bone gradually. The degradation behavior of scaffold should vary based on the targeted application.[55]

Growth factor delivery: As discussed in **section 1.4**, the effective incorporation of growth factor can promote cell growth and enhance bone regeneration.

Easy fabrication: Conventional techniques for fabricating scaffolds include solvent casting, freeze-drying, thermally induced phase separation, gas forming, sol-gel, and electrospinning. However, it is generally difficult with any of these methods to control pore size

and porosity, which influence bone regeneration.[56] Recently, 3D-printing together with computational topology design (CTD) has been demonstrated as a powerful way to fabricate scaffold with controlled pore size and porosity.[57]

1.6 Current Materials Options and Limitations

Until now, various materials have been explored as BTE scaffolds. As shown in **Table 1.1**, these systems include biodegradable polymers, ceramics, and composites.[58,59] Generally, these material systems have acceptable biocompatibility and produce nontoxic degradation products; however, none of them can meet the entire set of criterion discussed in **Section 1.5**. There are limitations with each material system, as discussed below.

Biodegradable polymers: Various polymers - either from natural origin (collagen (Col), gelatin (Gel), alginate, chitin, etc.)[60,61] or synthetic origin (polycaprolactone (PCL), polylactic acids (PLA), poly(glycolic acid) (PGA), etc.)[62] - have been explored for bone scaffold application.[63] The main drawbacks for these polymers are their low mechanical strength (i.e. they cannot sustain stress loading in the implanted site over a long period of time) and poor formability. Moreover, the degradation rate of these polymers is too fast for bone regeneration (i.e. materials erode in body fluid at a fast rate, leading to a quick loss of massive amount of materials), which results in low bulk corrosion resistance.[64] Thus, for synthetic polymers to be a viable option for BTE, it needs to display a more controllable degradation rate, tunable mechanical properties and can be prepared with easy fabrication techniques. Finally, it is also desirable to design polymers that can improve cell attachment and demonstrate potential to deliver growth factors.

Bioactive ceramics: These can be from either natural or synthetic in origin such as HAp, calcium phosphate, bioactive glass and calcium silicate. Due to the chemical similarity between

ceramics and our natural bone, they have shown high compressive strength, providing high resistance to deformation.[65] Another advantage of ceramics is that they can be easily fabricated into scaffold. Nevertheless, the utilization of ceramics is impeded by two reasons. First, they only show relatively slow degradation, which is not favored for BTE. Second, ceramics are often brittle, which would likely to cause fracture after implantation.

Composite: The composite systems, consisting of two or more materials, have emerged with the hope to incorporate strength from each material to this complex system.[58,59] In general, there are three types of combinations, namely co-polymers, polymer-polymer blends, and polymer-ceramic composites. For instance, poly(lactic-*co*-glycolic acid) (PLGA) is a copolymer of polylactide and polyglycolide, which has been regarded as a promising option for BTE application due to its biodegradability and ease of fabrication. Moreover, to address necrosis, caused by the acidic degradation product of PLGA, polyphosphazenes have been blended with PLGA to neutralize the acidic degradation product by releasing only neutral or basic products.[66] Recently, polymer-ceramic composites combining the advantages of polymers and ceramics have emerged as the most promising option for scaffold since they have shown tunable mechanical strength, adjustable degradation rate and good biocompatibility. In fact, bone itself is a polymer-ceramic composite material, consisting of biopolymer collagen and bioceramic HAp, thus bone is strong but also tough. In spite of these advantages of composite materials, their development is rather slow, due to processing constraints and the formation of undesired microstructures in these composites. Thus, significant efforts are still warranted in pursuit of ideal materials for bone scaffold.[67]

Table 1.1. Current material options and related properties

	Polymers	Bioceramics	Composites
Compressive strength	Poor (2-40MPa)	Good (50-400MPa)	Fair (60-150 MPa)
Degradation	Very Fast (2-12 mo.)	Slow	Tunable
Formability	Poor	Good	Tunable
Examples	Collagen (COL) Gelatin (GEL) Alginate, Chitin PCL, PLA, PGA	Hydroxyapatite (HAp) Bioactive glass Tricalcium phosphate Calcium silicate	HAp-Gel HAp-Col PLGA

1.7 Biomimetic Hydroxyapatite-Gelatin Composite Materials

For all these reasons, the You group in Chemistry and the Ko group in the Dental School have formed a strong collaboration to explore and develop polymer-ceramic composite-based materials for bone scaffolds. Specifically, we focused on mimicking natural bone since natural bone is perfect. In this decade long collaboration, we have developed several generations of biomimetic composites as shown in **Figure 1.5**.

HAp-Gel: We first developed a nanocomposite named HAp-Gel, mimicking hydroxyapatite-collagen (HAp-Col) in nature bone (i.e., gelatin (Gel) is denatured collagen (Col), mimicking the function of Col in nature bone). HAp-Gel was prepared by co-precipitation of calcium hydroxide ($Ca(OH)_2$) with phosphoric acid in the presence of gelatin. Similar to the interaction between various components in natural bone, HAp-Gel showed chemical bond formation between calcium cations of HAp nanocrystals and carboxyl anions of gelatin macromolecules. Furthermore, HAp-Gel has a self-organized structure along *c*-axis of crystalline of HAp nanocrystals, which would account for the improved mechanical strength of this composite.[68] However, HAp-Gel is a particulate powder and hard to form the scaffold.

Gemosil: To address the issue with formability, the Ko group used an aminosilane (bis[3-

(trimethoxysilyl) propyl] ethylenediamine (enTMOS)) as the chemical linker to facilitate the binding and solidification of HAp-Gel, and named the composite Gemosil (i.e., silane-modified HAp-Gel composite).[69] Compared to previously developed glutaraldehyde linker treated HAp-Gel,[70] this new composite, Gemosil, demonstrated increased compressive strength and good cell compatibility. Still, the compressive strength of Gemosil was only ~40% of the value achieved by cortical bone (80 MPa vs 205 MPa[11]). The biaxial flexural strength of Gemosil was merely ~18% of that achieved by the cortical bone (40 MPa vs 220 MPa[71]).

Gemosil-Poly: To further improve the mechanical strength of Gemosil, we have attempted to incorporate biocompatible polymers. For example, we designed a silane-functionalized poly(L-lactide-*co*-propargyl carbonate) (P(LLA-*co*-PC)) copolymer, which was blended into the Gemosil composite, aiming to enhance the long-range interactions among different components within the Gemosil composite. We named this new composite as Gemosil-Poly.[72] However, this polymer-enriched composite only improved the biaxial flexural strength from 40 MPa to 60 MPa, still much lower than that of the natural bone. This limited improvement was attributed to the poor solubility of polymer in the processing solvent MeOH, resulting in an inhomogeneous mixing of polymer with other components in the system and weak adhesion among different components.

Gemussel: Most recently, we introduced polydopamine (PDA) – a mussel adhesive protein inspired material that has shown excellent coating and adhesion properties – into Gemosil, aiming to improve the adhesion between the hydrophilic HAp-Gel and the hydrophobic siloxane matrix and named this latest generation of composite as Gemussel. However, the compressive strength improvement was still limited, only from 80 MPa to 120 MPa.[73] This caused by the lower molecular weight of PDA, which likely failed to reproduce the long-range

interaction of collagen in natural bone.

Thus, the aim of this dissertation is to further improve properties of HAp-Gel-based composite to make it a better material for scaffold for BTE application.

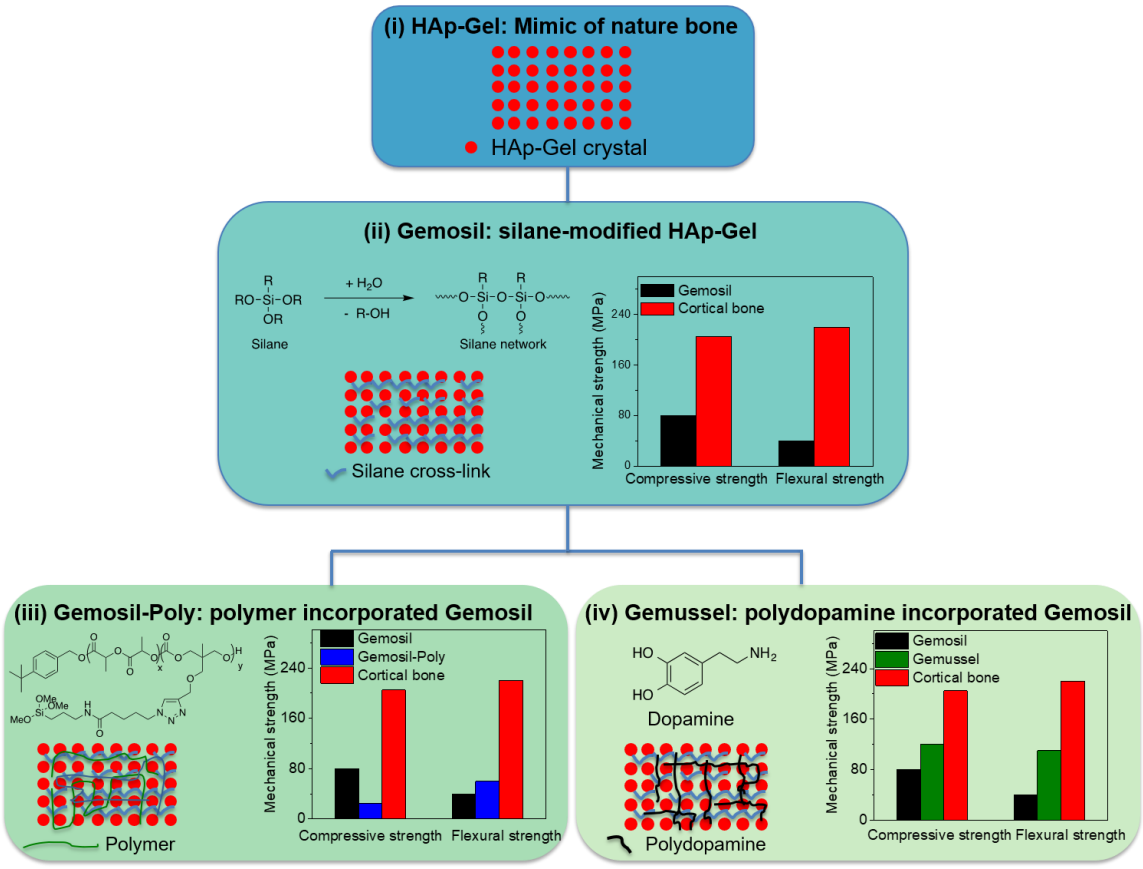

Figure 1.5. The evolution of different generations of HAp-Gel based composites.

Chapter 2 DRAMATIC IMPROVEMENT OF MECHANICAL STRENGTH OF SILANE-MODIFIED HYDROXYAPATITE-GELATIN COMPOSITES VIA PROCESSING WITH CO-SOLVENT

2.1 Introduction

While substantial improvements have been made in improving the mechanical strength of HAp-Gel based composites, the resulting composites still do not meet the requirements for BTE application. The limited improvement of composite mechanical strength with biocompatible polymer or polydopamine (PDA) made us speculate that the main reason for the poor mechanical strength of Gemosil (i.e. silane-modified HAp-Gel) might be the intrinsically weak silane network in this composite. Given that silane matrix is the major component of Gemosil composite (~ 46% by weight), engineering the silane network to dramatically improve its mechanical strength would be an alternative– perhaps an ideal – solution.

It has been well established that the silane network formation is a sol-gel process. This process starts with hydrolysis of alkoxide silane precursors to form silanol, followed by the condensation/polymerization between the silanol groups to form siloxane (Si-O-Si) linkages.[74] The gel structure (e.g., morphology and porosity), which decides the mechanical strength of as formed sliane network, can be significantly influenced by the processing method and specific conditions, including pH, R ratio (R=[H_2O]/alkoxide precursor),[75] solvents[76,77] and dry process.[74] As a result, to produce a gel with desirable properties, the processing method and conditions need to be carefully optimized. Processing conditions become even more important when

This chapter previously appeared as an article in ACS Omega. Reprinted with permission from H. Hu, B. W. Huang, Y. T. Lee, J. Hu, S. W. Wong, C. C. Ko, and W. You, ACS Omega, 2018, 3(3), pp 3592-3598. Copyright (2018) American Chemical Society.

preparing composite materials that contain the silane network. For instance, an inhomogeneous mixing of different components in the composite can induce fractures during drying,[74] which can significantly decrease the final mechanical strength of such composites.

Among the aforementioned factors that could influence the gel structure, controlling the drying process of the sol to gel formation has been shown to have a crucial impact on the mechanical property of the final composite.[74] To improve the ease of drying while minimizing cracking, co-solvents[78,79] have often been employed. Moreover, different co-solvents exert different control on the kinetics of hydrolysis and condensation, resulting in the formation of sliane network with different structures (**Scheme 2.1**) and different physical properties.[76,77] All these inspired us to explore a variety of co-solvents to further improve the mechanical properties of our Gemosil. Indeed, we find that by choosing the appropriate co-solvent, the mechanical strength of Gemosil can be greatly improved. Compared with the original Gemosil, the new Gemosil composite – processed with tetrahydrofuran (THF) as the co-solvent – demonstrated almost twice the mechanical strength as much as the original composite without THF (i.e., compressive strength: 97 MPa vs 195 MPa, biaxial flexural strength: 222 MPa vs 431 MPa). Furthermore, we show that the improvement of mechanical strength is due to the improved morphology of sliane network and the uniform distribution of HAp-Gel in the enTMOS matrix.

Scheme 2.1. enTMOS network formed in different solvent system

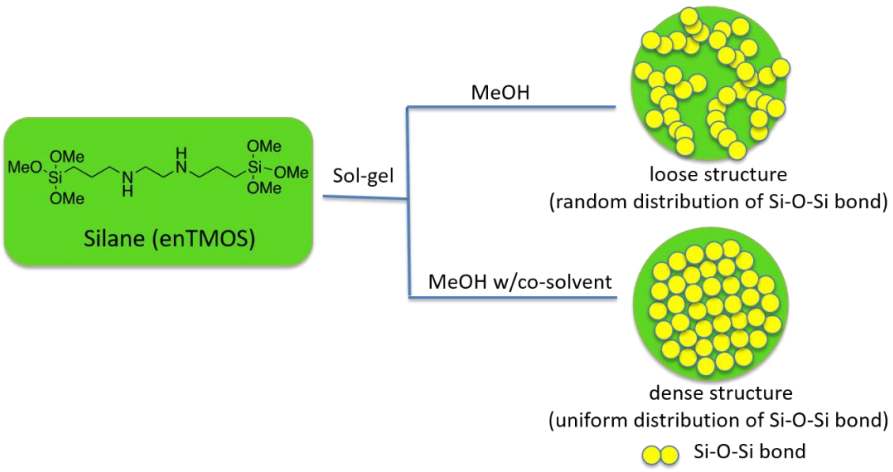

2.2 Co-Solvent Effect: Observation

According to previous findings, on the one hand, low viscosity solvents promote rapid hydrolysis, which would likely resulted in condensed network caused by fast condensation reactions to occur (due to the increased concentration of reactants for condensation).[76] On the other hand, non-polar aprotic solvent is preferred for a fast condensation reaction. This is because hydrogen bonding and/or electrostatic interactions between polar solvents and the nucleophilic substitution reaction intermediate will slow the rate of condensation.[77] To form a dense silane network and thereby achieve higher mechanical strength of such a gel, one would need rapid hydrolysis and fast condensation reactions. Thus, non-polar aprotic solvent with low viscosity would be ideal. To experimentally verify this hypothesis, we chose a number of co-solvents in this study (**Table 2.1**). These co-solvents have different viscosity values and can be categorized into three different groups (i.e., polar protic, polar aprotic and non-polar aprotic).

Table 2.1. Biaxial flexural strength of composite with different co-solvents

Type of co-solvent	**Entry**	**Co-solvent/MeOH** (v/v=9:5)	**Viscosity of co-solvent**	**b.p. of co-solvent (°C)**	**Biaxial flexural strength (MPa)**
Polar Protic	1	MeOH	0.55	64.7	222.83±54.80
	2	EtOH/MeOH	1.07	78.37	102.32±34.53
Polar aprotic	3	CH_3CN/MeOH	0.37	81.3	410.43±25.48
	4	DMSO/MeOH	1.99	189	138.01±19.40
Non-polar aprotic	5	THF/MeOH	0.46	66	431.35±58.72
	6	THP/MeOH	0.52	88	471.40±44.83
	7	Dioxane/MeOH	1.18	101.1	291.05±75.75
	8	DME/MeOH	1.1	85	408.73±51.38

Our results in **Table 2.1** clearly demonstrate that the co-solvents indeed have a strong influence on the biaxial flexural strength of the composite. First, as we expected, among the three types of co-solvents we studied, aprotic ones – with the exception of dimethyl sulfoxide (DMSO) – improve the mechanical strength of the composite more than protic ones. In some cases, we could even increase the mechanical strength over 100% when compared with that of the original Gemosil (prepared with MeOH only, entry 1 of **Table 2.1**). For instance, when using acetonitrile (CH_3CN) and tetrahydrofuran (THF) as the co-solvents, the flexural strength of such composites increases from 222 MPa to around 410 MPa and 431 MPa, respectively (entry 3 and entry 5 in **Table 2.1**). This can be explained by the fact that THF and CH_3CN are aprotic in nature, which can promote fast condensation reaction when compared with the protic ones (such as methanol (MeOH) and ethanol (EtOH)). Moreover, THF and CH_3CN also have relative lower viscosity values, which would likely promote fast hydrolysis reaction of enTMOS. For these

reasons, the addition of THF or CH_3CN would result in a dense silane network as shown in **Scheme 2.1** with higher flexural strength. This can be further supported by the impressive improvement of compressive strength, which increases from 97 MPa when processed with pure MeOH to 195 MPa when adding THF as the co-solvents (**Table A2.1,** entry 2 and 4, **Appendix**). However, if all MeOH was replaced by THF (i.e., THF only) or CH_3CN (i.e., CH_3CN only), the sol-gel reaction would be completed too fast (gelation time was reduced to 2 min from the original 5 min). The too fast cure rate would result in the incomplete condensation reaction, evidenced by the opaque colour of pure enTMOS (**Figure A2.5 (c)** and **(e)** in **Appendix**), leading to lower mechanical strength of such a composite. For instance, the compressive strength and biaxial flexural strength of THF only composite would decrease from 195 MPa to 72 MPa and 430 MPa to 152 MPa, respectively (entry 4 and entry 5 in **Table A2.1** in **Appendix)**. Second, for co-solvents in the same category, the boiling point of the co-solvents also plays a role in the mechanical strength of the composite. For instance, composites made from dioxane/MeOH and dimethoxyethane (DME)/MeOH have different flexural strengths, 291 MPa vs. 408 MPa (**Table 2.1**, entry 7 and 8). It appears that a close match of the boiling point of co-solvent with that of MeOH (65 °C) would help the drying process. In this specific case, the boiling point of dioxane (101 °C) is too far from MeOH compared to the boiling point of DME (85 °C). This could be explained by that having a co-solvent with a similar boiling point to that of the primary solvent can lead to a more uniform solvent evaporation, which can help reduce the large cracks in the final composite and result in higher mechanical strength. Finally, viscosity of the co-solvent does not appear to have any correlation with the biaxial flexural strength of the final composite. This can be seen from cases of

CH_3CN/MeOH, THF/MeOH, and DME/MeOH. A range of viscosity values (0.37, 0.52 and 1.1) were observed, yet all co-solvents offered similarly high flexural strength of the final composites (over 400 MPa).

2.3 Hypothesis for Co-solvent Effect

We hypothesize that the effect of co-solvent on the mechanical strength of the Gemosil composite is mainly due to the combined effects from hydrolysis and condensation of silanes that changed the morphology of the composite, rather than from co-solvent induced chemical reaction/interaction between different components within the composite. Specifically, adding co-solvent into the processing solvent (i.e., MeOH) can have two functions during the composite formation. First, mixing different co-solvents with MeOH increases the total volume of solvent when compared with the original processing method reported previously. The extra solvent would allow the various components, including HAp-Gel, $Ca(OH)_2$ and enTMOS, to mix more homogenously. Second, the co-solvent can have a subtle impact on the morphology of the enTMOS network in the final composite (i.e., branched or condensed network, shown in **Scheme 2.1**), likely caused by the different rates of hydrolysis and condensation when different co-solvent is applied. As discussed earlier, the polarity and boiling point of the co-solvent can have a direct impact on these fundamental steps (i.e., hydrolysis and condensation) in the sol-gel process. Macroscopically, composites processed with an appropriate co-solvent show less cracks/holes, which would benefit a higher mechanical strength. Finally, since the solvent can be completely removed during the drying process, the biocompatibility of these composites can be maintained in addition to the improved mechanical strength.

2.4 FT-IR Study

To experimentally verify the hypothesis, we first applied FT-IR spectroscopy to identify specific chemical bonds in the final gel structure and to monitor the sol-gel reaction process.[80] We started with pure enTMOS gels formed from different co-solvents/MeOH systems to probe whether the co-solvent reacted with enTMOS. Three representative co-solvents/MeOH systems from these three different types (**Table 2.1**) were selected, THF/MeOH, CH_3CN/MeOH and MeOH only. First, the FT-IR of pure enTMOS network prepared with CH_3CN/MeOH and THF/MeOH show characteristic peaks for enTMOS gels (e.g., Si-O-Si stretching at 1029 cm^{-1} and 1118 cm^{-1}), indicating the formation of aminosilica matrix. As expected, enTMOS gels made from different co-solvent/MeOH systems demonstrated almost identical absorption spectra (from 4000 cm^{-1} – 400 cm^{-1}) to that of the enTMOS gel made from MeOH only (**Figure 2.1 (a)**). This indicates that the co-solvents did not react with the enTMOS during the sol-gel process. Moreover, the almost identical absorbance of peaks corresponding to the Si-O-Si bond for enTMOS processed with different solvents indicates that the total amount of Si-O-Si bond is comparable across the samples. We also performed ^{29}Si solid state NMR to further investigate the variety of Si bonds (e.g., Si-O-Si and Si-OH) that were involved in the sol-gel process. As shown in **Figure A2.2** in Appendix, for all silane networks with different processing co-solvents, we observed two Si peaks. The signal at – 65 ppm is corresponding to the formation of Si-O-Si, whereas the other signal at – 58 ppm is attributed to the Si-OH structure from the incomplete condensation.[81] Again, the ^{29}Si NMR spectra are very similar across the samples, implying similar amount of Si species. Second, in order to examine whether the co-solvents would react with other components in the Gemosil composite, i.e., HAp-Gel and $Ca(OH)_2$ with chlorhexidine(CHX), we applied FT-IR to study the Gemosil composite. Again, these FT-IR

spectra of composites made from different co-solvents/MeOH systems are almost identical to each other (**Figure 2.1 (b)**), indicating that the co-solvents didn't react with the remaining components (i.e., HAp-Gel and $Ca(OH)_2$ with CHX) in the Gemosil system. Most importantly, we did not observe any co-solvents/MeOH characteristic absorption in all FT-IR spectra, indicating that solvent was completely removed after drying. This is ideal for BTE application since the residual co-solvent (if any) could be toxic.

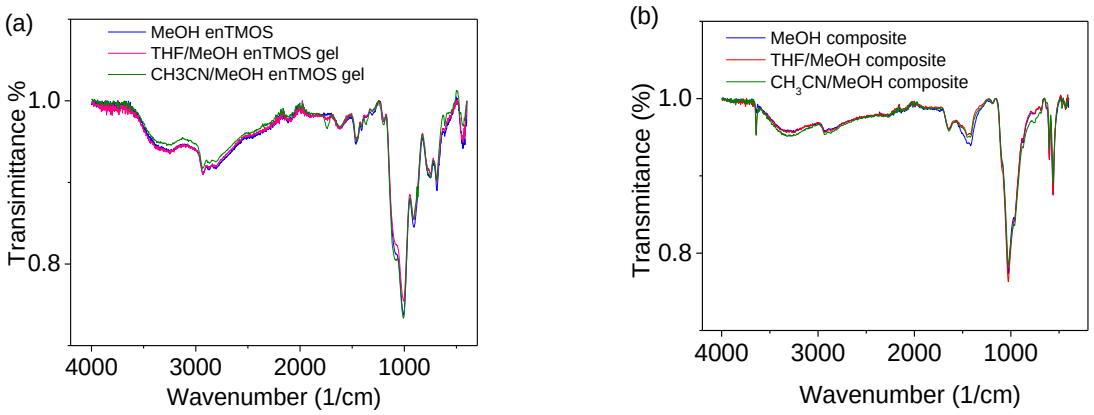

Figure 2.1. FT-IR spectra of (a) enTMOS gels and (b) Gemosil composites prepared from different solvent systems.

2.5 Morphology Study

Results from the FT-IR study rule out the possibility that the improvement of mechanical strength of these co-solvent-treated composites was from co-solvent-induced chemical interactions/reactions. Thus, it is very likely that the optimized morphology of the Gemosil composite is the main reason for the improved flexural strength. We next used SEM to investigate the morphology (i.e., phase distribution, porosity) of the composite formed from different co-solvent/MeOH systems and of the pure enTMOS network. We chose to study the cross-section of the composite made from two representative co-solvent/MeOH systems, namely, CH_3CN/MeOH and THF/MeOH. Composites made from only MeOH or THF were also

investigated as the reference. From the cross-section images of these composites (**Figure 2.2**), one can clearly observe that composite formed from CH_3CN/MeOH or THF/MeOH has a much smoother surface (less visual cracks), which agrees well with the greatly improved flexural strength of the composites (**Table 2.1**). In contrast, composite made from MeOH only has large cracks (**Figure 2.2(a)**). Furthermore, there are two distinct phases probed by EDS: one is enriched with HAp-Gel, while the other is enriched with silsesquioxane phase (**Figure A2.3** in **Appendix**). Comparing the phase distribution in composites made from MeOH only or THF only with that in composites made from CH_3CN/MeOH or THF/MeOH, the enTMOS phase and HAp-Gel distribute more homogenously with the addition of co-solvent (CH_3CN or THF). We attribute this homogenous phase distribution to the increased total volume of solvent with the addition of co-solvent, which would help the homogenous mixing of different components.

More importantly, these co-solvents can control the drying process of forming the Gemosil composite, since the mixed solvent (co-solvent+MeOH) would have a slower evaporation rate than that of the pure MeOH. If this were the case, a further deviation of the boiling point of co-solvent from that of the main solvent (i.e., MeOH) would have a more appreciable effect on the drying process and the morphology of as-formed composite. Indeed, the composite made from dioxane/MeOH (**Figure A2.4 (c)** in **Appendix**) shows larger cracks than the one made from THF/MeOH. This can be ascribed to the fact that the boiling point of dioxane (101 °C) is too far from that of MeOH than that of THF (66 °C).

While our results show that mixing co-solvent into the main solvent can be beneficial to improving the morphology and mechanical strength of our composites, having pure co-solvent alone (i.e., co-solvent as the sole solvent) cannot offer the same improvement. This can be seen by comparing the composite made from co-solvent/MeOH with that made from THF only. The

composite made with THF only shows less homogeneity and weaker mechanical strength (**Figure 2.2 (d)** and entry 5 in **Table A2.1** in **Appendix**). We speculate that a too fast gelation would occur when pure THF was used, which would lead to the inhomogeneous mixing of different components in the composite.

Finally, we applied TEM to investigate more details about each component in the composite. In principle, if the co-solvents did not react with the HAp-Gel crystal, we should be able to observe intact HAp-Gel crystals. Indeed, TEM images of composites show the Hap-gel nanocrystals remain intact after the processing with co-solvents (**Fig A2.6** in **Appendix**). This further proves that the improvement of mechanical strength by these co-solvents could be solely related to the optimized enTMOS matrix structure and the more homogenous mixing of different components in the composite.

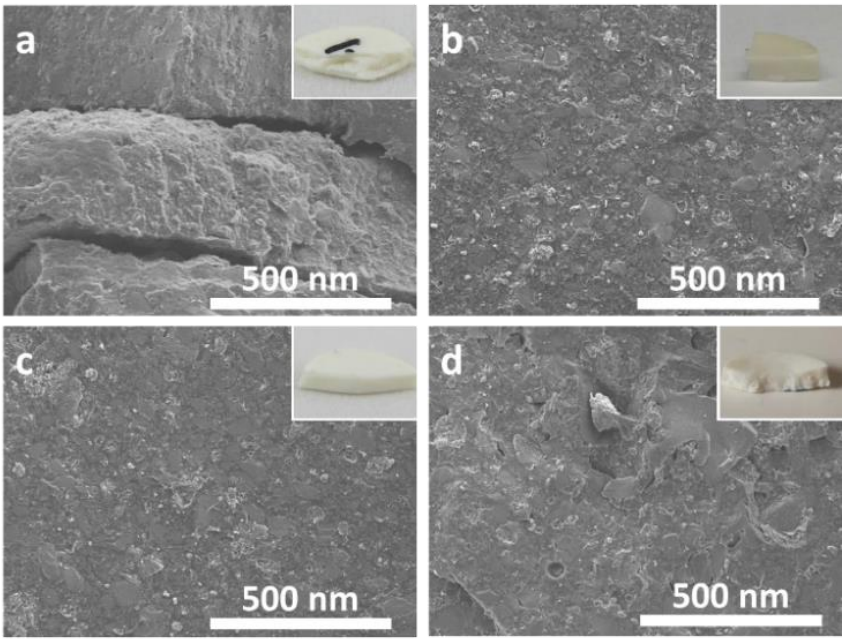

Figure 2.2. SEM images of composites made from (a) MeOH only; (b) CH_3CN/MeOH; (c) THF/MeOH; (d) THF only. Inset: the physical appearance of the composite under that condition.

2.6 Biocompatibility Study

Good biocompatibility of the composite is a prerequisite for BTE. Previous study has demonstrated that Gemosil has good biocompatibility.[69] In the current study, we add co-solvent and CHX as additional components during the processing, and there is a possibility that the residual co-solvent and CHX could lead to cell toxicity. To investigate this possible pitfall, the following experiments were carried out. We chose THF/MeOH as the representative co-solvent/MeOH system and varied the amount of co-solvent and CHX as independent variables. Experimentally, four different types of composites made from (a) MeOH, $Ca(OH)_2$, (b) MeOH, $Ca(OH)_2$ CHX, (c) THF/MeOH, $Ca(OH)_2$, (d) THF/MeOH, $Ca(OH)_2$ CHX were incubated with cells. The viability of the potential transplanted cells in BTE application, rMSCs, was monitored by RealTime-Glo^{TM} MT cell viability assay. We used this method to distinguish the direct toxicity monitored by the cells attached to the composites and the leaching toxicity measured by the cells in the well surrounding the bulk materials. However, a quick screening showed poor cells attachment on bulk composite made from $Ca(OH)_2$ with CHX and its surrounding area in the cell culture well, indicated acutely direct and leaching cytotoxicity resulting from CHX. We thus focused on comparing the cell toxicity of group (a) and group (c) to understand the impact of THF on cell viability. As shown in the **Figure 2.3**, the luminescent reading gradually increased from day 0 to day 1, suggesting the addition of THF during the composite processing did not decrease the cell viability compared with the non-toxic composite processed with MeOH only. The decreased luminescence on the day 2 may result from either the exhaustion of reagents or the confluency of cells on the composite. Importantly, we further discovered that when we replaced the $Ca(OH)_2$ CHX

with just $Ca(OH)_2$, the compressive strength of composites (with or without CHX) was comparable (**Table A2.2** in **Appendix**). Therefore, we recommend to replace $Ca(OH)_2$ CHX with $Ca(OH)_2$ for future use of the composites where good biocompatibility is required.

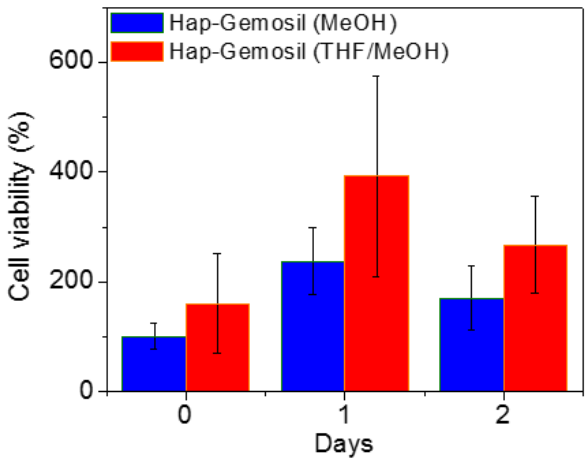

Figure 2.3. Cell viability test by RealTime-GloTM MT cell viability assay (two way ANOVA analysis, P=0.0012).

2.7 3D Porous Scaffold Fabrication and Mechanical Properties

In addition to biocompatibility, other important considerations for scaffolds intended for BTE include the feasibility of forming porous structures yet still maintaining good mechanical strength. To this end, we fabricated 3D porous scaffold with the Gemosil (THF/MeOH) composite via the aid of computational topology design (CTD) and 3D-printing. A good control on the porous architecture can be achieved (**Figure 2.4 (a)**). Moreover, porous scaffold processed with THF/MeOH has a compressive strength ~11.33±1.25 MPa, increased by ~60% compared to the compressive strength of scaffold processed with MeOH (6.94±1.01 MPa) (**Figure 2.4 (b)**). This increment further proves the effect of co-solvent in improving mechanical strength of Gemosil composite.

Furthermore, the achieved compressive strength of scaffold processed with co-solvent is comparable to that (1-13 MPa) of the cancellous bone.[13] All these indicate a great potential of such scaffold for BTE. Further in *vivo* test is in progress to access the feasibility of such scaffolds for biomedical applications.

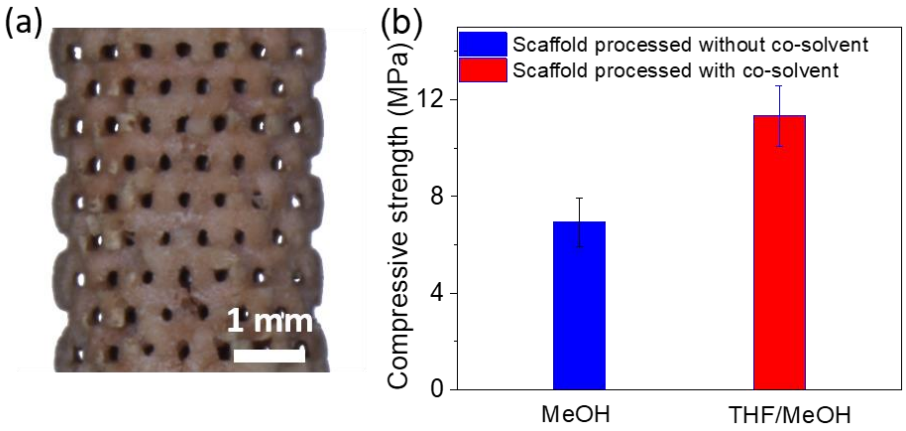

Figure 2.4. (a) Picture of the porous scaffold (pore size: 400 μm, porosity: 50%) and (b) compressive strength of porous scaffold processed with different co-solvents (student *t*-test, P=0.0001).

2.8 Conclusion

In conclusion, we successfully improved the mechanical strength of our previously developed Gemosil composite significantly with the aid of selected co-solvents (e.g., THF, CH_3CN, THP, etc.). We further demonstrated that the improvement of mechanical strength was not due to chemical interaction/reaction between the different components in Gemosil and co-solvents. Instead, adding co-solvents helped the enTMOS network formation and the composite processing. As a result, the likely uniformly cross-linked enTMOS matrix and the more homogenous composite would result in higher mechanical strength. Moreover, we showed that the co-solvent/MeOH could be completely removed from the composite during the drying process, thus having minimum impact on the

biocompatibility of this new Gemosil composite. Finally, we demonstrated that porous scaffold processed with co-solvent can be easily made yet maintained good compressive strength. All these results point to that this newly modified Gemosil composite is a very promising candidate for BTE. Currently, we are focus on evaluating the effect of this new scaffold for bone regeneration in *vivo*.

2.9 Experimental Section

Materials

HAp-Gel and $Ca(OH)_2$ powder was prepared by the method reported previously.[68] $Ca(OH)_2$ with CHX was prepared by doping 5%-10% CHX into $Ca(OH)_2$ powder. 95% bis[3-(trimethoxysilyl)-propyl]ethylenediamine (enTMOS) and 62% enTMOS in MeOH were purchased from Gelest, Inc. (Morrisville, PA, USA). Solvents, including MeOH, EtOH, CH_3CN, THF, tetrahydropyran (THP), DMSO, dimethoxyethane (DME), 1,4-dioxane were purchased from Alfa Aesar and used as received. Ammonium persulfate (APS) was purchased from Sigma-Aldrich and used as received.

Preparing the composite

The method for making the composites was adapted from previous report.[73] 300 mg HAp-Gel, 200 mg of $Ca(OH)_2$ with CHX powder were transferred into a mortar and ground into fine powder. Then, the powder mixture was spread on a glass sheet, which placed on a cold stage to maintain a depressed temperature of - 20 °C. The pre-mixed enTMOS solution, including 360 μL of co-solvent, 200 μL MeOH and 500 μL 95% enTMOS, was then added into the powder mixture quickly and mixed continuously with a spatula for 30 seconds. Then, 80 μL 7.5 % APS in MeOH/water (v/v=3:7) was added to trigger the sol-gel reaction. After mixing thoroughly, the mixture was poured into a disk

mold (size: diameter: 15.58 mm and thickness: 2.8 mm, designed for 3-point bending test), which lay on a smooth glass slide. Another smooth glass slide was carefully covered at the top of the mold to remove extra material. This "sandwich" structure (glass slides at the top and the bottom, material in the disk mold in between) was clamped and sealed into a plastic bag for one week to let the composite dry slowly. Finally, the sample was further dried in an oven at 54 °C for 5 days before the flexural strength test. The reason why the temperature was set at 54 °C is because gelatin has been shown to degrade gradually around 100°C and collagen has been shown to denature to gelatin between 60 °C and 80°C. Thus, we chose 54 °C to remove the remaining solvent as well as to avoid the degradation of gelatin or collagen. For comparison, composites without co-solvents, namely all MeOH, were also prepared according to the same procedure described above. Furthermore, previously reported Gemosil composite[69] made from 62% enTMOS was also repeated here as a reference. Additionally, cylinder-shaped samples with a 1:2 ratio of diameter (3.8 mm) to length (7.6 mm) were made according to our previous report[73] with the same composition described above. To prepare pure enTMOS network without HAp-Gel and $Ca(OH)_2$ CHX, APS was directly added to the pre-mixed enTMOS solution. After gelation, same drying process was applied as described above.

Compressive and biaxial flexural test

The testing procedures were performed according to methods established in our previous publication.[72] Cylinder-shaped samples (3.8 mm diameter by 7.6 mm length) or disk shape samples (13 mm diameter by 2.5 mm thickness) were used for compression test and 3-point bending test, respectively. Mechanical testing was performed on an Instron machine (model 4411, Instron Co., Norwood, MA, USA) with a cross-head speed

of 0.5 mm/min. Same calculation method[72] was used to get compressive strength and biaxial flexural strength. A minimum of three samples for each group were used in all mechanical testing.

FT-IR

Bulk composites were ground into fine powder. Then the fine powder was spread directly on diamond crystal and analyzed by Fourier-transform Infrared spectroscopy (FT-IR) using attenuated total reflection (ATR) mode.

^{29}Si solid state NMR

^{29}Si CPMAS NMR spectra were acquired on a Bruker DMX 360MHz WB NMR spectrometer operating at 71.55 MHz for ^{29}Si and 360.13 MHz for ^{1}H. A Q8M8 (i.e. octakis(trimethylsiloxy)silsequioxane) sample was used to calibrate the proton pulse width and the silicon power level for the contact pulse (10ms). A relaxation delay of 5 s and a sweep width of 27 kHz was used. Total number of scans ranged from 4k to 16k. Spectra were processed with 50Hz line broadening and referenced to an external TMS sample.

Morphology study

For scanning electron microscopy (SEM) analysis, a sample was carefully cut from bulk disk-shaped composite. Then the sample cross-section was sputter-coated with gold in a vacuum and imaged using a Hitachi S-4700 Cold Cathode Field Emission SEM (Hitachi High Technologies America, Inc.). Energy-dispersive X-ray spectroscopy (EDS) analysis was performed to examine at different phase on sample's cross-section, which were analyzed by Inca operator software. For transmission electron microscopy (TEM) analysis, the bulk composite was ground into a fine powder and suspended into MeOH with sonication. Then, a small drop

this solution was added to the TEM grid for imaging using a JEOL 2010F-FasTEM (JEOL USA, Inc.).

3D porous scaffold fabrication

A 3D cylindrical porous template (diameter: 5 mm and height: 10mm, pore size: 400 μm, porosity: 50%) was designed using SolidWorks software (Dassault Systems SolidWorks Corp.,Waltham, MA, USA). This template (stl format) was then used to print a 3D wax mold made of Solidcape® Model (Solidscape Inc., Merrimack, NH, USA) with 0.16 mm^2 trusses and 0.16 mm^2 pore sizes (continuous space) using a Solidscape 3D printer (Solidscape Inc., Merrimack, NH, USA). Next, the composite mixture was prepared on the cold stage as described above and injected to the 3D-printed mold before the materials was let to solidify. After setting for 3-5 minutes, the wax mold and the composite was immersed in acetone for 15 minutes to remove the wax template and release the 3D porous composite based scaffold, which is shown in **Figure 2.4(a)**. The porous scaffold was air dried for one week, followed by drying at 52 °C for 4 days prior to the compression test. Same method and data analysis were used here to obtain the compressive strength. The compressive strength of the porous scaffold was averaged from at least three samples.

Bulk material biocompatibility study via RealTime-Glo™ MT cell viability assay

Bulk disk samples (diameter: 6 mm, thickness: 1 mm) made from THF/MeOH or MeOH were leaching in H_2O for 3 days, followed by gas sterilization and balanced in the cell growth media for overnight. The disk samples were then seeded with rat mesenchymal stem cells (rMSCs) in a Costar 48-well plate and incubated at 37 °C for overnight to allow cell to attach. Then the disk samples were transferred into a new 96-well opaque plate to prevent inter-well

interference during measurement, followed by addition of NanoLuc® luciferase and a cell-permeant prosubstrate and incubated at 37 °C. At predetermined time points (i.e., 0 day, 1 day, 2 days), the illuminance of each well with substrate was measured by Cytation 5 cell imaging multi-mode reader. Each group with minimum of three samples was tested for each time. The cell viability result was averaged from three separate measurements.

Chapter 3 CATECHOL-FUNCTIONALIZED ADHESIVE POLYMER FOR ENHANCING MECHANICAL STRENGTH OF SILANE-MODIFIED HYDROXYAPATITE-GELATIN COMPOSITE IN WET CONDITION

3.1 Introduction

In **Chapter 2**, we optimized the silane (i.e., enTMOS) sol-gel reaction condition through applying selective co-solvent during processing and were able to dramatically improve the mechanical strength of Gemosil composite (i.e., silane-modified HAp-Gel composite). For instance, the new Gemosil composite processed with THF as co-solvent, demonstrated almost twice the compressive strength (195 MPa vs. 97 MPa) and biaxial flexural strength (431 MPa vs. 222 MPa) of the original Gemosil composite without THF, respectively. These findings offer valuable guidelines when selecting co-solvents to improve silane sol-gel processing and the mechanical strength of such composites. Moreover, the co-solvents can be completely removed during drying, thereby not compromising the biocompatibility of composite. Finally, we have shown that porous scaffolds could be easily fabricated, and such porous scaffolds demonstrated values of compressive strength around 11 MPa, comparable to those of cancellous bones.[13] However, there are challenges in using such porous scaffolds for bone regeneration *in vivo*. Our preliminary *in-vitro* degradation study showed that the scaffold degraded rapidly when immersed in water (H_2O). Compressive strength of the porous scaffold decreased from 11 MPa to 0.5 MPa after it was immersed in H_2O for 3 days. Therefore, our next goal was set to develop a more robust composite to be used as scaffolds for BTE application.

One possible option is to incorporate a water-insoluble, biocompatible and cross-linkable polymer with sufficient mechanical strength into the composite, assuming the strength of such polymer networks was able to be carried into the composite. There have been numerous reports on blending polymers with various inorganic materials to improve the performance of the final composites, for instance, tuning their degradation profiles and increasing the toughness.[54,82,83] Given that biocompatibility and biodegradability are required for our application, we turned our attention to synthetic polymers with these features, such as poly (L-lactide acid)(PLLA),[84,85] poly(lactic-*co*-glycolic acid)(PLGA),[86,87] polycaprolactone(PCL)[88], and poly(trimethylene carbonate)(PTMC).[89,90] These polymers have been long established as blends for a variety of medical applications due to their unique mechanical and degradation properties. Previously, our group designed a silane-functionalized P(LLA-*co*-PC) copolymer, aiming to enhance the long-range interactions among different components in Gemosil by incorporating this copolymer within the Gemosil composite.[72] In that study,[72] this copolymer demonstrated several advantages. First, copolymerization of PLLA with PC lowered the glass transition temperature (T_g) of pure PLLA,[91] which would help to 'soften' PLLA and provide better toughing effect to mitigate the brittle nature of the Gemosil composites.[92] Second, the PC monomer allowed the incorporation of a pendant alkyne group for further post-functionalization. In the previous study, we functionalized the P(LLA-*co*-PC) copolymer with silane side groups on the PC unit; such silane-functionalized P(LLA-*co*-PC) copolymers were designed to react with the enTMOS silane cross-linker in the Gemosil composite during the sol-gel process, which would incorporate these copolymers into the Gemosil composite to further reinforce the composite.[72] Indeed, we successfully increased the biaxial flexural strength of composite from 40 MPa to 60 MPa through the incorporation of this P(LLA-*co*-PC) polymer based network. Unfortunately, the compressive

strength of the polymer-incorporated composite greatly decreased (from 80 MPa to 30 MPa), likely due to the poor adhesion between the hydrophilic HAp-Gel and the hydrophobic polymers.

To increase the adhesion between the aforementioned components, we decided to seek inspiration by searching nature's methods of adhering biomaterials under aqueous conditions. A great example is mussels, which have demonstrated impressive adhesion to various substrates under wet conditions. These impressive adhesion properties are due to mussel adhesive proteins, which have several key structural features.[93] For example, mussel adhesive proteins' sequences have two main types of constituents, namely, catecholic amino acid (e.g., L-3,4-dihydroxyphenylalanine (L-DOPA)), and amine-containing amino acids (e.g., lysine, histidine and arginine).[93] Further studies revealed that the catechol groups in L-DOPA were able to form: a) adhesive interactions at the substrate surface through hydrogen bonding, π- π electron interaction and cation- π interaction,[94,95] and b) a cross-linked network to improve cohesive strength through metal chelating[95,96] or oxidative aryl-aryl coupling.[97,98] All these contributed to mussel's impressive adhesive properties. Moreover, amine group could provide a synergistic effect to mussel's adhesion through ionic bonding to negatively charged surfaces [99] and intermolecular cross-linking with *o*-quinones through Michael addition or Schiff-base formation.[95] Inspired by these findings, various synthetic polymers with catechol alone,[97] or coupled together with amine [100] have been investigated to develop functional polymers with strong adhesive properties under wet condition.[101] Among these, dopamine, perhaps the simplest molecule that covalently linking catechol and amine, has shown impressive adhesive and coating properties with its polymers.[102] Recently, we introduced polydopamine (PDA) into our Gemosil composite, aiming to improve the adhesion between the hydrophilic HAp-Gel and the hydrophobic siloxane matrix. However, we observed limited improvement in compressive

strength, from 80 MPa to 100 MPa.[73] This might be caused by the low molecular weight of PDA,[103] which would not reproduce the long-range interaction of collagen in nature bones.

These previous results motivated us to design a new polymer that could provide long-range interactions as well as good adhesive properties. We envisioned a copolymer, P(LLA-*co*-PC) decorated with cross-linkable adhesive catechol functional group (**Scheme 3.1**), would a potential candidate. We chose P(LLA-*co*-PC) as the parent polymer in order to introduce the favorable mechanical properties, biocompatibility and degradability, offered by P(LLA-*co*-PC). Moreover, the cross-linkable adhesive catechol functional group, newly added to P(LLA-*co*-PC) in our design, would provide two advantages. First, the interfacial adhesion between different components in the composite could be improved due to the impressive adhesive property of catechol; second, long-range interactions could be increased through the formation of polymer network via catechol aryl-aryl coupling between polymer and dopamine under oxidative condition. It should be mentioned that using dopamine small molecule together with catechol-functionalized copolymer would further promote the network formation. It was expected that the combination of copolymer and dopamine would enhance the mechanical reinforcement effect compared to using copolymer only or dopamine only. In short, introducing of this newly designed cross-linkable adhesive polymer together with dopamine would likely help to mitigate the degradation issue by the presence of extra structural support from network and enhanced adhesion within composite, thereby improving the mechanical strength of composite under wet condition.

Scheme 3.1. Proposed polymer network formed through the catechol oxidative coupling between polymer and dopamine

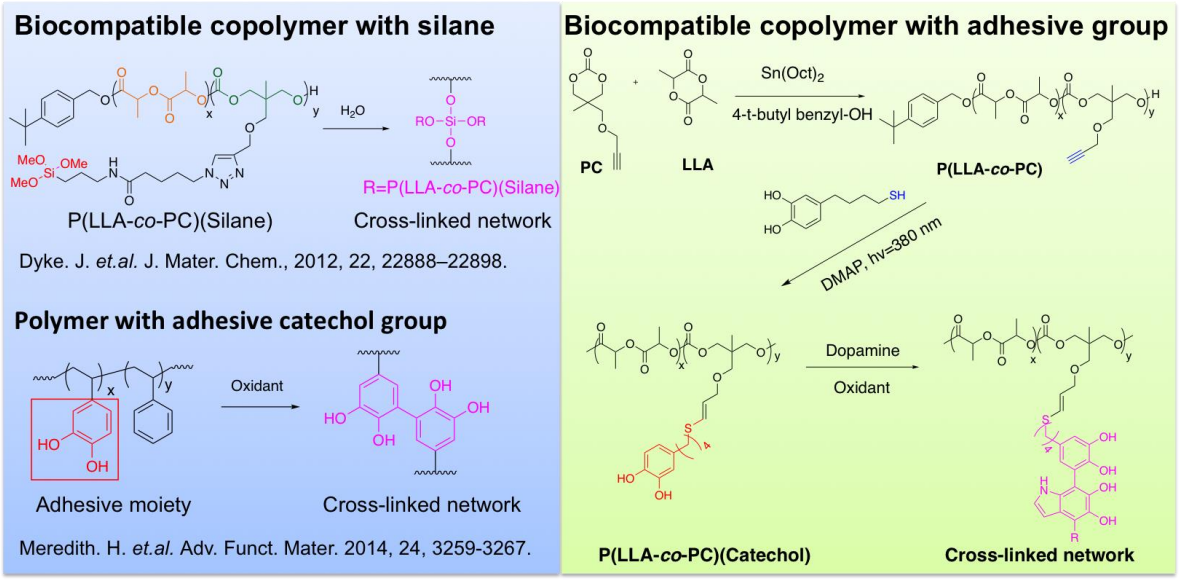

As shown in **Scheme 3.1**, we first synthesized P(LLA-*co*-PC) with pendant acetylene groups, following our previous report.[72] A post-functionalization of the P(LLA-*co*-PC) with catechol functional groups through "thiol-yne" click chemistry, where the "yne" functionality comes from copolymer and "thiol" functionality was linked with catechol (i.e., catechol-4C-SH), offered the P(LLA-*co*-PC)(catechol). Having successfully prepared this new copolymer, we probed how the mechanical properties of our Gemosil composites would change upon incorporation of this copolymer and dopamine. A number of variables were investigated. From the copolymer point of view, we studied the ratio of catechol incorporation on the copolymer, the molecular weight of the copolymer; from the formulation point of view, we studied the ratio of copolymer vs. free dopamine in the composite. We found that with optimized polymer composition (catechol amount ~ 15%) and molecular weight (~16 kDa) as well as optimized copolymer and dopamine amount (i.e., 30 mg and 10 mg, respectively), the compressive strength

of scaffold could be improved by 20% under wet condition with the addition of the copolymer of and dopamine.

3.2 Synthesis of Monomer and Cross-linker

The synthesis of PC monomer, as shown in **Scheme 3.2**, was adapted from our previous report,[72] and the targeted cross-linker molecule, 4-(4-mercaptobutyl) benzene-1,2-diol (i.e., Catechol-4C-SH), was prepared according to **Scheme 3.3**. Specifically, a Friedel-Crafts acylation of the commercially available 3,4-dimethoxybenzene, followed by a $NaBH_4$ reduction, readily afforded the key intermediate (**3.2'**).[104] This intermediate then went through a nucleophilic substitution of the bromide with the thioacetate to accomplish compound (**3.3'**). Treating compound (**3.3'**) with the strong Lewis acid BBr_3 smoothly removed the methyl protecting groups, revealing the catechol group, which was then followed by the removal of acetate group to reveal the thiol group under acidic condition and afforded the target molecule (**3.4'**). The chemical structure of the product formed after each step was confirmed by ^1H NMR (**Appendix** for Chapter 3).

Scheme 3.2. Synthesis route of PC monomer

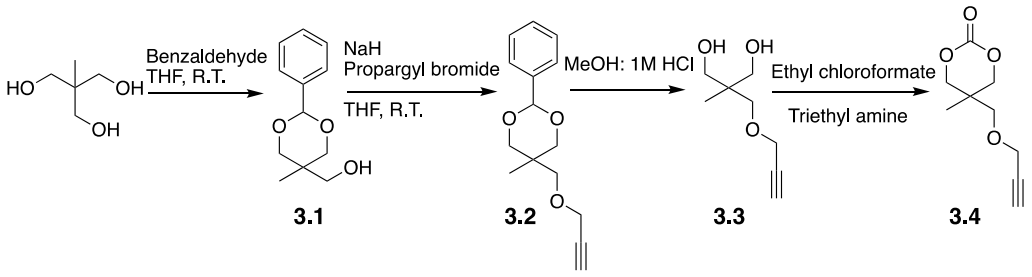

Scheme 3.3. Synthesis route of Catechol-4C-SH

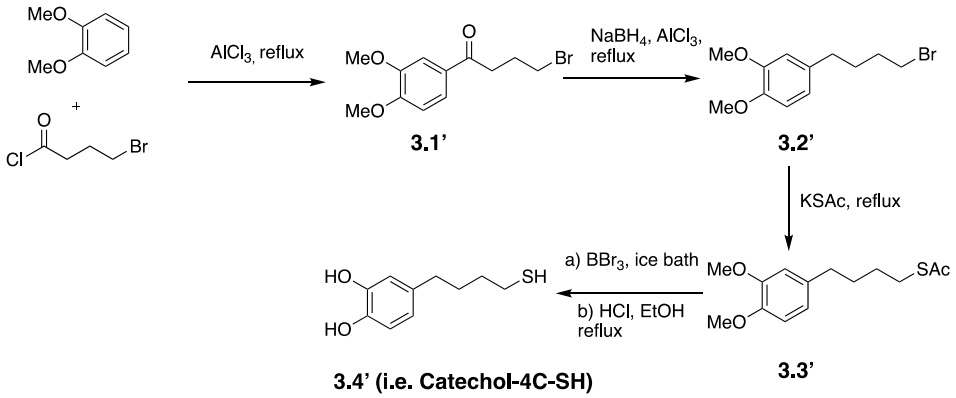

3.3 Synthesis of P(LLA-*co*-PC) Copolymers and Post-functionalization with Catechol

The PLLA-*co*-PC copolymer was prepared according to our previous report.[72] The successful synthesis of copolymer was characterized by ^{1}H NMR spectra (**Figure 3.1** and **Appendix** for Chapter 3). As demonstrated in our previous report,[72] copolymers with different amount of PC in the backbone, as shown in **Table 3.1**, could be readily obtained by varying the loading mol% of PC (0-50 mol%). We also observed that the number average molecular weight (M_n) of copolymer, characterized by gel permeation chromatography (GPC), gradually decreased with the increasing amount of loaded PC monomer (**Figure A3.1** in **Appendix**). This was attributed to a faster consumption rate of LLA compared to PC during the copolymerization.[72]

Table 3.1. Summarized polymerization data for P(LLA-*co*-PC) copolymers

Entry	PC loading (mol%)	PC incorporation (mol%)	M_n (kg/mol)	M_w (kg/mol)	Dispersity (Đ)
1	16.7	11.7	16.4	22.4	1.36
2	20	19.5	12.6	17.1	1.35
3	30	24.0	9.3	12.7	1.36
4	50	48.3	6.1	8.6	1.41
5	100	100	4.2	4.7	1.13

Scheme 3.4. Synthesis of PLLA-*co*-PC copolymer functionalized with catechol through "thiol-yne" click chemistry

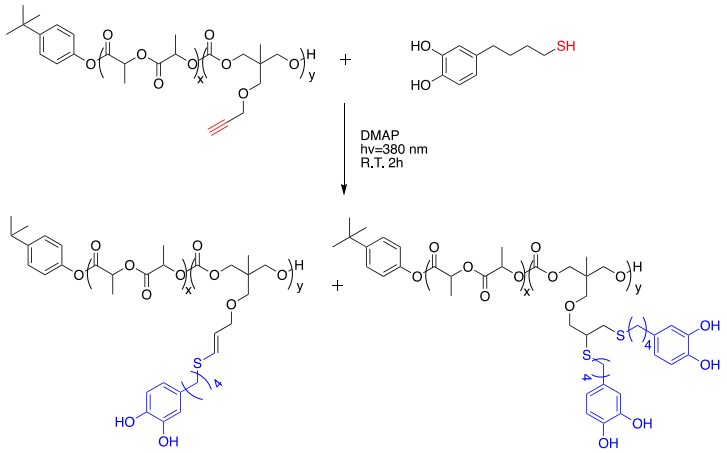

Having successfully obtained the P(LLA-*co*-PC) copolymer, we next attempted to functionalize the pendant acetylene of PC with catechol through "thiol-yne" click chemistry as shown in **Scheme 3.4**. "Thiol-yne" click chemistry [105] has been demonstrated as a powerful method for post-functionalization of polymers. Mechanistically, each yne moiety first reacts with one thiol functionality to form a vinyl sulfide (i.e., monoaddition product), followed by subsequent reaction of the vinyl sulfide with the second thiol to yield the 1,2-disubstitued adduct (i.e., bisaddition product).[106] Interesting, according to previous report,[107] for post-functionalization of polymers with the "thiol-yne" method, one would need to have thiols in a large stoichiometric excess (usually 10 ×) to obtain close to 100% bisaddition product. In our case, we found under the stoichiometric (2 thiols:1 yne) condition, successful post-functionalization of the copolymer with catechol were achieved, evidenced by the disappearance of pendant acetylene protons at δ=2.45 ppm and appearance of the phenyl protons at δ=6.56 ppm (associated with the phenyl ring of Catechol-4C-SH) in ^{1}H NMR spectra (**Figure 3.1**). Additionally, through comparing the integrations of signals of phenyl protons (δ=6.56 ppm) with

lactide methane protons (δ=5.18 ppm) in ^{1}H NMR spectra, we were able to calculate the incorporated catechol amount. We found that both monoaddition product and bisaddition product were obtained. For instance, when functionalizing P(LLA-*co*-PC)$_{11.7\%}$ (i.e., entry 1 of **Table 3.1**, 11.7 mol% of PC in the polymer backbone) with catechol, we found that the ratio of incorporated catechol to lactide in the polymer is around 14.3% (i.e., in average 1 yne reacted with 1.22 thiols). Accordingly, we named the final copolymer as P(LLA-*co*-PC)$_{11.7\%}$(Catechol)$_{14.3\%}$ for clarity.

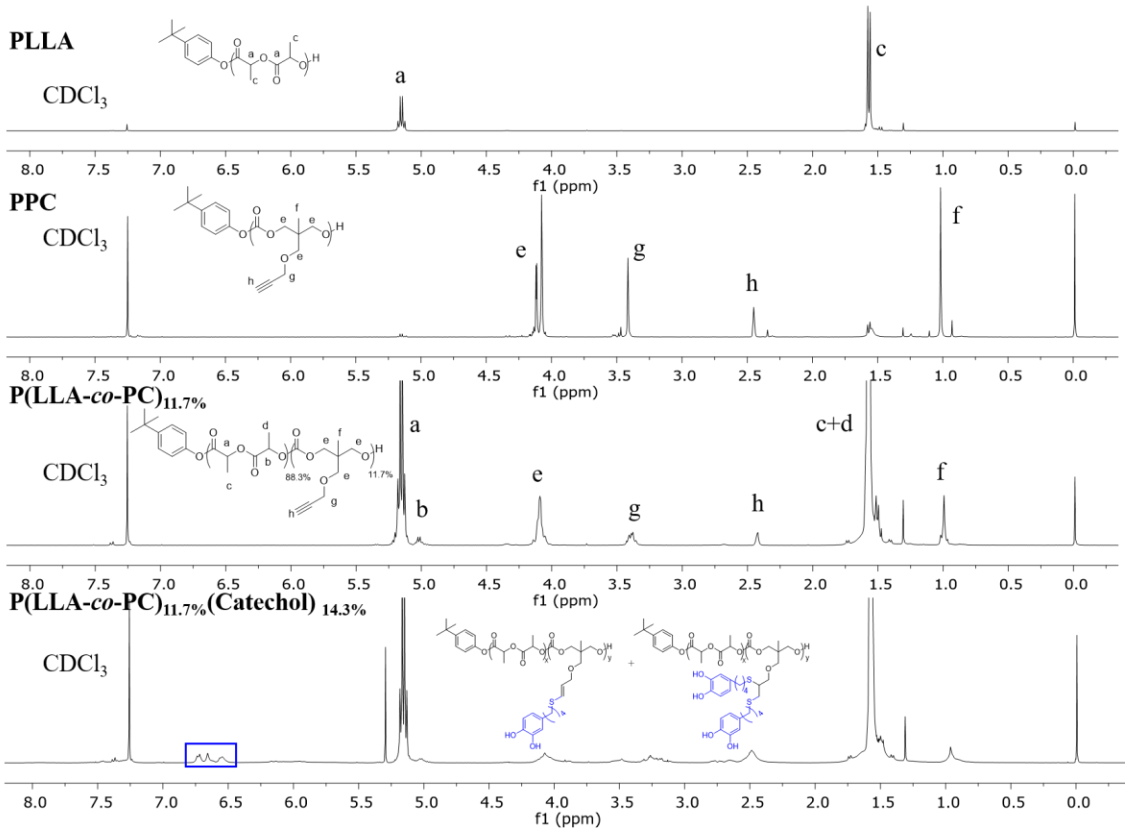

Figure 3.1. The ^{1}H NMR spectra of homopolymers, copolymer and catechol functionalized copolymer.

3.4 Optimization of Catechol Amount

Previous studies have demonstrated that the amount of catechol on its functionalized

polymers can substantially influence the adhesive properties of catechol-bearing polymers. For instance, the Wilker group discovered that their mussel-mimic adhering copolymers, i.e. poly(3,4-dihydroxystyrene)-*co*-styrene, achieved the highest adhesive strength with the copolymer having an equivalent of ~ 33 mol% catechol.[108,109] The authors believed this specific amount of incorporated catechol (33 mol%) would strike a balance between the cohesive and adhesive bonding; further increasing the catechol amount would likely cause too much crosslinking, causing the decrease of adhesive bonding to the surface. Given that our polymers also have catechol as the pendant group, similar to the polymer reported by the Wilker group, it would not be surprising that the amount of catechol in our copolymer would also have a strong impact on the adhesive property. Furthermore, since catechol has a much better solubility in common organic solvents than our copolymer backbone (i.e., P(LLA-*co*-PC)), the amount of incorporated catechol would also influence the solubility of the catechol-functionalized copolymer and related processability. In short, all these factors will exert influence on the mechanical strength of the final composite after the copolymer is introduced. Therefore, it is necessary to find the optimized amount of catechol incorporated with our copolymer.

To examine the influence of the amount of incorporated catechol on the mechanical strength of the final composite, we prepared three polymers of varied amount of catechol. We chose to fix the loading molar ratio of yne:thiol to 1:2 to ensure similar click reaction efficiency (e.g., 1 yne would produce 1.22 pendant catechols, in average); this strategy allowed us to vary the amount of incorporated catechol by simply varying the amount of PC in the copolymer backbone. Specifically, in addition to PLLA-*co*-$PC_{11.7\%}$ (entry 1 in **Table 3.1**), we also applied the thiol-yne chemistry to attach the catechol functionality to PLLA-*co*-$PC_{19.5\%}$ (entry 2 in **Table 3.1**) and PLLA-*co*-$PC_{24\%}$ (entry 3 in **Table 3.1**), bearing 19.5 mol% and 24 mol% of PC

monomer in the copolymer backbone, respectively. The successful incorporation of catechol to each polymer was evidenced by the appearance of phenyl protons at δ= 6.56 ppm in ^{1}H NMR spectra, which was associated with the original catechol-4C-SH (**Appendix** in Chapter 3). Similarly, through comparing the integration of signals from the phenyl protons at δ= 6.56 ppm and lactide methane protons at δ= 5.18 ppm, the amount of the incorporated catechol (mol%) was calculated (**Table 3.2**). Again, it was demonstrated that for all post-functionalization, both monoaddition and bisaddition product were obtained. Interestingly, for PLLA-*co*-$PC_{24\%}$, we obtained a higher click reaction efficiency (entry 3, **Table 3.2**, i.e., 1 yne would produce 1.5 pendant catechols, in average), which could be caused by the lower molecular weight of PLLA-*co*-$PC_{24\%}$ and relative higher alkyne amount in polymer backbone. Unfortunately, copolymers with high amount of catechol, such as PLLA-*co*-$PC_{19.5\%}$-$Catechol_{25\%}$ and PLLA-*co*-$PC_{24\%}$-$Catechol_{36\%}$, were easily cross-linked in THF, likely due to the formation of hydrogen-bonding between catechol groups from different polymer chains. Such gels posed a significant challenge in further blending these catechol-functionalized copolymers into our composites; thus, we chose to fix the catechol amount around 15 mol% on the copolymer for our next investigation. This amount (15 mol%) would allow the maximum loading of catechol yet still maintain the solubility of such copolymer in common organic solvents.

Table 3.2. P(LLA-*co*-PC) copolymers with different amount of catechol

Entry	PC incorporation (mol%)	Catechol amount (mol%)	Gelation behavior
1	11.7	14.3	No
2	19.5	25.0	Yes
3	24.0	36.0	Yes

3.5 Optimization of the Molecular Weight of Copolymer

After establishing the maximum allowable amount of catechol in the copolymer to be ~ 15%, we next explored the impact of the molecular weight of catechol-functionalized copolymer on the mechanical strength of the final composite. The molecular weight can influence many key properties of polymers that influence mechanical strength, for example, the glass transition temperature (T_g), stiffness, strength, viscosity and toughness.[110] We synthesized several copolymers with a variety of molecular weight by altering the monomer/initiator ratio during the polymerization. Please note that we attempted to fix the amount of incorporated catechol (i.e., optimized catechol amount ~15 mol%) in this series of copolymers through fixing the loading molar ratio of PLLA/PC at 85/15 during the polymerization. Based on the "thiol-yne" click reaction efficiency in our system discussed in **Section 3.4**, it is very likely to obtain ~15 mol% catechol incorporation in copolymer with 15 mol% of PC loading. Specifically, we varied the monomer/initiator molar ratio from 12.5 to 200 and four polymers with M_n ranging from 10.7 kg/mol to 37.4 kg/mol were successfully obtained as shown in **Table 3.3**. Through similar "thiol-yne" click chemistry, the four polymers prepared here displayed final catechol amount within a range of 13.9 -15.4 mol%. Representative ^{1}H NMR spectra of P(LLA-*co*-PC)(Catechol) are provided in the **Appendix** for Chapter 3.

Table 3.3. P(LLA-*co*-PC)(Catechol) with different polymer molecular weight

Entry	Monomer/ Initiator molar ratio	PC loading/incorporation (mol%)	Catechol amount (mol%)	M_n (kg/mol)	M_w (kg/mol)	Dispersity (Đ)
1	12.5	15/11.7	14.3	10.7	12.3	1.15
2	33.3	15/11.8	14.3	16.4	19.7	1.20
3	100	15/12.2	13.9	24.3	34.5	1.42
4	200	15/12.7	15.4	37.4	50.2	1.34

We then blended each copolymer to our original composites (i.e. Gemosil, silane-modified HAp-Gel composite) and measured the compressive strength and biaxial flexural strength of the final composite. We first used THF/MeOH (v/v=9:5), a mixed solvent system, to dissolve the copolymer, followed by blending the copolymer solution with HAp-Gel powder. There are two reasons for choosing this processing method. First, as shown in **Chapter 2**, THF/MeOH would likely promote the formation of a condensed structure of enTMOS silane network, offering good mechanical strength. Second, dissolving the copolymer in this mixed solvent would also provide a more homogenous mixing of copolymer with other components in the composites, such as HAp-Gel and enTMOS. After successfully forming new composites with the blended copolymer, we then carried out the mechanical testing to determine the effect of the molecular weight of our copolymers on the mechanical properties of the final composite. The results are compared in **Figure 3.2**. Interestingly, we find that the molecular weight of the copolymer does not seem to have a significant impact on the mechanical strength of the final composite, for both compressive strength and flexural strength. Nevertheless, the copolymer with a moderate molecular weight, around 16.4 kg/mol (entry 2 in **Table 3.3**), appeared to offer

slightly better mechanical performance of the final composite than others (**Figure 3.2**). Thus, we chose this particular molecular weight, i.e., P(LLA-*co*-PC)$_{11.7\%}$Catechol$_{14.3\%}$ with a M_n of ~ 16.4 kg/mol for further study.

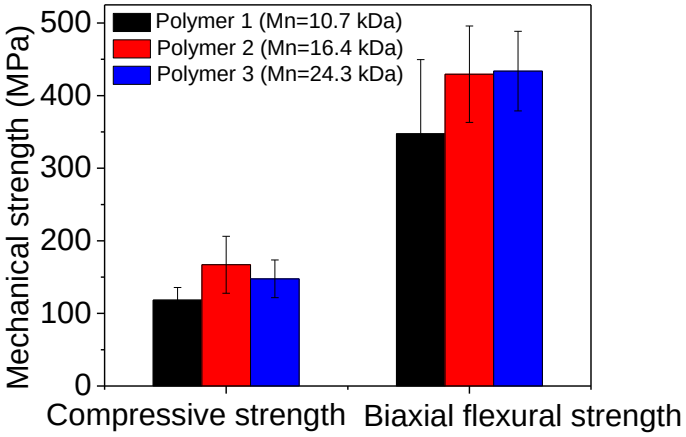

Figure 3.2. Mechanical strength of composite processed with different molecular weight of P(LLA-*co*-PC)(Catechol).

3.6 Optimization of Relative Amount of Catechol Functionalized Copolymer and Dopamine

Having optimized the catechol incorporation amount and polymer molecular weight, the last part is to optimize the relative amount of catechol functionalized copolymer and dopamine. To further improve the internal adhesion within the composite, the mussel-inspired small molecule dopamine was incorporated to promote the network formation through participating in the oxidative catechol coupling during network formation. Since there are two variables here, i.e., the amount of dopamine and the amount of copolymer, we performed a statistical design and stimulation. Based on the statistical design of experiment, we tested the mechanical strength (both compressive strength and biaxial flexural strength) with various amount of dopamine and copolymer. The preliminary results are shown in **Table 3.4**.

Table 3.4. Mechanical strength of bulk composite with different amount of copolymer and dopamine

Copolymer (mg)	Dopamine (mg)	Compressive strength (MPa)	Biaxial Flexural strength (MPa)
4.4	1.5	194.74	247.63
4.4	8.5	158.21	239.43
25.6	1.5	123.51	342.88
25.6	8.5	145.69	524.56
15	5	113.64	355.94
15	5	107.35	306.82
15	5	122.45	248.58
15	5	122.78	258.98
15	5	121.26	246.04
15	5	186.90	378.39
15	5	182.77	313.30
15	10	144.79	428.72
15	0	103.17	345.75

With statistical stimulation, we displayed these results in **Table 3.4** through a contour plot shown in **Figure 3.3**. For compressive strength, two maximum values (indicated by the red arrows in **Figure 3.3(a)**) were observed with all different combinations of copolymer and dopamine amount. One maximum value appeared at very low dopamine and copolymer amount, which can be explained by the fact that copolymer and dopamine haven't exert their function due to the relative low amount. Interestingly, the compressive strength decreased as we further

increased the copolymer and dopamine amount. This could be ascribed to that the cross-linked network between copolymer and dopamine hasn't formed yet. As a result, the copolymer and dopamine functioned as defects in the composite. As expected, with further increasing the copolymer and dopamine amount, the compressive strength of composite started to increase, which is attributed to the enhancing effect from the formation of copolymer and dopamine network in the composite. For the biaxial flexural strength (**Figure 3.3(b)**), a similar trend was observed. The highest biaxial flexural strength was achieved with high amount of copolymer and dopamine. Combining the stimulation results for both compressive and biaxial flexural strength, the optimized amount of copolymer and dopamine for achieving the largest enhancement of mechanical strength in composite was 30 mg and 10 mg, respectively.

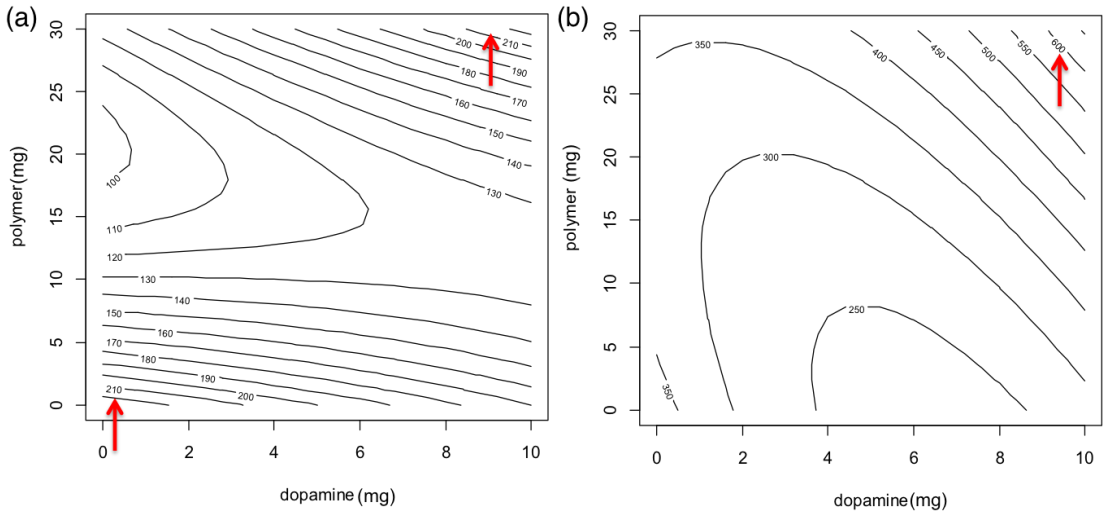

Figure 3.3. Contour plot for (a) compressive strength and (b) biaxial flexural strength of composite with various amount of copolymer/dopamine.

3.7 Compressive Strength of Scaffold Under Wet Condition

With the optimized catechol amount (~ 15%), polymer molecular weight (~ 16 kg/mol) and copolymer and dopamine amount (30 mg and 10 mg, respectively), we fabricated 3D porous scaffold (pore size: 400 μm and porosity: 50%) with copolymer/dopamine using the same

method described in **Chapter 2** to see whether the formation of copolymer/dopamine network could help to mitigate the degradation of scaffold in H_2O, thus improve the compressive strength of scaffold in wet condition (i.e. immersing the scaffold in H_2O for 3 days before testing the compressive strength of scaffold). Scaffolds made with Gemosil and Gemussel (i.e., polydopamine-reinforced Gemosil) were also studied as references. As shown in **Figure 3.4**, Gemussel and Gemussel-polymer (i.e., Gemussel with copolymer) has demonstrated a compressive strength of ~1.9 MPa and ~2.3 MPa, respectively, which are increased by 1.7 and 2.3 times compared to the compressive strength of Gemosil scaffold (~0.7 MPa). It should be mentioned that the incorporation of copolymer network into the Gemussel system could further improve the compressive strength of scaffold by 20%. This mechanical strength improvement allows this Gemussel-polymer system to be further studied in *vivo* to evaluate its performance for scaffold application.

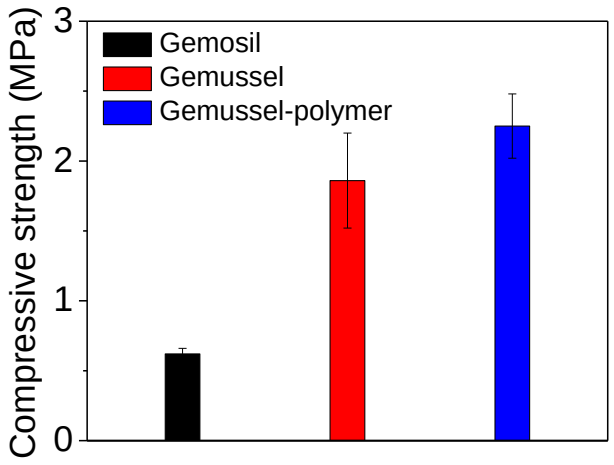

Figure 3.4. Compressive strength of scaffold under wet condition.

3.8 Conclusion

In summary, we have designed and synthesized a new biocompatible and biodegradable copolymer PLLA-*co*-PC with "cross-linkable" and adhesive catechol group. It has been

demonstrated that after incorporation of the copolymer together with dopamine into the previously developed Gemosil composite, the catechol-functionalized copolymer and dopamine together was capable of providing enhanced long-range interaction and improving the internal adhesion within the composite. Through optimizing the catechol incorporation amount, copolymer molecular weight and copolymer/dopamine amount, we were able to improve the compressive strength of the Gemosil scaffold significantly (from ~ 0.7 MPa to 2.3 MPa). Moreover, the incorporation of copolymer network into the Gemussel system could further improve the compressive strength of Gemussel scaffold by 20%. Our current focus is to investigate the cell toxicity of copolymer incorporated composite and further in *vivo* study.

3.9 Experimental Section

Materials

1,1,1-Tris(hydroxyl methyl) ethane (THME, Aldrich, 99%), triethylamine (TEA, Aldrich, 99%), 2,2-dimethoxy-2-phenylacetophenone (DMPA, Aldrich 99%), benzaldehyde (Aldrich, 98%), p-toluene sulfonic acid (TsOH, Aldrich, 98.5%), tin(II) 2-ethyl hexanoate ($SnOct_2$,98%, MP Biomedicals), and propargyl bromide (80% in toluene, TCI) were used as received. Ethyl chloroformate (99%) and CaH_2 (60% in mineral oil), and 4-tert butyl benzyl alcohol (98%) were obtained from Acros Organics and used as received. 4-bromobutanoyl chloride and sodium borohydride (98%) was purchased from Alfa Aesar and used as received. Potassium thioaetate (98%) was obtained from Sigma Aldrich and used as received. L-Lactide was generously donated by Purac and used without further purification. N,N-bis [(3-trimethoxysilyl)propyl]ethylene diamine (enTMOS, 95% in MeOH) was purchased from Gelest, Inc. and used as received. HAp-Gel and $Ca(OH)_2$ powder was prepared by the method reported previously.[68] Glutaraldehyde solution (50 wt.% in H_2O) and glycine were purchased from Sigma

Aldrich and used as received. Hexanes, acetone, chloroform, dichloromethane (DCM), anhydrous toluene, anhydrous MeOH, ethyl acetate (EtOAc) and THF were obtained from Fisher. THF was freshly distilled over sodium before use.

Synthesis of propargyl carbonate (PC) monomer

Synthesis of PC monomer is adapted from previously reported work by Dyke et al.[72] ^{1}H NMR (400 MHz, $CDCl_3$): δ 1.11 (s, 3H), 2.46 (s, 1H), 3.49 (s, 2H), 4.07 (d, 2H), 4.17 (s, 2H), 4.33 (d, 2H).

Synthesis of catechol-4C-SH

3.1' and **3.2'** was synthesized according to previous literature report and their structure was evidenced by ^{1}H NMR.[104] **3.1'**: ^{1}H NMR (400 MHz, $CDCl_3$): δ 2.29 (m, J=6.8, 6.4Hz, 2H), 3.13 (t, J=6.8 Hz, 2H), 3.54 (t, J=6.4 Hz, 2H), 3.93 (s, 3H), 3.94(s, 3H), 6.88(d, J=8.4 Hz, 1H), 7.52 (d, J=2 Hz, 1H), 7.61(dd, J=8.4, 2 Hz, 1H). **3.2'**: ^{1}H NMR (400 MHz, $CDCl_3$): δ 1.75 (m, J=7.6, 6.8 Hz, 2H), 1.88(m, J=7.2, 6.4 Hz, 2H), 2.58 (t, J=6.8, 6.4 Hz, 2H), 3.41 (t, J=7.6, 7.2 Hz, 2H), 3.85 (s, 3H), 3.87 (s, 3H), 6.70 (s, 1H), 6.72(d, J=2 Hz, 1H), 6.78 (d, J=8.8 Hz, 1H).

***S*-(4-(3,4-dimethoxyphenyl)butyl) ethanethoate (3.3')** compound **3.2'** (1.01g, 3.75 mmol) was dissolved in anhydrous THF, then potassium thioacetate (0.64g, 5.63 mmol) was added and stir at R.T. for 1.5 h. Rotary evaporation was used to remove the THF, and the concentrated residue was dissolved in EtOAc and washed with water 3 times before drying with $MgSO_4$ and concentrating again. Purification via a column using 4:1 hexane: EtOAc affords pure product as a yellow liquid (0.93g, yield: 92.3%). ^{1}H NMR (400 MHz, $CDCl_3$): δ 1.62 (m, 4H), 2.32 (s, 3H), 2.57 (t, J=8 Hz, 2H), 2.89(t, J=8 Hz, 3H), 3.85(s, 3H), 3.87(s, 3H), 6.69(d, J=8Hz, 1H), 6.71(d, J=4 Hz, 1H), 6.79(dd, J=8, 4 Hz, 1H).

Catechol-4C-SH (3.4') compound **3.3'** (0.93g, 3.5 mmol) was dissolved in anhydrous DCM and degassed with argon for 15 minutes in an ice bath. 1M BBr_3 in DCM solution was then added dropwise under argon. The reaction mixture was stirred for 2 hours before it was quenched with water slowly. After concentrating by rotary evaporation, the reaction mixture was dissolved in EtOAc and washed with water 3 times, then the organic phase was dried over $MgSO_4$ and concentrated by rotary evaporation again. The crude product was then dissolved in 1:1 v/v EtOH/12M HCl and heated to reflux for overnight to removal protection group to generate final product. The reaction mixture was concentrated by rotary evaporation again. The residue was subject to column chromatography using 1:1 hexane and EtOAc as the eluent to afford pure product as white solid (471mg, yield: 68%). ^{1}H NMR (400 MHz, $CDCl_3$): δ 1.33 (t, J=8 Hz, 1H), 1.63 (m, 4H), 2.52 (m, 4H), 6.59(dd, J=8,4 Hz, 1H), 6.69(d, J=4 Hz, 1H), 6.76 (d, J=8 Hz, 1H).

Synthesis of copolymers by $Sn(Oct)_2$ catalyzed ROP

Polymerization was carried out based on previous reported.[72] For all polymerizations, monomers/catalyst/initiator was fixed at 100/1/1. To synthesize copolymer with 16.7 mol% PC loading, first, under argon atmosphere, LLA (1.19g, 8.26 mmol) and PC (303 mg, 1.65 mmol) were added to a high pressure flask with 10 ml anhydrous toluene. Followed by adding $Sn(Oct)_2$ (stock solution in toluene:175.2 mM, 565 μL) and 4-tert-butylbenzyl alcohol (stock solution in toluene: 175.2 mM, 565 μL) quickly. The reaction container was then quickly transferred to a preheated oil bath (120 °C) for polymerization. The polymerization was then quenched with MeOH after 20 hours and the resulting copolymer was purified by precipitation into cold MeOH for 3 times. ^{1}H NMR analysis indicated this polymer contain 11.7 mol% PC in the backbone and thus was denoted as P(LLA-*co*-PC)$_{11.7\%}$ for clarity.

Post-functionalization of copolymer with catechol via click chemistry

All post-functionalization through "thiol-yne" click chemistry was performed in anhydrous THF with UV light under argon atmosphere. A typical synthesis for functionalization of P(LLA-*co*-PC)$_{11.7\%}$ with catechol-4C-SH is as follows: P(LLA-*co*-PC)$_{11.7\%}$ (2 g, yne amount:1.183 mmol), catechol-4C-SH (466 mg, 2.366 mmol) and photoinitiator DMPA (606.75mg, 2.366 mmol) were loaded into flamed-dried 100 mL two neck round flask and dissolved with anhydrous THF under Argon atmosphere. After the reagents are totally dissolved, UV light was used to initiate the polymerization. After 2 hours, the reaction was quenched by adding small amount of MeOH. Catechol-functionalized copolymer was obtained by precipitating into cold MeOH to yield product as yellow powder. ^{1}H NMR analysis indicated this polymer contain 14.3 mol% catechol in the backbone and thus was denoted as P(LLA-*co*-PC)$_{11.7\%}$-Catechol$_{14.3\%}$ for clarity.

Characterization of polymers

^{1}H NMR was used to determine the monomer incorporation ratio. $CDCl_3$ was used as the solvent. The molecular weight and polydispersity of the copolymers were determined by a Waters 1515 gel permeation chromatograph (GPC) using THF as the eluent as a flow rate of 1.0 mL/min at 30 °C. A series of narrow polystyrene standards were used for the calibration of the columns.

Fabrication of bulk composite with catechol-functionalized copolymer

The method for making the composites was similar to the method described in the experimental section in **Chapter 2**. The processing method for additional copolymer and dopamine is dissolving them in THF/MeOH mixing solvent first and then mixing them with enTMOS to make a homogenous solution. This homogenous solution with

copolymer, dopamine and enTMOS was then added to HAp-Gel and $Ca(OH)_2$ powder and made bulk cylinder and disk composite for compressive strength test and flexural strength test, respectively.

Fabrication of porous scaffold with catechol-functionalized copolymer

Porous template with pore size 400 um and porosity 50% was fabricated by 3D-printing technique. Then polymer (25.6mg) and dopamine (8.5mg) was dissolved in THF/MeOH mixing solvent (v/v=9:5, total volume 280 μL) with 250 μL 95% enTMOS solution. The premixed stock solution was then added to HAp-Gel (150 mg) and $Ca(OH)_2$ (100 mg) powder and injected to the 3D-printed mold before the materials were left to solidify. Similar to the post-treatment process described in **Chapter 2** experimental section, after setting for 3-5 minutes, the wax mold and the composite was immersed in acetone for 15 minutes to remove the wax template and release the 3D porous composite based scaffold. The porous scaffold was air dried for one week, followed by drying at 52 °C for 4 days. Then scaffold was immersed in 5% glutaraldehyde solution for further cross-linking of gelatin and 5% glycine solution for 1 day to react with remaining glutaraldehyde before compression test.

Compressive and biaxial flexural test

The testing procedures were performed according to methods established in our previous publication.[72,73] Cylinder-shaped samples (3.8 mm diameter by 7.6 mm length) or disk shape samples (13 mm diameter by 2.5 mm thickness) were used for compression test and 3-point bending test, respectively. Mechanical testing was performed on an Instron machine (model 4411, Instron Co., Norwood, MA, USA) with a cross-head speed of 0.5 mm/min. Same calculation method was used to get compressive strength and

biaxial flexural strength. A minimum of three samples for each group were used in all mechanical testing.

Chapter 4 INVESTIGATION OF DOPAMINE ANALOGUES: SYNTHESIS, MECHANISTIC UNDERSTANDING, AND STRUCTURE-PROPERTY RELATIONSHIP

4.1 Introduction

In our previously developed Gemussel composite, we introduced polydopamine(PDA) – a mussel adhesive proteins inspired material which has impressive adhesive property – to improve the internal adhesion between different components within composite. It was demonstrated that the incorporation of dopamine/PDA could effectively improve the mechanical strength of our composite. Even though dopamine/PDA has shown its application in our composite and many other areas, dopamine/PDA has its own limitations. For instance, PDA's dark/black color is not favored for clinical applications and its polymerization mechanism is still elusive. In this chapter, dopamine and other catecholamines are studied more extensively to try to get a better understanding about dopamine polymerization mechanism and expand the scope of current mussel-inspire adhesive and coating materials for future applications.

Recently, the unique moisture-resistant adhesion of marine mussels has attracted scientists' attention.[101] Studies revealed that the mussel-adhesion is mediated by five unique adhesive proteins, all of which contain a significant amount of catechol-containing amino acid, L-3,4-dihydroxyphenylalanine (L-DOPA), and amine-containing amino acids, such as lysine, histidine and arginine.[93] Unsurprisingly, fundamental understanding of the functions of these

This chapter previously appeared as an article in *Langmuir*. Reprinted with permission from H. Hu, J. C. Dye, B. A. Bowman, C. C. Ko and W. You, *Langmuir*, 2016, 32(38), pp 9873-9882.

mussel adhesive proteins[93,111] has facilitated the design of synthetic small molecules/polymers to mimic the unique adhesive property of mussels.[97,112,113] Reciprocally, investigating these mussel protein-inspired small molecules/polymers, in particular, the structure-property relationship, has helped to identify the key functional components and the working mechanism for these unique adhesion/coating behaviors. Pioneering work by the Deming group[114] demonstrated that the catechol functionality of L-DOPA is the primary component required to replicate the moisture-resistant adhesion. Further studies have shown that catechol and its oxidized *o*-quinone form are largely responsible for the adhesive behavior through hydrogen bonding[94,95] and cross-linking via metal chelating[95,96] as well as aryl-aryl coupling,[97,98] respectively.[115] These discoveries have promoted the incorporation of catechol and its derivatives into various polymer backbones to achieve functional hydrogels and adhesives, among others. [97,109,112,116-119]

While the importance of having the catechol functional group to reproduce mussel's adhesive properties has been generally agreed upon, the potential involvement of the amine group in achieving mussel's adhesive properties is much less studied. Researchers suggested that the amine may contribute to the mussel's adhesion via ionic bonding to negatively charged surfaces[99,120] and intermolecular cross-linking with *o*-quinones through Michael addition or Schiff-base formation.[95] Thus, having both catechol and amine would create a synergistic effect to reproduce the mussel's adhesive properties.[100] Indeed, in 2007, the Messersmith group first reported that dopamine, a small molecule that covalently links both catechol and amine, could form polydopamine (PDA) under mild conditions, e.g., under a buffer condition of pH = 8.5. More impressively, PDA demonstrated an almost universal adhesion/coating property to a variety of substrates, including metals, ceramics and polymers, among others. Inspired by the formation mechanism of the eumelanin polymer, Messersmith and co-workers proposed a similar

polymerization mechanism to explain the formation of PDA (**Scheme 4.1**). This proposed mechanism first involves the oxidation of dopamine to dopaminequinone, which can then cyclize to form dopaminechrome. Subsequent oxidation and rearrangement would form the pre-monomer, which can then polymerize via oxidative coupling into the PDA.[102] Though a generally agreed formation mechanism of PDA and its exact chemical structure remain elusive,[121-124] the easy synthesis of PDA and its impressive coating/adhesive property have promoted the application of PDA and its derivative materials in various fields, including energy, environment and biomedical engineering.[113]

However, PDA and its related materials have their own limitations. For instance, the dark brown/black color associated with PDA and its related materials[102] are not desirable for certain clinical applications. Further structural functionalization of dopamine molecule without impacting its polymerization behavior also appears to be difficult; the only reported strategy to covalently incorporate dopamine with other polymers/organic materials is through its amine group, which, for example, can form amide with the pendent carboxylic acid from the parent polymer.[118,119,125,126] This status quo motivated us to explore new mussel adhesive inspired molecules that could maintain notable features of dopamine/PDA, including water-solubility, facile polymerization, and the extraordinary coating ability, while mitigating issues in current systems.

Based on all these previous studies, we hypothesized that any molecule that covalently links the catechol and primary amine functional groups would likely show similar polymerization and coating behavior as dopamine/PDA have demonstrated. However, the polymerization mechanism could be molecule dependent, in particular, when factoring in the proposed ring-formation process in the dopamine polymerization. In general, forming a cyclic

product from a linear precursor would be affected by both entropy and enthalpy. For example, in the series of dopamine analogues shown in **Scheme 4.1**, 3C-DA and 4C-DA would likely undergo cyclization during their polymerization, leading to the formation of cyclic structures (e.g., six-membered ring for 3C-DA) in their polymers, similar to the proposed five-membered ring formation in the case of dopamine (i.e., 2C-DA). This is because five- and six-membered rings are the most stable cyclics. Indeed, an earlier computational study of the intramolecular amine addition to ortho-quinones[127] indicated the possibility of forming six- and seven-membered rings. On the other hand, it is hard to imagine that 5C-DA and 12C-DA, having longer alkyl chains, would be able to undergo cyclization and form eight-membered ring (for 5C-DA) and larger ring structure (for 12C-DA). This is because the large ring formation via intramolecular ring-closure is entropically unfavored. Therefore, having all these new dopamine analogues and investigating their polymerization behaviors would help shed more light on the polymerization mechanisms of dopamine and its analogues. Furthermore, comparing the adhesive and coating properties shown by these dopamine analogues would help to disclose how these subtle structural changes (i.e., the length of alkyl chain between the catechol and the amine) would influence the adhesive/coating ability of PDA and its derivative materials.

Thus, the objective of our study is three-fold: synthesis, mechanistic investigation, and structure-property relationships. We find that all of these new dopamine analogues are able to polymerize, albeit likely via different mechanisms, based on experimental observations. While 3C-DA and 4C-DA could go through similar polymerization pathways (e.g., cyclization followed by oxidative coupling) to the one proposed for dopamine (**Scheme 4.1**), 5C-DA and 12C-DA appear to go through a simpler reaction pathway to polymerize (e.g., without cyclization). Importantly, the adhesive properties of polymers from these dopamine analogues (including

dopamine) are tightly correlated with the amount of catechol and amine functionalities in the system, with negligible influence by the length of the alkyl chain that links catechol and amine. Furthermore, even the alkyl linkage between catechol and amine does not seem to be a prerequisite to achieve the adhesive property. In fact, non-covalently linked catechol and amine based molecular systems (e.g., catechol and "free" propyl amine) – when subjected to the same polymerization condition – also form materials that show comparable shear adhesive strength to those achieved with covalently linked catechol and amine via an alkyl chain. On the other hand, this covalent linkage via an alkyl chain seems to be critical in achieving the coating ability of these analogous catechol-amine systems: while the covalently linked catechol and amine systems also show comparable coating ability with their polymers to that of PDA, materials formed with un-linked catechol and amine only show mediocre coating abilities.

Scheme 4.1. Overview of mussel-inspired materials and proposed polymer structure

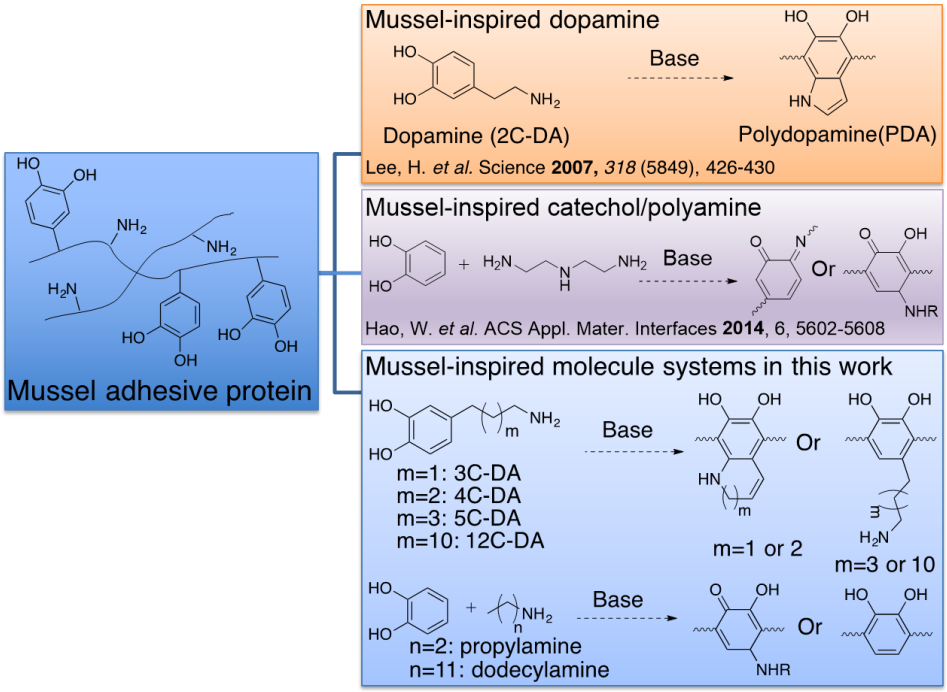

4.2 Synthesis of Dopamine Analogues

Due to the high reactivity of dopamine analogues that have unprotected amine and catechol groups, all these analogues were synthesized in their HCl salt form, similar to the commercially available dopamine (also as its HCl salt). **Scheme 4.2** outlines the synthetic route that successfully offered the 3C-DA in its HCl salt form. A condensation of commercially available 3,4-dimethoxybenzaldehyde with cyanoacetic acid, followed by a $NaBH_4$ reduction, leads to compound (**4.3**). Decarboxylation of (**4.3**) gives 3-(3,4-dimethoxyphenyl)propylnitrile (**4.4**), which undergoes another reduction by $LiAlH_4$ to afford the key intermediate, 3-(3,4-dimethoxyphenyl) propylamine (**4.5**).[128] Multiple attempts to remove the methyl from the methoxy group (e.g., via BBr_3 treatment) to directly convert (**4.5**) into the targeted 3C-DA failed, possibly due to the interference of the primary amine functionality of (**4.5**). Thus we decided to protect the primary amine with a trifluoroacetyl (Tfa) group, converting (**4.5**) into (**4.6**), following a similar protocol previously reported.[129] Treating (**4.6**) with the strong Lewis acid BBr_3 can then smoothly remove these two methyl groups, revealing the catechol of (**4.7**). In the last step, the Tfa protecting group is readily cleaved under strong acidic condition to generate the target molecule (3C-DA), however, in its HCl salt form (**4.8**). The chemical structure of the product formed after each step was confirmed by ^1H NMR and ^{13}C NMR spectra, respectively, and the chemical formula of target molecule (**4.8**) was further verified by ESI-MS.

Scheme 4.2. Synthesis route of 3C-DA Analogue

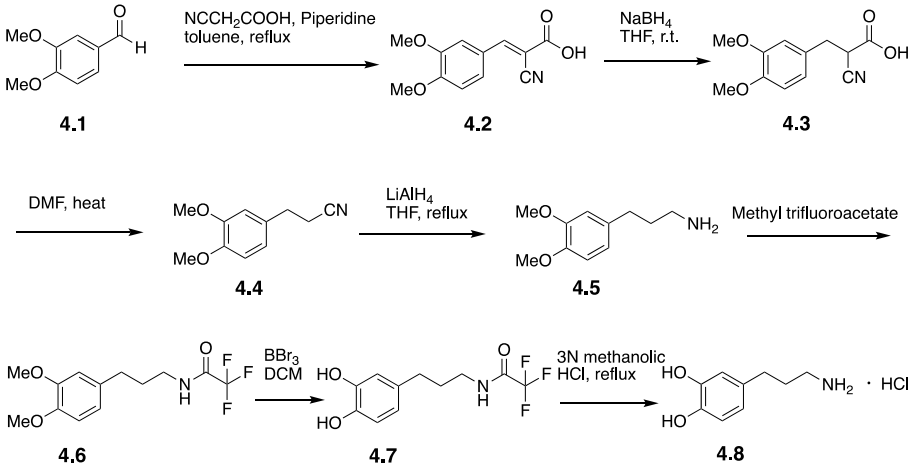

The general synthesis of dopamine analogues (4C-DA, 5C-DA and 12C-DA) is largely similar to that of 3C-DA; the major difference lies in the preparation of 3-(3,4-dimethoxyphenyl)alkylnitrile, molecule (**4.4'**) in **Scheme 4.3**. Specifically, a Friedel-Crafts acylation of the commercially available 3,4-dimethoxy benzene (**4.1'**), followed by a $NaBH_4$ reduction, readily affords (**4.3'**). A nuccleophilic substitution of the bromide in (**4.3'**) with the cyano offers (**4.4'**), which is the structural analogue to (**4.4**) in **Scheme 4.2**. The molecule (**4.4'**) can then to through similar reactions outlined in the **Scheme 4.2** (i.e., from (**4.4**) to (**4.8**) to afford the targeted molecule (**4.8'**), also in its HCl salt form.

Scheme 4.3. Synthesis route of 4C-DA, 5C-DA and 12C-DA Analogues

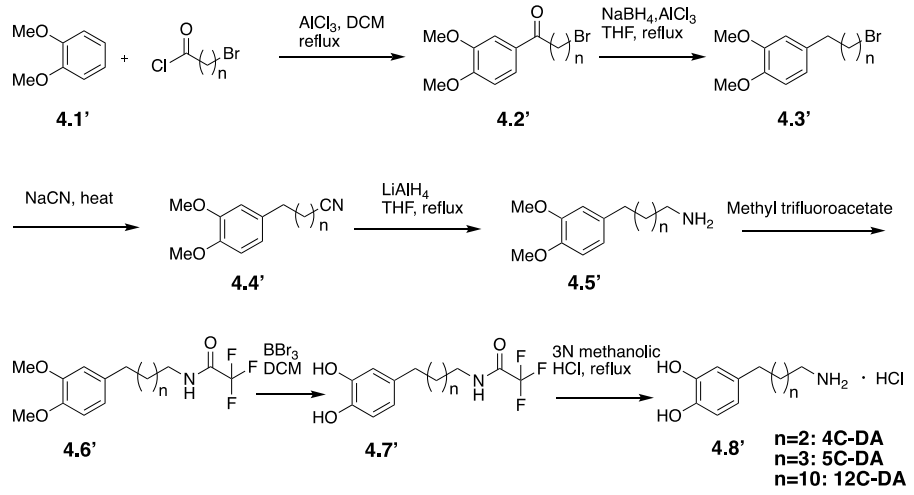

4.3 Polymerization Behavior Studied by UV-Vis Spectra

After having obtained substantial quantity of these dopamine analogues (in their HCl form), we next explored their polymerization behavior with dopamine·HCl as the control/reference. Given the difficulty in separating reaction intermediates from the polymerization, we chose to monitor the polymerization process by UV-Vis spectroscopy, which has been previously used to track the polymerization progress of dopamine.[130,131] Though Tris buffer has been a popular medium for the polymerization of dopamine, we have noticed that Tris buffer could be incorporated into the PDA structure,[122] which could interfere with our study on the polymerizations. Thus, we simplified the polymerization condition and carried out the polymerization of different dopamine analogues in aqueous solution with excess NaOH base.[132] Through comparing the time-dependent UV-Vis absorption spectra during the polymerization to the absorption feature of known reaction intermediates,[116,130,131] we can identify plausible reaction pathways.

Experimentally, after adding excess amount of base (dopamine analogue: 1M NaOH=1:8, molar ratio) to a dilute aqueous solution (1mM) of dopamine/3C-DA/4C-DA/5C-DA (NOTE: 12C-DA is not soluble in water), UV-Vis absorbance spectra were recorded at different time intervals for 24 h. **Figure 4.1(a)** shows the time-dependent UV-Vis spectra of the polymerization of dopamine, which agrees well with a previous literature report.[131] The most notable feature of the UV-Vis spectra is the appearance of an absorbance peak at 420 nm immediately after the base addition, which gradually develops its intensity in the first 25 min and then attenuates. As the polymerization progresses, this absorption peak broadens and gradually decreases; and the whole spectrum becomes almost featureless but widely absorptive after 4 h, which explains the black/brown color of polydopamine (PDA). Similar time-dependent UV-Vis spectra for the

polymerization of 3C-DA was observed (**Figure 4.1(b)**); however, the absorption peak position shifts to 470 nm, and the maximum peak intensity ever reached is much lower than that of the 420 nm absorption peak observed in the dopamine polymerization. Nevertheless, the absorption spectrum loses this absorption peak (~ 470 nm) as the polymerization proceeds. More interestingly, the spectrum after 4 h does not bear much intensity after 450 nm, hence the solution containing poly(3C-DA) appears almost colorless (at low concentration) or much lighter color (at high concentration) than the solution of poly(2C-DA) (i.e., PDA). Interestingly, with one more methylene in its structure than 3C-DA, 4C-DA does not show any obvious absorption peaks during its polymerization, even at the very beginning (i.e., 2 min). This could be caused by a fast polymerization rate, which would render the observation of the reaction intermediate more difficult, given the "transient" nature of such reaction intermediate. Similar to 3C-DA, 4C-DA almost loses the absorption intensity entirely in the range of 400 nm to 600 nm during its polymerization (**Figure 4.1(c)**), whereas 5C-DA regains the absorption in the same region in the UV-Vis spectrum (**Figure 4.1(d)**). Finally, the polymerization of catechol and propylamine (i.e., the non-covalently linked molecular system of 3C-DA) also has noticeable absorption within the range of 400 nm to 600 nm (**Figure 4.1(e)**), though no clearly defined peak can be identified in the same range. Nevertheless, in all cases, the UV-Vis absorption spectrum becomes almost featureless after 24 h, with much less intensity in the visible region than that of the spectrum from the polymerization of dopamine.

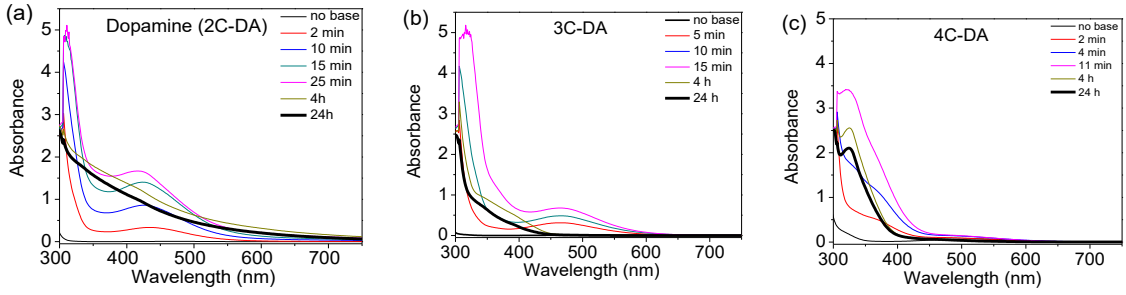

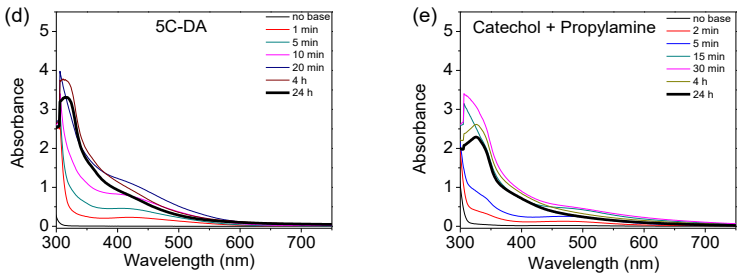

Figure 4.1. Time dependent UV-Vis spectroscopy for the polymerization of dopamine analogues in aqueous solution after adding 1M NaOH.

Given that alcohol-water mixed solvent has been used to affect the polymerization rate of dopamine[133,134] and 12C-DA is insoluble in water but soluble in methanol (MeOH), we next chose methanol as the solvent to conduct the polymerization and aimed to spectroscopically capture the reaction intermediates. After adding the same excess amount of base (dopamine analogues: 1 M NaOH= 1:8, molar ratio) to a dilute MeOH solution (1 mM) of dopamine/3C-DA/4C-DA/5C-DA/12-DA, we again monitored their polymerization by UV-vis (**Figure 4.2**). A few interesting observations can be noted. First, the noticeable absorption peak at 420 nm in the early stage of the dopamine polymerization in water (**Figure 4.1(a)**) loses its intensity for the same polymerization in the mixed solvent (**Figure 4.2(a)**), though a hump at 470 nm can still be identified in this broad absorption. Second, the UV-Vis spectrum for the 3C-DA polymerization in the mixed solvent (**Figure 4.2(b)**) is qualitatively similar to that in water (**Figure 4.1(b)**). However, the 470 nm peak has shown a higher intensity in the early stage of the polymerization and the time it takes for reaching the highest absorbance intensity is twice that as in water. Interestingly, the 4C-DA polymerization in the mixed solvent develops a new absorption peak around 480 nm, which eventually disappears after 24 h (**Figure 4.2(c)**). If we assume that the 470 (480) nm absorption peak indicates the formation of the polymerization intermediate, a

shorter time to reach the maximum intensity and a faster disappearance of this absorption peak would imply more rapid formation of the polymer (**Figure A4.1** and **Figure A4.2** in **Appendix**). Under this assumption, it appears that the polymerization of either 3C-DA or 4C-DA in the mixed solvent (MeOH:water=125:1, v/v) is slower than the corresponding polymerization in water. Third, the dopamine analogues with longer aliphatic linkers (5C-DA and 2C-DA) show qualitatively similar time-dependence UV-Vis spectra (**Figure 4.2(d)** and **4.2(e)**), with a noticeable absorption peak at 410 nm in the early stage of the polymerization. Nevertheless, in all these polymerizations of dopamine and its analogues in the mixed solvent, the UV-Vis spectra do not contain identifiable absorption peak beyond 350 nm after 24 h, similar to what were observed for the polymerizations in water. In contrast, the UV-vis spectra for the non-covalently linked catechol/propylamine has developed an absorption peak at 326 nm, whose intensity continues to rise even after 24 h (**Figure 4.2(f)**). Increasing the alkyl chain length for the non-covalently linked system has negligible impact on the polymerization, evidenced by the fact that almost identical UV-Vis spectra were observed for catechol/dodecylamine (**Figure A4.2g** in **Appendix**).

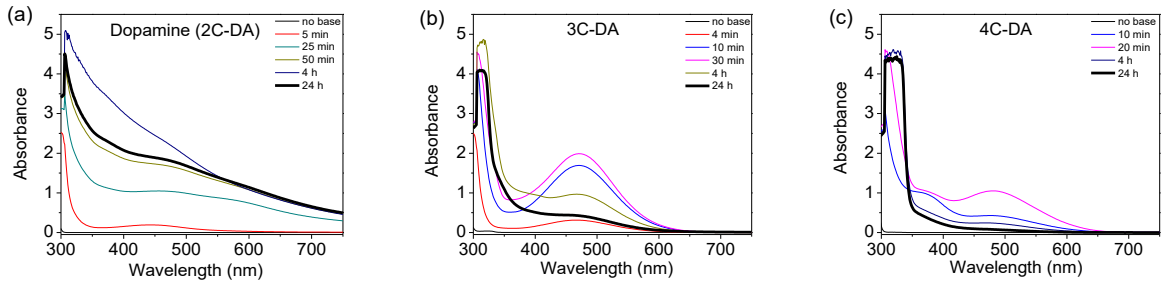

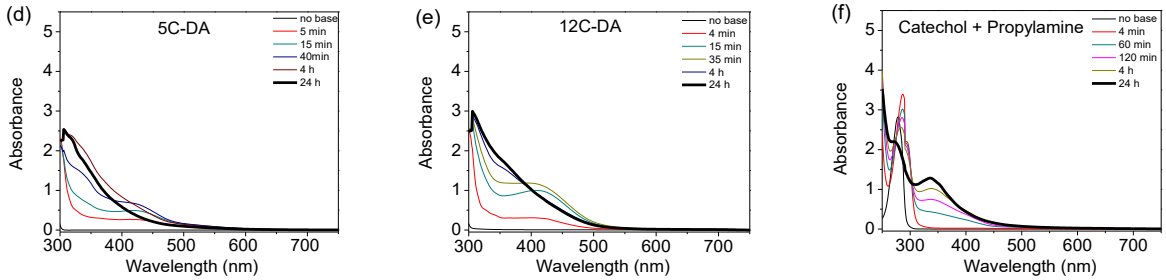

Figure 4.2. Time dependent UV-Vis spectroscopy for dopamine analogues in MeOH (1mM) after adding 1M NaOH (MeOH:water=125:1, v/v).

Combining our time-dependent UV-Vis data in both H_2O and MeOH with literature reports on the polymerization mechanism of dopamine,[121-124] we propose plausible mechanisms for the observed polymerizations as follows. First, the absorbance peak of ~470 nm (480 nm) (**Figure 4.1(b), 4.2(b), 4.2(c)**), appearing in the early stage of the polymerization of 3C-DA and 4C-DA the early stage of the polymerization of 3C-DA and 4C-DA agrees well with the absorbance of dopachrome, which has been previously identified during the biosynthesis of eumelanin from L-DOPA and has a λmax of 473 nm.[116] Therefore, we tentatively assign this peak to the formation of 3C-dopachrome and 4C-dopachrome (**Scheme 4.4**) via a similar formation process for dopachrome, i.e., intramolecular cyclization and then oxidation. On the other hand, for entropic reasons, it would be difficult for similar cyclization occurring during the polymerization of 5C-DA or 12C-DA, both having longer aliphatic chains between the catechol and the amine. Thus, we tentatively ascribe the 410 nm absorbance peak, which appeared during the 5C-DA and 12C-DA polymerization (**Figure 4.2(d)** and **4.2(e)**) to the presence of 5C-dopaquinone and 12C-dopaquinone (**Scheme 4.4**). In fact, this 410 nm peak agrees well with the ~ 400 nm absorption peak for dopaquinone.[98] In all cases (3C- to 12C-DA), the intensity of the absorption peak would decrease after a short period of time, because cross-coupling between the

structural units of catechol and/or quinone would increasingly dominate the reaction progress to form the polymer (**Scheme A4.3** in **Appendix**).

However, for dopamine polymerization, the UV-Vis spectrum is more complicated. First, in H_2O/NaOH, we did not observe any absorbance peak at ~ 470 nm (**Figure 4.1(a)**), which was believed to indicate the formation of dopaminechrome, a known reaction intermediate for dopamine polymerization. This could be caused by the high pH (8 mM NaOH) and thereby rapid spectral evolution, which could mask the initial ~ 470 nm peak.[135] Furthermore, we speculate the observed unique absorbance peak at ~ 420 nm (**Figure 4.1(a)**), which has also been observed by others,[131] might indicate the formation of some oligomers (e.g., coupling of phenols) in the early stage of the dopamine polymerization. Interestingly, when we decreased the polymerization rate for dopamine polymerization with MeOH-H_2O (v/v=125:1), we observed a broad absorption over the entire spectral range (**Figure 4.2(a)**) with a hump near 470 nm, which implies the formation of dopaminechrome. Nevertheless, the broad absorption which rendered the dark color of PDA, is believed to be a result of its complicated, presumably cross-linked structure analogous to that of eumelanin.[102] It is very likely that PDA is a mixture of oligomers/polymers with various monomeric components (e.g., dopamine, dihydroxyindole, indoledione, etc.), tied together via cross-linking and non-covalent interactions.[123,124] In contrast, the much lighter color of these new dopamine analogues after polymerization, supported by the much attenuated absorption in the visible region after 24 h (**Figure 4.2(b) to 4.2(e)**), suggests simpler structures that have less conjugation than PDA. Given the structural similarity between dopamine and these dopamine analogues, further investigation of the polymerization mechanism of these dopamine analogues – ideally, together with other dopamine analogues – can offer more insights on a clearer picture of the formation of PDA.

On the other hand, when the amine is not covalently linked with the catechol, the UV-Vis spectra of polymerizations with these molecular systems (i.e., catechol/propylamine and catechol/dodecylamine) are distinctly different from those observed with covalently linked ones (**Figure A4.2(f)** and **Figure A4.2(g)** in **Appendix** vs. **Figure 4.2(a)** to **4.2(e)**). In particular, the absorption peak at 326 nm gains more intensity as polymerization continues and becomes much more visible after 24 h. We tentatively assign this absorbance peak at 326 nm to the Michael addition product between the quinone and amine or phenol coupling (**Scheme 4.4**). The polymerization of such non-covalently linked systems could undergo the coupling among semiquinone and/or quinones as well as products from Michael addition to form the polymers.[136]

Lastly, please note that the proposed mechanisms are largely postulated based on the time-dependent UV-Vis absorption data for the studied molecular systems in the mixed solvent (MeOH:water = 125:1, v/v). The noticeable difference of UV-Vis spectra for the same molecular system in different solvents imply that the polymerization mechanism could also depend on the given solvent system, in particular, the water dominant system vs. the methanol dominant system.

Scheme 4.4. Proposed reaction intermediates during polymerization

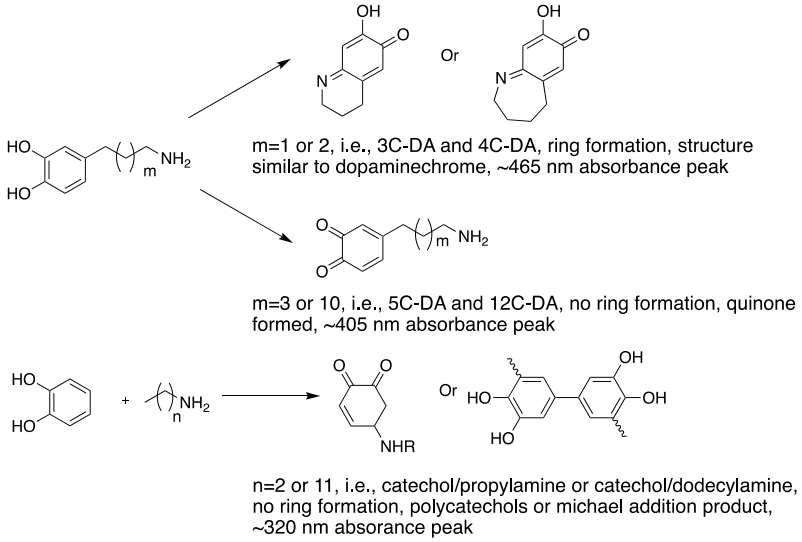

4.4 Adhesive Property Studied by Lap-shear Testing

Many mussel-inspired materials have significant adhesive properties;[102,109,112] since dopamine and the analogues in this study are also inspired by mussel, we next investigated the bulk adhesive properties of all molecular systems in our study. Specifically, we measured the lap shear adhesion of two glass substrates sandwiching the polymer, following a protocol established by the Wilker group.[109] We first dissolved some monomers (including 2C-DA, 3C-DA, 4C-DA, 5C-DA and catechol/propylamine) in water, or all monomers (2C-DA, 3C-DA, 4C-DA, 5C-DA, 12C-DA, catechol/propylamine and catechol/dodecylamine) in isopropanol/water (1:2, v/v). Please note that isopropanol (IPA) was used here instead of methanol in order to further mitigate the solubility issue of 12C-DA. In fact, these two solvent systems appear to offer similar polymers via similar polymerization mechanisms for each studied molecular system, since UV-Vis spectra for the polymerization in the mixed solvent where H_2O was dominant (IPA-H_2O, v/v=1:2) (**Figure A4.3** in **Appendix**) are very comparable to those obtained in H_2O (**Figure A4.1** in **Appendix**), for each studied molecular system.

We then added excess base (100 μL 1M NaOH aqueous solution) to induce the polymerization. After 5 minutes, we applied 30 μL of the polymer solution onto one side of the glass slide, which was then covered with another identical glass slide with an overlapping area of 1 inch × 1 inch. A binder clip was employed to maintain this sandwich structure for the next 48 hours to ensure the completion of the polymerization (**Figure 4.3(a)**, left). This binder clip was removed before the sandwich structure was tested via an Instron (**Figure 4.3(a)**, right). After measuring three maximum load at break point for each polymer, adhesive strength was calculated by maximum load/sandwich area, i.e., 1 inch × 1 inch in our case. A load vs extension curve was obtained for each sample, which was qualitatively similar to literature

results[109](**Figure A4.8** in **Appendix**), indicating the complete removal of the solvent. In addition, we measured the UV-Vis spectra of the polymers sandwiched in between the glass substrates. The UV-Vis spectrum of the polymer does not contain characteristic absorption features of the reaction intermediate (for each studied system), and the overall spectrum is very similar to the final UV-Vis spectrum (i.e., measured after 24 h) of the same molecular system obtained in H_2O. These results confirmed that it was the polymers that were tested in the lap shear testing (**Figure A4.9** in **Appendix**).

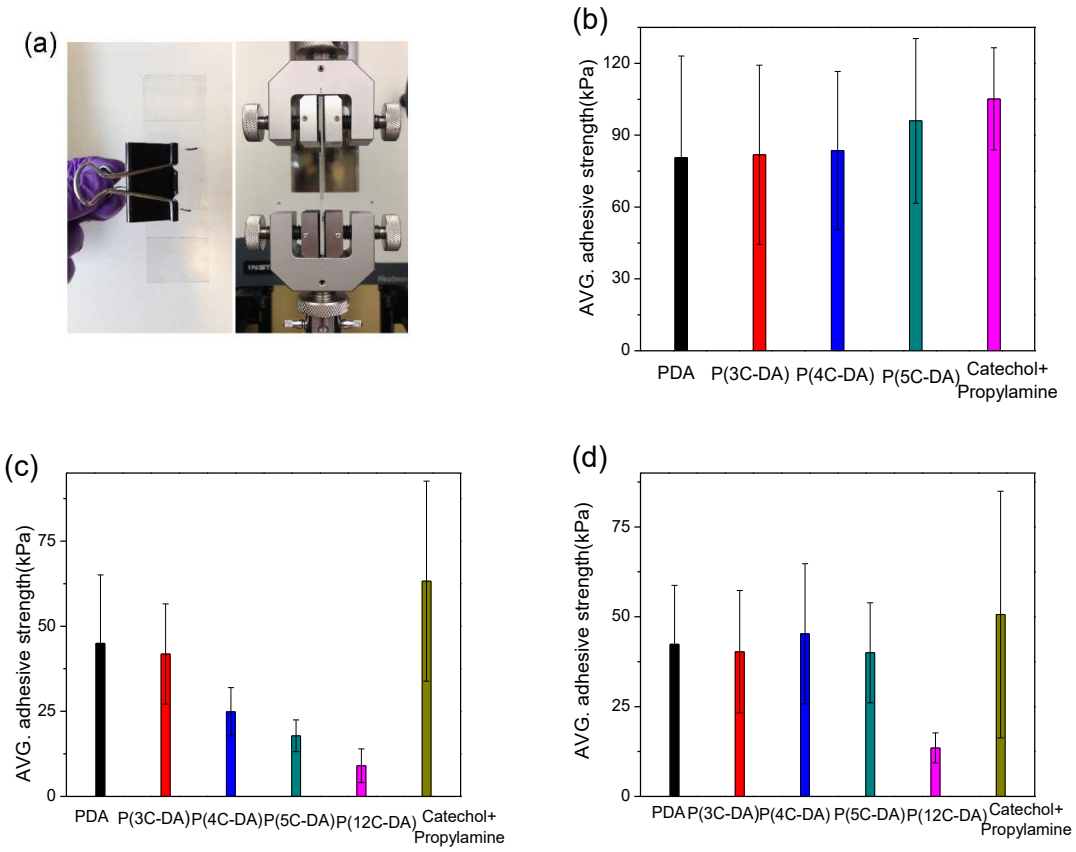

Figure 4.3. (a) Image of test sample (left) and main part of Instron machine (right) for lap-shear testing; (b) results for adhesive strength for PDA, poly(3C-DA), poly(4C-DA), poly(5C-DA) and catechol/propylamine in water at 6.7 mg/mL;(c) results for adhesive strength for PDA, poly(3C-DA), poly(4C-DA), poly(5C-DA), catechol/propylamine and catechol/dodecylamine in IPA:

H_2O at 6.7 mg/mL (IPA:H_2O=1:2, v/v); (d) results for adhesive strength for PDA, poly(3C-DA), poly(4C-DA), poly(5C-DA), catechol/propylamine and catechol/dodecylamine in IPA: H_2O at 33.3 mM (IPA:H_2O=1:2, v/v).

As shown in **Figure 4.3(b)**, polydopamine (i.e., PDA), poly(3C-DA), poly(4C-DA) and poly(5C-DA) have demonstrated comparable adhesive strength (~ 90 kPa) from the identical polymerization in water (i.e., same mass concentration of 6.7 mg/mL), indicating that the increment of the aliphatic chain length between the amine and the catechol only negligibly influence the adhesive property of the polymer. Interestingly, the polymer from reacting catechol/propylamine under the same condition (i.e., catechol and propylamine together at 6.7 mg/mL with 1:1 molar ratio) demonstrated almost identical adhesion strength as that of covalently-linked dopamine analogues, implying that the covalent bonding (i.e. the alkyl linkage) between the amine and the catechol is not necessary to achieve the adhesive strength of the polymer.

Again, since 12C-DA is not soluble in water, we switched to the mixed solvent, IPA:water (1:2, v/v). For comparison with the results obtained with polymers synthesized in water, we used the same mass concentration (6.7 mg/mL) in the mixed solvent as well. Surprisingly, for each of dopamine and its analogues with longer aliphatic chains, the adhesive strength of the polymer created in the mixed solvent is significantly smaller than that of the counterpart synthesized in water. We offer two plausible explanations. First, the mixed solvent (IPA:H_2O, v/v=1:2), which has a different solvent evaporation rate than that of pure H_2O, might lead to incomplete film formation under our experimental condition. Alternatively, pure H_2O may generate more polymers than the mixed solvent of IPA:H_2O (though the structure of the polymers could be identical, regardless of the solvent system, as we previously discussed).

Furthermore, the adhesive strength of the polymer decreases monotonically from dopamine to 12C-DA (**Figure 4.3(c)**). However, when the same polymerizations were done with an identical molar concentration (i.e., 33 mM) in the mixed solvent, the adhesive strength from the different polymers becomes comparable (**Figure 4.3(d)**), except the polymer from 12C-DA. We tentatively ascribe the weaker adhesive strength demonstrated by the polymer from 12C-DA in the mixed solvent to its limited solubility (even in the mixed solvent), which would significantly impede its polymerization. Nevertheless, these results indicate that the amount of catechol and amine in the system is proportional to the adhesive strength of polymers from these dopamine analogues in the mixed solvent. This conclusion is further supported by the fact that the polymers created from the non-covalently linked analogues (i.e., catechol/propylamine and catechol/dodecylamine) also show comparable adhesive strength to that of their covalently linked counterparts, when the same molar concentration (33 mM) was used for the polymerization in the mixed solvent (**Figure 4.3(d)**). This observation also supports the previous conclusion that the covalent bonding between the amine and the catechol is not a prerequisite for achieving the adhesive strength of the polymer.

4.5 Coating Property Studied by XPS

The most impressive property of polydopamine (PDA) is its ability to coat almost any substrates, effectively serving as an ad-layer to change the surface property of the coated substrate and allow further functionalization. Thus, our last task was to investigate the coating ability of these newly prepared polymers. To compare the coating ability of our newly synthesized dopamine analogues to that of PDA, we followed a protocol reported earlier by the Messersmith group, i.e.,10 mM Tris buffer, pH=8.5.[102] To investigate whether the Tris buffer solution would have any impact to the polymerization when compared with the NaOH solution,

we conducted a similar time-dependence UV-Vis study of these dopamine analogs in the Tris buffer solution. Comparing the additional data (**Figure A4.4** in **Appendix**) with the UV-Vis data acquired in H_2O/NaOH (**Figure A4.1** in **Appendix**), we did not discern any significant difference. Thus, we believe the polymerization mechanisms (and related polymers) in the Tris buffer condition would be comparable to those under the H_2O/NaOH condition.

We chose PTFE, which is known for its anti-fouling ability, as our target to study the coating ability of these polymers. Experimentally, PTFE substrate was immersed into dilute aqueous solutions of 3C-DA, 4C-DA, 5C-DA and catechol/propylamine, respectively (i.e., 2 mg/mL in 10 mM Tris buffer, pH=8.5, following a protocol reported earlier by the Messersmith group),[102] which were then gently stirred overnight. A control experiment with dopamine·HCl was also carried out in parallel. The first observation is the noticeable coloration of the substrate after it was coated with the polymer (**Figure 4.4(a)**). While the PTFE substrate coated with PDA has a black brown/grey color in appearance, the ones coated with poly(3C-DA), poly(4C-DA) and poly (5C-DA) show lighter color instead. More importantly, X-ray photoelectron spectroscopy (XPS) characterization of the substrates coated with these dopamine analogues reveals a complete absence of the signals specific to the substrate (e.g., fluorine) after the coating, demonstrating a similar "shielding" effect as PDA has shown[102] (**Figure 4.4(a)** and **Figure A4.11** in **Appendix**). Further chemical analyses (via XPS) of the surface of these PTFE substrates after coating with these new polymers disclose that the nitrogen/carbon ratio is very close to the theoretical value of each dopamine analogue (**Figure 4.4(b)**, rightmost column). This further supports a complete surface coating of the PTFE substrate by polymers from these dopamine analogues, similar to the coating ability of PDA.[102] However, the non-covalently linked system, i.e., catechol and amine, is not able to achieve the complete coating of the PTFE

substrate, as the fluorine signal (from the PTFE substrate) is still present after the coating (**Figure 4.4(a)**). These results suggest that the covalent bonding between the amine and the catechol might play an important role to maximize the coating ability of these dopamine analogues.

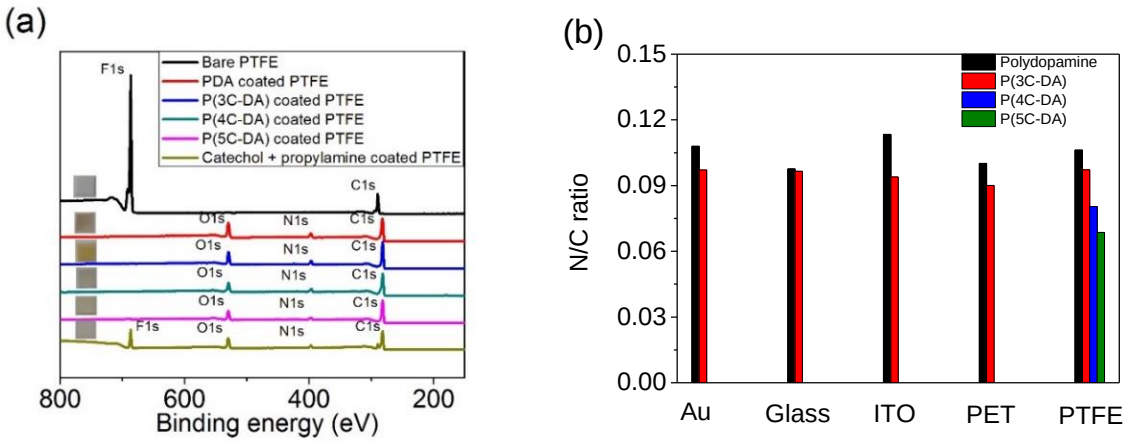

Figure 4.4. (a) XPS spectra of bare PTFE substrates, PDA coated PTFE and poly(3C-DA) coated PTFE, poly(4C-DA) coated PTFE, and poly(5C-DA) coated PTFE; (b) the quantitative analysis of nitrogen/carbon (N/C) ratio of different substrates coated with PDA and poly(3C-DA) as indicated by the black bar and red bar, respectively. Blue bar and green bar represent the N/C ratio of PTFE substrate coated with poly(4C-DA) and poly(5C-DA), respectively.

To further investigate whether the excellent coating ability on PTFE demonstrated by these new dopamine analogues – similar to that of PDA – is also universal as PDA has shown,[102] we chose 3C-DA as the example to test the coating of its polymer on other substrates. For comparison, dopamine was also included in this set of experiments. Four different substrates having representative surface properties, gold, indium tin oxide (ITO), glass, and poly(ethyleneterephalate) (PET), were coated with poly(3C-DA) or PDA, following the same protocol as illustrated above. Not surprisingly, there is a visible change in the color appearance of the substrate after it was coated with the polymer (i.e., PDA or poly(3C-DA)) (**Figure**

A4.10(a) in **Appendix**). XPS characterization of the surface of these substrates after coating reveals a complete disappearance of substrate signals, demonstrating comparable coating ability of poly(3C-DA) to that of PDA (**Figure A4.10(b)** in **Appendix**). In addition, the nitrogen/carbon ratio, ranging from 0.902 to 0.972 on these coated substrates, is very close to the theoretical value of 3C-DA (0.1111) (**Figure 4.4(b)**, red bar), suggesting a complete surface coverage on all these substrates by poly(3C-DA), similar to that achieved by PDA (**Figure 4.4(b)**, black bar). These results strongly suggest that the 3C-DA, after polymerization, offers a similar coating ability and general applicability to those of dopamine/PDA.

4.6 Conclusion

In summary, through a series of molecular systems that are structurally analogous to dopamine, we demonstrate that the intriguing polymerization behaviors of dopamine are not unique to dopamine; in fact, it appears that all molecular systems that contain catechol and amine – covalently linked via an alkyl chain or not – are able to polymerize. However, the exact polymerization mechanism for individual molecular system appears to be dependent on (a) whether or not the catechol and amine are covalently linked via alkyl chain, and (b) the length of the alkyl chain that links the catechol and amine. Furthermore, the solvent system chosen to carry out the polymerization also seems to have an impact on the polymerization mechanism. It appears conditions where water is dominant (i.e., IPA:H_2O, H_2O and Tris buffer) should offer similar polymers via similar mechanism, whereas the polymerization mechanism in methanol is different. Further mechanistic studies on these molecular systems and other related systems are needed to elucidate the polymerization mechanisms.

Furthermore, our results indicate that the covalent attachment of catechol and amine (e.g., as in the case of dopamine) appears to have only a negligible influence on the adhesive property

shown by polydopamine; almost all studied molecular systems show comparable adhesive strength when normalized with the amount of catechol and amine. However, such covalent linking between catechol and amine via an alkyl chain is crucial in reproducing the impressive coating ability that polydopamine has shown; noncovalently linked catechol and amine only show mediocre coating behaviors. All of these findings offer valuable guidelines in selecting and designing mussel adhesive protein-inspired materials for specific applications, including BTE application in the near future.

4.7 Experimental Section

The synthesis of 2-cyano-3-(3,4-dimethoxyphenyl)acrylic acid (**4.1**),[128] 2-cyano-3-(3,4-dimethoxyphenyl)propionic acid (**4.2**),[128] 3-(3,4-dimethoxyphenyl) propanenitrile (**4.4**)[128] and 3-(3,4-dimethoxyphenyl) propylamine (**4.5**)[137] were adapted from previous literature reports.

2-cyano-3-(3,4-dimethoxyphenyl)acrylic acid (4.2) 3,4-dimethoxybenzaldehyde (15.00 g, 89.78 mmol) and cyanoacetic acid (15.28g, 179.96 mmol) were dissolved in anhydrous toluene. Piperidine (17.78 mL, 179.96 mmol) was then added slowly to this reaction mixture and stirred under reflux for 17 hours. The reaction mixture was concentrated by rotary evaporation and the residue was dissolved in EtOAc and washed 3 times with 1 M HCl aqueous solution first and then washed with water 3 times. The organic phase was dried over anhydrous $MgSO_4$ and concentrated by rotary evaporation to yield crude product **4.2** as a yellow solid. Purification through recrystallization in MeOH twice yielded pure product **4.2** as yellow needle-like crystals (16.75 g, yield: 80%). ^{1}H NMR (400 MHz, $CDCl_3$): δ 3.97 (s, 3H), 3.98 (s, 3H), 6.96 (d, J=8.5 Hz, 1H), 7.50 (dd, J=8.5, 2.0 Hz, 1H), 7.85 (d, 1H, J=2.0 Hz), 8.22 (s, 1H).

2-cyano-3-(3,4-dimethoxyphenyl)propionic acid (4.3) Compound **4.2** (5g, 21.43 mmol) was dissolved in THF and stirred at room temperature. $NaBH_4$ (2.03g, 53.58 mmol) was then

added to this solution by portion and allowed to react for 15 hours. The reaction was quenched in an ice bath with dropwise addition of water and concentrated by rotary evaporation. The residue was then dissolved in EtOAc and washed with water three times before the organic layer was concentrated by rotary evaporation to afford product **4.3** as a white solid (4.54g, yield: 90%). ^{1}H NMR (400MHz, d6-DMSO): δ 3.00 (dd, J=14 Hz, 8.8 Hz, 1H), 3.11 (dd, J=14, 5.2 Hz, 1H), 3.73 (s, 6H), 4.26 (q, J=5.6 Hz, 1H), 6.80 (dd, J=8.4, 2 Hz, 1H), 6.88 (d, J=8.4 Hz, 1H), 6.91 (d, J=2.0 Hz, 1H).

3-(3,4-dimethoxyphenyl) propanenitrile (4.4) Compound **4.3** (4.54g, 19.28 mmol) was dissolved in DMF (30 mL) and refluxed for 12 hours. The solvent DMF was then removed by blowing with a gentle stream of air for a few hours. The reaction mixture was then dissolved in EtOAc and washed with water 3 times. The organic phase was concentrated by rotary evaporation. The residue that contained the crude product was further purified by column chromatography using 2:1 hexane and ethyl acetate as the eluent to afford product **4.4** as a white solid (2.14 g, yield: 58%). ^{1}H NMR (400MHz, $CDCl_3$): δ 2.59 (t, J=7.2 Hz, 2H), 2.89 (t, J=7.2 Hz, 2H), 3.86 (s, 3H), 3.87 (s, 3H), 6.74 (dd, J=8, 2 Hz, 1H), 6.77 (d, J=2 Hz, 1H), 6.82 (d, J=8 Hz, 1H). ^{13}C NMR (400MHz, $CDCl_3$) δ 19.9, 31.5, 56.16, 56.19, 111.8, 111.8, 119.6, 120.6, 130.9, 148.5, 149.3.

Trifluoroacetyl (tfa) protected (4.5) (i.e., molecule 4.6) $LiAlH_4$ (0.34g, 8.84 mmol) was dissolved in anhydrous THF and refluxed for 15 minutes. To this reflux solution, product **4.4** (4.42 mmol, 0.85g) dissolved in anhydrous THF was added dropwise. After 2 hours, the reaction was cooled in an ice bath and quenched with saturated NaOH solution dropwise. After filtration to remove insoluble salts, the reaction mixture was concentrated by rotary evaporation to remove the THF, and the residue was dissolved in ethyl acetate and washed with water 3 times before the

organic phase was concentrated by rotary evaporation again to yield crude product **4.5** (3-(3,4-dimethoxyphenyl) propylamine) as a white solid. Crude product **4.5** (0.55g, 2.82 mmol) was then dissolved in methanol and stirred at room temperature, followed by addition of methyl trifluoroacetate (0.31 mL, 3.10 mmol) and triethylamine (0.47 mL, 3.38mmol). After stirring overnight, the mixture was concentrated by rotary evaporation and then dissolved in EtOAc and washed 3 times with 1 N HCl followed by water, respectively. The organic phase was dried over $MgSO_4$, and concentrated by rotary evaporation. The residue was subject to column chromatography using 2:1 hexane and EtOAc as the eluent to afford product **4.6** as a colorless liquid (0.40 g, yield: 31%). ^{1}H NMR (400 MHz, $CDCl_3$): δ 1.92 (m, J=7.2 Hz, 2H), 2.65 (t, J=7.2 Hz, 2H), 3.40 (m, J=6.8 Hz, 2H), 3.86 (s, 3H), 3.88 (s, 3H), 6.26 (s, 1H), 6.71 (d, 1H), 6.73 (s, 1H), 6.80 (d, J=8 Hz, 1H). ^{13}C NMR (400MHz, $CDCl_3$): δ 30.7, 32.9, 39.8, 56.0, 56.2, 111.7, 111.9, 117.6, 120.4, 133.6, 147.8, 149.3, 157.6.

Tfa protected 3C-DA (4.7) Compound **4.6** (0.40g, 1.37 mmol) was dissolved in DCM and degassed with argon for 15 minutes in an ice bath. 1 M BBr_3 in DCM solution (5.48 mL) was then added dropwise under argon. The reaction mixture was stirred for 2 hours before it was quenched with water slowly. After concentrating by rotary evaporation, the reaction mixture was dissolved in EtOAc and washed with water 3 times, then the organic phase was dried over $MgSO_4$ and concentrated by rotary evaporation again. The residue was subject to column chromatography using 1:1 hexane and EtOAc as the eluent to afford pure product **4.7** as a light yellow viscous liquid at room temperature (0.78g, yield: 85%). ^{1}H NMR (400 MHz, $CDCl_3$): δ 1.85 (m, J=7.2, 6.8 Hz, 2H), 2.56 (t, J=7.2 Hz, 2H), 3.36 (m, J=6.8 Hz, 2H), 5.46 (s, 1H), 5.71 (s, 1H), 6.34 (s, 1H), 6.59 (dd, J=8.4, 2 Hz, 1H), 6.69 (d, J=2Hz, 1H), 6.78 (d, J=8.4 Hz, 1H). ^{13}C

NMR (100 MHz, d6-DMSO): δ 31.4, 32.9, 115.8, 116.7, 116.9, 118.7, 120.1, 133.3, 144.6, 146.3, 157.4.

3C-DA·HCl (4.8) Compound **4.7** (0.31g, 1.16 mmol) was dissolved in 3N methanolic HCl solution (20 mL) and degassed with argon for 5 minutes before it was heated to reflux. The mixture was allowed to react overnight before it was concentrated by rotary evaporation to give a light yellow liquid. The crude product was then washed with ethyl acetate and ethyl ether three times, respectively, to generate the target 3C-DA·HCl as a white solid (0.22g, yield: 92%). ^{1}H NMR (400 MHz, d_6-DMSO): δ 1.76 (t, J=7.2 Hz, 2H), 2.44 (m, J=6.8 Hz, 2H), 2.71 (t, J=7.2, 6.8 Hz, 2H), 6.42 (d, J=8.0 Hz, 1H), 6.58 (s, 1H), 6.64 (d, J=8.0 Hz, 1H), 8.00 (s, 3H), 8.72 (s, 1H), 8.82 (s, 1H). ^{13}C NMR (400MHz, d6-DMSO): δ 30.2, 32.5, 39.6, 116.8, 117.0, 120.1, 132.8, 144.7, 146.4. HR-MS (LTQ FT-ICR MS) m/z: [M+] Calcd for $C_9H_{14}NO_2$ 168.1024; Found 168.1020.

3-bromo-1-(3,4-dimethoxyphenyl)propan-1-one (**4.2'**, n=2) The synthesis of **4.2'** was adapted from previously reported literature.[138] To a flame-dried 250 mL round bottle, $AlCl_3$(19.35g, 145.13 mmol) in anhydrous DCM was added. After stirring for 5 minutes, 3-bromopropyl chloride (12.4g, 72.33 mmol) was added into the mixture, followed by adding 1,2-dimethoxybenzene (10.00g, 72.37 mmol) slowly. The reaction mixture was heated to reflux for 1.5 h before it was quenched in an ice bath with H_2O. After concentrating by rotary evaporation, the reaction mixture was dissolved in EtOAc and washed with water 3 times, then the organic phase was dried over $MgSO_4$ and concentrated by rotary evaporation again. The residue was then subject to column chromatography using 4:1 hexane and EtOAc as the eluent. Recrystallization in mixed EtOAc and hexane twice affords pure product as a white crystal(7.12g, yield:37%). ^{1}H NMR (400 MHz, $CDCl_3$): δ 3.52 (t, J=7.2, 6.8 Hz, 2H), 3.72 (t, J=7.2, 6.8 Hz, 2H), 3.92 (s, 3H),

3.94(s, 3H), 6.88(d, J=8.4 Hz, 1H), 7.51 (d, J=2 Hz, 1H), 7.55(dd, J=8.4, 2 Hz, 1H). ^{13}C NMR (400MHz, CDCl3): δ 26.5, 41.3, 56.3, 56.4,110.37, 110.39, 123.1, 129.9, 149.5, 154.0, 195.8.

4-(3-bromopropyl)-1,2-dimethoxybenzene (**4.3'**, n=2) Sodium borohydride (1.47g, 39.36 mmol) and alumina chloride (1.57g, 11.80 mmol) were added to a flame-dried two neck flask, then anhydrous THF was added as solvent. After stirring in an ice bath for 5 minutes, compound **4.2'** (n=2) (2.15g, 7.87 mmol) dissolved in anhydrous THF was added dropwise. The reaction mixture was then heated to reflux for 2 h before it was quenched with H_2O slowly in an ice bath. Rotary evaporation was used to remove the THF, and the concentrated residue was dissolved in EtOAc and washed with H_2O 3 times before drying with $MgSO_4$ and concentrating again. Purification via a column using 4:1=hexane: EtOAc affords pure product as a colorless liquid (1.33g, 65.2%). ^{1}H NMR (400 MHz, $CDCl_3$): δ 2.14(m, J=7.2, 6.8 Hz, 2H), 2.73 (t, J=7.2 Hz, 2H), 3.39(t, J=6.8 Hz, 2H), 3.86 (s, 3H), 3.88(s, 3H), 6.72 (s, 1H), 6.75 (d, J=1.6 Hz, 1H), 6.80 (d, J=8 Hz, 1H). ^{13}C NMR (400MHz, $CDCl_3$): δ 33.5, 33.8, 34.6, 56.16, 56.24, 111.7, 112.2, 120.7, 133.4, 147.8, 149.2.

4-(3,4-dimethoxyphenyl)butanenitrile (**4.4'**, n=2) Compound **4.3'** (n=2) (878 mg, 3.36 mmol) and NaCN (247 mg, 5.04 mmol) were dissolved in anhydrous DMF, the reaction mixture was heated to 90 °C and reacted for 4 h. Then H_2O was added, and the reaction mixture was extracted with EtOAc for 3 times, the organic phase was dried with $MgSO_4$, and concentrated through rotary evaporation. Purification via a column using 2:1=hexane: EtOAc gave pure product as a colorless liquid (660 mg, yield: 96%). ^{1}H NMR (400 MHz, $CDCl_3$): δ 1.96 (m, J=7.2, 6.8 Hz, 2H), 2.32 (t, J=7.2 Hz, 2H), 2.73(t, J=6.8 Hz, 2H), 3.86 (s, 3H), 3.88(s, 3H), 6.71(dd, J=8, 2 Hz, 1H), 6.73 (d, J=2 Hz, 1H), 6.80 (d, J=8 Hz, 1H). ^{13}C NMR (400MHz, $CDCl_3$): δ 16.6, 27.4, 34.2, 56.17, 56.24, 111.7, 112.0, 119.9, 120.7, 132.6, 148.0, 149.4.

Trifluoroacetyl (tfa) protected 4 (i.e., compound **4.5',** n=2**)** Follow the same procedure for the synthesis of 3C-DA as described above. Starting with compound **4.4'**(n=2) (660 mg, 3.22 mmol) will afford final product as a colorless liquid (565 mg, yield: 57%). ^{1}H NMR (400 MHz, $CDCl_3$): δ 1.63(m, J=7.2, 6.8, 6.4 Hz, 4H), 2.60 (t, J=7.2,6.8 Hz, 2H), 3.38(q, J=6.8, 6.4 Hz, 2H), 3.85 (s, 3H), 3.87 (s, 3H), 6.23 (s, 1H), 6.69 (s, 1H), 6.71 (d, J=2 Hz, 1H), 6.79 (d, J=7.6 Hz, 1H). ^{13}C NMR (400MHz, $CDCl_3$): δ 28.8, 28.9, 35.2, 40.1, 56.2, 56.3, 111.7, 112.1, 117.5, 120.5, 134.6, 147.9, 149.4, 157.8.

Tfa protected 4C-DA (4.6', n=2**)** Follow the same procedure for the synthesis of 3C-DA as described above. Starting with compound **4.5'** (n=2) (535mg, 1.75 mmol) will afford pure product as a light yellow liquid (415mg, yield: 86%). ^{1}H NMR (400 MHz, d6-DMSO): δ 1.46 (t, J=3.6, 3.2 Hz, 4H), 2.38 (t, J=6.8, 6.4 Hz, 2H), 3.17 (b, 2H), 6.39 (dd, J=8, 2 Hz, 1H), 6.53 (d, J=2 Hz, 1H), 6.59 (d, J=8 Hz, 1H), 8.62 (b, 2H), 9.34 (b, 1H).^{13}C NMR (400MHz, d_6-DMSO): δ 29.1, 29.5, 35.3, 40.2, 116.7, 116.9, 120.1, 134.0, 144.4, 146.2, 157.2.

4C-DA·HCl (4.7', n=2**)** Follow the same procedure for 3C-DA·HCl synthesis. Starting with compound **4.6'** (250 mg, 0.90 mmol) will give product as a white solid (179 mg, yield: 91%). ^{1}H NMR (400 MHz, d6-DMSO): δ 1.51(m, 4H), 2.38 (t, J=6.8, 6.4 Hz, 2H), 2.74 (b, J=6.8, 6.4 Hz, 2H), 6.41 (dd, J=8, 2 Hz, 1H), 6.56 (d, J=2 Hz, 1H), 6.62 (d, J=8 Hz, 1H), 7.88 (b, 1H), 8.66(s, 1H), 8.73 (s, 1H). ^{13}C NMR (400MHz, d6-DMSO): δ 27.8, 29.2, 35.2, 39.9, 116.8, 117.1. 120.1, 133.7. 144.5, 146.3. HR-MS (LTQ FT-ICR MS) m/z: [M+] Calcd for $C_{10}H_{16}NO_2$ 182.1171; Found 182.1176.

4-bromo-1-(3,4-dimethoxyphenyl)butan-1-one (4.1', n=3**)** Similar to the synthesis of compound **4.1'** (n=2): $AlCl_3$(15.44g, 115.8 mmol) in anhydrous DCM was added to a flame-dried flask which was cooled to 0 °C. After stirring for 5 minutes, 4-bromobutyl chloride

(10.74g, 57.9 mmol) was added into the mixture, followed by adding 1,2-dimethoxybenzene (8.00g, 57.9 mmol) slowly. Same to the reaction condition and post-reaction procedure for synthesizing 3-bromo-1-(3,4-dimethoxyphenyl)propan-1-one will afford the pure product as a light yellow crystal (7.8g, yield: 47%). ^{1}H NMR (400 MHz, $CDCl_3$): δ 2.29 (m, J=6.8, 6.4Hz, 2H), 3.13 (t, J=6.8 Hz, 2H), 3.54 (t, J=6.4 Hz, 2H), 3.93 (s, 3H), 3.94(s, 3H), 6.88(d, J=8.4 Hz, 1H), 7.52 (d, J=2 Hz, 1H), 7.61(dd, J=8.4, 2 Hz, 1H). ^{13}C NMR (400MHz, $CDCl_3$): δ 27.6, 34.1, 36.4, 56.3, 56.4, 110.4, 110.4, 123.1, 130.4, 149.4, 153.8, 197.8.

4-(4-bromobutyl)-1,2-dimethoxybenzene (4.2', n=3**)** Similar to the synthesis of compound **4.2'** (n=2), sodium borohydride (1.46g, 38.8 mmol) and alumina chloride (1.55g, 11.64 mmol) were added to a flame-dried two neck flask, then anhydrous THF was added as solvent. After stirring in an ice bath for 5 minutes, compound **4.1'** (n=3) (2.21g, 7.76 mmol) dissolved in anhydrous THF was added drop by drop. The reaction mixture was then heated to reflux for 2 h before it was quenched with H_2O slowly in an ice bath. Following the same procedure for synthesizing compound **4.2**'s (n=2) affords product also as a colorless liquid (1.67g, yield: 77%). ^{1}H NMR (400 MHz, $CDCl_3$): δ 1.75 (m, J=7.6, 6.8 Hz, 2H), 1.88(m, J=7.2, 6.4 Hz, 2H), 2.58 (t, J=6.8, 6.4 Hz, 2H), 3.41 (t, J=7.6, 7.2 Hz, 2H), 3.85 (s, 3H), 3.87 (s, 3H), 6.70 (s, 1H), 6.72(d, J=2 Hz, 1H), 6.78 (d, J=8.8 Hz, 1H). ^{13}C NMR (400MHz, $CDCl_3$): δ 30.2, 32.5, 34.0, 34.8, 56.1, 56.2, 111.6, 112.0, 120.5, 134.7, 147.5, 149.2.

5-(3,4-dimethoxyphenyl)pentanenitrile (4.3', n=3**)** Same procedure to the synthesis of compound **4.3'** (n=2). Compound **4.2'** (n=3) (1.20g, 4.43 mmol) and NaCN (325 mg, 6.64 mmol) were dissolved in 20 mL anhydrous DMF, the reaction mixture was heated to 90 °C and reacted for 4 h. Same post-reaction procedure with compound **4.3'** (n=2) affords product also as a colorless liquid (900 mg, yield: 93%). ^{1}H NMR (400 MHz, $CDCl_3$): δ 1.78(m, 2H), 1.68 (m,

2H), 2.35(t, J=7.2 Hz, 2H), 2.61(t, J=6.8 Hz, 2H), 3.86(s, 3H), 3.88(s, 3H), 6.69 (s, 1H), 6.71 (d, J=2 Hz, 1H), 6.79 (d, J=7.6 Hz, 1H). ^{13}C NMR (400MHz, $CDCl_3$): δ 17.4, 25.1, 30.7, 34.9, 56.15, 56.23, 111.6, 111.9, 120.0, 120.5, 134.2, 147.7, 149.2.

Trifluoroacetyl (tfa) protected 4 (i.e. compound **4.5',** n=3**)** Follow the same procedure for the synthesis of 3C-DA as described above. Starting with compound **4.4'**(n=3) (685 mg, 3.39 mmol) will afford final product as a colorless liquid (585 mg, yield: 54%).^{1}H NMR (400 MHz, $CDCl_3$): δ 1.38 (m, 2H), 1.63(m, 2H), 2.56 (t, J=7.6 Hz, 2H), 3.36 (q, J=6.8 Hz, 2H), 3.86 (s, 3H), 3.87 (s, 3H), 6.27(s, 1H), 6.69 (s, 1H), 6.71 (d, J=2 Hz, 1H), 6.79 (d, J=8.4 Hz, 1H). ^{13}C NMR (400MHz, $CDCl_3$): δ 26.6, 29.2, 31.4, 35.6, 40.3, 56.2, 56.3, 111.6, 112.1, 117.8, 120.5, 135.2, 147.8, 149.1, 157.4.

Tfa protected 5C-DA (4.6', n=3**)** Follow the same procedure for the synthesis of 3C-DA as described above. Starting with compound **4.5'** (n=3) (560mg, 1.75 mmol) will afford pure product as a light yellow viscous liquid (451 mg, yield: 89%). ^{1}H NMR (400 MHz, d6-DMSO): δ 1.24 (m, 2H), 1.48(m, 4H), 2.36(t, J=7.6 Hz, 2H), 3.14(t, J=6.8 Hz, 2H), 6.39 (dd, J=7.6, 2 Hz, 1H), 6.53 (d, J=2 Hz, 1H), 6.59 (d, J=7.6 Hz, 1H), 8.60 (b, 2H), 9.38 (b, 1H).^{13}C NMR (400MHz, d6-DMSO): δ 27.0, 29.3, 32.0, 35.6, 116.6, 116.9, 118.8, 120.1, 134.2, 144.4, 146.2, 157.4.

5C-DA·HCl (4.7', n=3**)** Deprotection of Tfa protecting group by strong acid will give the targetted molecule in its HCl salt form. Follow the same procedure for 3C-DA·HCl synthesis. Starting with compound **4.6'** (n=3) (250 mg, 0.86 mmol) will generate product as a white solid (169 mg, yield: 85%). ^{1}H NMR (400 MHz, d6-DMSO): δ 1.28 (m, 2H), 1.48 (q, J=7.6 Hz, 2H), 1.56 (q, J=7.6 Hz, 2H), 2.38 (t, J=7.6, 7.2 Hz, 2H), 2.73 (m, 2H), 6.41(dd, J=8, 2 Hz, 1H), 6.56 (d, J=2 Hz, 1H), 6.62 (d, J=8 Hz, 1H), 7.90 (b, 3H), 8.63 (s, 1H), 8.72 (s, 1H).^{13}C NMR

(400MHz, d6-DMSO): δ 26.7, 28.1, 31.9, 35.5, 39.9, 116.8, 117.1. 120.1, 134.0, 144.4, 146.2. HR-MS (LTQ FT-ICR MS) m/z: [M+] Calcd for $C_{11}H_{18}NO_2$ 196.1333; Found 196.1332.

12-(3,4-dimethoxyphenyl)dodecanenitrile (**4.3'**, n=10) Start with 4-(11-bromoundecyl)-1,2-dimethoxybenzene(**4.2'**, n=10) (1.6 g, 4.3 mmol) (which was synthesized according to previous literature report), then follow the same synthesis procedure of compound **4.3'** (n=2) will give product as a colorless liquid (1.24g, yield: 91%). ^{1}H NMR (400 MHz, $CDCl_3$): δ 1.29 (m, 12H), 1.41(m, 2H), 1.58(m, 2H), 1.60(m, 2H), 2.31(t, J=7.2 Hz, 2H), 2.54 (t, J=8.0 Hz, 2H), 3.84 (s, 3H), 3.86 (s, 3H), 6.70 (d, J=2 Hz, 1H), 6.71 (d, J=2 Hz, 1H), 6.77 (dd, J=8.4, 2 Hz, 1H). ^{13}C NMR (400MHz, $CDCl_3$): δ 17.4, 25.6, 28.9, 29.0, 29.4, 29.6, 29.8, 32.0, 35.8, 56.1, 56.2, 111.5, 112.1, 120.1, 120.4, 135.9, 147.3, 149.0.

Trifluoroacetyl (tfa) protected 4 (i.e. compound **4.5',** n=10**)** Follow the same procedure for the synthesis of 3C-DA as described above. Starting with compound **4.4'**(n=2) (354 mg, 1.11 mmol) will afford final product as a white solid (215 mg, yield: 48%).^{1}H NMR (400 MHz, $CDCl_3$): δ 1.28 (m, 16H), 1.57 ((m, 4H), 2.54 (t, J=8.0 Hz, 2H), 3.35 (q, J=6.8 Hz, 2H), 3.85 (s, 3H), 3.87 (s, 3H), 6.36(s, 1H), 6.70(d, J=2.0Hz,1H), 6.72(d, J=2.0Hz,1H), 6.78 (dd, J=8, 2Hz, 1H). ^{13}C NMR (400MHz, $CDCl_3$): δ 27.0, 29.2, 29.4, 29.6, 29.8, 29.9, 32.0, 35.9, 40.4, 56.1, 56.3, 111.6, 112.2, 117.7, 120.5, 136.0, 147.3, 149.1, 157.5.

Tfa protected 12C-DA (4.6', n=10**)** Follow the same procedure for the synthesis of 3C-DA as described above. Starting with compound **4.5'** (n=10) (215mg, 0.54 mmol) will afford pure product as a white solid (202 mg, yield: 96%). ^{1}H NMR (400 MHz, $CDCl_3$): δ 1.24-1.29 (b, 16H), 1.55 (m, 4H), 2.48 (t, J=7.6 Hz, 2H), 3.35(q, J=6.8 Hz, 2H), 5.30 (s, 1H), 5.44 (s, 1H), 6.37 (s, 1H), 6.59 (dd, J=8.4, 2 Hz, 1H), 6.69 (d, J=2 Hz, 1H), 6.76 (d, J=8.4 Hz, 1H). ^{13}C NMR

(400MHz, $CDCl_3$): δ 27.4, 29.4, 29.8, 29.9, 30.17, 30.21, 30.3, 32.5, 35.8, 116.6, 116.9, 118.7, 120.0 134.4, 114.3, 146.2, 157.3.

12C-DA·HCl (4.7', n=10**)** Follow the same procedure for 3C-DA·HCl synthesis. Starting with compound **4.6'** (n=10) (202 mg, 0.52mmol) will generate product as a white solid (150mg, yield: 87%). ^{1}H NMR (400 MHz, d6-DMSO): δ 1.24 (b, 16H), 1.45(m, 2H), 1.52(m, 2H), 2.37 (t, J=7.6 Hz, 2H), 2.74 (m, 2H), 6.39 (dd, J=8,2 Hz, 1H), 6.53 (d, J=2 Hz, 1H), 6.60 (d, J=8 Hz, 1H), 7.99 (b, 3H), 8.60 (s, 1H), 8.68 (s, 1H).^{13}C NMR (400MHz, d6-DMSO): δ 27.1, 28.2, 29.8, 30.1, 30.2, 30.3, 32.5, 35.8, 116.7.117.0, 120.0, 134.3, 144.3, 146.2. HR-MS (LTQ FT-ICR MS) m/z: [M+] Calcd for $C_{18}H_{32}NO_2$ 294.2424; Found 294.2427.

Chapter 5 CONCLUSION AND FUTURE DIRECTION

5.1 Conclusion

In summary, an ideal scaffold is essential for successful BTE applications. Despite the fact that there are various scaffold materials, none of them are ideal. The primary goal of this dissertation was to further improve the properties of established Gemosil composite consisting of HAp-Gel with silane cross-linker, aiming to achieve a better material for BTE application. We have explored a few different approaches with various degree of success. In **Chapter 2**, we successfully doubled the mechanical strength of the Gemosil composite through developing a new processing method with the aid of selected co-solvents (e.g., THF, CH_3CN, etc.). We further demonstrated that the improvement of mechanical strength was due to improved morphology of both silane network and composite. In **Chapter 3**, we designed and synthesized a biocompatible and biodegradable copolymer P(LLA-*co*-PC) with "cross-linkable" and adhesive catechol groups. We demonstrated that through incorporating this catechol-functionalized copolymer together with dopamine into our previously developed Gemosil scaffold, the compressive strength of scaffold in wet condition could be significantly improved due to the enhanced effect from the formed polymer network as well as improved internal adhesion. Moreover, the compressive strength of Gemussel scaffold (i.e., Gemosil with dopamine/polydopamine) was further improved by 20% under wet condition with the addition of this catechol-functionalized copolymer. In **Chapter 4**, we investigated the synthesis, polymerization behavior of dopamine analogues as well as the adhesive and coating properties of their polymers formed from these dopamine analogues. This study expanded the scope of current mussel-inspired adhesive and

Coating materials, thus providing more options for replacing dopamine in our composite for further improving composite properties, for instance, color issue. More importantly, it has offered new insights in the dopamine polymerization mechanism and better understanding of structure-property relationship. The exploration in this dissertation demonstrated that designing an ideal scaffold requires interdisciplinary efforts, involving chemistry, processing and fundamental understanding of mechanisms (e.g., network formation). Based on the results presented in this dissertation, we are able to identify several directions that could further improve the properties of the HAp-Gel based composite to serve as better scaffolds for BTE.

5.2 Future Direction

5.2.1 Exploring new polymers with better processability

Our preliminary results in **Chapter 3** indicated that the incorporation of catechol-functionalized copolymer was capable of improving the compressive strength of Gemussel scaffold (i.e., Gemosil with dopamine/polydopamine) in wet condition through providing enhanced adhesion and long-range interactions within the composite. Nevertheless, the mechanical strength improvement was limited, only by 20%. We suspect that the main reason for the limited mechanical strength improvement is caused by the poor solubility of P(LLA-*co*-PC)(Catechol) (**Figure 5.1(a)**) in the processing solvent, i.e. THF/MeOH mixed solvent (Note: P(LLA-*co*-PC) backbone is insoluble in MeOH). The limited solubility may result in an inhomogeneous distribution of copolymer in the composite and incomplete cross-linking of copolymer. To address this issue, future work will focus on designing new polymer with better solubility in current processing solvent (i.e. THF/MeOH). We plan to synthesize a new polymer as shown in **Figure 5.1(b)** with biocompatible polyethylene oxide (PEO) backbone and functionalizable ethylene side group.[139] Since PEO has been shown to have a good solubility in

MeOH and many other organic solvents, we expect this new polymer would demonstrate a better solubility than P(LLA-*co*-PC)(Catechol) in THF/MeOH mixing solvent. Furthermore, the ethylene side group in the polymer backbone will allow post-functionalization with "cross-linkable" and adhesive catechol group through "thiol-ene" click chemistry. Through incorporating this new polymer with catechol to our composite, we hope to further improve the mechanical strength of our current composite.

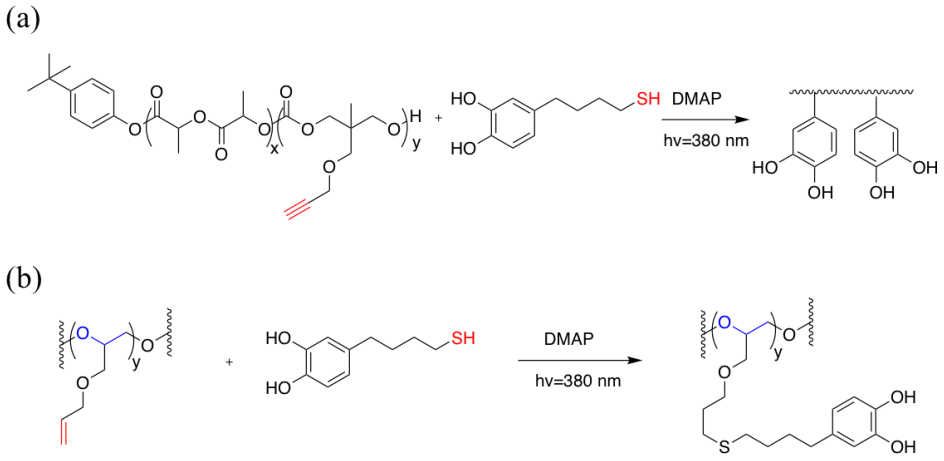

Figure 5.1. Polymer design (a) old copolymer, and (b) new copolymer.

5.2.2 Replacing dopamine with other catecholamines

We have found that covalent-linkage of catechol and amine is not required for achieving good adhesive strength, we next plan to replace dopamine with non-covalent linked catechol and propylamine in our composite. This is because non-covalent linked catechol and propylamine are much cheaper than dopamine and they have better solubility in THF/MeOH mixing solvent (Note: commercial available dopamine is in the form of HCl salt, thus, it's not soluble in THF solvent) (**Figure 5.2 (a)**). It is expected that non-covalent linked catechol and propylamine should be able to demonstrate comparable mechanical strength enhancement effect on the composite as dopamine has showed in our previous study. We further noticed that among the various dopamine analogues studied in **Chapter 4**, 3C-DA displayed a lighter color after

polymerization than dopamine; moreover, its polymer (i.e., P(3C-DA)) has demonstrate comparable adhesive and coating ability as PDA. Thus, we plan to use 3C-DA to replace dopamine for achieving lighter color of the scaffold, which could be desirable for specific applications (e.g., dental) (**Figure 5.2(b)**).

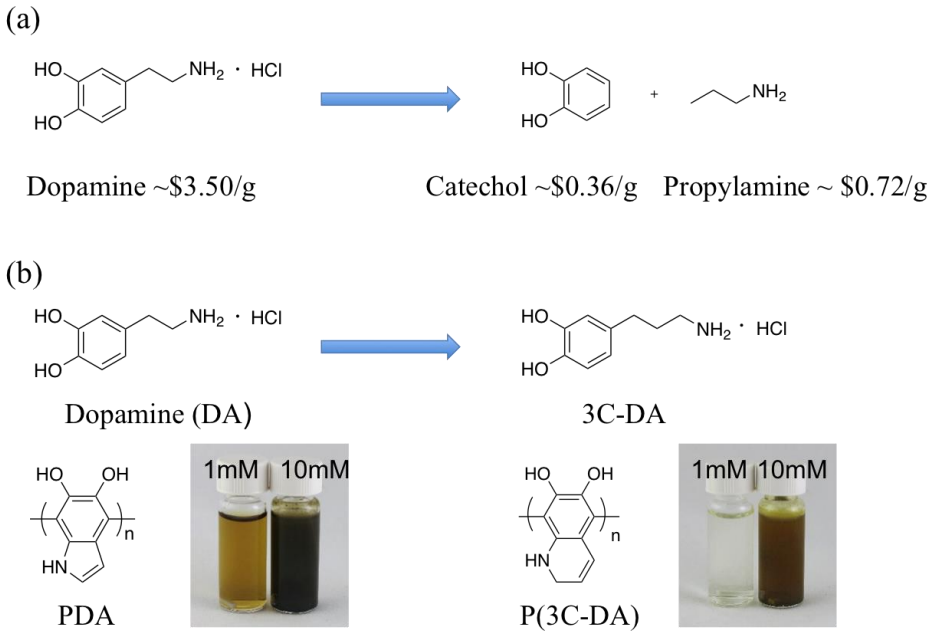

Figure 5.2. Replace dopamine with (a) catechol/propylamine, and (b) 3C-DA.

5.2.3 Exploring new materials: graphene oxide (GO)

Finally, we have shown that imparting the polymer network strength into the composite could help to enhance the long-range interaction within the composite, thereby improving the mechanical strength of composite. Therefore, we envision that replacing the polymer network with materials that demonstrate better mechanical strength in composite would likely give further enhancement of the mechanical strength of our composite. We plan to use graphene to replace the polymer network. Graphene has been well-known for its impressive mechanical properties and good biocompatibility.[140] Moreover, graphene can be easily oxidized to graphene oxide (GO), which bearing several functionalizable group, such as carboxyl and epoxy group.[141] We

have successfully functionalized GO with cross-linkable silane or catechol group through the esterification reaction between carboxyl group in GO and amine group in (3-aminopropyl) trimethoxysilane or dopamine as shown in **Figure 5.3**. It will be interesting to incorporate this cross-linkable GO into our composite and investigate their effect on the mechanical strength of the composite.

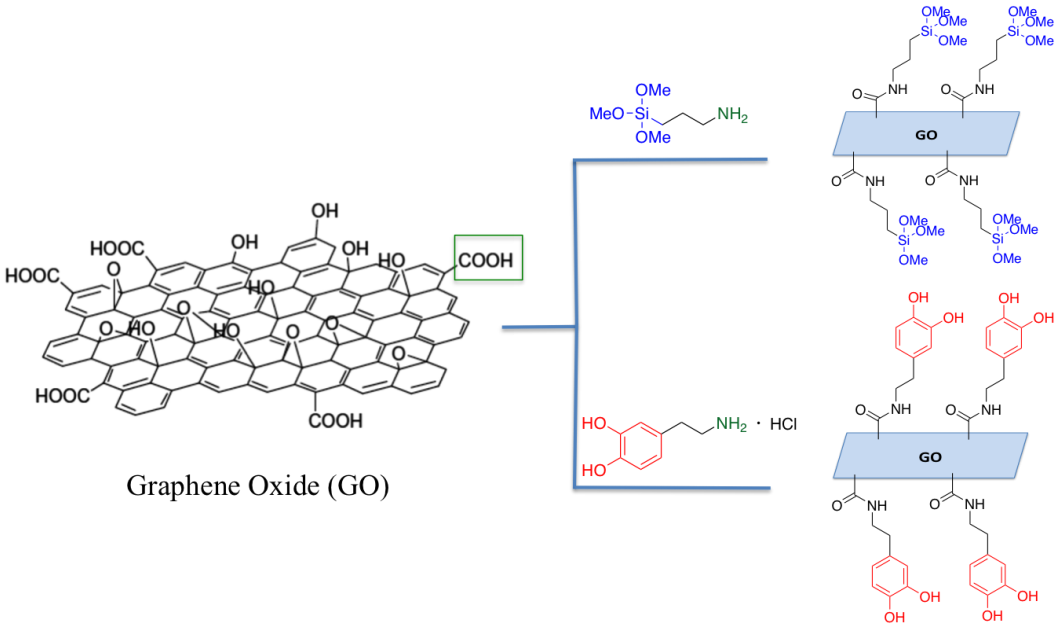

Figure 5.3. Silane or catechol functionalized GO as new materials for enhancing composite mechanical property.

5.3 Concluding Remarks

The efforts in synthetic bone scaffolds discussed in this dissertation are just a small component of the larger puzzle of BTE. Apart from the challenges in developing a sturdy scaffold with sufficient mechanical strength during whole bone regeneration process, exploring effective techniques to delivery biochemical factors and directing appropriate cell behavior in scaffold are also crucial for BTE, as briefly summarized in **Chapter 1**. Therefore, synergistic research efforts from materials scientists, biologists, engineers and medical doctors are required to continuously improve the BTE.

APPENDIX

Appendix for Chapter 2

Table A2.1. Mechanical strength for composites processed with co-solvents.

Entry	Co-solvent/MeOH	Compressive strength (MPa)	Biaxial flexural strength (MPa)
1	62% enTMOS in MeOH	143.11±27.27	141.88±20.19
2	MeOH	97.09±20.3	222.83±54.80
3	1,4-dioxane/MeOH	103.77±6.57	291.05±75.75
4	THF/MeOH	195.24±1.98	437.94±49.95
5	THF	72.23±12.40	152.14±19.69

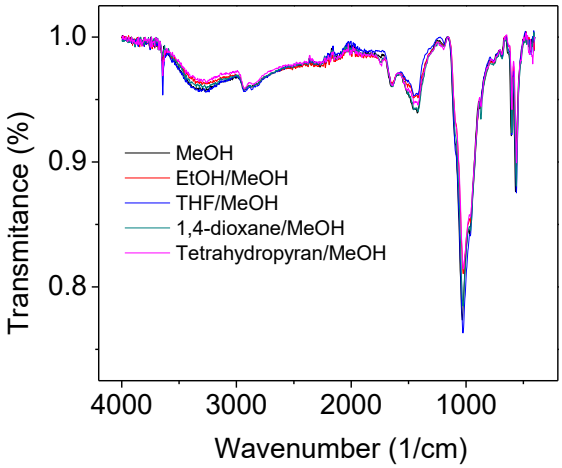

Figure A2.1. FT-IR spectra of Gemosil composite processed with different co-solvents.

Table A2.2. Biaxial flexural strength for Gemosil composites with $Ca(OH)_2$ and $Ca(OH)_2$ CHX.

No	Solvent	Material	Biaxial flexural strength (MPa)
1	THF/MeOH	$Ca(OH)_2$ CHX	437.94±49.95
2	THF/MeOH	$Ca(OH)_2$	420.67±44.54

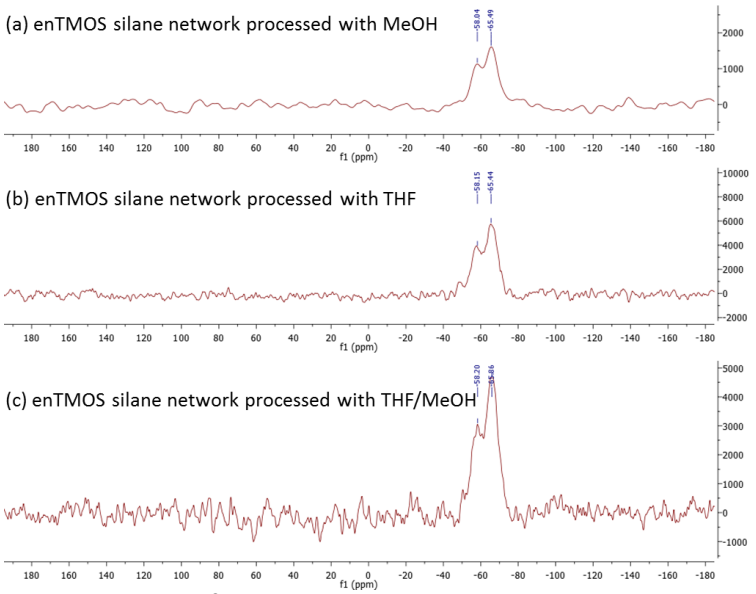

Figure A2.2. Solid-state ^{29}Si NMR of enTMOS silane network processed with different co-solvent.

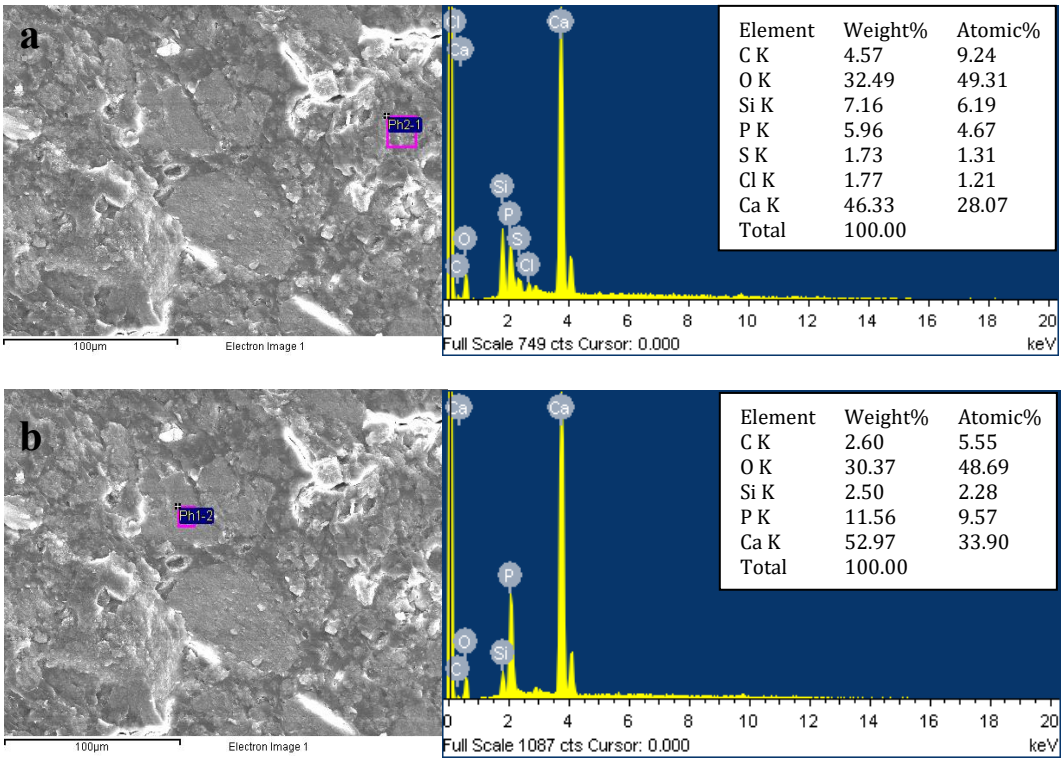

Figure A2.3. EDS data of HAp-Gemosil: (a) one is enTMOS phase rich and (b) the other phase is HAp-Gel rich.

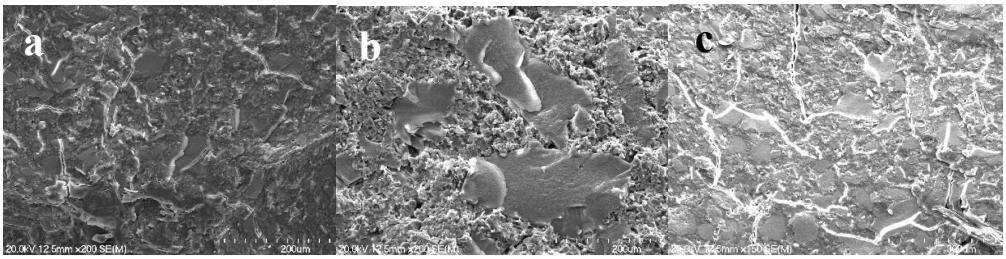

Figure A2.4. SEM images of Gemosil composite processed with a) MeOH, b) THF/MeOH(v/v=22.4), c)1,4-dioxane/MeOH (v/v=1.6).

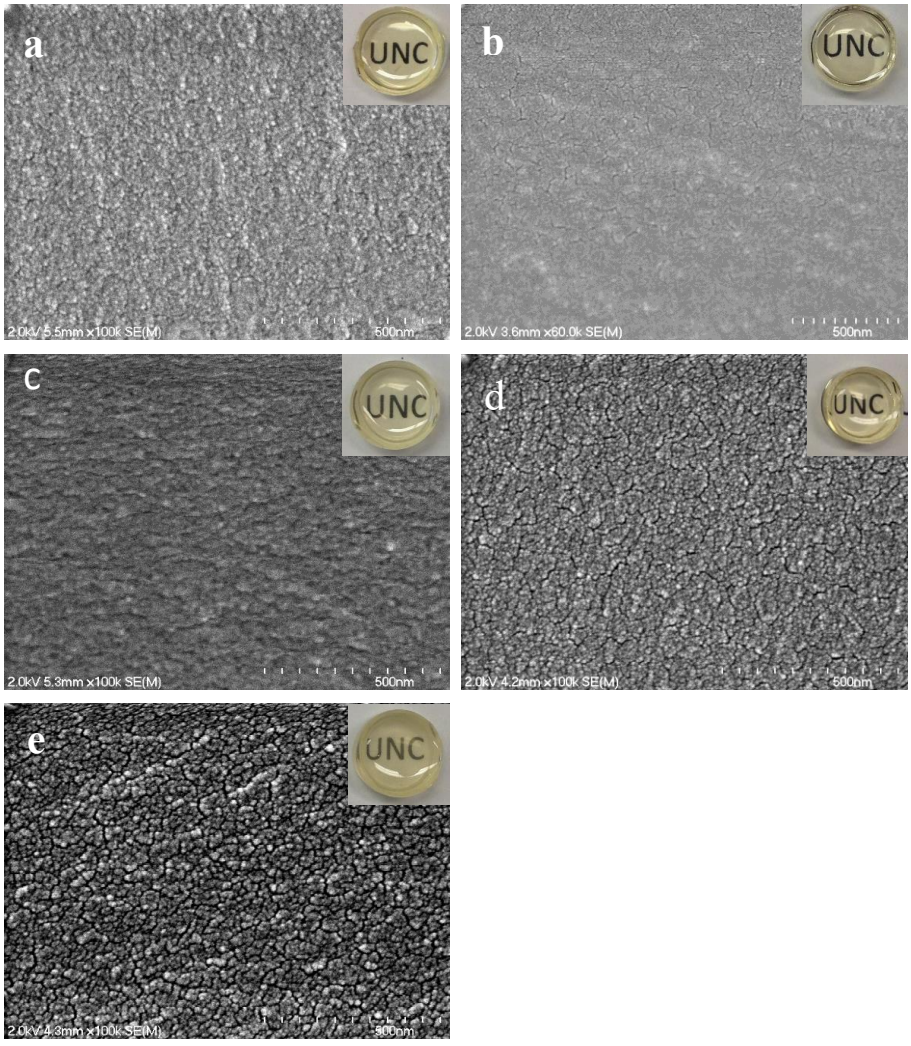

Figure A2.5. SEM images of pure enTMOS network processed with different co-solvents: a) MeOH, b)THF/MeOH (v/v=1.6), c)THF/MeOH (v/v=22.4), d) CH_3CN/MeOH (v/v=1.6), e) CH_3CN/MeOH (v/v=22.4).

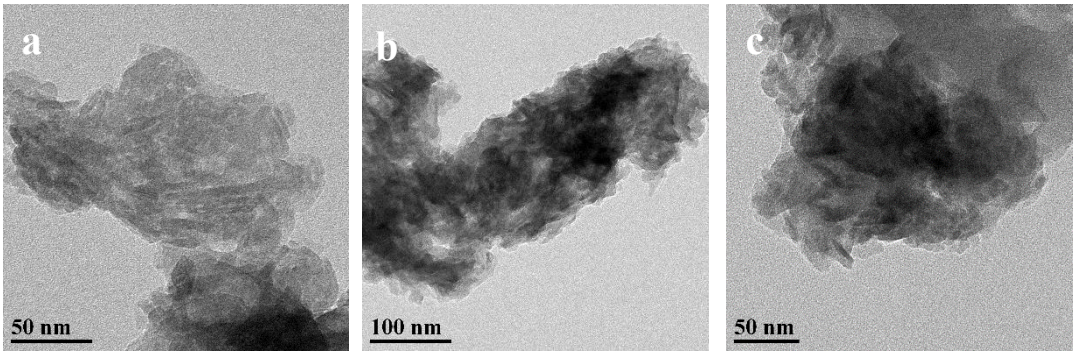

Figure A2.6. TEM images of Gemosil composite processed with a) all methanol, b)THF/MeOH (v/v=1.6), c) THF/MeOH(v/v=22.4).

Appendix for Chapter 3

^{1}H and ^{13}C NMR spectra

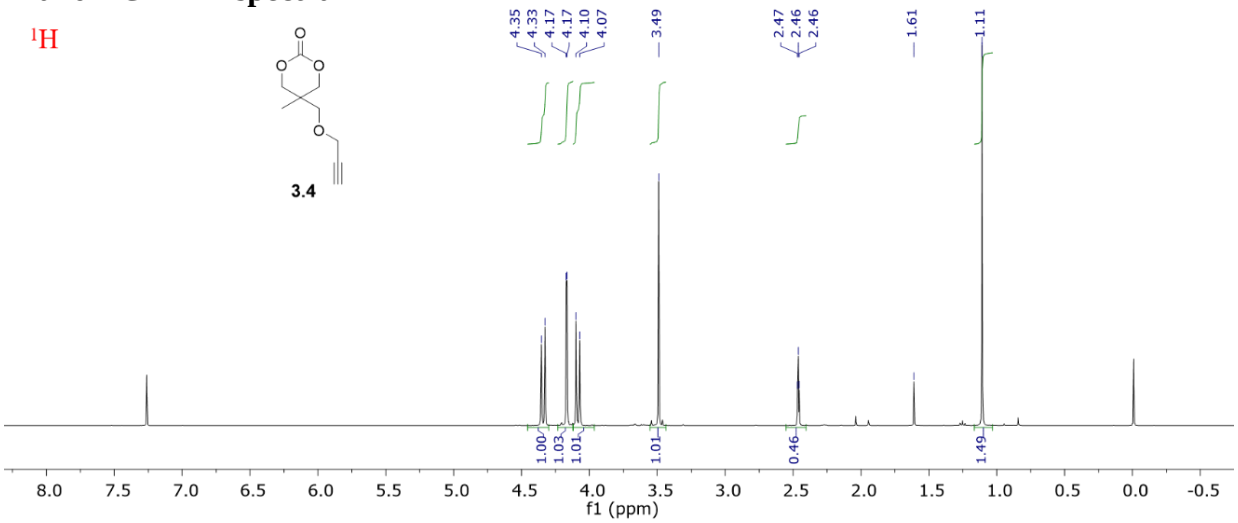

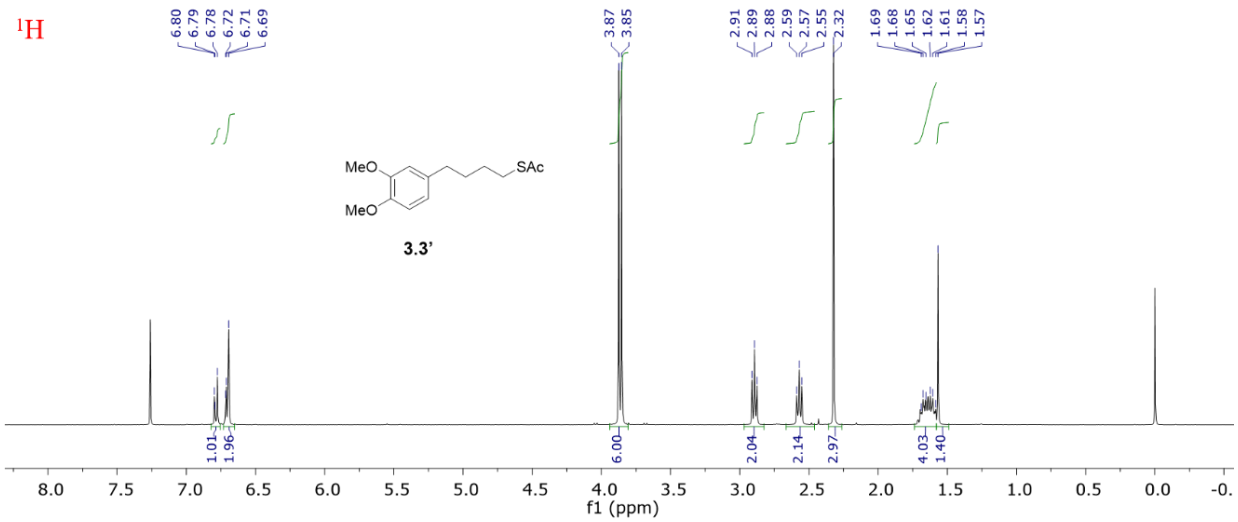

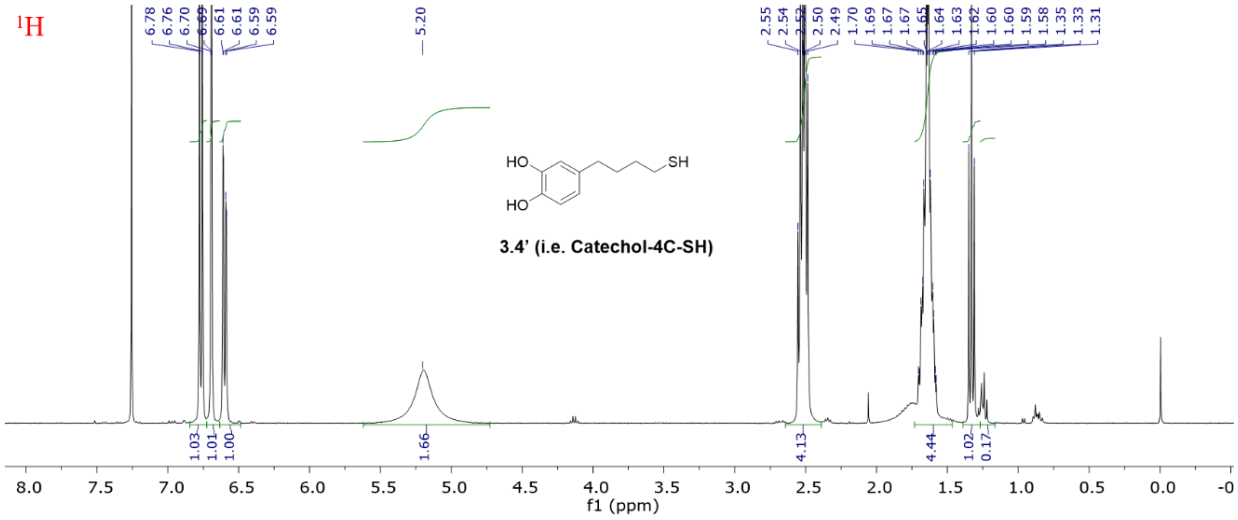

^{1}H

PLLA

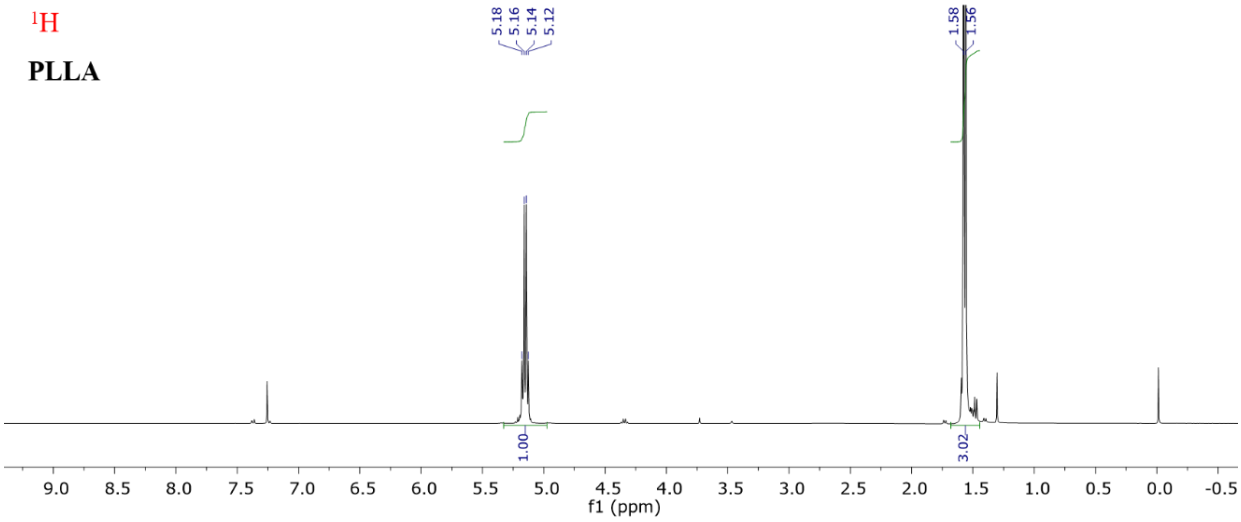

^{1}H

PPC

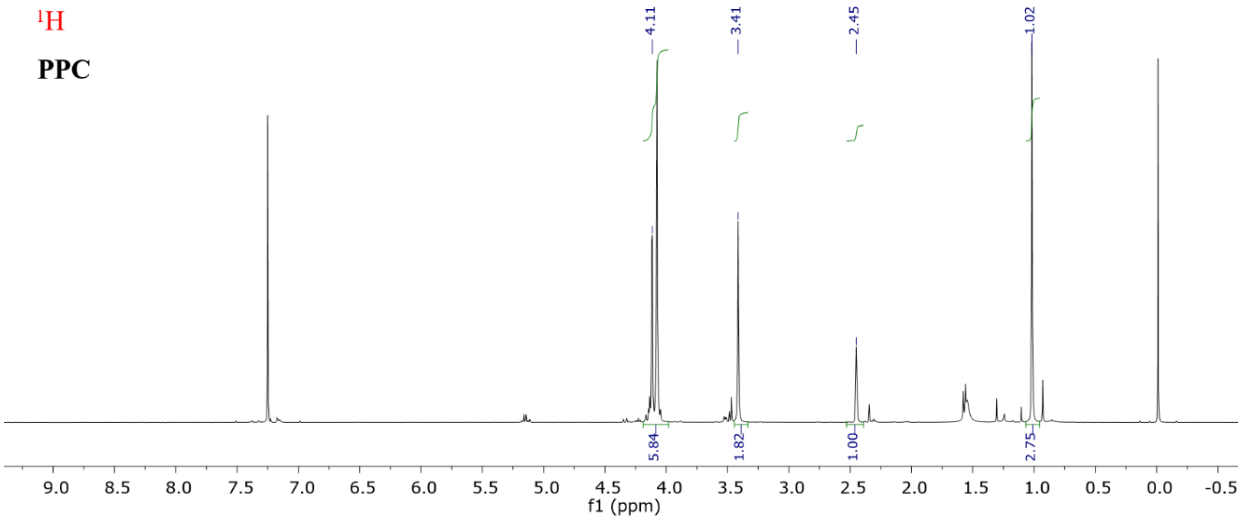

^{1}H **P(LLA-*co*-PC)$_{11.7\%}$**
(PC loading 16.7%)

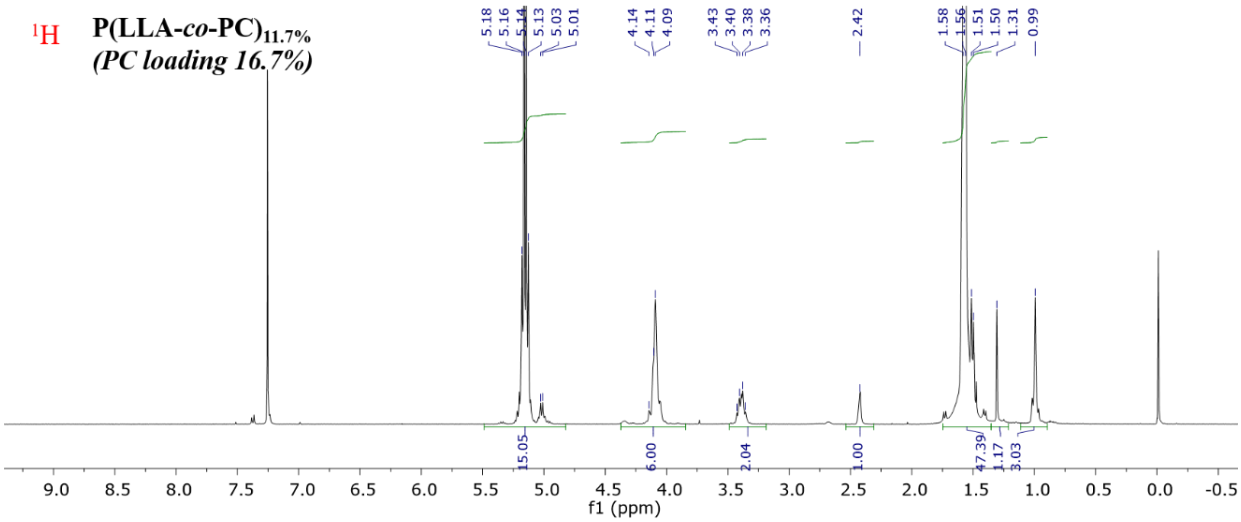

^{1}H **P(LLA-*co*-PC)$_{19.5\%}$**
(PC loading 20%)

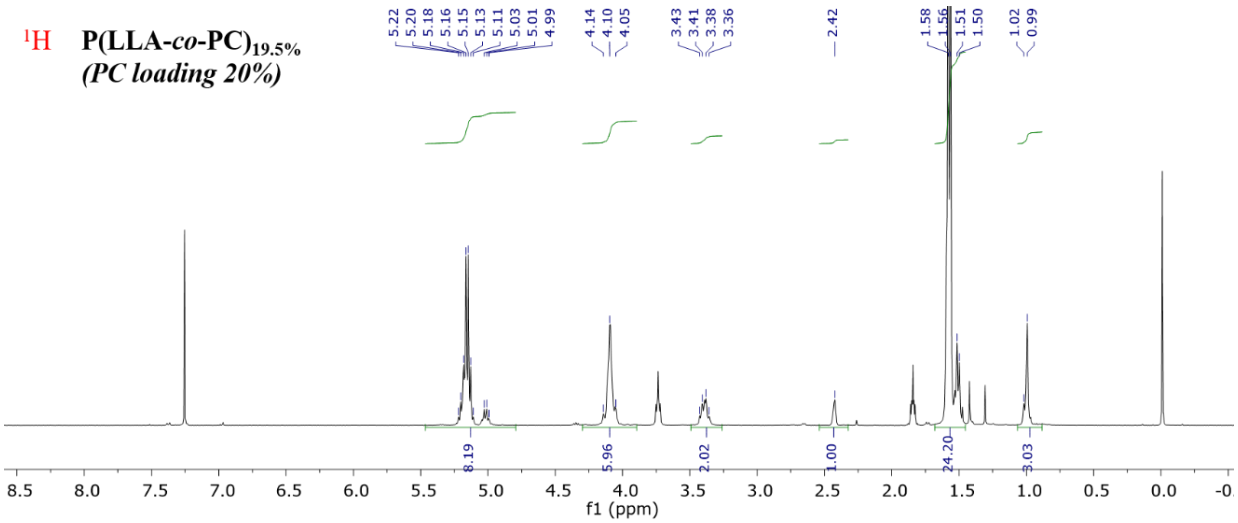

^{1}H **P(LLA-*co*-PC)$_{24.0\%}$**
(PC loading 30%)

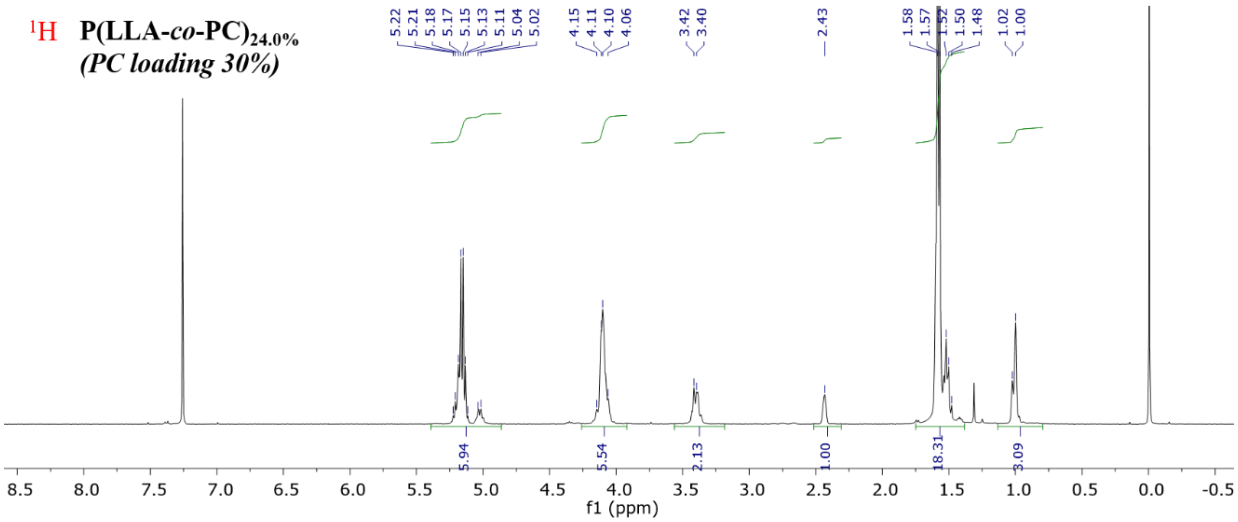

^{1}H **P(LLA-*co*-PC)$_{48.5\%}$**
(PC loading 50%)

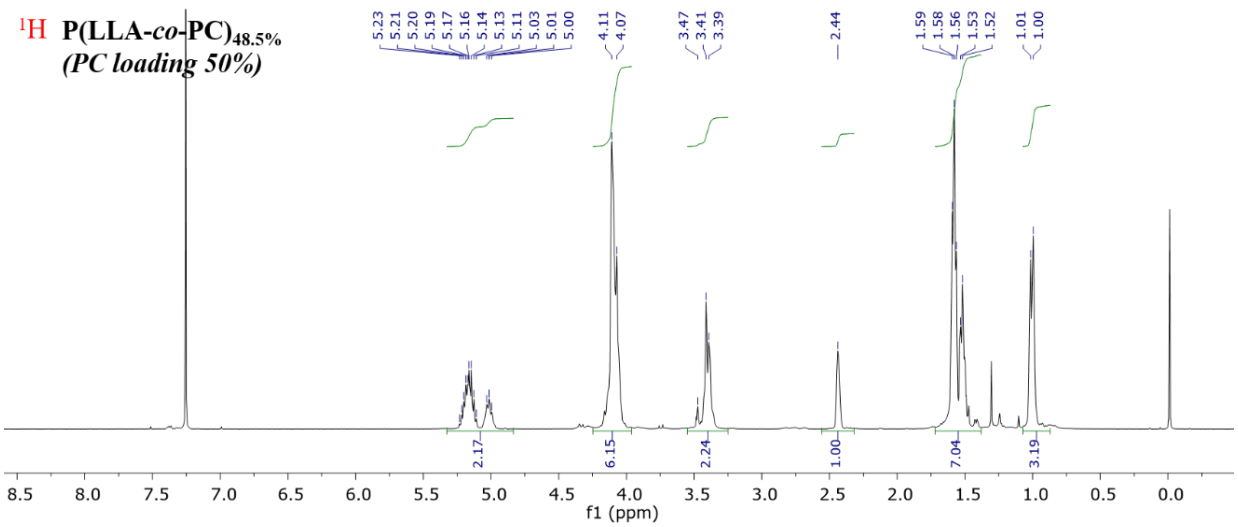

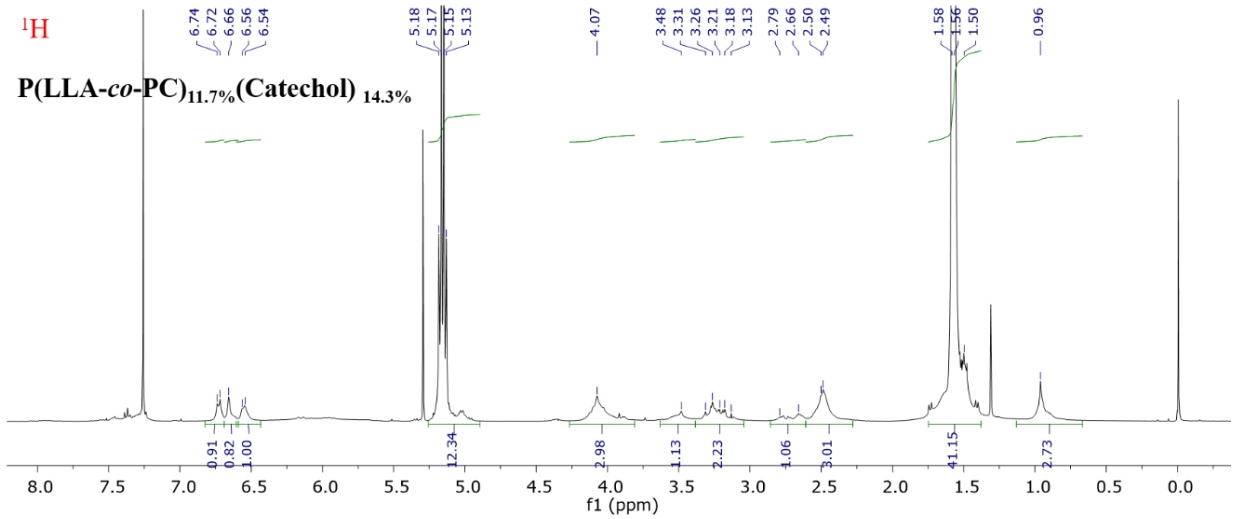
1H
P(LLA-co-PC)11.7%(Catechol) 14.3%
6.74
6.72
6.66
6.56
6.54
5.18
5.17
5.15
5.13
4.07
3.48
3.31
3.26
3.21
3.18
3.13
2.79
2.66
2.50
2.49
1.58
1.56
1.50
0.96
0.91
0.82
1.00
12.34
2.98
1.13
2.23
1.06
3.01
41.15
2.73
f1 (ppm)

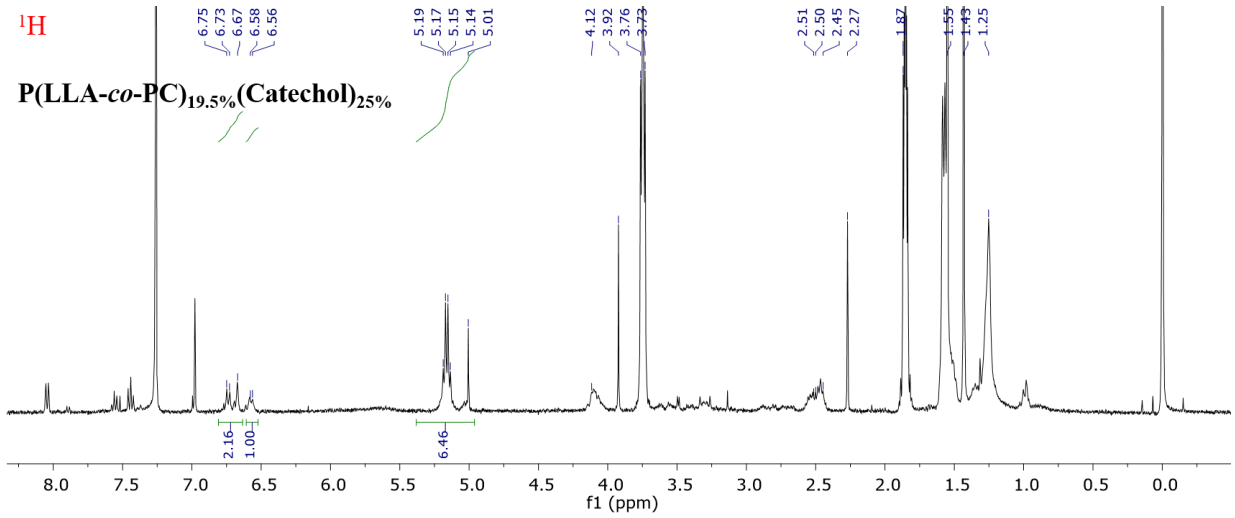
1H
P(LLA-co-PC)19.5%(Catechol)25%
6.75
6.73
6.67
6.58
6.56
5.19
5.17
5.15
5.14
5.01
4.12
3.92
3.76
3.73
2.51
2.50
2.45
2.27
1.87
1.55
1.43
1.25
2.16
1.00
6.46
f1 (ppm)

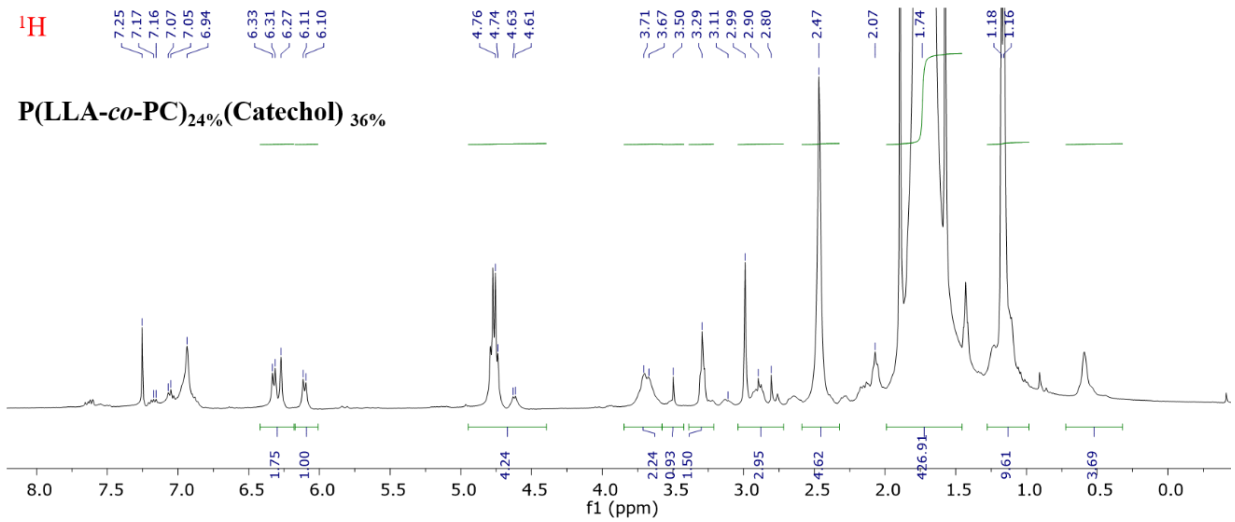
1H
P(LLA-co-PC)24%(Catechol) 36%
7.25
7.17
7.16
7.07
7.05
6.94
6.33
6.31
6.27
6.11
6.10
4.76
4.74
4.63
4.61
3.71
3.67
3.50
3.29
3.11
2.99
2.90
2.80
2.47
2.07
1.74
1.18
1.16
1.75
1.00
4.24
2.24
0.93
1.50
2.95
4.62
26.91
9.61
3.69
f1 (ppm)

^{1}H **P(LLA-*co*-PC)$_{11.8\%}$**
(Mn=10.7 kDa)

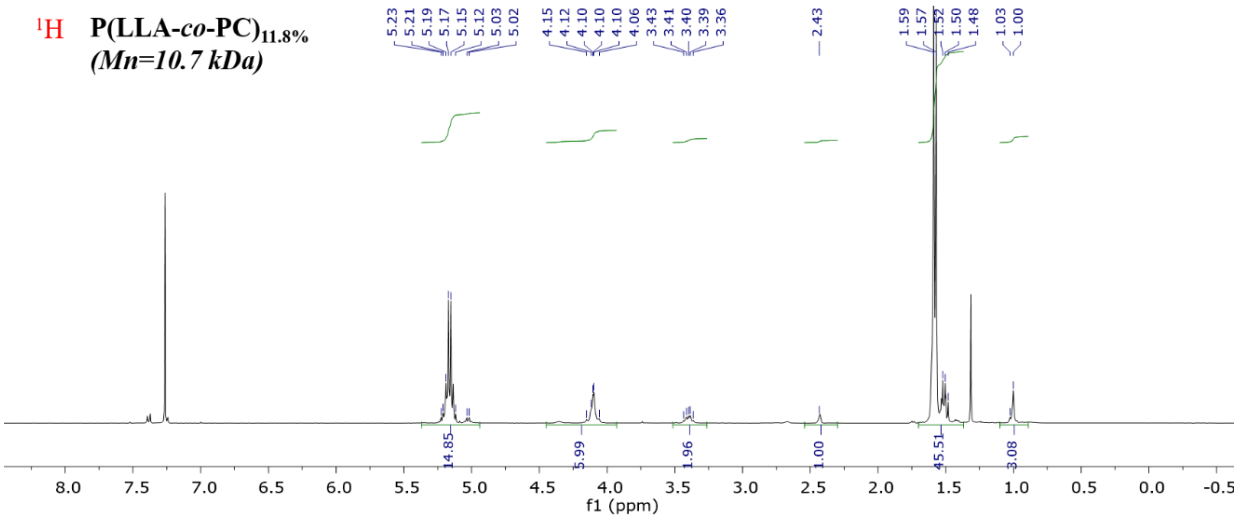

^{1}H
P(LLA-*co*-PC)$_{11.8\%}$(Catechol) $_{14.3\%}$

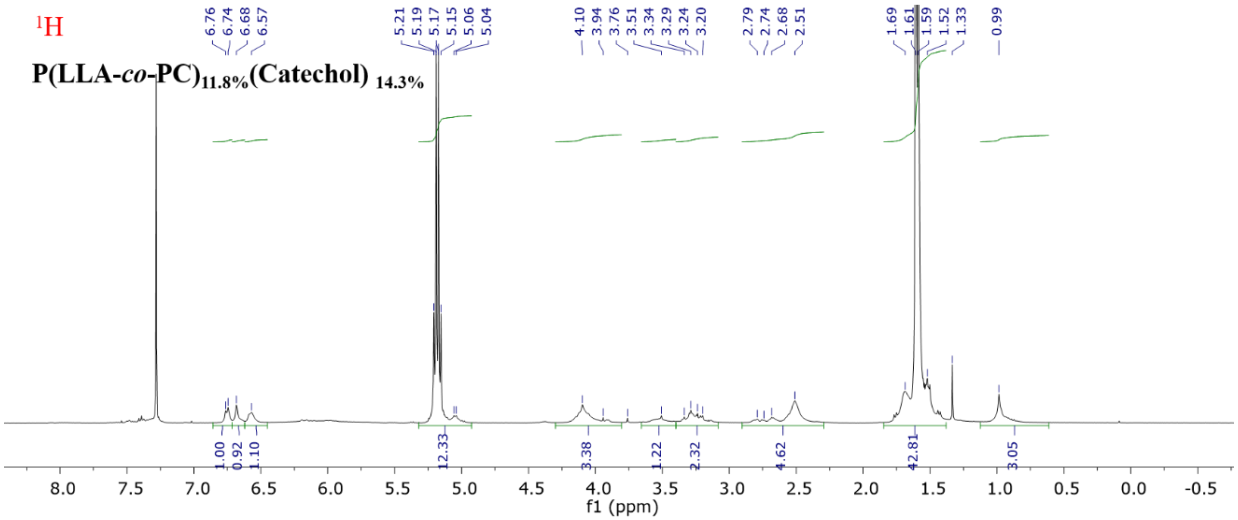

^{1}H **P(LLA-*co*-PC)$_{12.2\%}$**
(Mn=16.4 kDa)

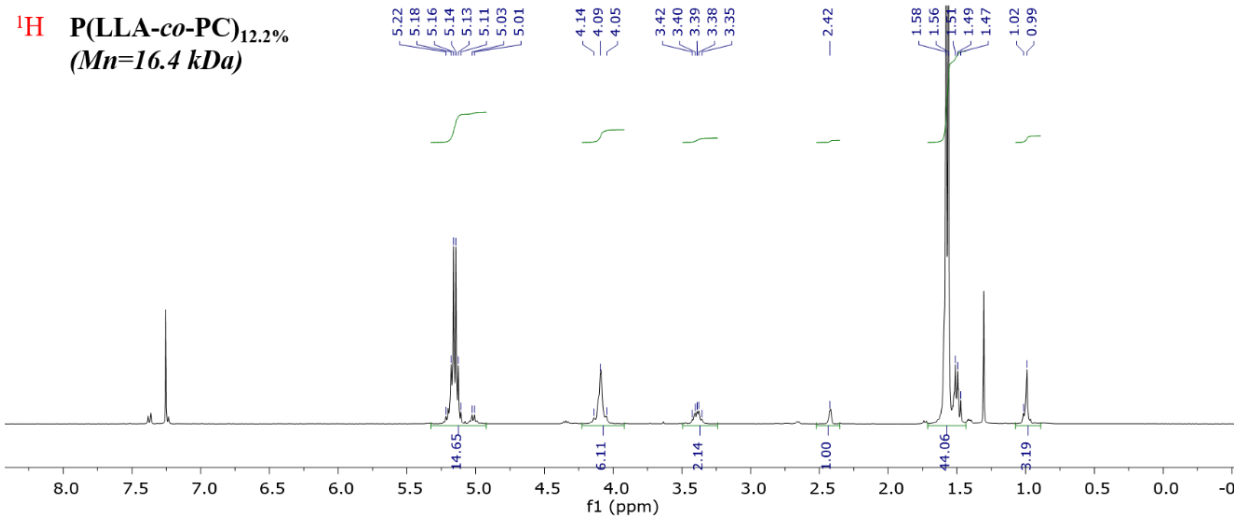

^{1}H

P(LLA-*co*-PC)$_{12.2\%}$(Catechol) $_{13.9\%}$

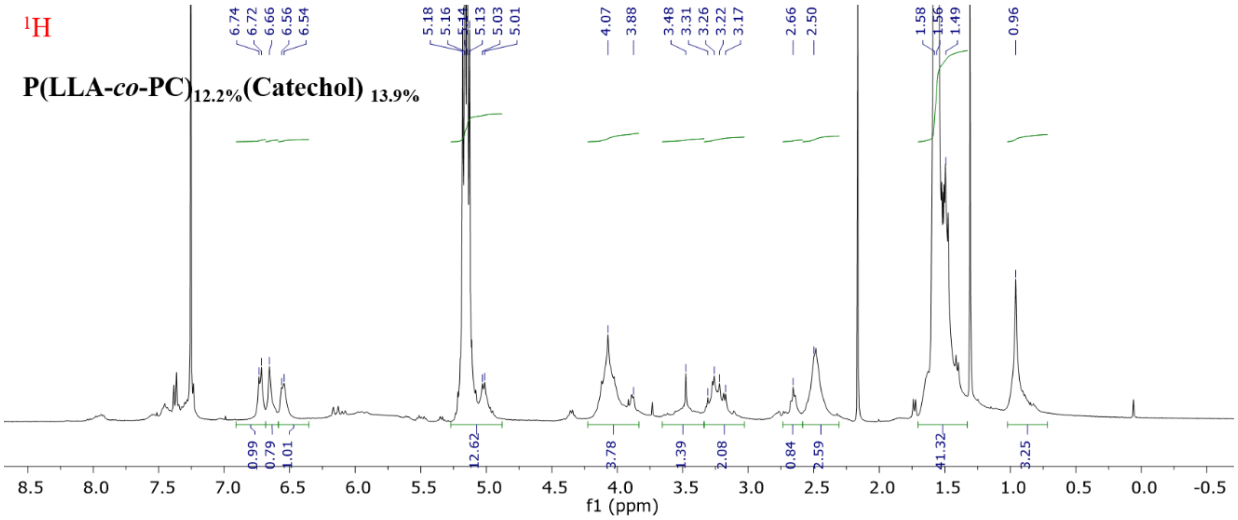

^{1}H **P(LLA-*co*-PC)$_{12.7\%}$**

(Mn=37.4 kDa)

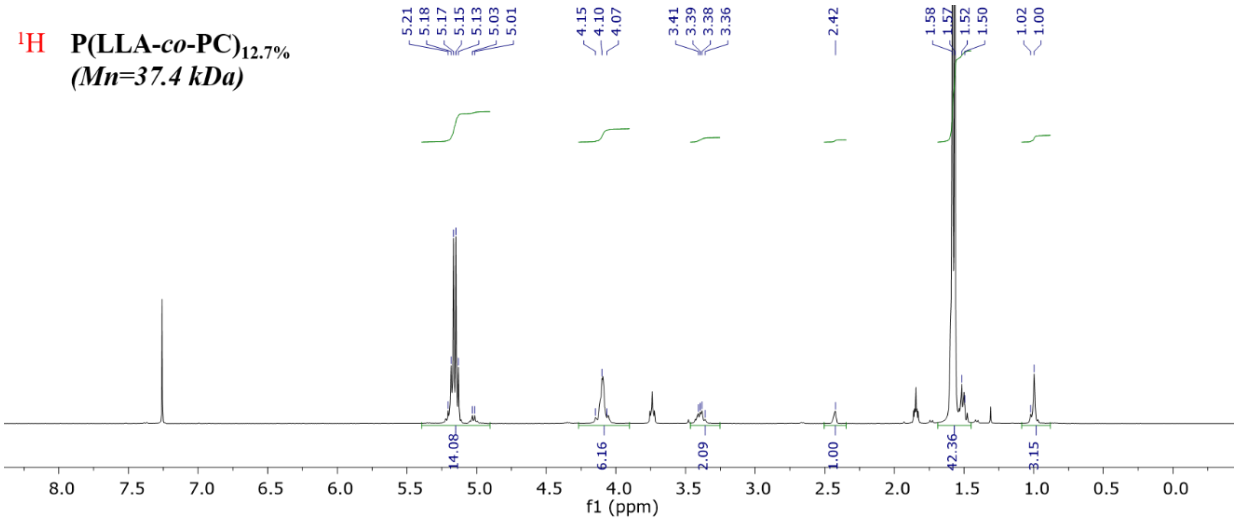

^{1}H

P(LLA-*co*-PC)$_{12.7\%}$(Catechol) $_{15.4\%}$

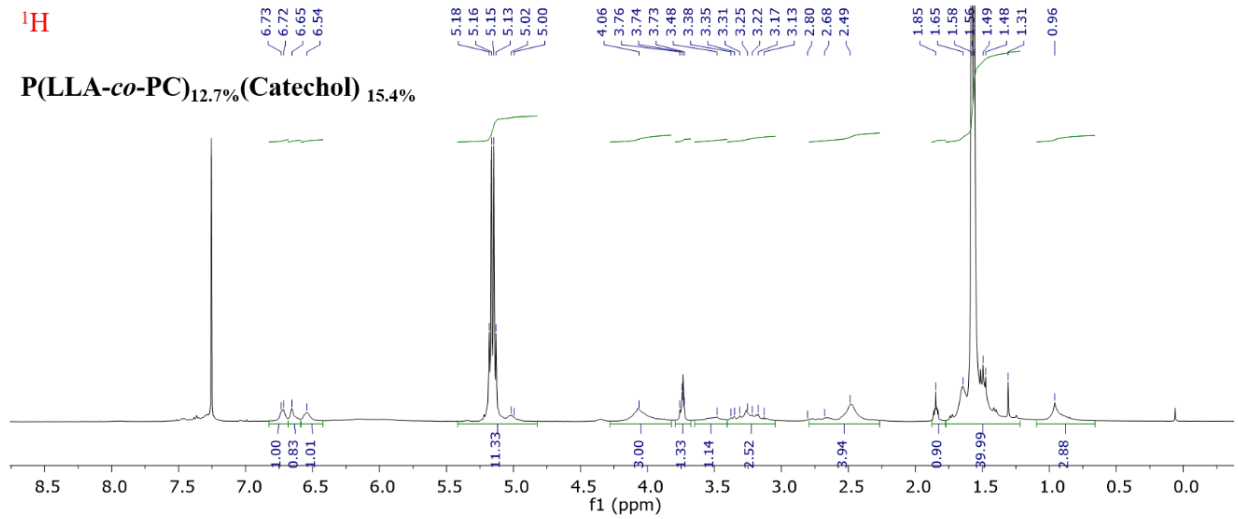

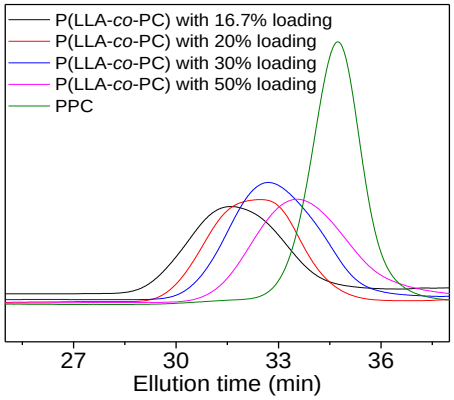

Figure A3.1. GPC curve for P(LLA-co-PC) with different PC loading.

Appendix for Chapter 4

UV-Vis absorbance spectra in H_2O

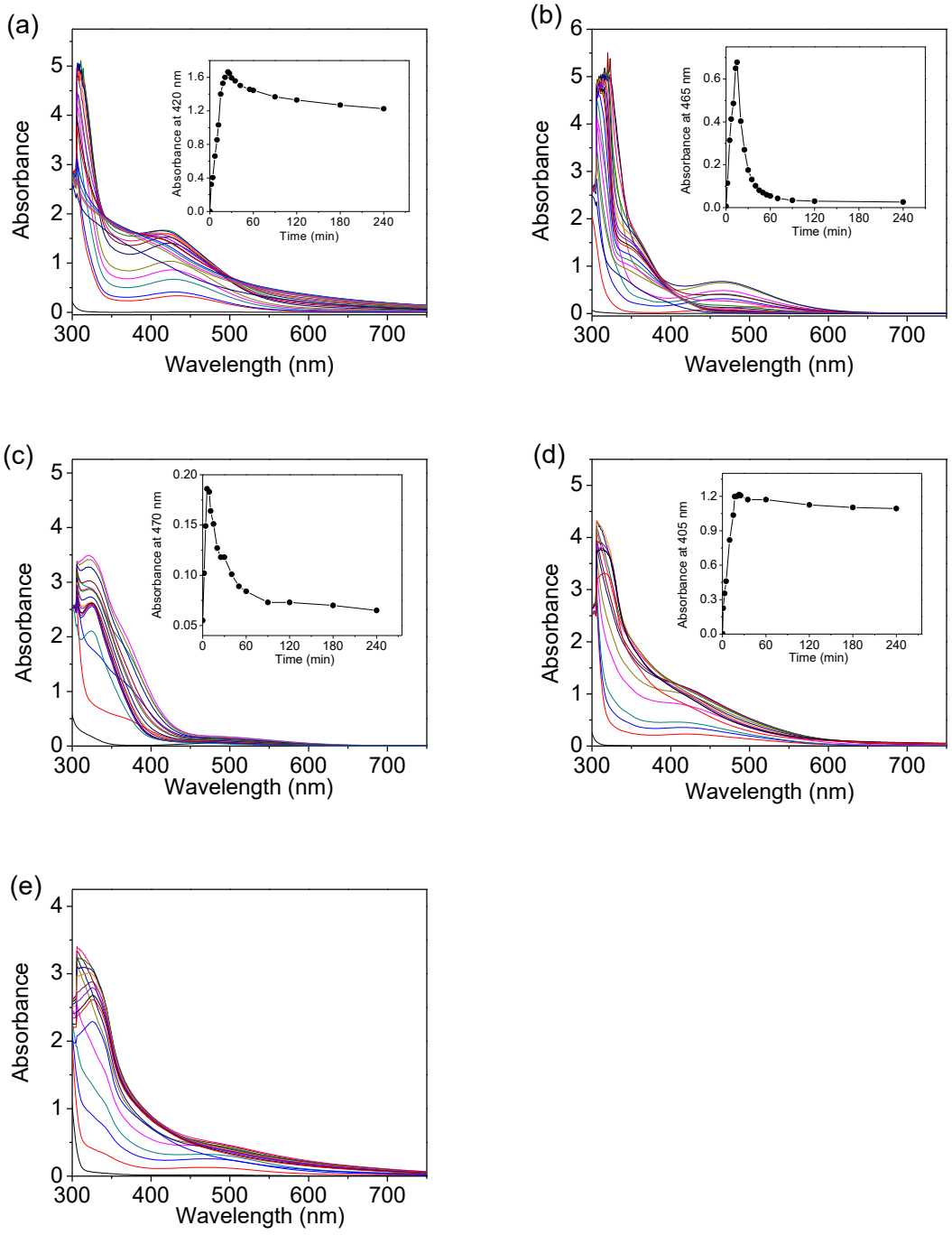

Figure A4.1. Time dependent UV-Vis spectroscopy for (a) dopamine, (b) 3C-DA, (c) 4C-DA, (d) 5C-DA, and (e) catechol and propylamine aqueous solution after adding 1M NaOH. Inserted figure is the time-dependent change of characteristic absorbance peak.

UV-Vis absorbance spectra in MeOH-H_2O (v/v=125:1)

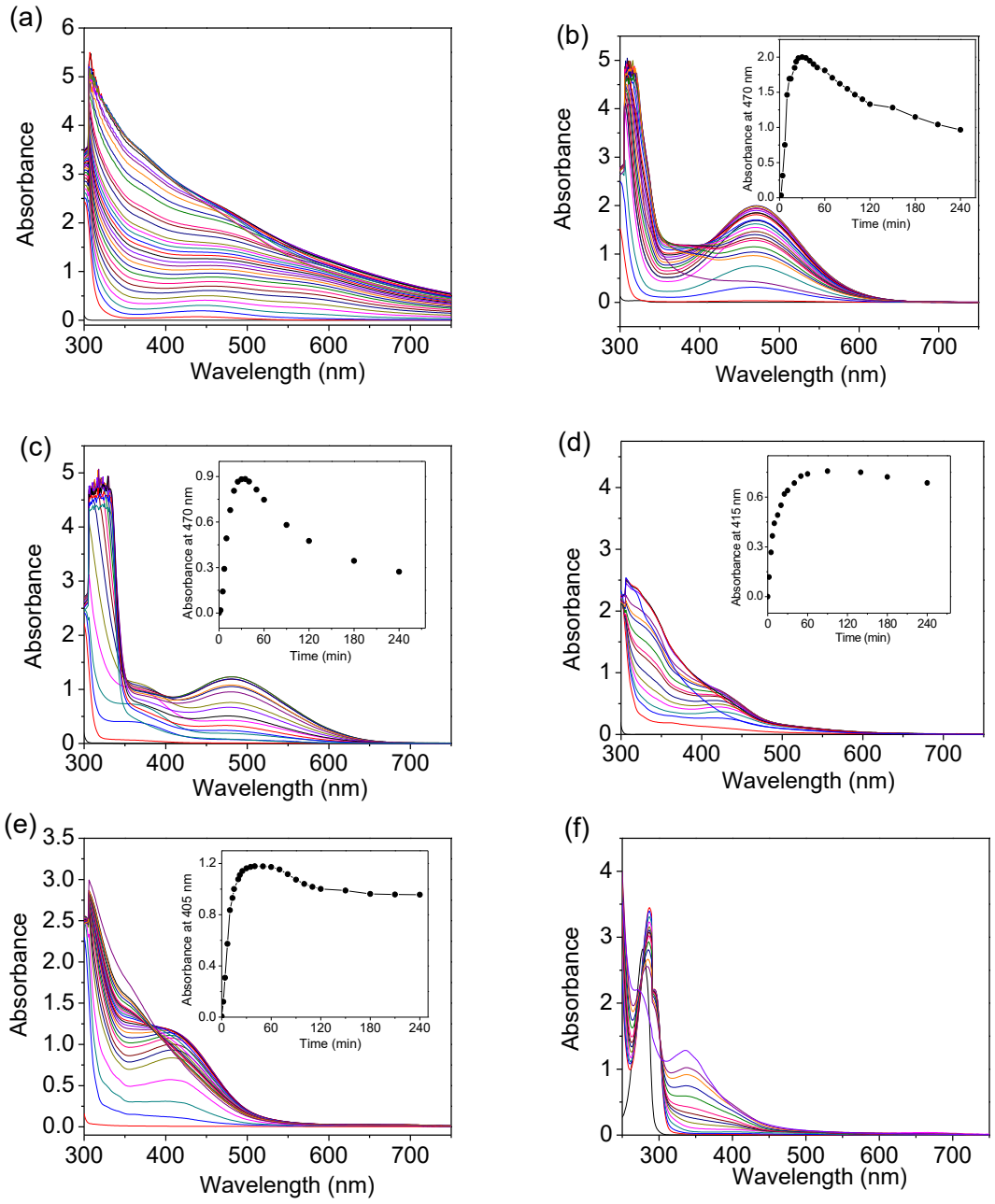

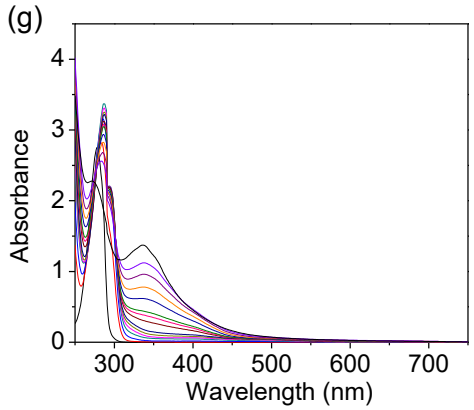

Figure A4.2. Time dependent UV-Vis spectroscopy for (a) dopamine, (b) 3C-DA, (c) 4C-DA, (d) 5C-DA, (e) 12C-DA, (f) catechol and propylamine and (g) catechol and dodecylamine in MeOH (1mM) after adding 1M NaOH. Inserted figure is the time-dependent change of characteristic absorbance peak.

UV-Vis absorbance spectra in IPA-H_2O (v/v=1:2)

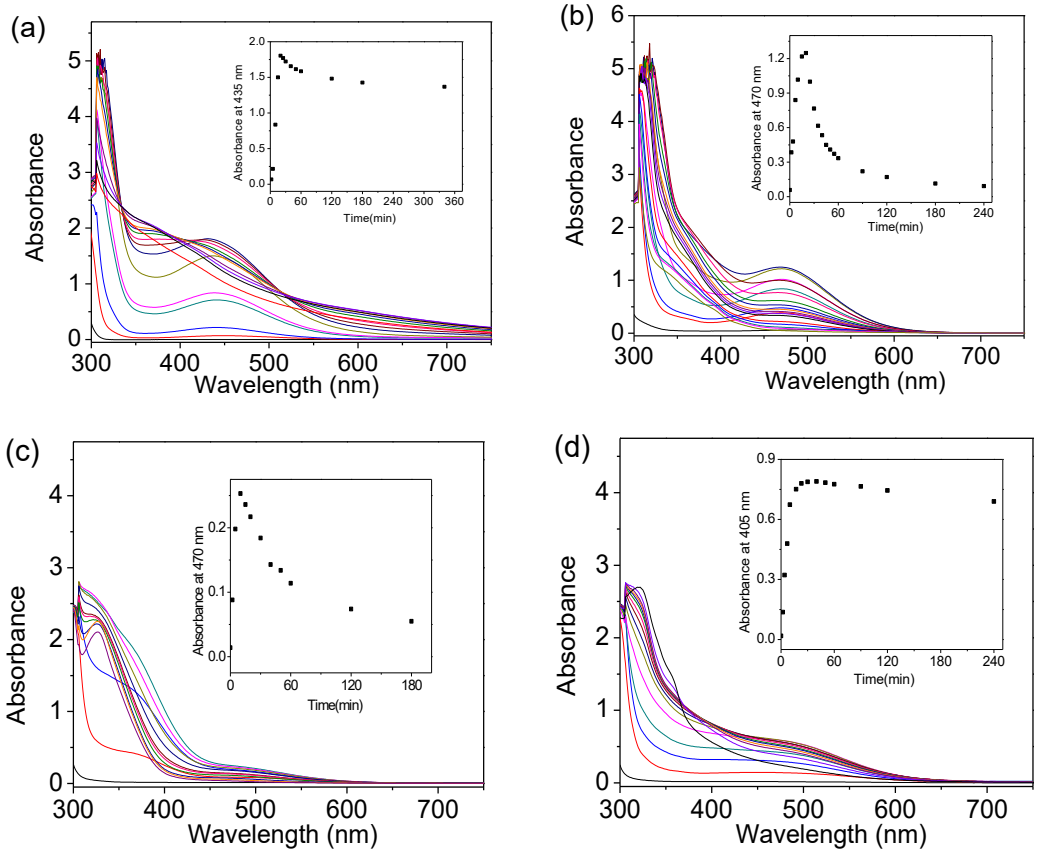

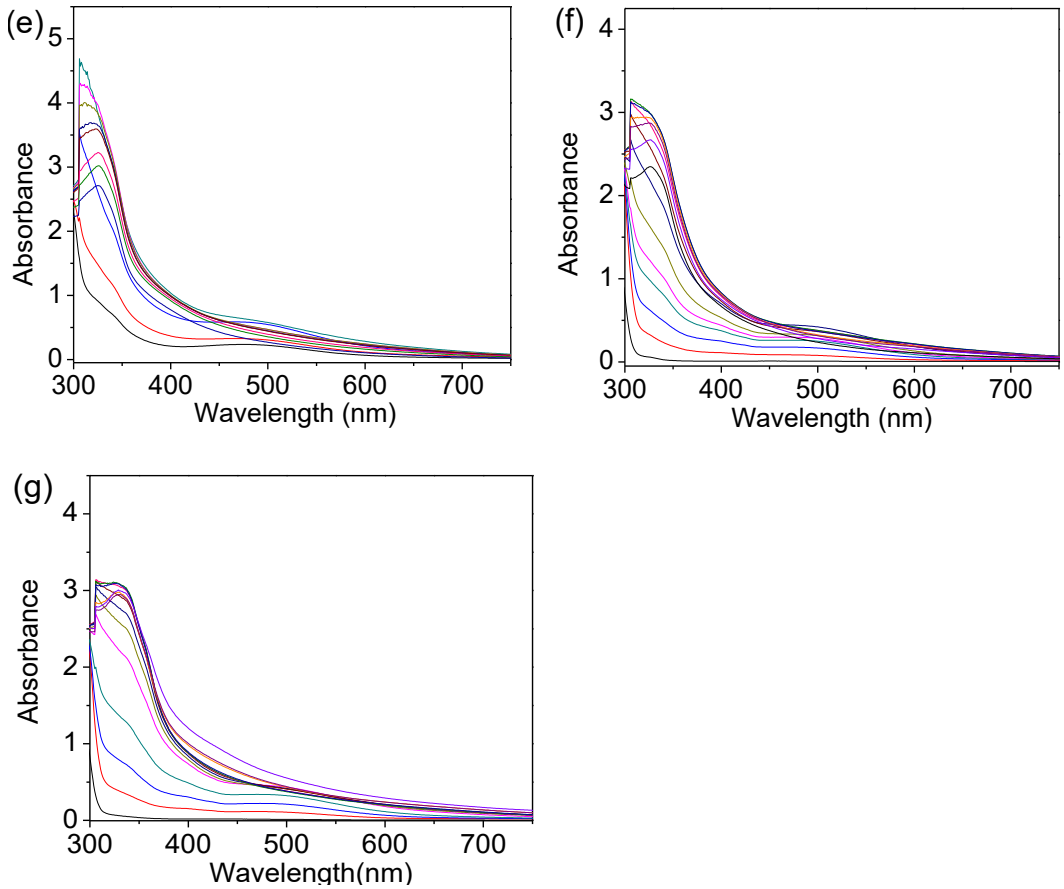

Figure A4.3. Time dependent UV-Vis spectroscopy for (a) dopamine, (b) 3C-DA, (c) 4C-DA, (d) 5C-DA, (e) 12C-DA, (f) catechol and propylamine and (g) catechol and dodecylamine (1 mM) in IPA: H2O, v/v=1:2, after adding 1M NaOH. Inserted figure is the time-dependent change of characteristic absorbance peak.

UV-Vis absorbance spectra in Tris buffer

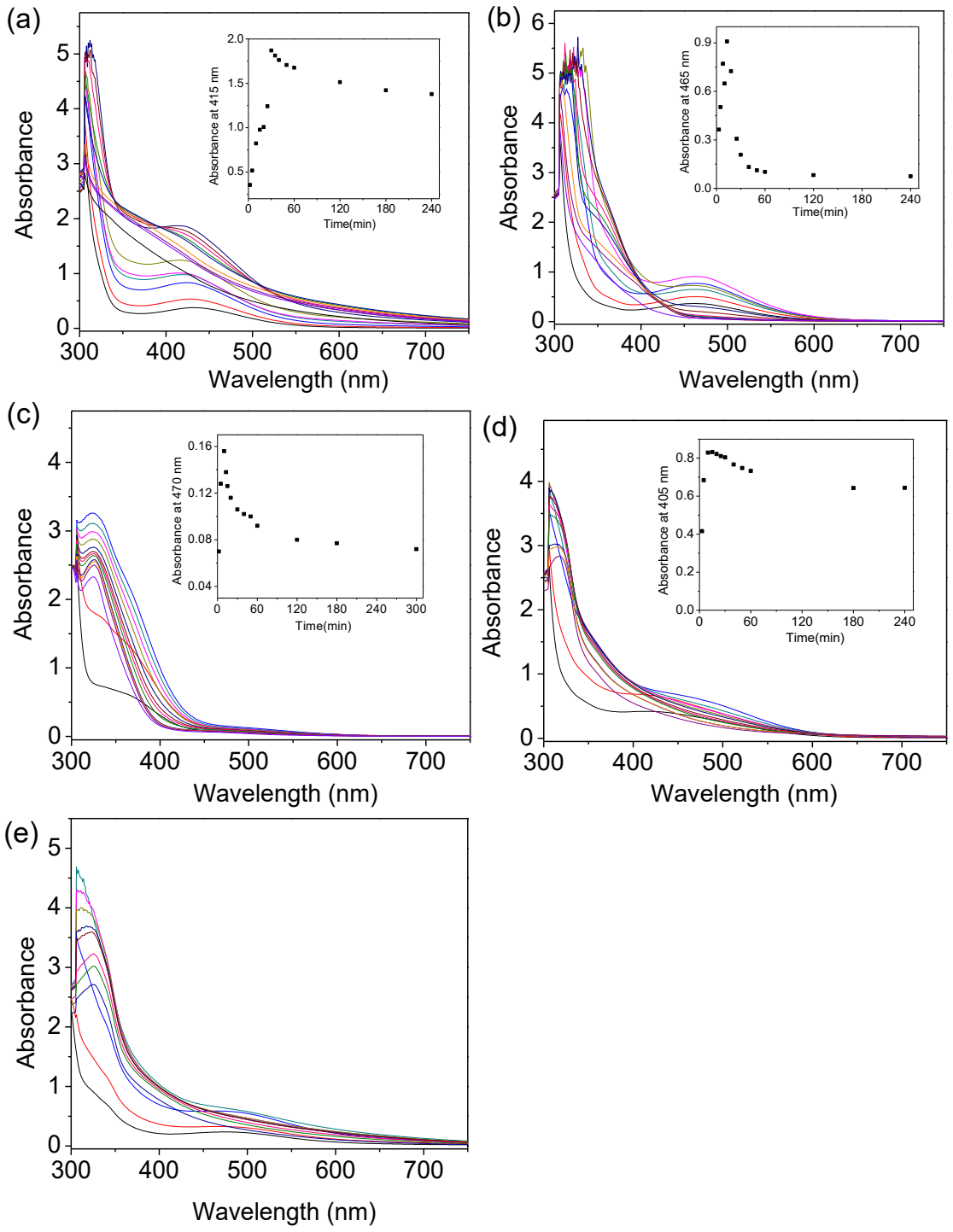

Figure A4.4. Time dependent UV-Vis spectroscopy for (a) dopamine, (b) 3C-DA, (c) 4C-DA, (d) 5C-DA, and (e) catechol and propylamine (1 mM) in 10 mM Tris buffer (pH=8.5). Inserted figure is the time-dependent change of characteristic absorbance peak.

Proposed polymerization mechanism for dopamine and dopamine analogues

Scheme A4.1. Proposed polymerization mechanism for (a)dopamine (b)3C-DA and 4C-DA (c)5C-DA and 12C-DA (d) catechol and alkylamine

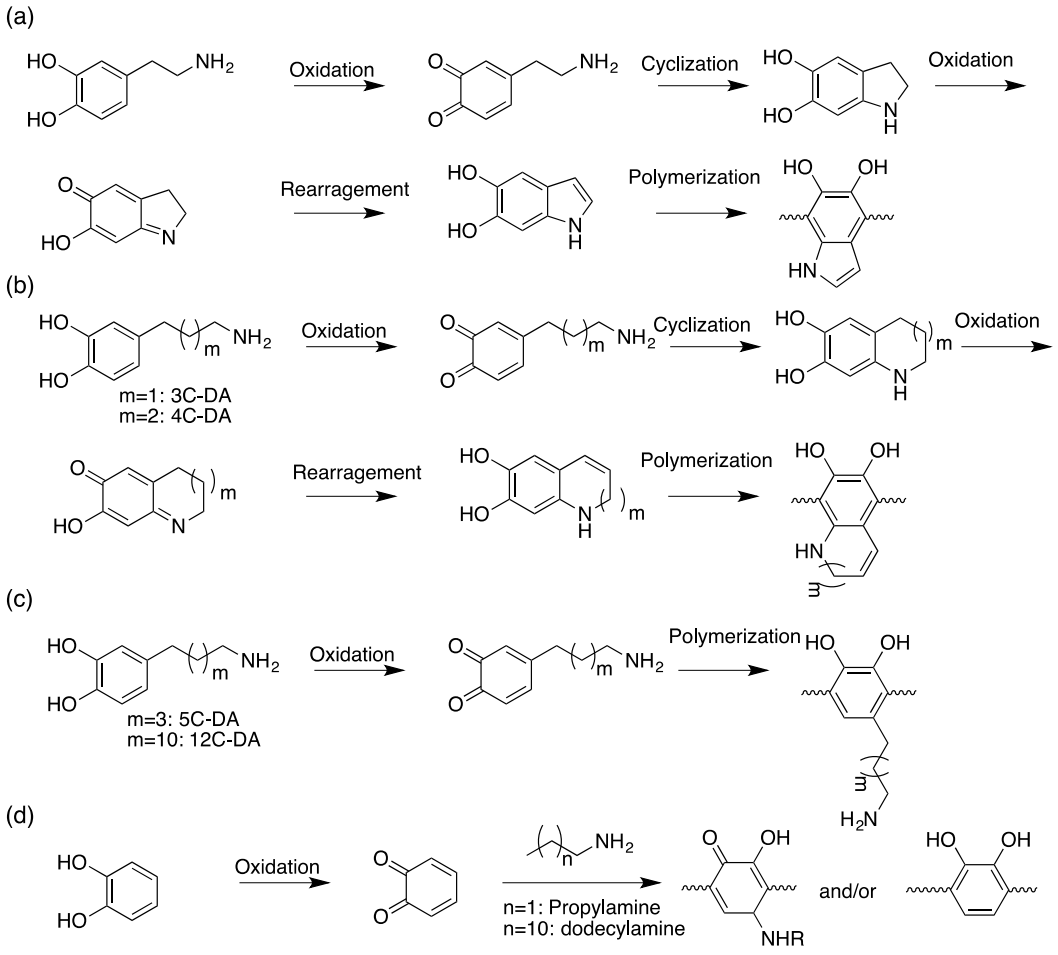

Adhesive strength result

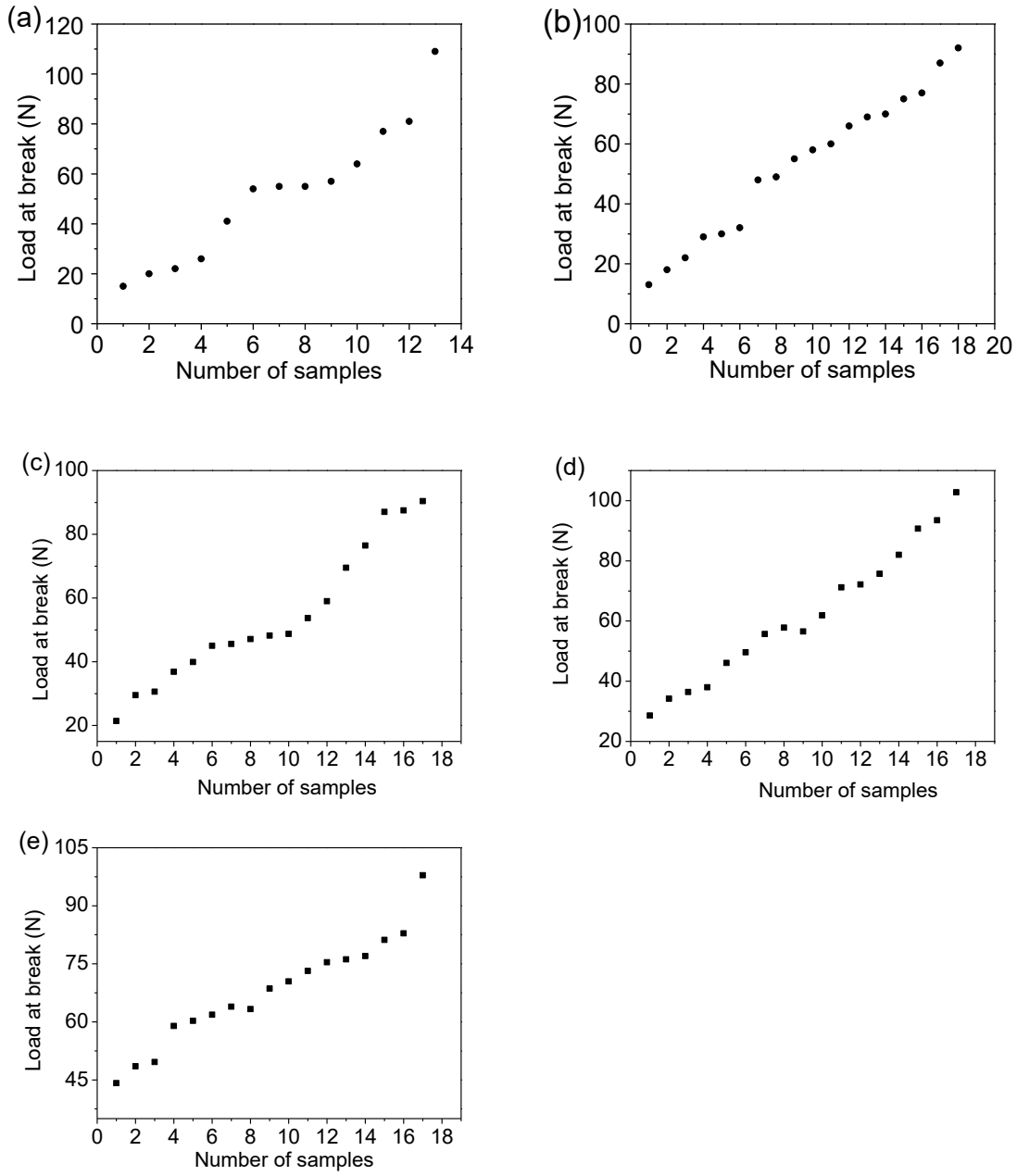

Figure A4.5. Histogram of load at break at same mass concentration in H_2O for (a) PDA; (b) P(3C-DA);(c) P(4C-DA); (d) P(5C-DA); (e) Catechol and propylamine.

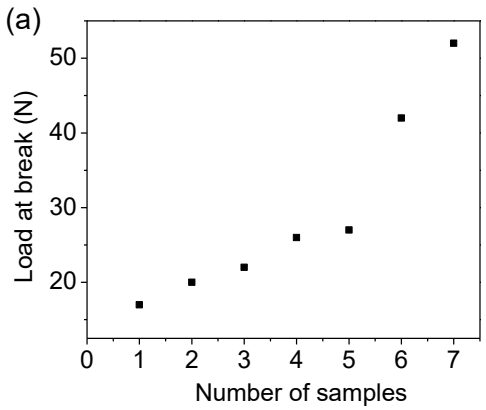
(a)
Load at break (N)
Number of samples

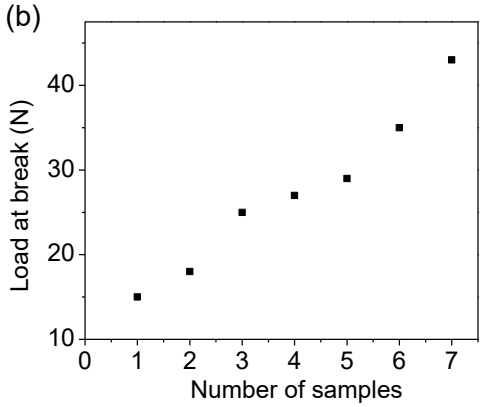
(b)
Load at break (N)
Number of samples

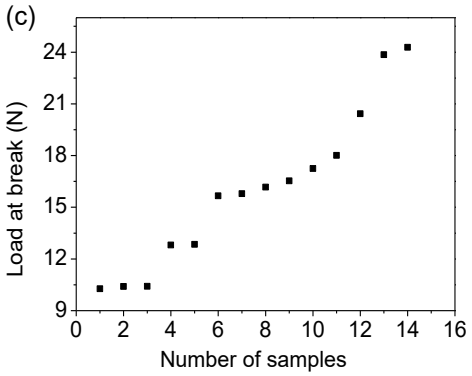
(c)
Load at break (N)
Number of samples

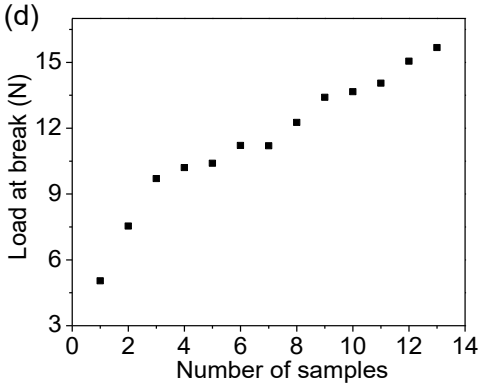
(d)
Load at break (N)
Number of samples

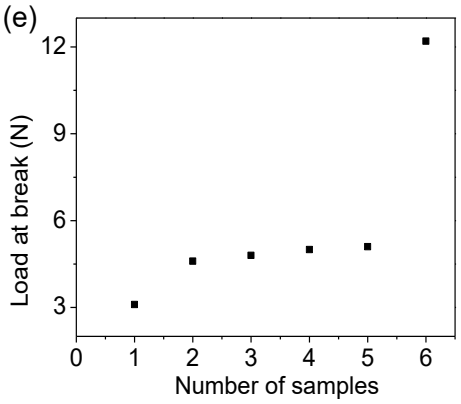
(e)
Load at break (N)
Number of samples

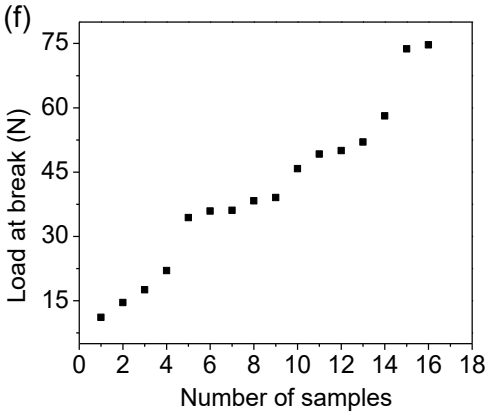
(f)
Load at break (N)
Number of samples

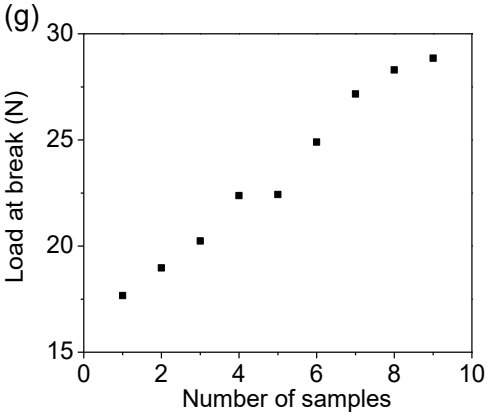
(g)
Load at break (N)
Number of samples

Figure A4.6. Histogram of load at break at same mass concentration in IPA-H2O for (a) PDA; (b) P(3C-DA);(c) P(4C-DA); (d) P(5C-DA); (e) P(12C-DA); (f) Catechol and propylamine; (g) Catechol and dodecylamine.

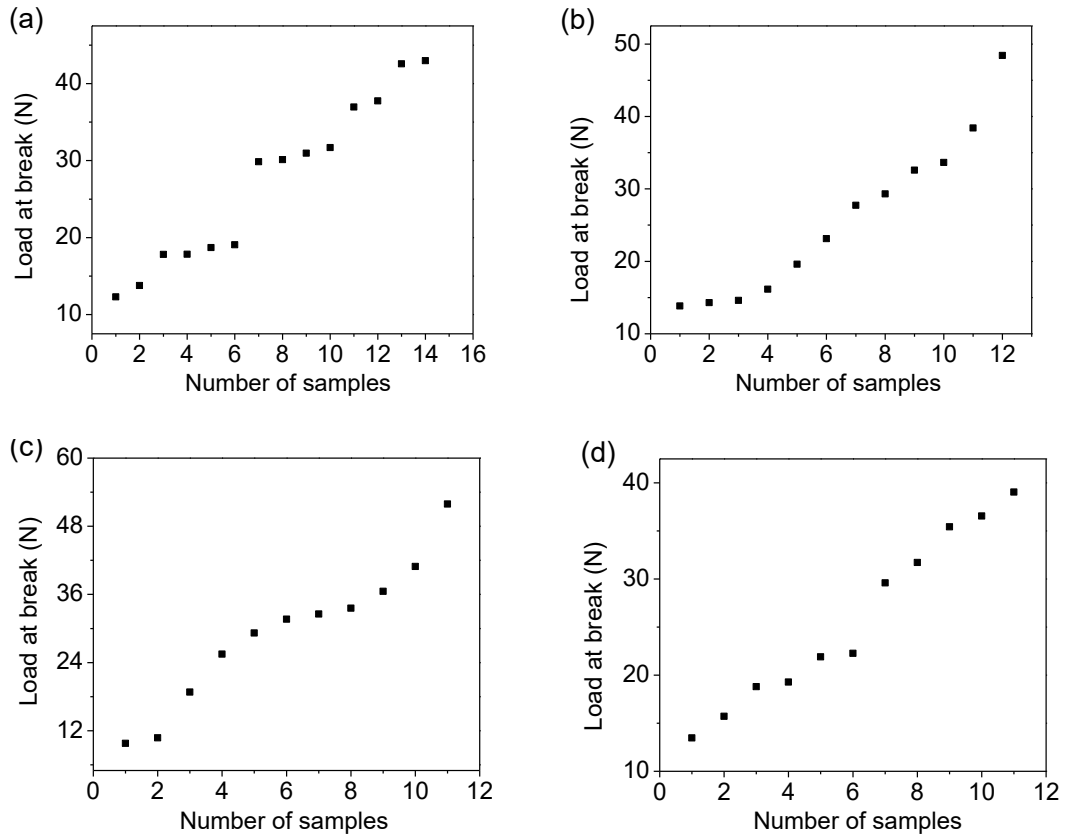

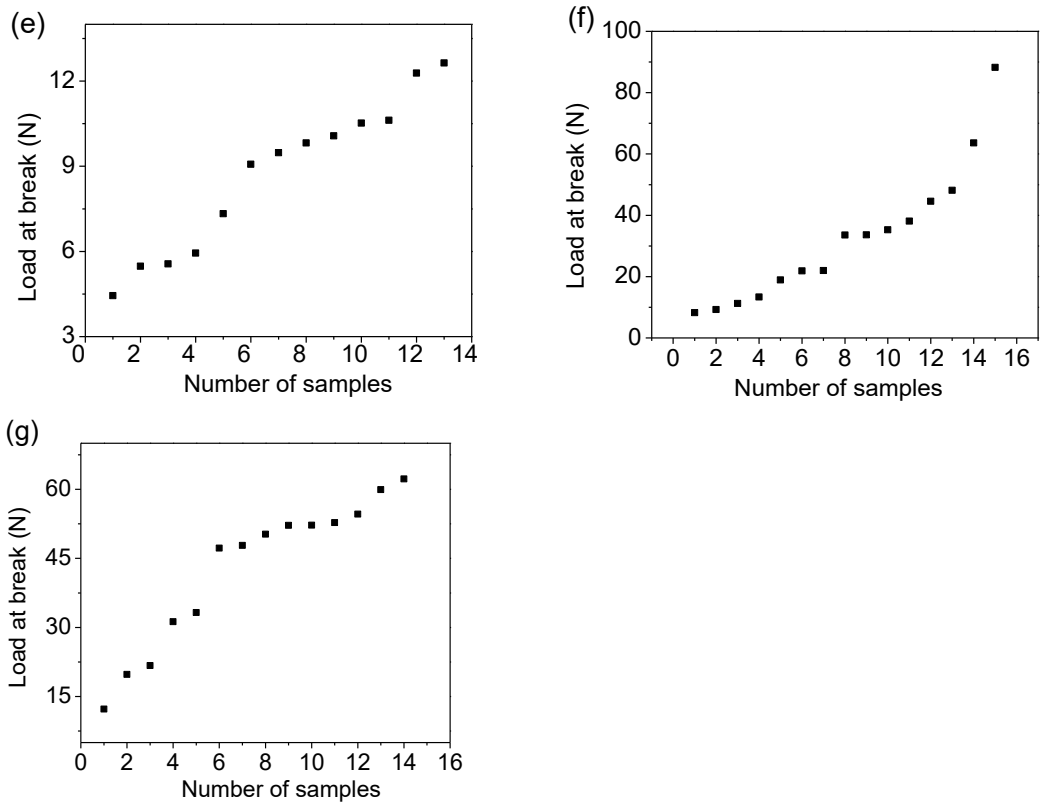

Figure A4.7. Histogram of load at break at same molar concentration in IPA-H2O for (a) PDA; (b) P(3C-DA);(c) P(4C-DA); (d) P(5C-DA); (e) P(12C-DA); (f) Catechol and propylamine; (g) Catechol and dodecylamine.

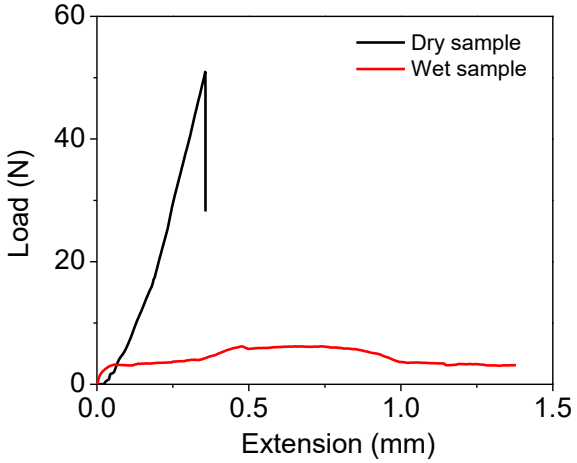

Figure A4.8. Typical load vs extension curve for lap shear testing.

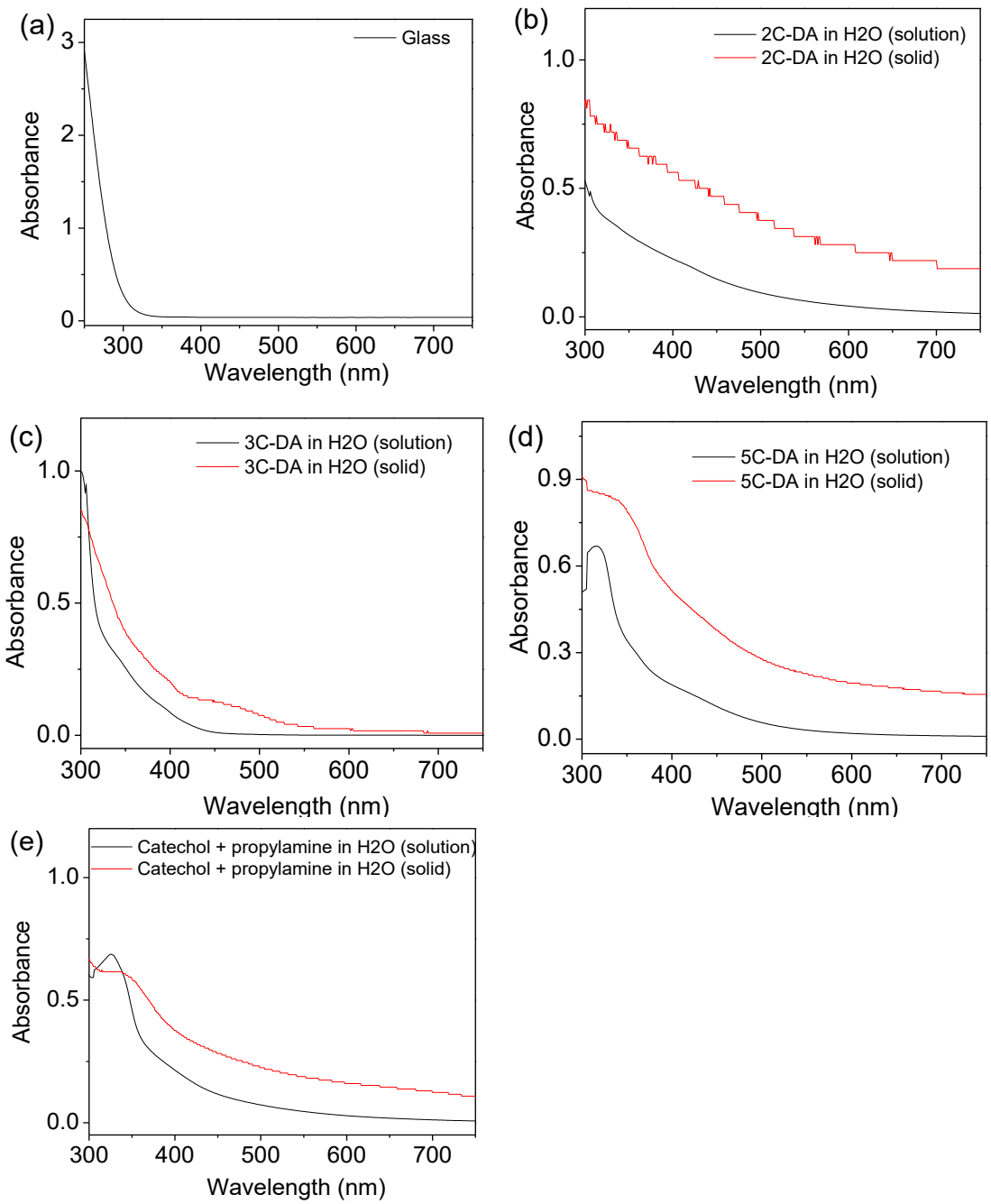

Figure A4.9. Normalized UV-Vis absorption spectra for (a) glass, (b) PDA, (c) P(3C-DA), (d) P(5C-DA), (e) Catechol and propylamine in H_2O (solution) (i.e., UV-Vis spectra of polymers formed from monomers (1 mM) polymerized in H_2O/NaOH after 24 h) and H_2O (solid) (i.e., UV-Vis spectra of polymers between glass slides for lap-shear testing prepared from monomers (6.7 mg/mL) polymerized in H_2O/NaOH).

Coating images and XPS result

(a)

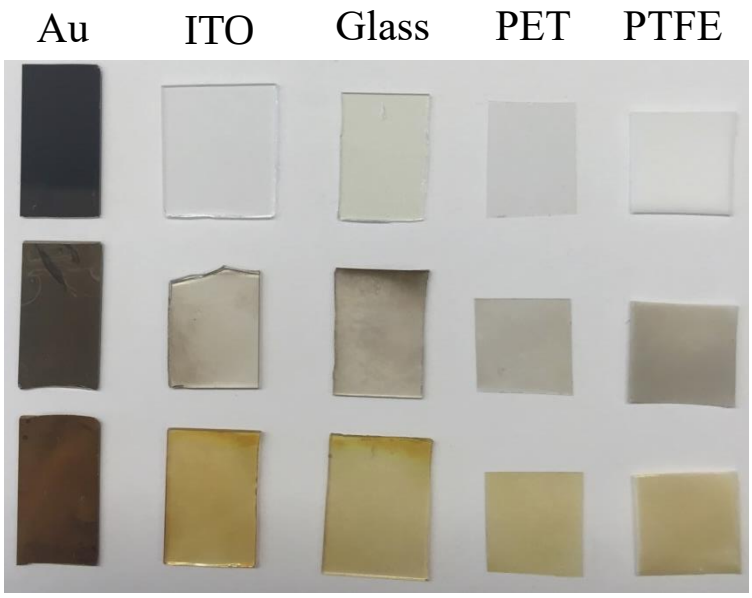

(b)

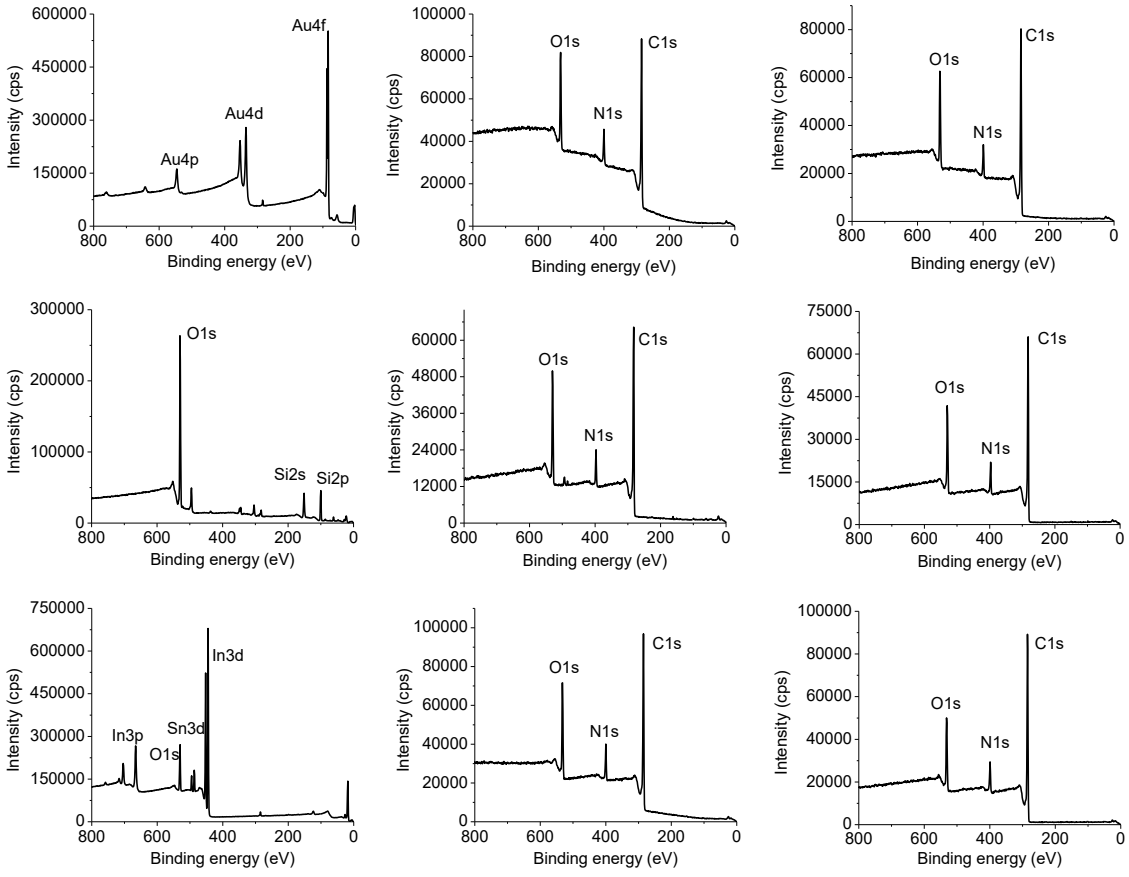

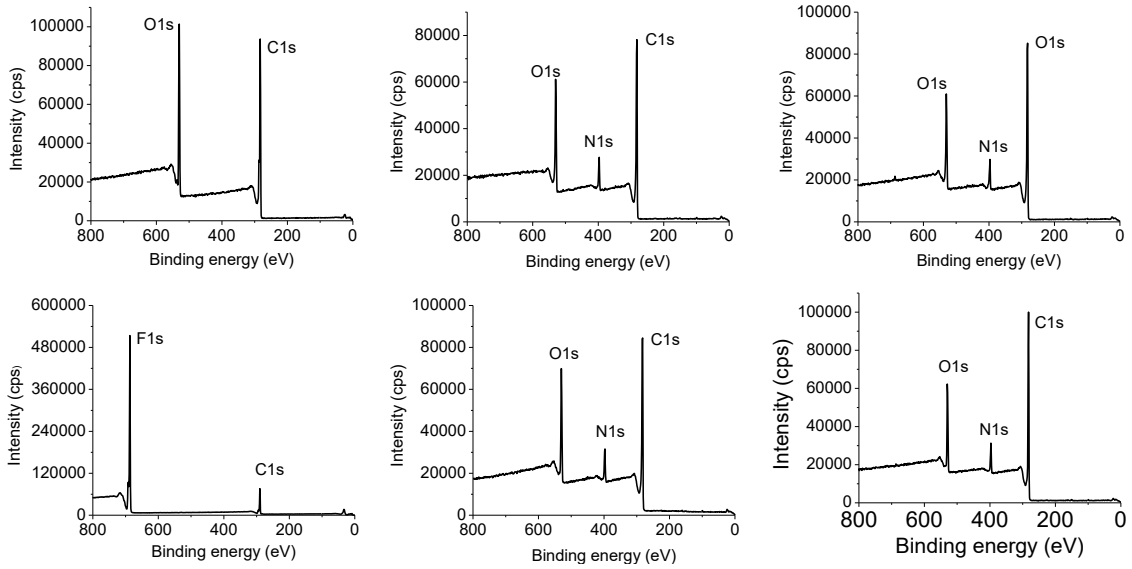

Figure A4.10. (a) Visual image of different substrates with no coating, coated with PDA and P(3C-DA); (b) XPS spectra of bare substrates (left), PDA coated substrates (middle) and P(3C-DA) coated substrates (right).

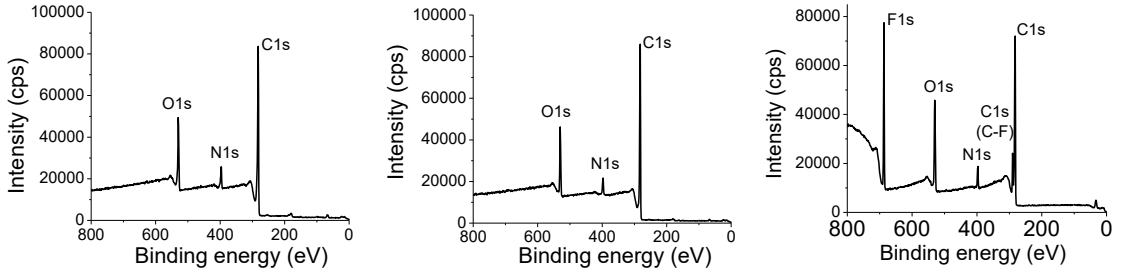

Figure A4.11. XPS spectra of P(4C-DA) coated PTFE (left), P(5C-DA) coated PTFE (middle) and Catechol and propylamine coated PTFE(right).

^{1}H and ^{13}C NMR spectra

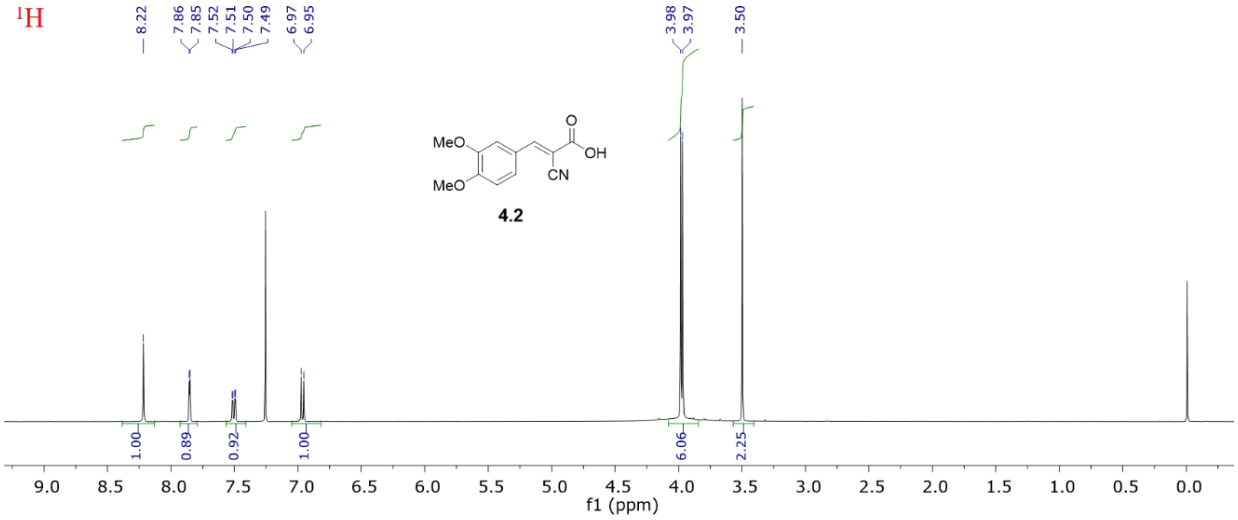

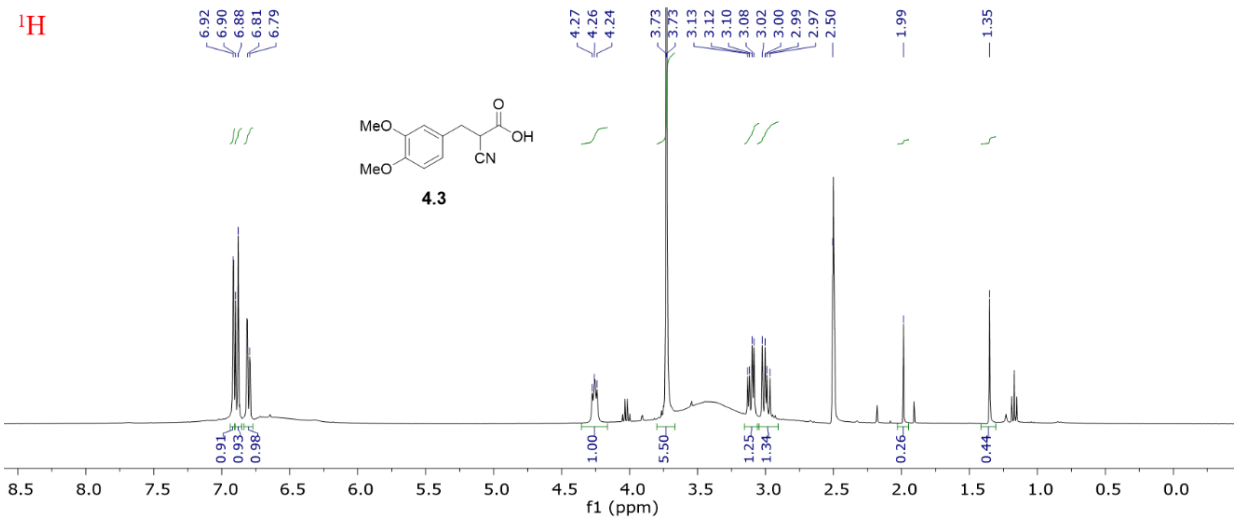

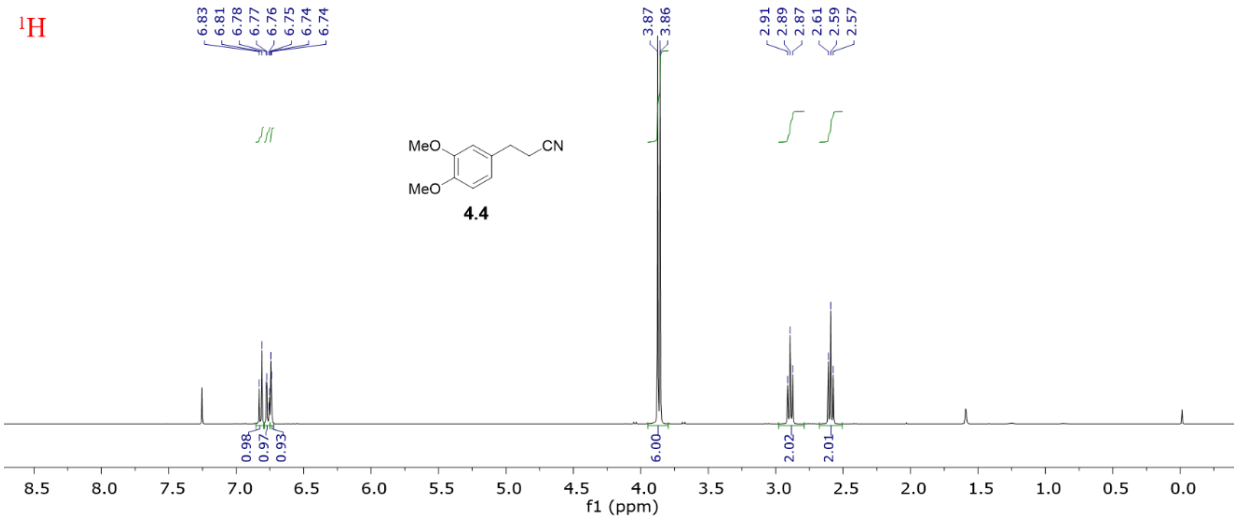

^{13}C

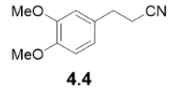

4.4

149.38
148.46
130.94
120.58
119.54
111.76
56.19
56.16
31.47
19.88

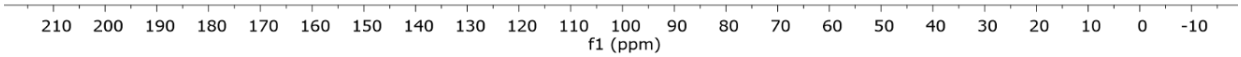

^{1}H

6.81
6.79
6.72
6.72
6.70
6.33
3.87
3.85
3.41
3.40
3.38
3.36
2.65
2.63
2.61
1.94
1.93
1.91
1.89
1.87

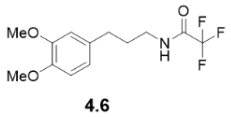

4.6

1.13
2.18
1.00
6.64
2.07
2.18
2.10

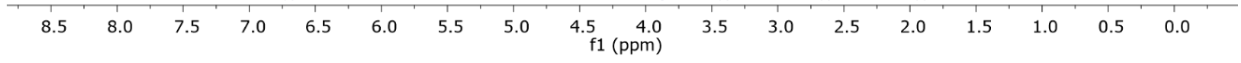

^{13}C

157.71
157.34
149.36
147.84
133.54
120.45
117.57
114.70
111.91
111.77
56.24
56.13
39.88
32.94
30.75
28.04

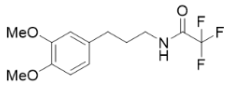

4.6

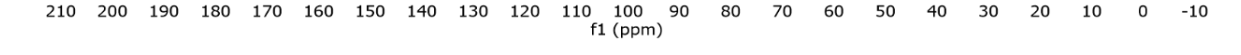

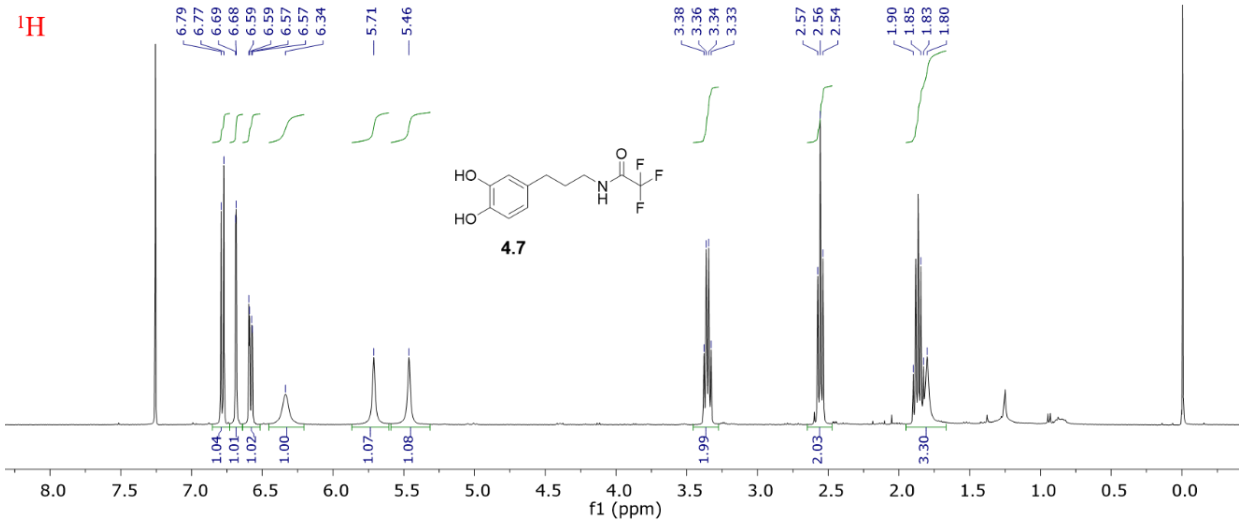
1H
6.79
6.77
6.69
6.68
6.59
6.59
6.57
6.57
6.34
5.71
5.46
3.38
3.36
3.34
3.33
2.57
2.56
2.54
1.90
1.85
1.83
1.80
HO
HO
O
F
F
F
N
H
4.7
1.04
1.01
1.02
1.00
1.07
1.08
1.99
2.03
3.30
8.0
7.5
7.0
6.5
6.0
5.5
5.0
4.5
4.0
3.5
3.0
2.5
2.0
1.5
1.0
0.5
0.0
f1 (ppm)

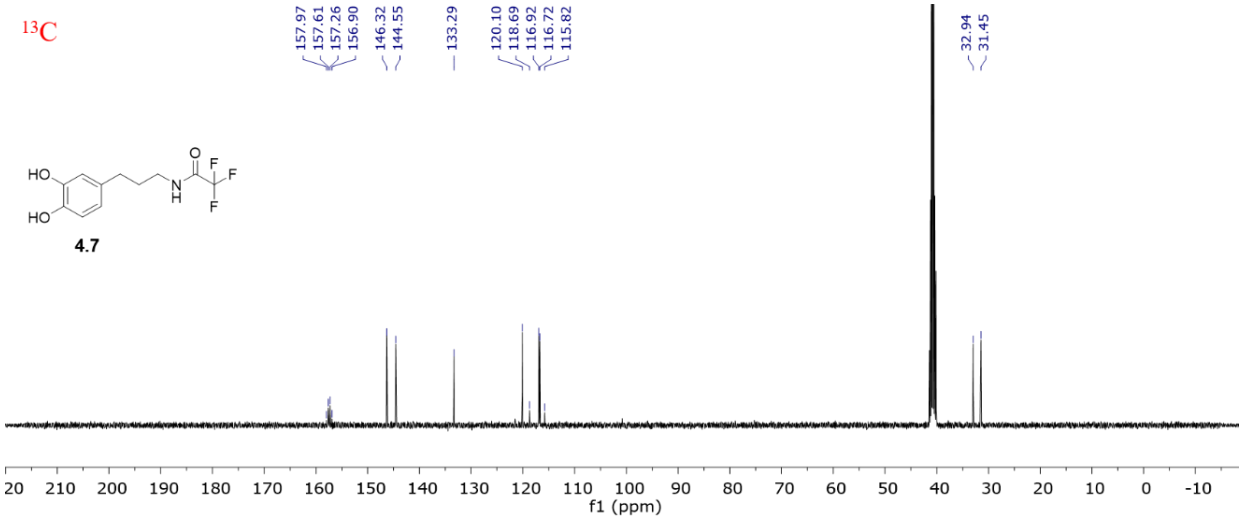
13C
157.97
157.61
157.26
156.90
146.32
144.55
133.29
120.10
118.69
116.92
116.72
115.82
32.94
31.45
HO
HO
O
F
F
F
N
H
4.7
20
210
200
190
180
170
160
150
140
130
120
110
100
90
80
70
60
50
40
30
20
10
0
-10
f1 (ppm)

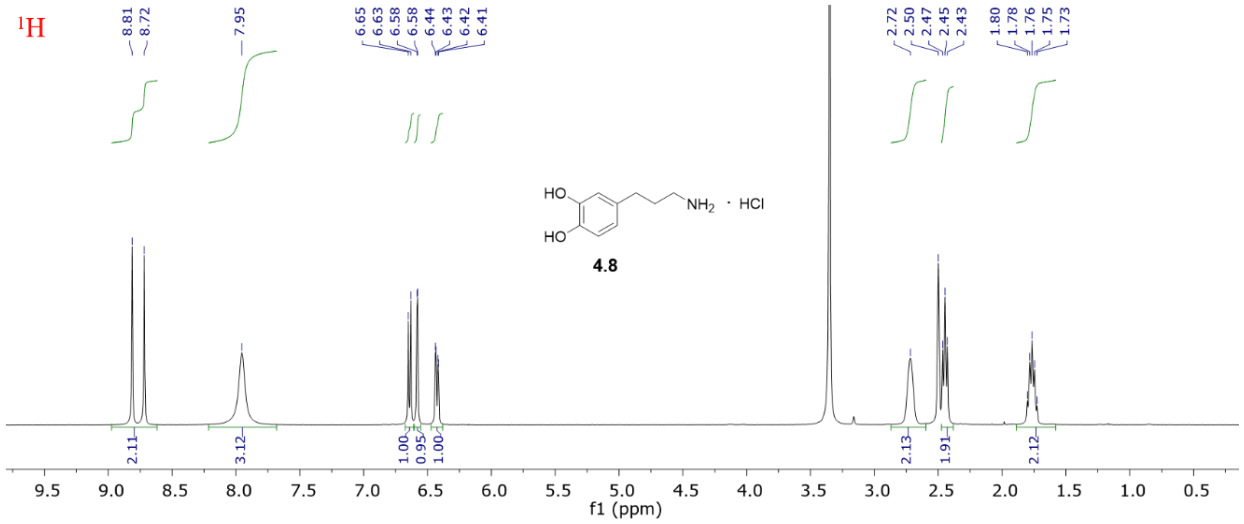
1H
8.81
8.72
7.95
6.65
6.63
6.58
6.58
6.44
6.43
6.42
6.41
2.72
2.50
2.47
2.45
2.43
1.80
1.78
1.76
1.75
1.73
HO
HO
NH2 · HCl
4.8
2.11
3.12
1.00
0.95
1.00
2.13
1.91
2.12
9.5
9.0
8.5
8.0
7.5
7.0
6.5
6.0
5.5
5.0
4.5
4.0
3.5
3.0
2.5
2.0
1.5
1.0
0.5
f1 (ppm)

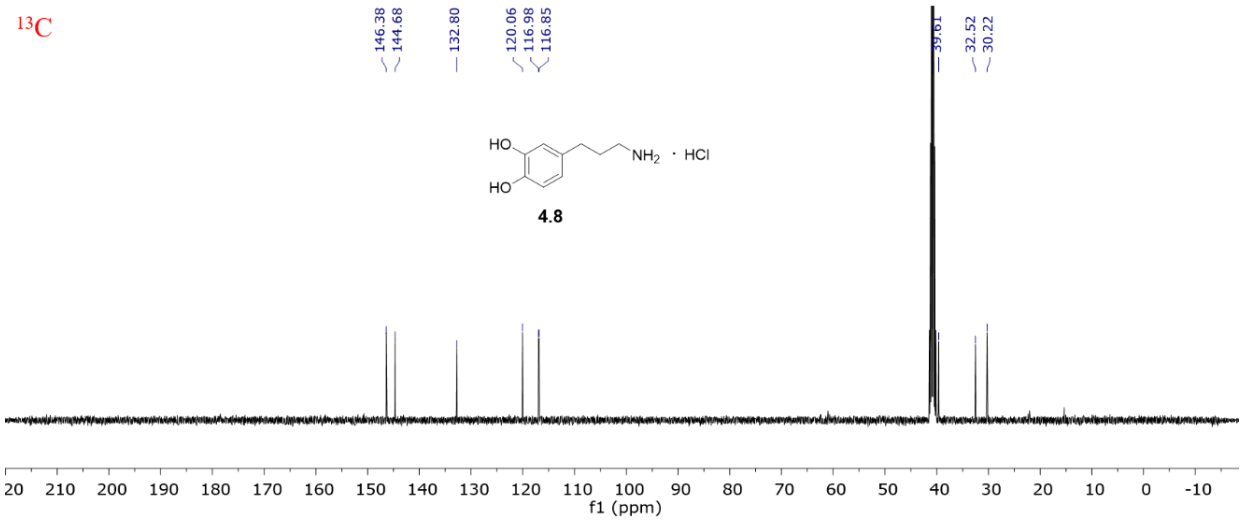
13C
146.38
144.68
132.80
120.06
116.98
116.85
39.61
32.52
30.22
HO
HO
NH2 · HCl
4.8
f1 (ppm)

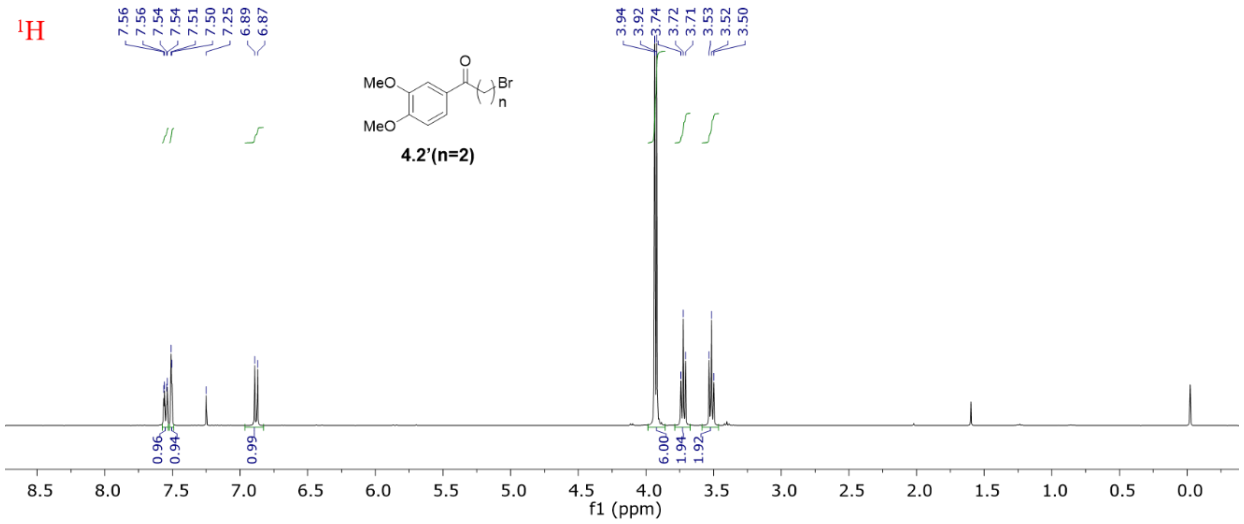
1H
7.56
7.56
7.54
7.54
7.51
7.50
7.25
6.89
6.87
3.94
3.92
3.74
3.72
3.71
3.53
3.52
3.50
MeO
MeO
Br
n
4.2'(n=2)
0.96
0.94
0.99
6.00
1.94
1.92
f1 (ppm)

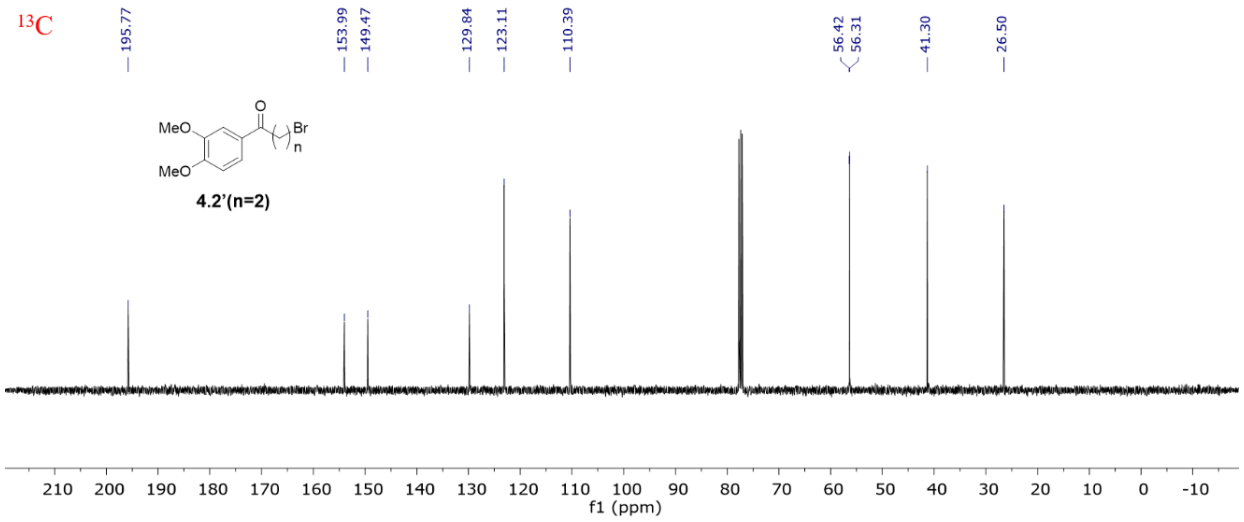
13C
195.77
153.99
149.47
129.84
123.11
110.39
56.42
56.31
41.30
26.50
MeO
MeO
Br
n
4.2'(n=2)
f1 (ppm)

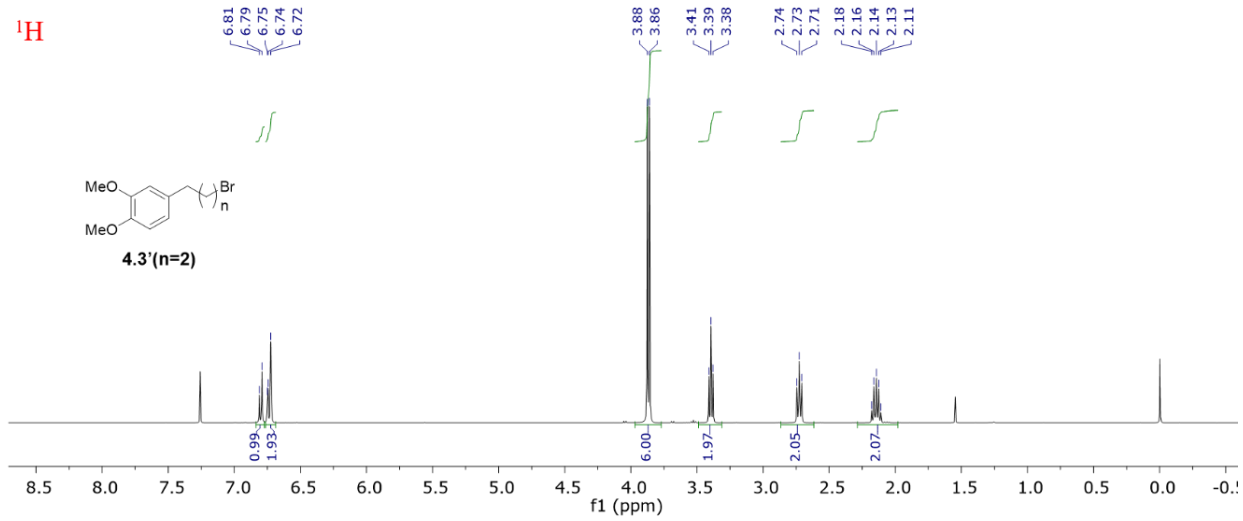
1H
6.81
6.79
6.75
6.74
6.72
3.88
3.86
3.41
3.39
3.38
2.74
2.73
2.71
2.18
2.16
2.14
2.13
2.11
MeO
MeO
Br
n
4.3'(n=2)
0.99
1.93
6.00
1.97
2.05
2.07
f1 (ppm)

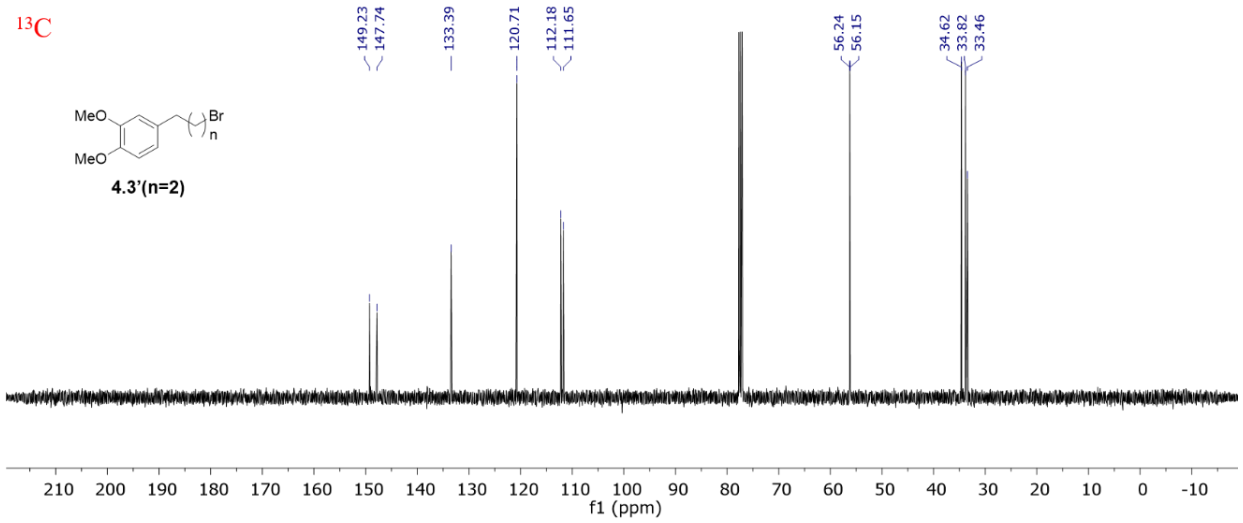
13C
149.23
147.74
133.39
120.71
112.18
111.65
56.24
56.15
34.62
33.82
33.46
MeO
MeO
Br
n
4.3'(n=2)
f1 (ppm)

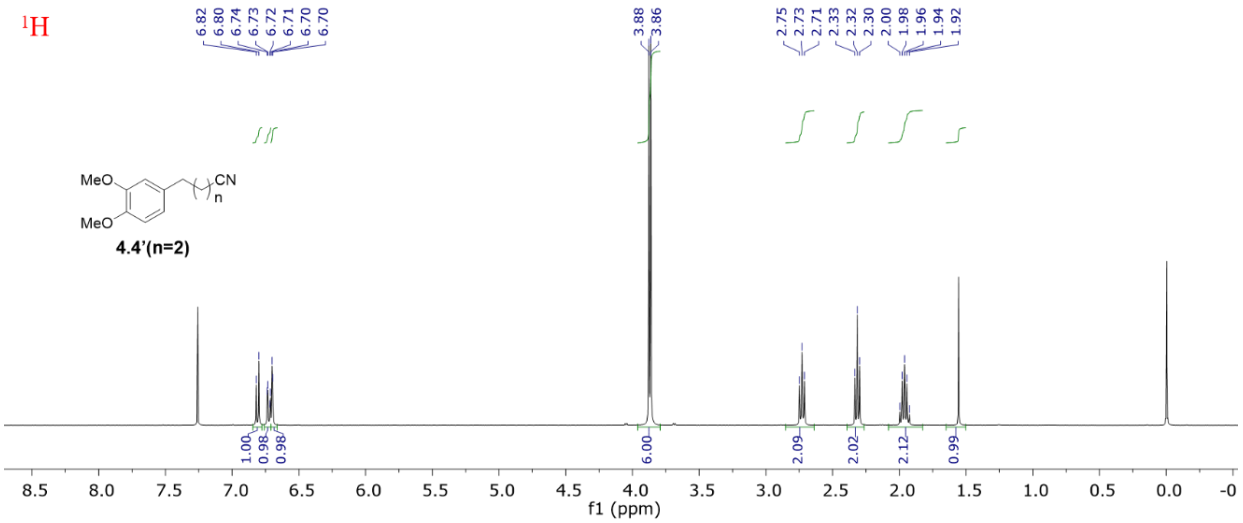
1H
6.82
6.80
6.74
6.73
6.72
6.71
6.70
6.70
3.88
3.86
2.75
2.73
2.71
2.33
2.32
2.30
2.00
1.98
1.96
1.94
1.92
MeO
MeO
CN
n
4.4'(n=2)
1.00
0.98
0.98
6.00
2.09
2.02
2.12
0.99
f1 (ppm)

^{13}C

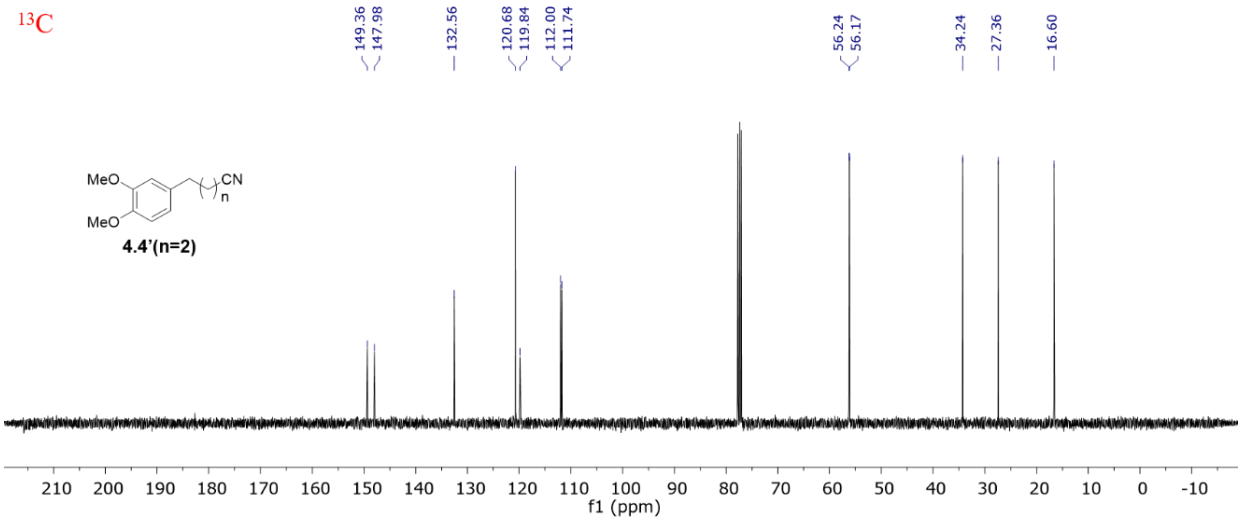
149.36
147.98
132.56
120.68
119.84
112.00
111.74
56.24
56.17
34.24
27.36
16.60
MeO
MeO
CN
n
4.4'(n=2)
210 200 190 180 170 160 150 140 130 120 110 100 90 80 70 60 50 40 30 20 10 0 -10
f1 (ppm)

^{1}H

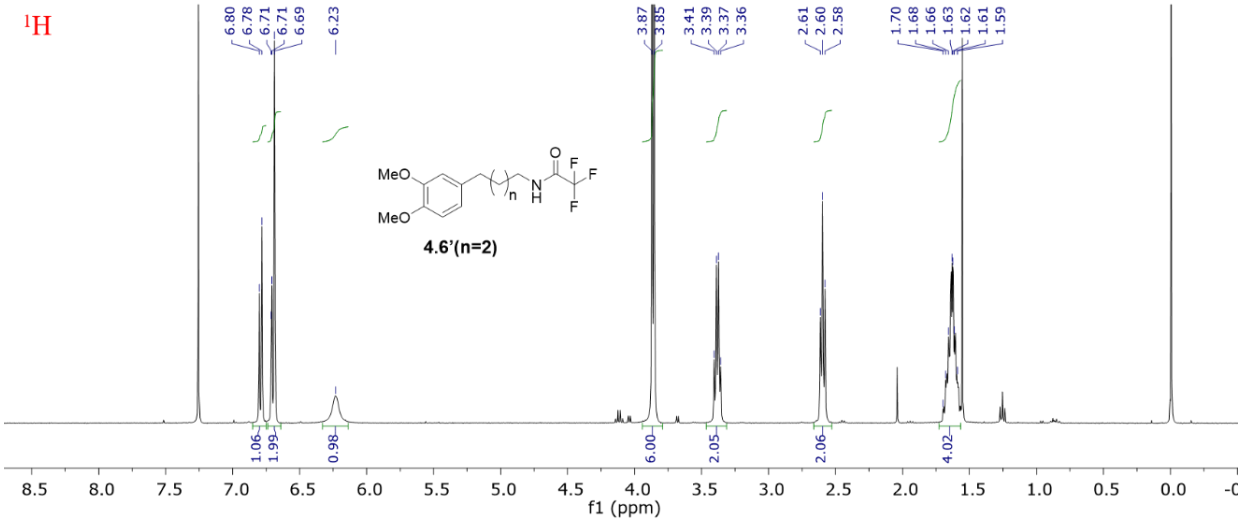
6.80
6.78
6.71
6.71
6.69
6.23
3.87
3.85
3.41
3.39
3.37
3.36
2.61
2.60
2.58
1.70
1.68
1.66
1.63
1.62
1.61
1.59
MeO
MeO
O
F
F
F
N
H
n
4.6'(n=2)
1.06
1.99
0.98
6.00
2.05
2.06
4.02
8.5 8.0 7.5 7.0 6.5 6.0 5.5 5.0 4.5 4.0 3.5 3.0 2.5 2.0 1.5 1.0 0.5 0.0
f1 (ppm)

^{13}C

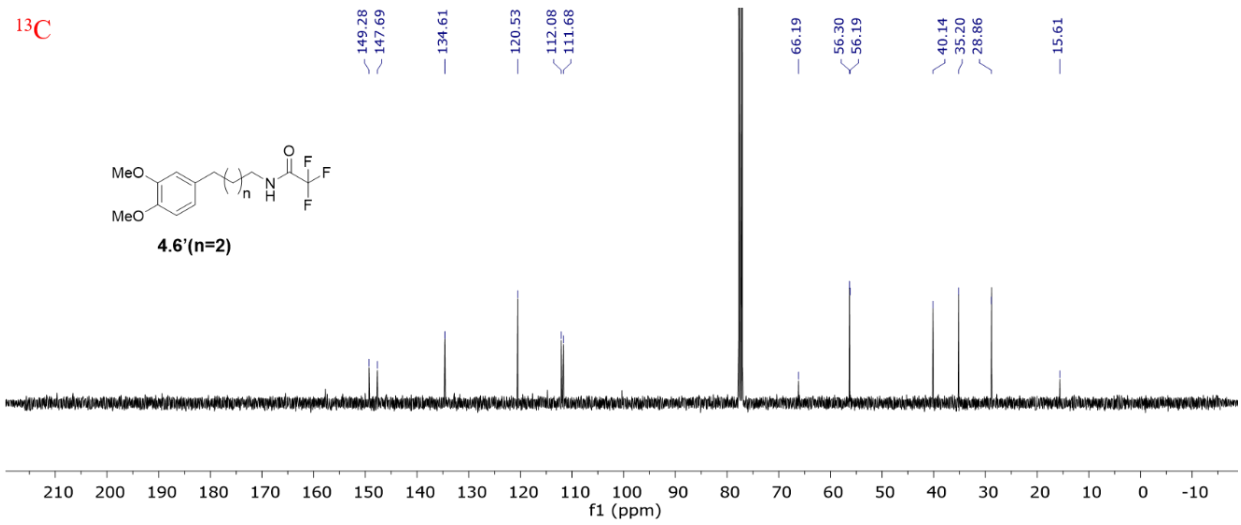
149.28
147.69
134.61
120.53
112.08
111.68
66.19
56.30
56.19
40.14
35.20
28.86
15.61
MeO
MeO
O
F
F
F
N
H
n
4.6'(n=2)
210 200 190 180 170 160 150 140 130 120 110 100 90 80 70 60 50 40 30 20 10 0 -10
f1 (ppm)

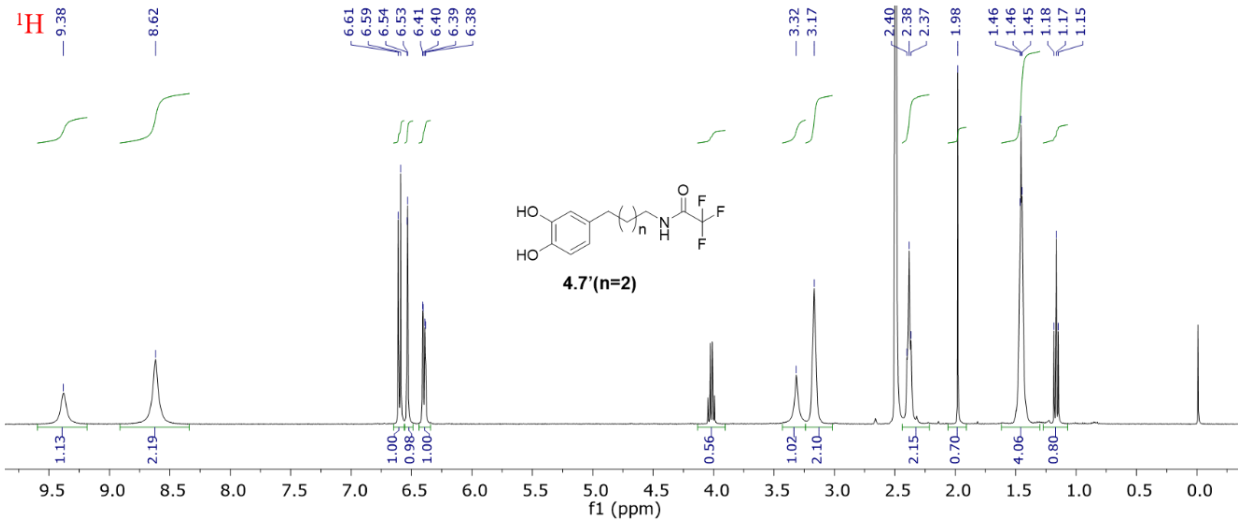
1H
9.38
8.62
6.61
6.59
6.54
6.53
6.41
6.40
6.39
6.38
3.32
3.17
2.40
2.38
2.37
1.98
1.46
1.46
1.45
1.18
1.17
1.15
HO
HO
n
N
H
O
F
F
F
4.7'(n=2)
1.13
2.19
1.00
0.98
1.00
0.56
1.02
2.10
2.15
0.70
4.06
0.80
f1 (ppm)

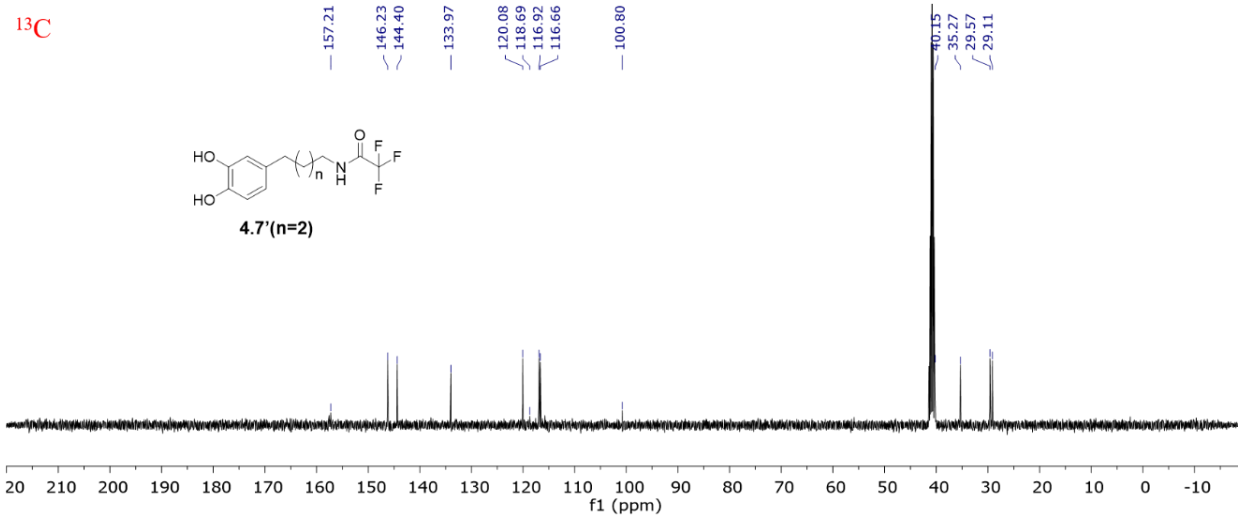
13C
157.21
146.23
144.40
133.97
120.08
118.69
116.92
116.66
100.80
40.15
35.27
29.57
29.11
HO
HO
n
N
H
O
F
F
F
4.7'(n=2)
f1 (ppm)

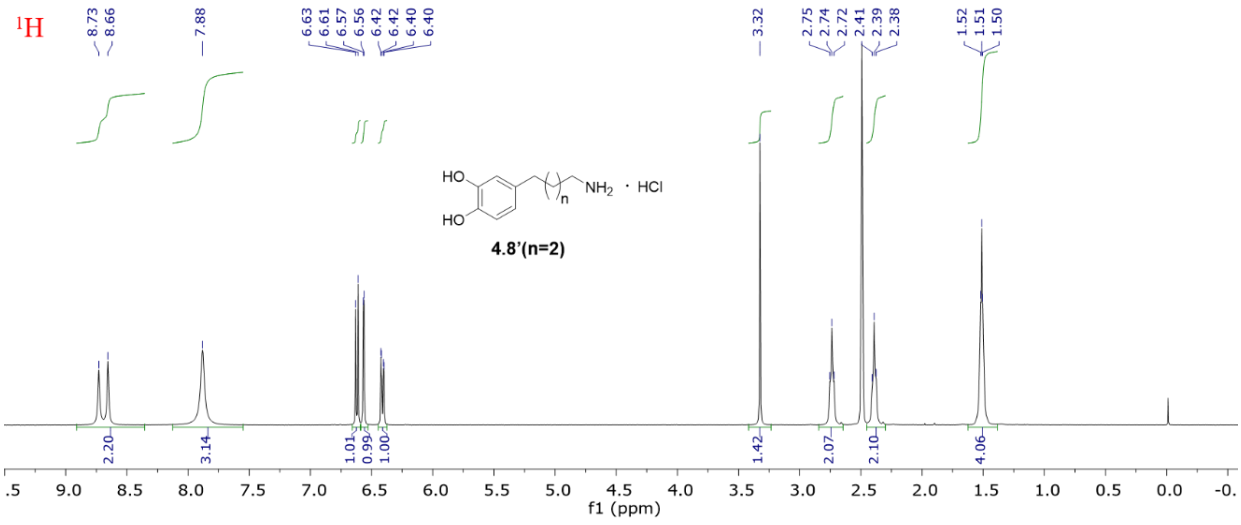
1H
8.73
8.66
7.88
6.63
6.61
6.57
6.56
6.42
6.42
6.40
6.40
3.32
2.75
2.74
2.72
2.41
2.39
2.38
1.52
1.51
1.50
HO
HO
n
NH2 · HCl
4.8'(n=2)
2.20
3.14
1.01
0.99
1.00
1.42
2.07
2.10
4.06
f1 (ppm)

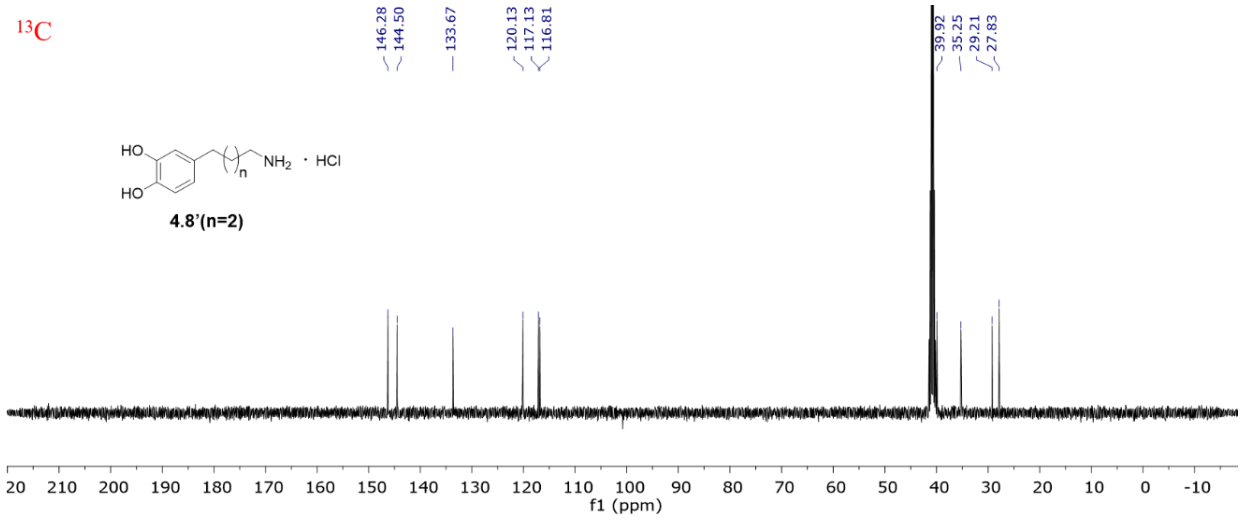
13C
146.28
144.50
133.67
120.13
117.13
116.81
39.92
35.25
29.21
27.83
HO
HO
NH2 · HCl
n
4.8'(n=2)
f1 (ppm)

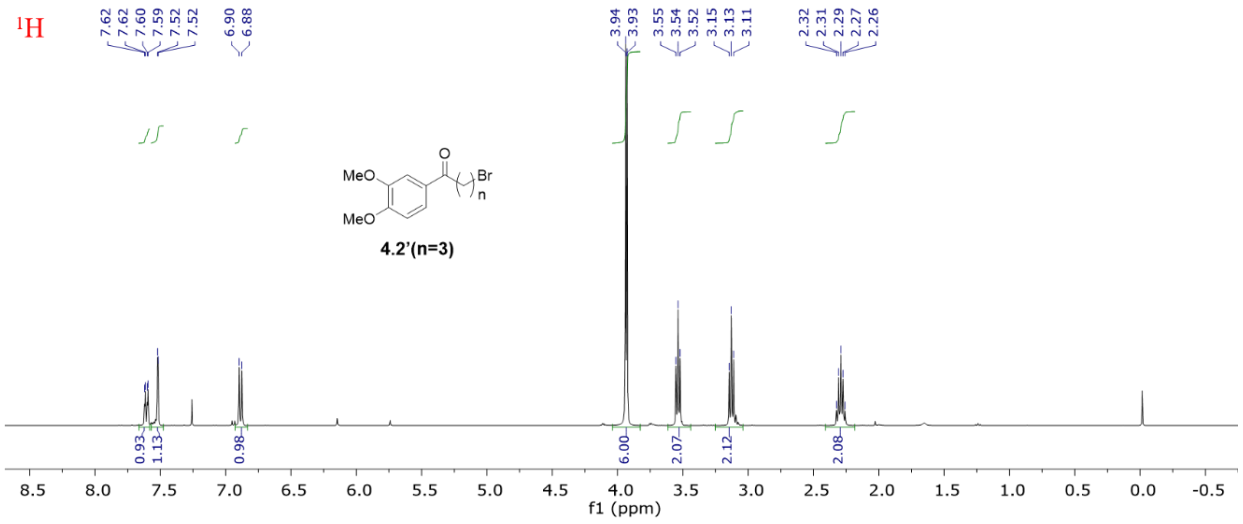
1H
7.62
7.62
7.60
7.59
7.52
7.52
6.90
6.88
3.94
3.93
3.55
3.54
3.52
3.15
3.13
3.11
2.32
2.31
2.29
2.27
2.26
MeO
MeO
O
Br
n
4.2'(n=3)
0.93
1.13
0.98
6.00
2.07
2.12
2.08
f1 (ppm)

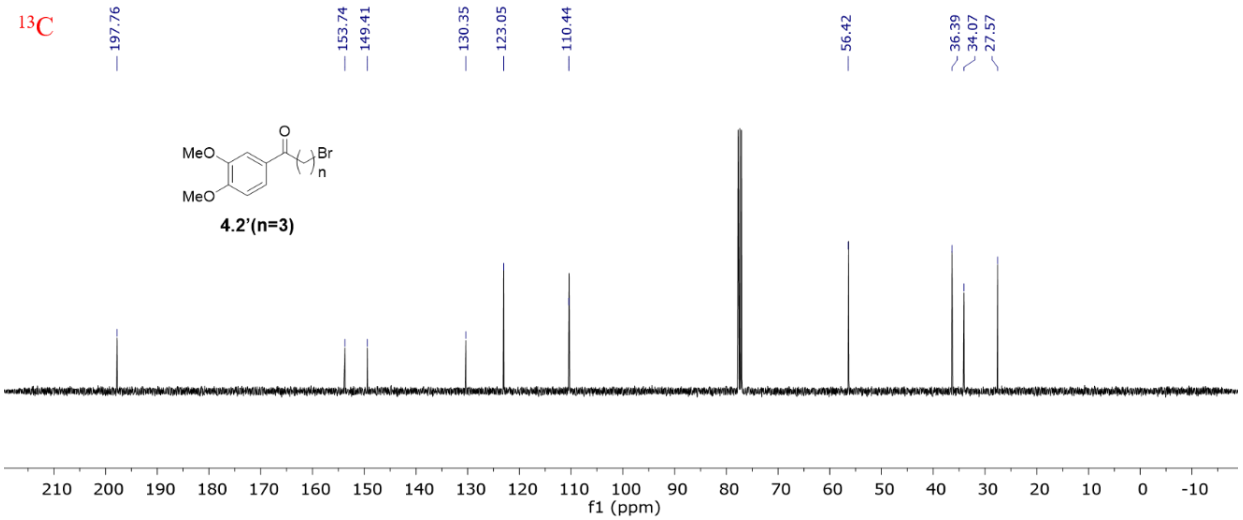
13C
197.76
153.74
149.41
130.35
123.05
110.44
56.42
36.39
34.07
27.57
MeO
MeO
O
Br
n
4.2'(n=3)
f1 (ppm)

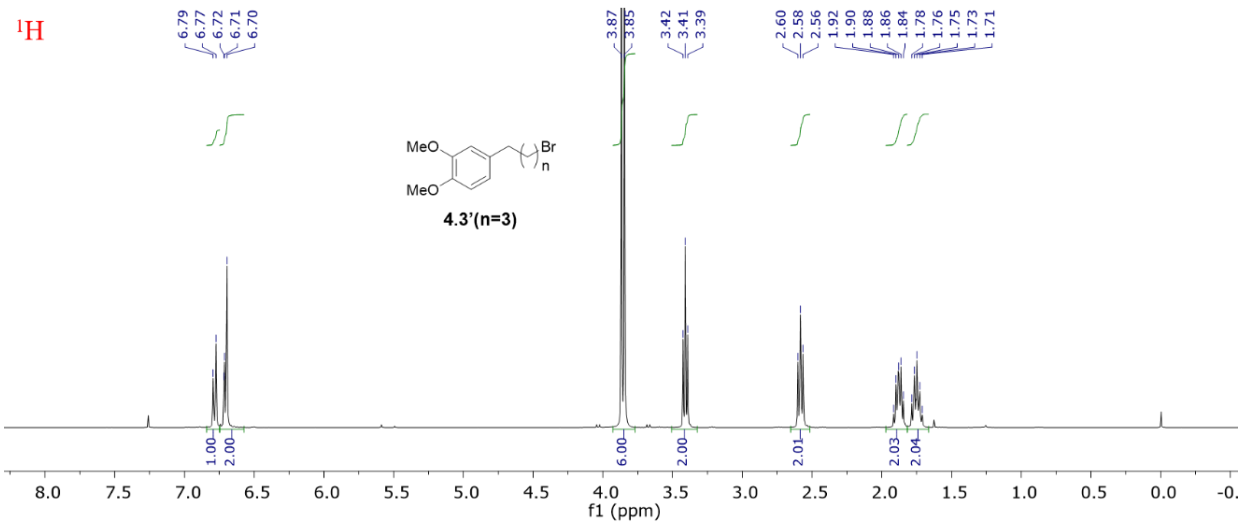
1H
6.79
6.77
6.72
6.71
6.70
3.87
3.85
3.42
3.41
3.39
2.60
2.58
2.56
1.92
1.90
1.88
1.86
1.84
1.78
1.76
1.75
1.73
1.71
MeO
MeO
Br
n
4.3'(n=3)
1.00
2.00
6.00
2.00
2.01
2.03
2.04
f1 (ppm)

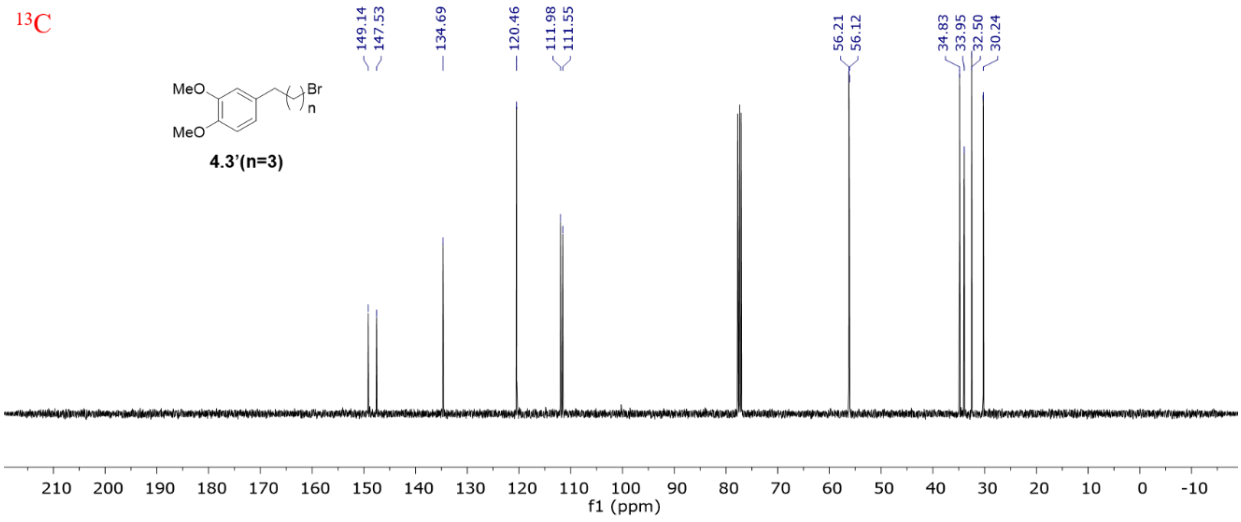
13C
149.14
147.53
134.69
120.46
111.98
111.55
56.21
56.12
34.83
33.95
32.50
30.24
MeO
MeO
Br
n
4.3'(n=3)
f1 (ppm)

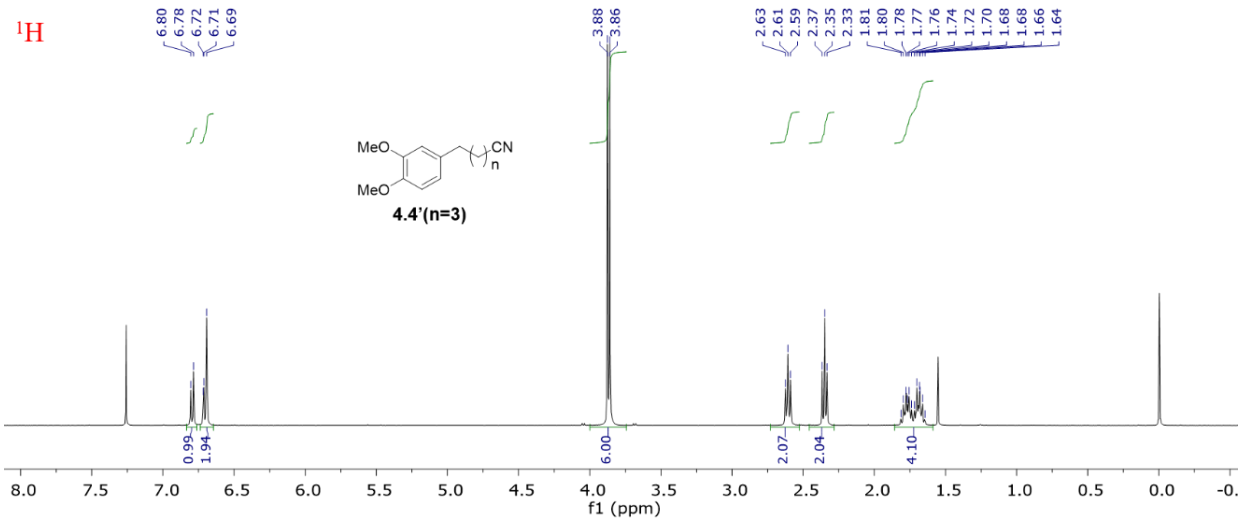
1H
6.80
6.78
6.72
6.71
6.69
3.88
3.86
2.63
2.61
2.59
2.37
2.35
2.33
1.81
1.80
1.78
1.77
1.76
1.74
1.72
1.70
1.68
1.68
1.66
1.64
MeO
MeO
CN
n
4.4'(n=3)
0.99
1.94
6.00
2.07
2.04
4.10
f1 (ppm)

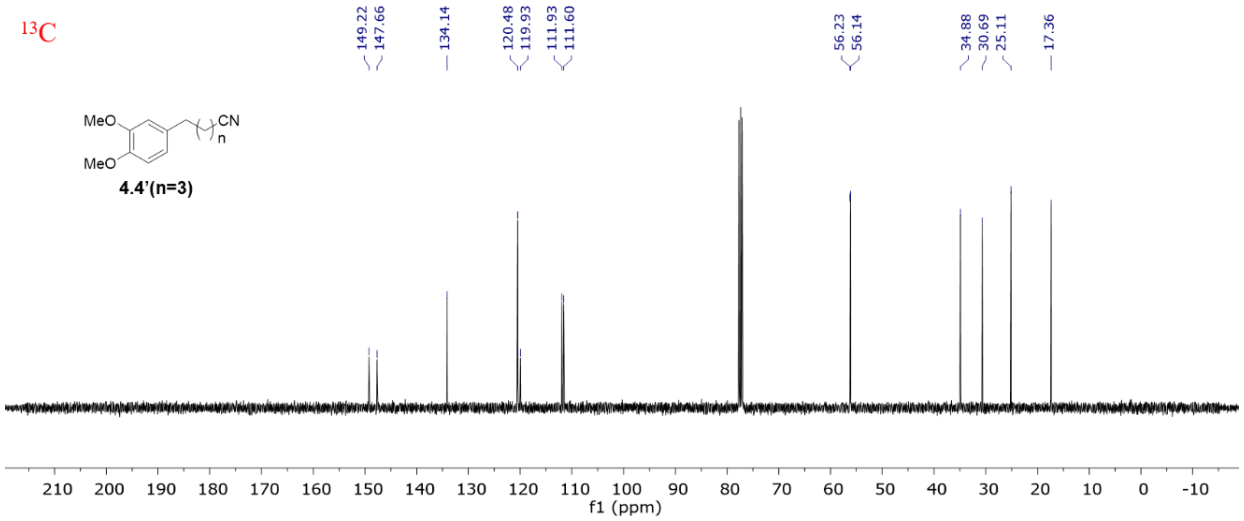
13C
149.22
147.66
134.14
120.48
119.93
111.93
111.60
56.23
56.14
34.88
30.69
25.11
17.36
MeO
MeO
CN
n
4.4'(n=3)
210 200 190 180 170 160 150 140 130 120 110 100 90 80 70 60 50 40 30 20 10 0 -10
f1 (ppm)

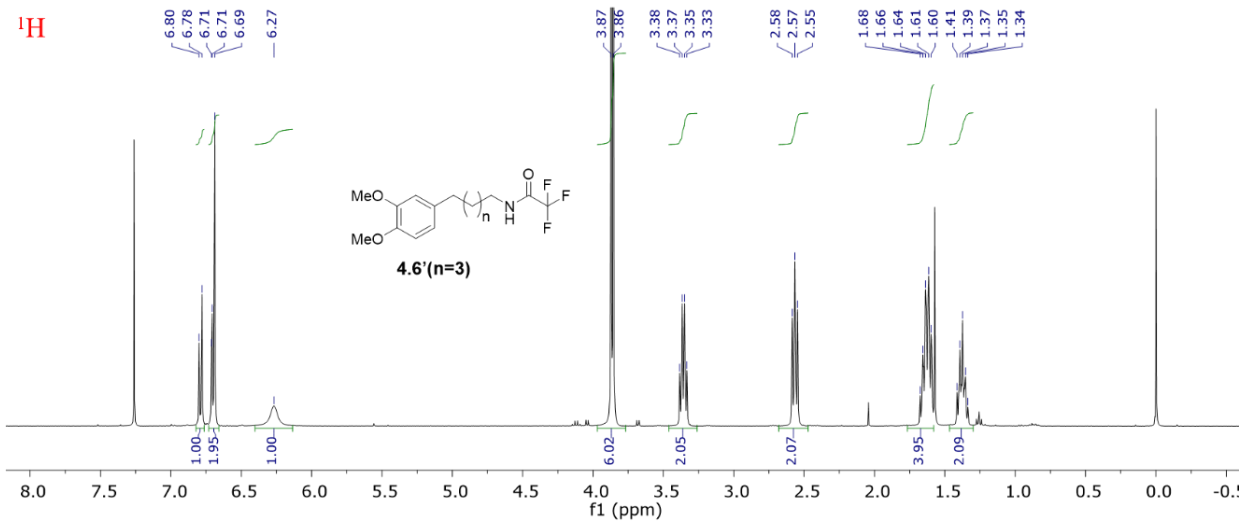
1H
6.80
6.78
6.71
6.71
6.69
6.27
3.87
3.86
3.38
3.37
3.35
3.33
2.58
2.57
2.55
1.68
1.66
1.64
1.61
1.60
1.41
1.39
1.37
1.35
1.34
MeO
MeO
n
N
H
O
F
F
F
4.6'(n=3)
1.00
1.95
1.00
6.02
2.05
2.07
3.95
2.09
8.0 7.5 7.0 6.5 6.0 5.5 5.0 4.5 4.0 3.5 3.0 2.5 2.0 1.5 1.0 0.5 0.0
f1 (ppm)

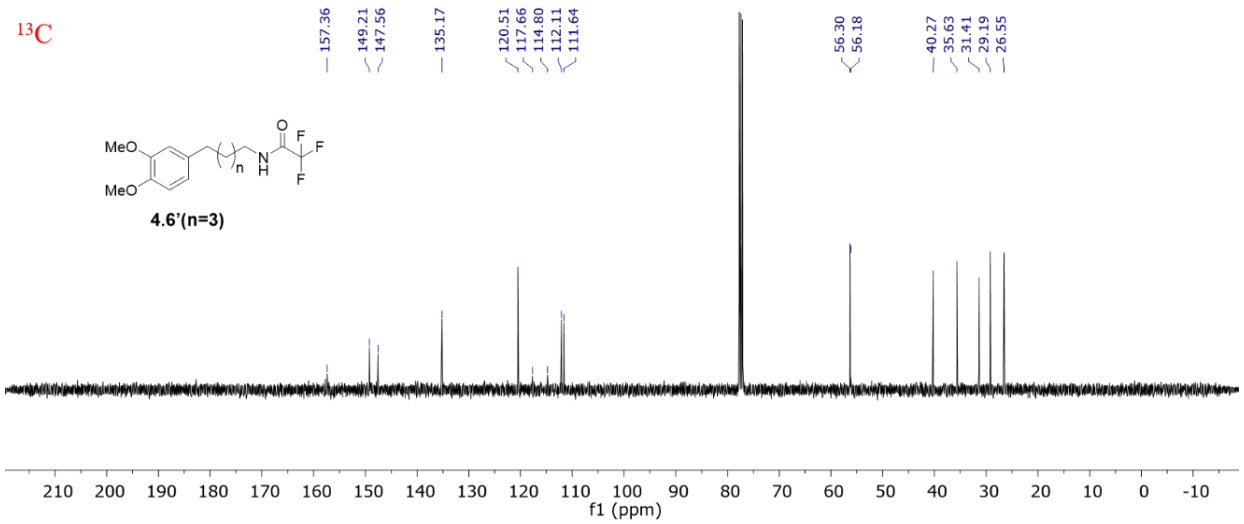
13C
157.36
149.21
147.56
135.17
120.51
117.66
114.80
112.11
111.64
56.30
56.18
40.27
35.63
31.41
29.19
26.55
MeO
MeO
n
N
H
O
F
F
F
4.6'(n=3)
210 200 190 180 170 160 150 140 130 120 110 100 90 80 70 60 50 40 30 20 10 0 -10
f1 (ppm)

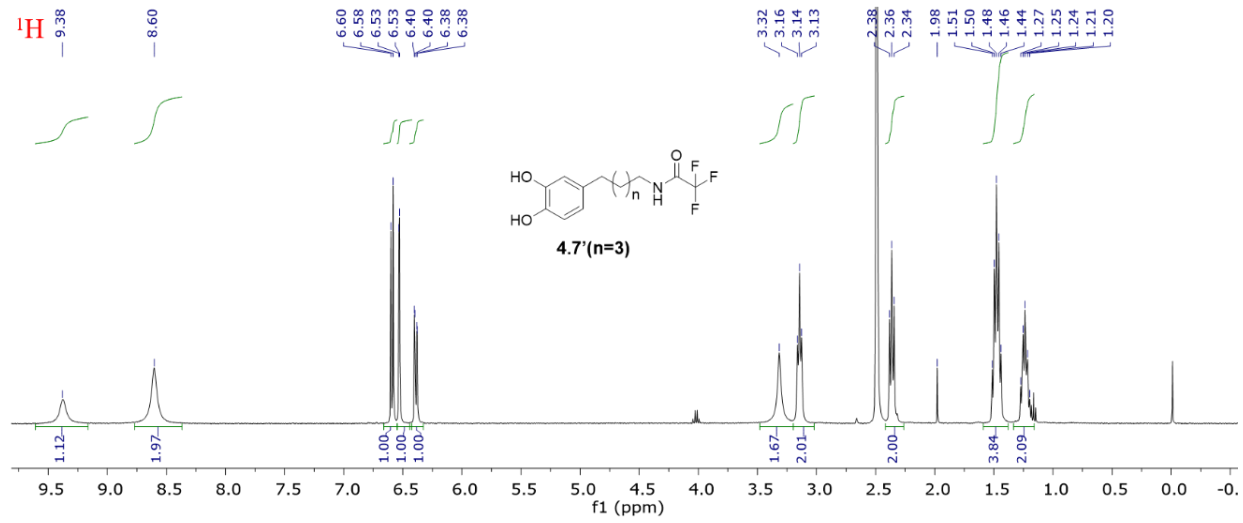
1H
9.38
8.60
6.60
6.58
6.53
6.53
6.40
6.40
6.38
6.38
3.32
3.16
3.14
3.13
2.38
2.36
2.34
1.98
1.51
1.50
1.48
1.46
1.44
1.27
1.25
1.24
1.21
1.20
HO
HO
n
N
H
O
F
F
F
4.7'(n=3)
1.12
1.97
1.00
1.00
1.00
1.67
2.01
2.00
3.84
2.09
f1 (ppm)

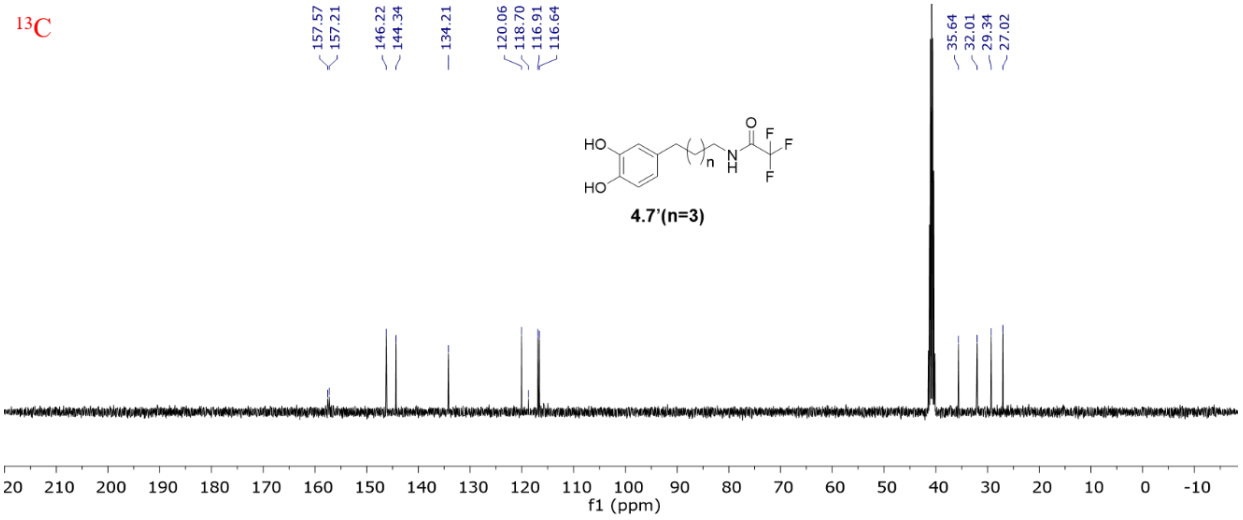
13C
157.57
157.21
146.22
144.34
134.21
120.06
118.70
116.91
116.64
35.64
32.01
29.34
27.02
HO
HO
n
N
H
O
F
F
F
4.7'(n=3)
f1 (ppm)

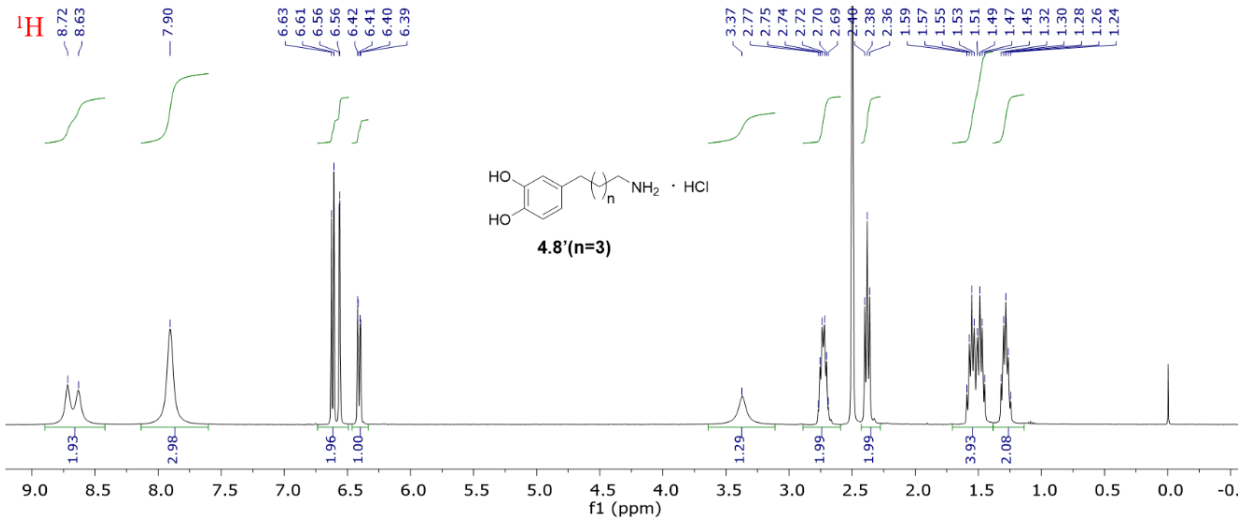
1H
8.72
8.63
7.90
6.63
6.61
6.56
6.56
6.42
6.41
6.40
6.39
3.37
2.77
2.75
2.74
2.72
2.70
2.69
2.40
2.38
2.36
1.59
1.57
1.55
1.53
1.51
1.49
1.47
1.45
1.32
1.30
1.28
1.26
1.24
HO
HO
n
NH2 · HCl
4.8'(n=3)
1.93
2.98
1.96
1.00
1.29
1.99
1.99
3.93
2.08
f1 (ppm)

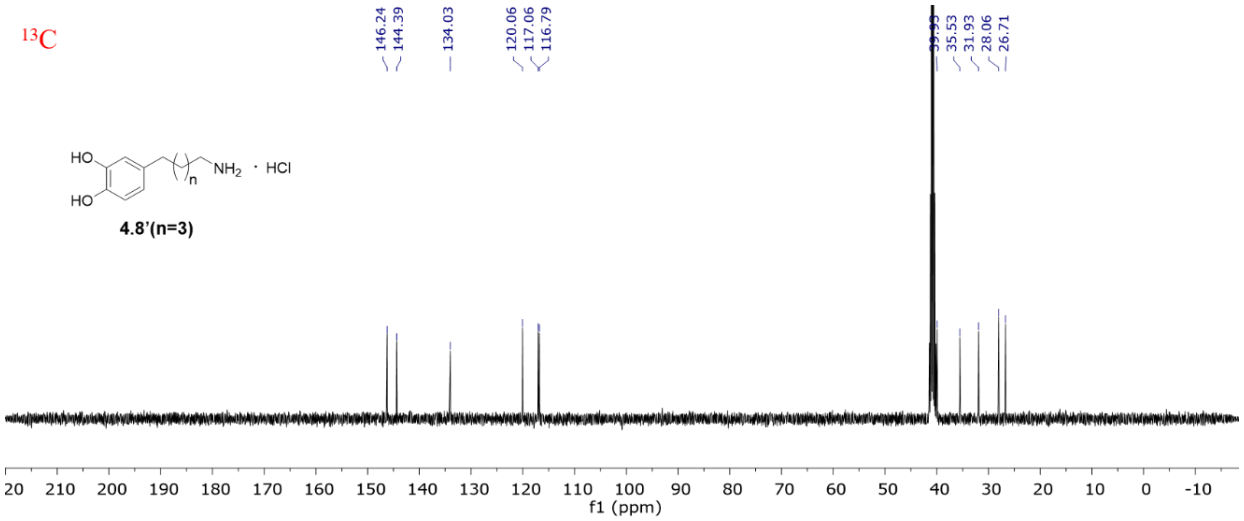
13C
146.24
144.39
134.03
120.06
117.06
116.79
39.93
35.53
31.93
28.06
26.71
HO
HO
NH2 · HCl
n
4.8'(n=3)
f1 (ppm)

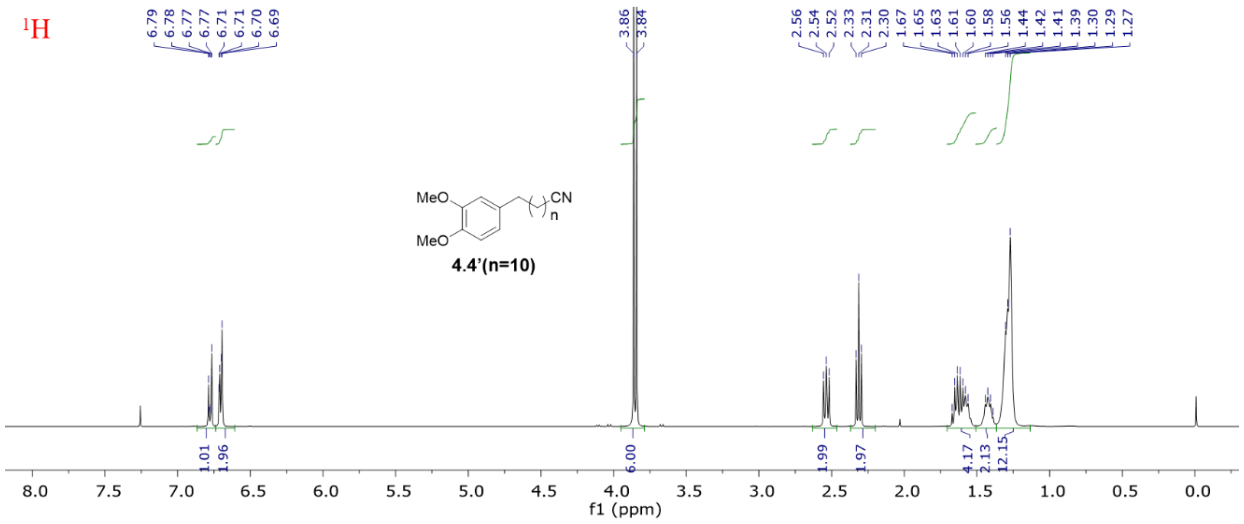
1H
6.79
6.78
6.77
6.77
6.71
6.71
6.70
6.69
3.86
3.84
2.56
2.54
2.52
2.33
2.31
2.30
1.67
1.65
1.63
1.61
1.60
1.58
1.56
1.44
1.42
1.41
1.39
1.30
1.29
1.27
MeO
MeO
CN
n
4.4'(n=10)
1.01
1.96
6.00
1.99
1.97
4.17
2.13
12.15
f1 (ppm)

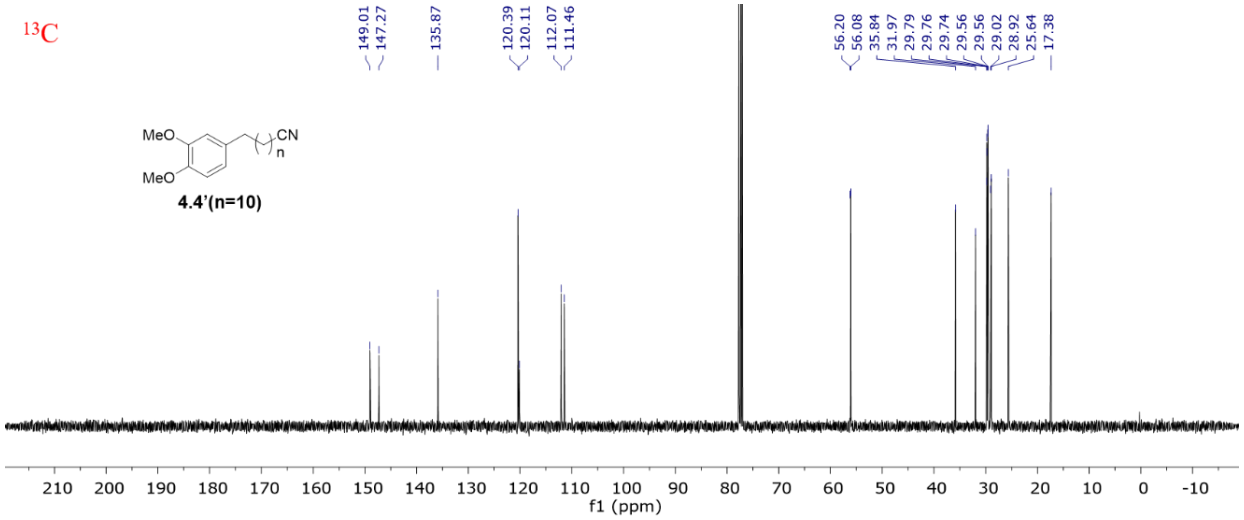
13C
149.01
147.27
135.87
120.39
120.11
112.07
111.46
56.20
56.08
35.84
31.97
29.79
29.76
29.74
29.56
29.56
29.02
28.92
25.64
17.38
MeO
MeO
CN
n
4.4'(n=10)
f1 (ppm)

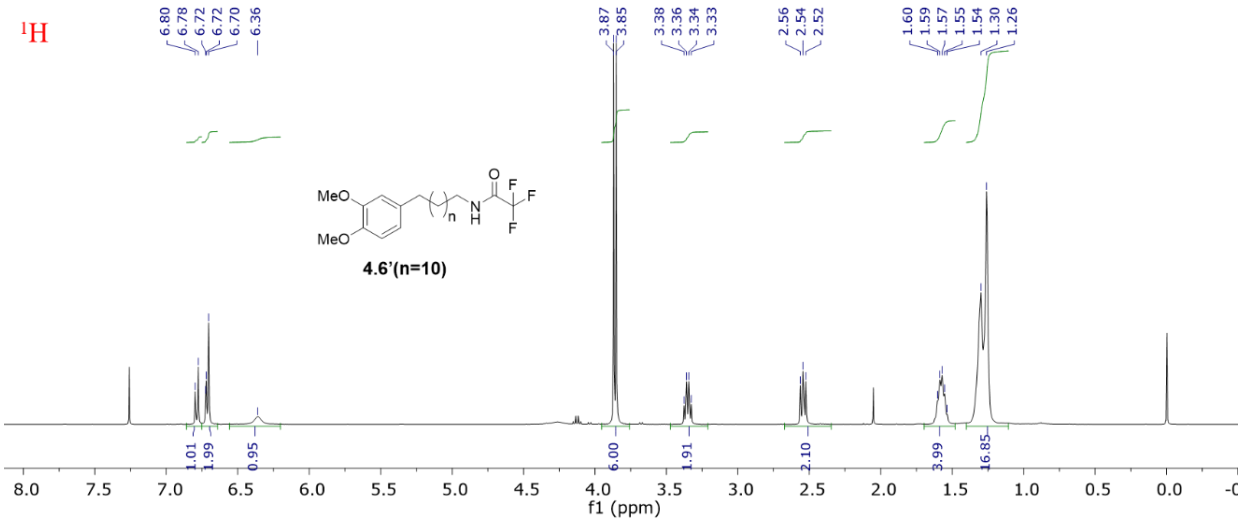
1H
6.80
6.78
6.72
6.72
6.70
6.36
3.87
3.85
3.38
3.36
3.34
3.33
2.56
2.54
2.52
1.60
1.59
1.57
1.55
1.54
1.30
1.26
MeO
MeO
n
N
H
O
F
F
F
4.6'(n=10)
1.01
1.99
0.95
6.00
1.91
2.10
3.99
16.85
f1 (ppm)

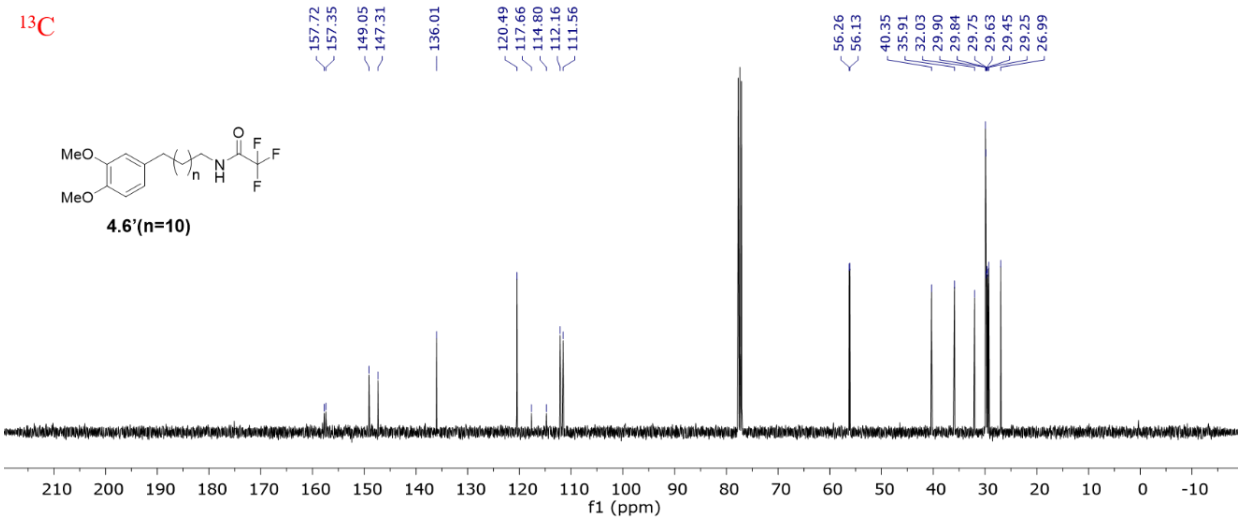
13C
157.72
157.35
149.05
147.31
136.01
120.49
117.66
114.80
112.16
111.56
56.26
56.13
40.35
35.91
32.03
29.90
29.84
29.75
29.63
29.45
29.25
26.99
MeO
MeO
n
N
H
O
F
F
F
4.6'(n=10)
f1 (ppm)

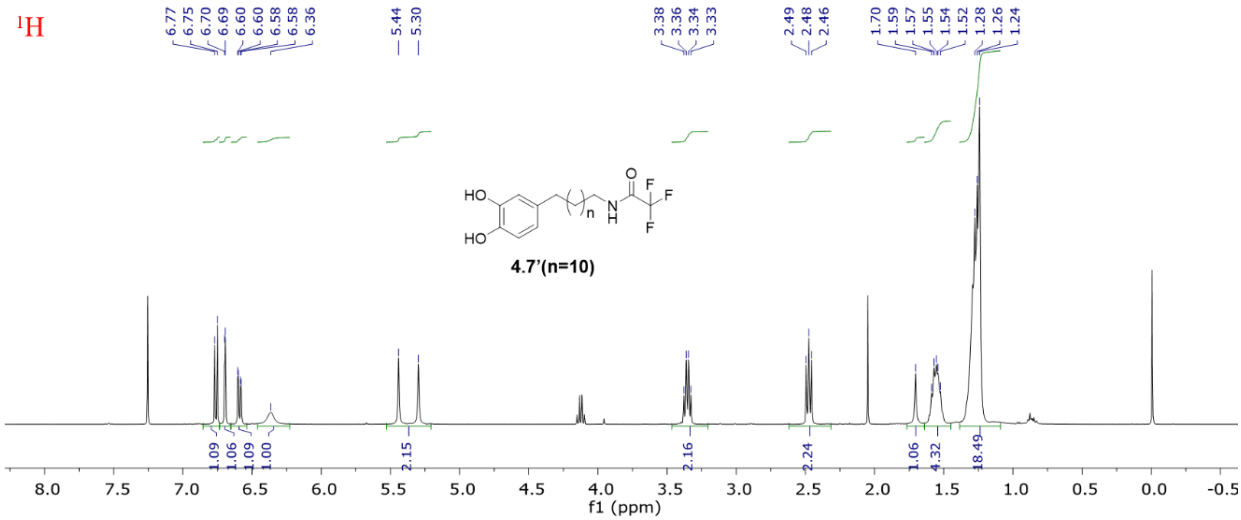
1H
6.77
6.75
6.70
6.69
6.60
6.60
6.58
6.58
6.36
5.44
5.30
3.38
3.36
3.34
3.33
2.49
2.48
2.46
1.70
1.59
1.57
1.55
1.54
1.52
1.28
1.26
1.24
HO
HO
n
N
H
O
F
F
F
4.7'(n=10)
1.09
1.06
1.09
1.00
2.15
2.16
2.24
1.06
4.32
18.49
f1 (ppm)

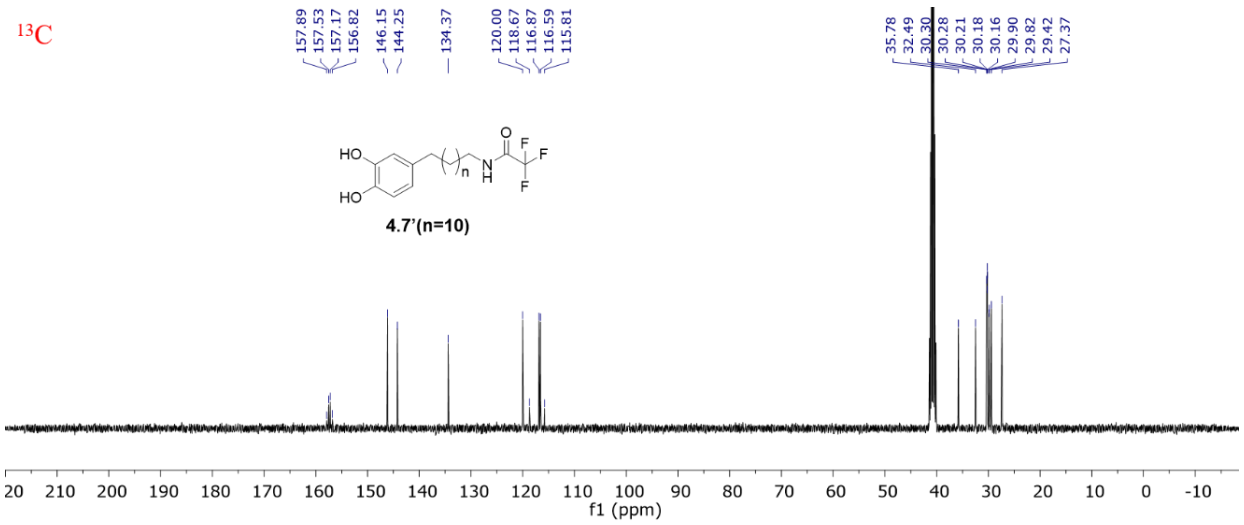
13C
157.89
157.53
157.17
156.82
146.15
144.25
134.37
120.00
118.67
116.87
116.59
115.81
35.78
32.49
30.30
30.28
30.21
30.18
30.16
29.90
29.82
29.42
27.37
HO
HO
n
N
H
O
F
F
F
4.7'(n=10)
20 210 200 190 180 170 160 150 140 130 120 110 100 90 80 70 60 50 40 30 20 10 0 -10
f1 (ppm)

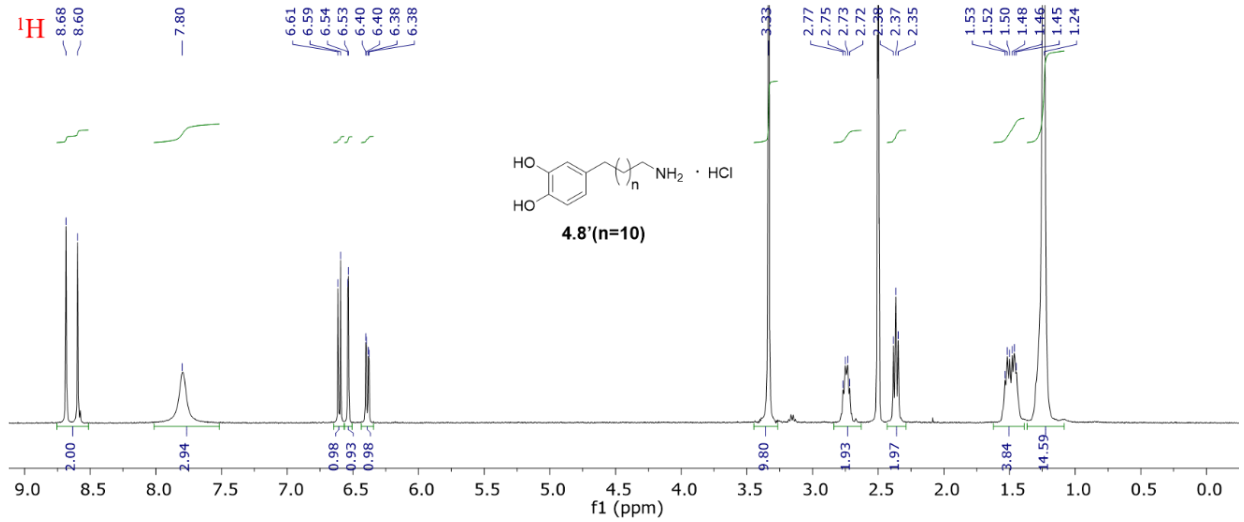
1H
8.68
8.60
7.80
6.61
6.59
6.54
6.53
6.40
6.40
6.38
6.38
3.33
2.77
2.75
2.73
2.72
2.38
2.37
2.35
1.53
1.52
1.50
1.48
1.46
1.45
1.24
HO
HO
n
NH2 · HCl
4.8'(n=10)
2.00
2.94
0.98
0.93
0.98
9.80
1.93
1.97
3.84
14.59
9.0 8.5 8.0 7.5 7.0 6.5 6.0 5.5 5.0 4.5 4.0 3.5 3.0 2.5 2.0 1.5 1.0 0.5 0.0
f1 (ppm)

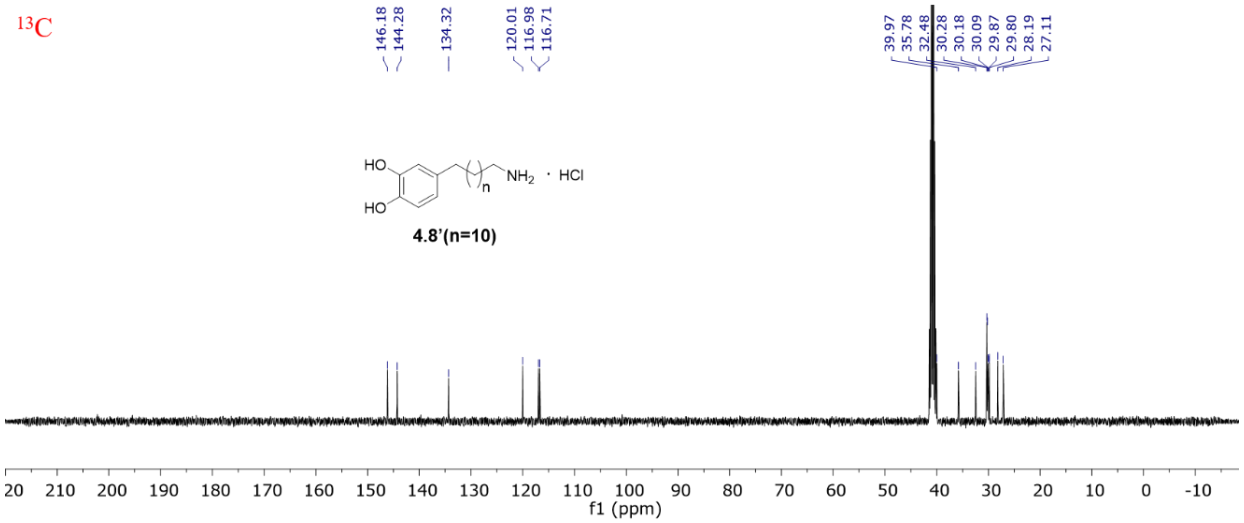
13C
146.18
144.28
134.32
120.01
116.98
116.71
39.97
35.78
32.48
30.28
30.18
30.09
29.87
29.80
28.19
27.11
HO
HO
n
NH2 · HCl
4.8'(n=10)
20 210 200 190 180 170 160 150 140 130 120 110 100 90 80 70 60 50 40 30 20 10 0 -10
f1 (ppm)

REFERENCES

(1) Loi, F.; Córdova, L. A.; Pajarinen, J.; Lin, T.-h.; Yao, Z.; Goodman, S. B.: Inflammation, Fracture and Bone Repair. *Bone* **2016**, *86*, 119-130.

(2) Porter, J. R.; Ruckh, T. T.; Popat, K. C.: Bone tissue engineering: A review in bone biomimetics and drug delivery strategies. *Biotechnology Progress* **2009**, *25*, 1539-1560.

(3) Buckwalter, J. A.; Glimcher, M. J.; Cooper, R. R.; Recker, R.: Bone Biology. PART I: Structure, Blood Supply, Cells, Matrix, and Mineralization *. *JBJS* **1995**, *77*, 1256-1275.

(4) Field, R. A.; Riley, M. L.; Mello, F. C.; Corbridge, J. H.; Kotula, A. W.: Bone Composition in Cattle, Pigs, Sheep and Poultry. *Journal of Animal Science* **1974**, *39*, 493-499.

(5) Buck, D. W. I.; Dumanian, G. A.: Bone Biology and Physiology: Part I. The Fundamentals. *Plastic and Reconstructive Surgery* **2012**, *129*, 1314-1320.

(6) McNally, E. A.; Schwarcz, H. P.; Botton, G. A.; Arsenault, A. L.: A Model for the Ultrastructure of Bone Based on Electron Microscopy of Ion-Milled Sections. *PLOS ONE* **2012**, *7*, e29258.

(7) Arsenault, A. L.: Image analysis of collagen-associated mineral distribution in cryogenically prepared turkey leg tendons. *Calcified Tissue International* **1991**, *48*, 56-62.

(8) Skedros, J. G.; Holmes, J. L.; Vajda, E. G.; Bloebaum, R. D.: Cement lines of secondary osteons in human bone are not mineral-deficient: New data in a historical perspective. *The Anatomical Record Part A: Discoveries in Molecular, Cellular, and Evolutionary Biology* **2005**, *286A*, 781-803.

(9) Ritchie, R. O.: The conflicts between strength and toughness. *Nature Materials* **2011**, *10*, 817.

(10) Zimmermann, E. A.; Busse, B.; Ritchie, R. O.: The fracture mechanics of human bone: influence of disease and treatment. *BoneKEy Rep* **2015**, *4*.

(11) Reilly, D. T.; Burstein, A. H.: The elastic and ultimate properties of compact bone tissue. *Journal of Biomechanics* **1975**, *8*, 393-405.

(12) Keaveny, T. M.: Cancellous bone. In *Handbook of Biomaterial Properties*; Black, J., Hastings, G., Eds.; Springer US: Boston, MA, 1998; pp 15-23.

(13) Goldstein, S. A.; Wilson, D. L.; Sonstegard, D. A.; Matthews, L. S.: The mechanical properties of human tibial trabecular bone as a function of metaphyseal location. *Journal of Biomechanics* **1983**, *16*, 965-969.

(14) Amini, A. R.; Laurencin, C. T.; Nukavarapu, S. P.: Bone Tissue Engineering: Recent Advances and Challenges. *Critical reviews in biomedical engineering* **2012**, *40*, 363-408.

(15) Hadjidakis, D. J.; Androulakis, I. I.: Bone Remodeling. *Annals of the New York Academy of Sciences* **2006**, *1092*, 385-396.

(16) Frost, H. M.: Wolff's Law and bone's structural adaptations to mechanical usage: an overview for clinicians. *The Angle Orthodontist* **1994**, *64*, 175-188.

(17) Giannoudis, P. V.; Dinopoulos, H.; Tsiridis, E.: Bone substitutes: An update. *Injury* **2005**, *36*, S20-S27.

(18) Pollock, R.; Alcelik, I.; Bhatia, C.; Chuter, G.; Lingutla, K.; Budithi, C.; Krishna, M.: Donor site morbidity following iliac crest bone harvesting for cervical fusion: a comparison between minimally invasive and open techniques. *European Spine Journal* **2008**, *17*, 845-852.

(19) Carter, G.: Harvesting and Implanting Allograft Bone. *AORN Journal* **1999**, *70*, 659-670.

(20) Lanza, R. P.; Butler, D. H.; Borland, K. M.; Staruk, J. E.; Faustman, D. L.; Solomon, B. A.; Muller, T. E.; Rupp, R. G.; Maki, T.; Monaco, A. P.: Xenotransplantation of canine, bovine, and porcine islets in diabetic rats without immunosuppression. *Proceedings of the National Academy of Sciences* **1991**, *88*, 11100-11104.

(21) Mankin, H. J.; Hornicek, F. J.; Raskin, K. A.: Infection in Massive Bone Allografts. *Clinical Orthopaedics and Related Research* **2005**, *432*, 210-216.

(22) Hou, C. H.; Yang, R. S.; Hou, S. M.: Hospital-based allogenic bone bank—10-year experience. *Journal of Hospital Infection* **2005**, *59*, 41-45.

(23) Yoo, D.; Giulivi, A.: Xenotransplantation and the potential risk of xenogeneic transmission of porcine viruses. *Canadian Journal of Veterinary Research* **2000**, *64*, 193-203.

(24) Yang, Y.-G.; Sykes, M.: Xenotransplantation: current status and a perspective on the future. *Nature Reviews Immunology* **2007**, *7*, 519.

(25) Moore, W. R.; Graves, S. E.; Bain, G. I.: Synthetic bone graft substitutes. *ANZ Journal of Surgery* **2001**, *71*, 354-361.

(26) Brånemark, P.; Breine, U.; Johansson, B.; Roylance, P.; Röckert, H.; Yoffey, J.: Regeneration of bone marrow. *Cells Tissues Organs* **1964**, *59*, 1-46.

(27) El-Ghannam, A.: Bone reconstruction: from bioceramics to tissue engineering. *Expert review of medical devices* **2005**, *2*, 87-101.

(28) Charnley, J.: Anchorage of the femoral head prosthesis to the shaft of the femur. *Bone & Joint Journal* **1960**, *42*, 28-30.

(29) Navarro, M.; Michiardi, A.; Castaño, O.; Planell, J. A.: Biomaterials in orthopaedics. *Journal of The Royal Society Interface* **2008**, *5*, 1137-1158.

(30) Anderson, J. M.: Biological Responses to Materials. *Annual Review of Materials Research* **2001**, *31*, 81-110.

(31) Polo-Corrales, L.; Latorre-Esteves, M.; Ramirez-Vick, J. E.: Scaffold Design for Bone Regeneration. *Journal of nanoscience and nanotechnology* **2014**, *14*, 15-56.

(32) Huiskes, R.; Weinans, H.; Van Rietbergen, B.: The relationship between stress shielding and bone resorption around total hip stems and the effects of flexible materials. *Clinical orthopaedics and related research* **1992**, 124-134.

(33) Teoh, S.: Fatigue of biomaterials: a review. *International Journal of Fatigue* **2000**, *22*, 825-837.

(34) Crane, G. M.; Ishaug, S. L.; Mikos, A. G.: Bone tissue engineering. *Nature Medicine* **1995**, *1*, 1322.

(35) Vallet-Regí, M.; Colilla, M.; González, B.: Medical applications of organic–inorganic hybrid materials within the field of silica-based bioceramics. *Chemical society reviews* **2011**, *40*, 596-607.

(36) Mistry, A. S.; Mikos, A. G.: Tissue engineering strategies for bone regeneration. In *Regenerative medicine II*; Springer, 2005; pp 1-22.

(37) Warnke, P.; Springer, I.; Wiltfang, J.; Acil, Y.; Eufinger, H.; Wehmöller, M.; Russo, P.; Bolte, H.; Sherry, E.; Behrens, E.: Growth and transplantation of a custom vascularised bone graft in a man. *The Lancet* **2004**, *364*, 766-770.

(38) Bruder, S. P.; Jaiswal, N.; Ricalton, N. S.; Mosca, J. D.; Kraus, K. H.; Kadiyala, S.: Mesenchymal stem cells in osteobiology and applied bone regeneration. *Clinical Orthopaedics and Related Research®* **1998**, *355*, S247-S256.

(39) Rada, T.; Reis, R. L.; Gomes, M. E.: Adipose tissue-derived stem cells and their application in bone and cartilage tissue engineering. *Tissue Engineering Part B: Reviews* **2009**, *15*, 113-125.

(40) Kotobuki, N.; Hirose, M.; Takakura, Y.; Ohgushi, H.: Cultured autologous human cells for hard tissue regeneration: preparation and characterization of mesenchymal stem cells from bone marrow. *Artificial organs* **2004**, *28*, 33-39.

(41) Mao, J. J.; Prockop, D. J.: Stem cells in the face: tooth regeneration and beyond. *Cell stem cell* **2012**, *11*, 291-301.

(42) Ikada, Y.: Challenges in tissue engineering. *Journal of the Royal Society Interface* **2006**, *3*, 589-601.

(43) Hollister, S. J.; Murphy, W. L.: Scaffold translation: barriers between concept and clinic. *Tissue Engineering Part B: Reviews* **2011**, *17*, 459-474.

(44) Weiss, S.; Baumgart, R.; Jochum, M.; Strasburger, C.; Bidlingmaier, M.: Systemic regulation of distraction osteogenesis: a cascade of biochemical factors. *Journal of Bone and Mineral Research* **2002**, *17*, 1280-1289.

(45) Yilgor, P.; Tuzlakoglu, K.; Reis, R. L.; Hasirci, N.; Hasirci, V.: Incorporation of a sequential BMP-2/BMP-7 delivery system into chitosan-based scaffolds for bone tissue engineering. *Biomaterials* **2009**, *30*, 3551-3559.

(46) Vo, T. N.; Kasper, F. K.; Mikos, A. G.: Strategies for controlled delivery of growth factors and cells for bone regeneration. *Advanced drug delivery reviews* **2012**, *64*, 1292-1309.

(47) Awad, H. A.; O'Keefe, R. J.; Lee, C. H.; Mao, J. J.: Chapter 83 - Bone Tissue Engineering: Clinical Challenges and Emergent Advances in Orthopedic and Craniofacial Surgery A2 - Lanza, Robert. In *Principles of Tissue Engineering (Fourth Edition)*; Langer, R., Vacanti, J., Eds.; Academic Press: Boston, 2014; pp 1733-1743.

(48) Navarro, M.; Michiardi, A.; Castano, O.; Planell, J.: Biomaterials in orthopaedics. *Journal of the Royal Society Interface* **2008**, *5*, 1137-1158.

(49) Blokhuis, T.; Arts, J. C.: Bioactive and osteoinductive bone graft substitutes: definitions, facts and myths. *Injury* **2011**, *42*, S26-S29.

(50) Hutmacher, D. W.: Scaffolds in tissue engineering bone and cartilage. *Biomaterials* **2000**, *21*, 2529-2543.

(51) Olszta, M. J.; Cheng, X.; Jee, S. S.; Kumar, R.; Kim, Y.-Y.; Kaufman, M. J.; Douglas, E. P.; Gower, L. B.: Bone structure and formation: a new perspective. *Materials Science and Engineering: R: Reports* **2007**, *58*, 77-116.

(52) Yang, S.; Leong, K.-F.; Du, Z.; Chua, C.-K.: The design of scaffolds for use in tissue engineering. Part I. Traditional factors. *Tissue engineering* **2001**, *7*, 679-689.

(53) Woodard, J. R.; Hilldore, A. J.; Lan, S. K.; Park, C.; Morgan, A. W.; Eurell, J. A. C.; Clark, S. G.; Wheeler, M. B.; Jamison, R. D.; Johnson, A. J. W.: The mechanical properties and osteoconductivity of hydroxyapatite bone scaffolds with multi-scale porosity. *Biomaterials* **2007**, *28*, 45-54.

(54) Rezwan, K.; Chen, Q.; Blaker, J.; Boccaccini, A. R.: Biodegradable and bioactive porous polymer/inorganic composite scaffolds for bone tissue engineering. *Biomaterials* **2006**, *27*, 3413-3431.

(55) Lichte, P.; Pape, H.; Pufe, T.; Kobbe, P.; Fischer, H.: Scaffolds for bone healing: concepts, materials and evidence. *Injury* **2011**, *42*, 569-573.

(56) Thavornyutikarn, B.; Chantarapanich, N.; Sitthiseripratip, K.; Thouas, G. A.; Chen, Q.: Bone tissue engineering scaffolding: computer-aided scaffolding techniques. *Progress in biomaterials* **2014**, *3*, 61-102.

(57) Bose, S.; Vahabzadeh, S.; Bandyopadhyay, A.: Bone tissue engineering using 3D printing. *Materials today* **2013**, *16*, 496-504.

(58) Matassi, F.; Nistri, L.; Paez, D. C.; Innocenti, M.: New biomaterials for bone regeneration. *Clinical cases in mineral and bone metabolism* **2011**, *8*, 21.

(59) Pignatello, R.: *Advances in biomaterials science and biomedical applications*; InTech, 2013.

(60) Ferreira, A. M.; Gentile, P.; Chiono, V.; Ciardelli, G.: Collagen for bone tissue regeneration. *Acta biomaterialia* **2012**, *8*, 3191-3200.

(61) Solchaga, L. A.; Dennis, J. E.; Goldberg, V. M.; Caplan, A. I.: Hyaluronic acid-based polymers as cell carriers for tissue-engineered repair of bone and cartilage. *Journal of Orthopaedic Research* **1999**, *17*, 205-213.

(62) Ishaug-Riley, S. L.: Bone formation by three-dimensional osteoblast culture in biodegradable poly (alpha-hydroxy ester) scaffolds. Rice University, 1997.

(63) O'Brien, F. J.: Biomaterials & scaffolds for tissue engineering. *Materials Today* **2011**, *14*, 88-95.

(64) Cheung, H.-Y.; Lau, K.-T.; Lu, T.-P.; Hui, D.: A critical review on polymer-based bio-engineered materials for scaffold development. *Composites Part B: Engineering* **2007**, *38*, 291-300.

(65) Gao, C.; Deng, Y.; Feng, P.; Mao, Z.; Li, P.; Yang, B.; Deng, J.; Cao, Y.; Shuai, C.; Peng, S.: Current progress in bioactive ceramic scaffolds for bone repair and regeneration. *International journal of molecular sciences* **2014**, *15*, 4714-4732.

(66) Krogman, N. R.; Weikel, A. L.; Kristhart, K. A.; Nukavarapu, S. P.; Deng, M.; Nair, L. S.; Laurencin, C. T.; Allcock, H. R.: The influence of side group modification in polyphosphazenes on hydrolysis and cell adhesion of blends with PLGA. *Biomaterials* **2009**, *30*, 3035-3041.

(67) Roseti, L.; Parisi, V.; Petretta, M.; Cavallo, C.; Desando, G.; Bartolotti, I.; Grigolo, B.: Scaffolds for Bone Tissue Engineering: State of the art and new perspectives. *Materials Science and Engineering: C* **2017**, *78*, 1246-1262.

(68) Chang, M. C.; Ko, C.-C.; Douglas, W. H.: Preparation of hydroxyapatite-gelatin nanocomposite. *Biomaterials* **2003**, *24*, 2853-2862.

(69) Luo, T.-J. M.; Ko, C.-C.; Chiu, C.-K.; Llyod, J.; Huh, U.: Aminosilane as an effective binder for hydroxyapatite-gelatin nanocomposites. *Journal of sol-gel science and technology* **2010**, *53*, 459-465.

(70) Chang, M. C.; Ko, C.-C.; Douglas, W. H.: Conformational change of hydroxyapatite/gelatin nanocomposite by glutaraldehyde. *Biomaterials* **2003**, *24*, 3087-3094.

(71) Ko, C. C.; Wang, Z.; Tseng, H.; Lee, D. J.; Guez, C.: Design, synthesis, and evaluation of polydopamine-laced gelatinous hydroxyapatite nanocomposites for orthopedic applications. *McKittrick JM, Narayan R, Lin H. Advances in Bioceramics and Biotechnologies II: Ceramic Transactions* **2014**, 135-148.

(72) Dyke, J. C.; Knight, K. J.; Zhou, H.; Chiu, C.-K.; Ko, C.-C.; You, W.: An investigation of siloxane cross-linked hydroxyapatite–gelatin/copolymer composites for potential orthopedic applications. *Journal of materials chemistry* **2012**, *22*, 22888-22898.

(73) Dyke, J. C.; Hu, H.; Lee, D. J.; Ko, C.-C.; You, W.: The role of temperature in forming sol–gel biocomposites containing polydopamine. *Journal of Materials Chemistry B* **2014**, *2*, 7704-7711.

(74) Hench, L. L.; West, J. K.: The sol-gel process. *Chemical reviews* **1990**, *90*, 33-72.

(75) Milea, C.; Bogatu, C.; Duta, A.: The influence of parameters in silica sol-gel process. *Bulletin of TheTransilvania University of Brasov* **2011**, *4*, 53.

(76) Artaki, I.; Zerda, T.; Jonas, J.: Solvent effects on hydrolysis stage of the sol-gel process. *Materials Letters* **1985**, *3*, 493-496.

(77) Artaki, I.; Zerda, T.; Jonas, J.: Solvent effects on the condensation stage of the sol-gel process. *Journal of non-crystalline solids* **1986**, *81*, 381-395.

(78) Orcel, G.; Hench, L.: Effect of formamide additive on the chemistry of silica sol-gels: Part I: NMR of silica hydrolysis. *Journal of non-crystalline solids* **1986**, *79*, 177-194.

(79) Orcel, G.; Hench, L. L.; Artaki, I.; Jonas, J.; Zerda, T.: Effect of formamide additive on the chemistry of silica sol-gels II. Gel structure. *Journal of Non-Crystalline Solids* **1988**, *105*, 223-231.

(80) Lenza, R. F.; Vasconcelos, W. L.: Study of the influence of some DCCAs on the structure of sol–gel silica membranes. *Journal of Non-crystalline solids* **2003**, *330*, 216-225.

(81) Pissetti, F. L.; Araújo, P. L. d.; Silva, F. A.; Poirier, G. Y.: Synthesis of poly (dimethylsiloxane) networks functionalized with imidazole or benzimidazole for copper (II) removal from water. *Journal of the Brazilian Chemical Society* **2015**, *26*, 266-272.

(82) Boccaccini, A. R.; Blaker, J. J.; Maquet, V.; Day, R.; Jérôme, R.: Preparation and characterisation of poly (lactide-co-glycolide)(PLGA) and PLGA/Bioglass® composite tubular foam scaffolds for tissue engineering applications. *Materials Science and Engineering: C* **2005**, *25*, 23-31.

(83) Habraken, W.; Wolke, J.; Jansen, J.: Ceramic composites as matrices and scaffolds for drug delivery in tissue engineering. *Advanced drug delivery reviews* **2007**, *59*, 234-248.

(84) Oh, J. K.: Polylactide (PLA)-based amphiphilic block copolymers: synthesis, self-assembly, and biomedical applications. *Soft Matter* **2011**, *7*, 5096-5108.

(85) Declercq, H.; Cornelissen, M.; Gorskiy, T.; Schacht, E.: Osteoblast behaviour on in situ photopolymerizable three-dimensional scaffolds based on D, L-lactide, ε-caprolactone and trimethylene carbonate. *Journal of Materials Science: Materials in Medicine* **2006**, *17*, 113-122.

(86) Gentile, P.; Chiono, V.; Carmagnola, I.; Hatton, P. V.: An overview of poly (lactic-co-glycolic) acid (PLGA)-based biomaterials for bone tissue engineering. *International journal of molecular sciences* **2014**, *15*, 3640-3659.

(87) Jiang, T.; Nukavarapu, S. P.; Deng, M.; Jabbarzadeh, E.; Kofron, M. D.; Doty, S. B.; Abdel-Fattah, W. I.; Laurencin, C. T.: Chitosan–poly (lactide-co-glycolide) microsphere-based scaffolds for bone tissue engineering: In vitro degradation and in vivo bone regeneration studies. *Acta biomaterialia* **2010**, *6*, 3457-3470.

(88) Shokrollahi, P.; Mirzadeh, H.; Scherman, O. A.; Huck, W. T.: Biological and mechanical properties of novel composites based on supramolecular polycaprolactone and functionalized hydroxyapatite. *Journal of Biomedical Materials Research Part A* **2010**, *95*, 209-221.

(89) Zhang, Z.; Kuijer, R.; Bulstra, S. K.; Grijpma, D. W.; Feijen, J.: The in vivo and in vitro degradation behavior of poly (trimethylene carbonate). *Biomaterials* **2006**, *27*, 1741-1748.

(90) Pego, A.; Siebum, B.; Van Luyn, M.; Gallego y Van Seijen, X.; Poot, A. A.; Grijpma, D. W.; Feijen, J.: Preparation of degradable porous structures based on 1, 3-trimethylene carbonate and D, L-lactide (co) polymers for heart tissue engineering. *Tissue engineering* **2003**, *9*, 981-994.

(91) Mano, J.; Ribelles, J. G.; Alves, N.; Sanchez, M. S.: Glass transition dynamics and structural relaxation of PLLA studied by DSC: Influence of crystallinity. *Polymer* **2005**, *46*, 8258-8265.

(92) Zhu, K.; Hendren, R.; Jensen, K.; Pitt, C.: Synthesis, properties, and biodegradation of poly (1, 3-trimethylene carbonate). *Macromolecules* **1991**, *24*, 1736-1740.

(93) Silverman, H. G.; Roberto, F. F.: Understanding marine mussel adhesion. *Marine biotechnology* **2007**, *9*, 661-681.

(94) Waite, J. H.; Andersen, N. H.; Jewhurst, S.; Sun, C.: Mussel adhesion: finding the tricks worth mimicking. *The journal of adhesion* **2005**, *81*, 297-317.

(95) Lee, H.; Scherer, N. F.; Messersmith, P. B.: Single-molecule mechanics of mussel adhesion. *Proceedings of the National Academy of Sciences* **2006**, *103*, 12999-13003.

(96) Fant, C.; Hedlund, J.; Höök, F.; Berglin, M.; Fridell, E.; Elwing, H.: Investigation of adsorption and cross-linking of a mussel adhesive protein using attenuated total internal reflection Fourier transform infrared spectroscopy (ATR-FTIR). *The Journal of Adhesion* **2010**, *86*, 25-38.

(97) Sedó, J.; Saiz-Poseu, J.; Busqué, F.; Ruiz-Molina, D.: Catechol-based biomimetic functional materials. *Advanced Materials* **2013**, *25*, 653-701.

(98) Yu, M.; Hwang, J.; Deming, T. J.: Role of L-3, 4-dihydroxyphenylalanine in mussel adhesive proteins. *Journal of the American Chemical Society* **1999**, *121*, 5825-5826.

(99) Suci, P. A.; Geesey, G. G.: Influence of sodium periodate and tyrosinase on binding of alginate to adlayers of Mytilus edulis foot protein 1. *Journal of colloid and interface science* **2000**, *230*, 340-348.

(100) Maier, G. P.; Rapp, M. V.; Waite, J. H.; Israelachvili, J. N.; Butler, A.: Adaptive synergy between catechol and lysine promotes wet adhesion by surface salt displacement. *Science* **2015**, *349*, 628-632.

(101) Lee, B. P.; Messersmith, P. B.; Israelachvili, J. N.; Waite, J. H.: Mussel-inspired adhesives and coatings. *Annual review of materials research* **2011**, *41*, 99-132.

(102) Lee, H.; Dellatore, S. M.; Miller, W. M.; Messersmith, P. B.: Mussel-inspired surface chemistry for multifunctional coatings. *science* **2007**, *318*, 426-430.

(103) Dreyer, D. R.; Miller, D. J.; Freeman, B. D.; Paul, D. R.; Bielawski, C. W.: Perspectives on poly (dopamine). *Chemical Science* **2013**, *4*, 3796-3802.

(104) Hu, H.; Dyke, J. C.; Bowman, B. A.; Ko, C.-C.; You, W.: Investigation of Dopamine Analogues: Synthesis, Mechanistic Understanding, and Structure–Property Relationship. *Langmuir* **2016**, *32*, 9873-9882.

(105) Lowe, A. B.; Hoyle, C. E.; Bowman, C. N.: Thiol-yne click chemistry: A powerful and versatile methodology for materials synthesis. *Journal of Materials Chemistry* **2010**, *20*, 4745-4750.

(106) Fairbanks, B. D.; Scott, T. F.; Kloxin, C. J.; Anseth, K. S.; Bowman, C. N.: Thiol− Yne photopolymerizations: novel mechanism, kinetics, and step-growth formation of highly cross-linked networks. *Macromolecules* **2008**, *42*, 211-217.

(107) Lowe, A. B.: Thiol-yne 'click'/coupling chemistry and recent applications in polymer and materials synthesis and modification. *Polymer* **2014**, *55*, 5517-5549.

(108) Meredith, H. J.; Jenkins, C. L.; Wilker, J. J.: Enhancing the Adhesion of a Biomimetic Polymer Yields Performance Rivaling Commercial Glues. *Advanced Functional Materials* **2014**, *24*, 3259-3267.

(109) Matos-Pérez, C. R.; White, J. D.; Wilker, J. J.: Polymer composition and substrate influences on the adhesive bonding of a biomimetic, cross-linking polymer. *Journal of the American Chemical Society* **2012**, *134*, 9498-9505.

(110) Jenkins, C. L.; Meredith, H. J.; Wilker, J. J.: Molecular weight effects upon the adhesive bonding of a mussel mimetic polymer. *ACS applied materials & interfaces* **2013**, *5*, 5091-5096.

(111) Waite, J. H.: The phylogeny and chemical diversity of quinone-tanned glues and varnishes. *Comparative Biochemistry and Physiology Part B: Comparative Biochemistry* **1990**, *97*, 19-29.

(112) Ye, Q.; Zhou, F.; Liu, W.: Bioinspired catecholic chemistry for surface modification. *Chemical Society Reviews* **2011**, *40*, 4244-4258.

(113) Liu, Y.; Ai, K.; Lu, L.: Polydopamine and its derivative materials: synthesis and promising applications in energy, environmental, and biomedical fields. *Chemical reviews* **2014**, *114*, 5057-5115.

(114) Yu, M.; Deming, T. J.: Synthetic polypeptide mimics of marine adhesives. *Macromolecules* **1998**, *31*, 4739-4745.

(115) Yang, J.; Stuart, M. A. C.; Kamperman, M.: Jack of all trades: versatile catechol crosslinking mechanisms. *Chemical Society Reviews* **2014**, *43*, 8271-8298.

(116) Lee, B. P.; Dalsin, J. L.; Messersmith, P. B.: Synthesis and gelation of DOPA-modified poly (ethylene glycol) hydrogels. *Biomacromolecules* **2002**, *3*, 1038-1047.

(117) Ryu, J. H.; Hong, S.; Lee, H.: Bio-inspired adhesive catechol-conjugated chitosan for biomedical applications: A mini review. *Acta biomaterialia* **2015**, *27*, 101-115.

(118) Lee, S.-B.; González-Cabezas, C.; Kim, K.-M.; Kim, K.-N.; Kuroda, K.: Catechol-functionalized synthetic polymer as a dental adhesive to contaminated dentin surface for a composite restoration. *Biomacromolecules* **2015**, *16*, 2265-2275.

(119) Wu, H.; Sariola, V.; Zhu, C.; Zhao, J.; Sitti, M.; Bettinger, C. J.: Transfer Printing of Metallic Microstructures on Adhesion-Promoting Hydrogel Substrates. *Advanced Materials* **2015**, *27*, 3398-3404.

(120) Olivieri, M. P.; Wollman, R. M.; Hurley, M. I.; Swartz, M. F.: Using conformational analysis to identify structurally conserved regions of MAP peptides that exhibit cellular attachment ability. *Biofouling* **2002**, *18*, 149-159.

(121) Dreyer, D. R.; Miller, D. J.; Freeman, B. D.; Paul, D. R.; Bielawski, C. W.: Elucidating the structure of poly (dopamine). *Langmuir* **2012**, *28*, 6428-6435.

(122) Hong, S.; Na, Y. S.; Choi, S.; Song, I. T.; Kim, W. Y.; Lee, H.: Non-covalent self-assembly and covalent polymerization co-contribute to polydopamine formation. *Advanced Functional Materials* **2012**, *22*, 4711-4717.

(123) Della Vecchia, N. F.; Avolio, R.; Alfè, M.; Errico, M. E.; Napolitano, A.; d'Ischia, M.: Building-block diversity in polydopamine underpins a multifunctional eumelanin-type platform tunable through a quinone control point. *Advanced Functional Materials* **2013**, *23*, 1331-1340.

(124) Liebscher, J. r.; Mrówczyński, R.; Scheidt, H. A.; Filip, C.; Hădade, N. D.; Turcu, R.; Bende, A.; Beck, S.: Structure of polydopamine: a never-ending story? *Langmuir* **2013**, *29*, 10539-10548.

(125) Lee, H.; Lee, Y.; Statz, A. R.; Rho, J.; Park, T. G.; Messersmith, P. B.: Substrate-independent layer-by-layer assembly by using mussel-adhesive-inspired polymers. *Advanced materials* **2008**, *20*, 1619-1623.

(126) Liu, Y.; Meng, H.; Konst, S.; Sarmiento, R.; Rajachar, R.; Lee, B. P.: Injectable dopamine-modified poly (ethylene glycol) nanocomposite hydrogel with enhanced adhesive property and bioactivity. *ACS applied materials & interfaces* **2014**, *6*, 16982-16992.

(127) Land, E. J.; Ramsden, C. A.; Riley, P. A.: An MO study of regioselective amine addition to ortho-quinones relevant to melanogenesis. *Tetrahedron* **2006**, *62*, 4884-4891.

(128) Vincze, Z.; Bíró, A. B.; Csékei, M.; Timári, G.; Kotschy, A.: The palladium-catalyzed preparation of condensed tetracyclic heterocycles and their application to the synthesis of rac-mangochinine. *Synthesis* **2006**, *2006*, 1375-1385.

(129) Liu, Z.; Hu, B.-H.; Messersmith, P. B.: Acetonide protection of dopamine for the synthesis of highly pure N-docosahexaenoyldopamine. *Tetrahedron letters* **2010**, *51*, 2403-2405.

(130) Wei, Q.; Zhang, F.; Li, J.; Li, B.; Zhao, C.: Oxidant-induced dopamine polymerization for multifunctional coatings. *Polymer Chemistry* **2010**, *1*, 1430-1433.

(131) Du, X.; Li, L.; Li, J.; Yang, C.; Frenkel, N.; Welle, A.; Heissler, S.; Nefedov, A.; Grunze, M.; Levkin, P. A.: UV-Triggered Dopamine Polymerization: Control of Polymerization, Surface Coating, and Photopatterning. *Advanced Materials* **2014**, *26*, 8029-8033.

(132) Ju, K.-Y.; Lee, Y.; Lee, S.; Park, S. B.; Lee, J.-K.: Bioinspired polymerization of dopamine to generate melanin-like nanoparticles having an excellent free-radical-scavenging property. *Biomacromolecules* **2011**, *12*, 625-632.

(133) Yan, J.; Yang, L.; Lin, M. F.; Ma, J.; Lu, X.; Lee, P. S.: Polydopamine spheres as active templates for convenient synthesis of various nanostructures. *Small* **2013**, *9*, 596-603.

(134) Jiang, X.; Wang, Y.; Li, M.: Selecting water-alcohol mixed solvent for synthesis of polydopamine nano-spheres using solubility parameter. *Scientific Reports* **2014**, *4*, 6070.

(135) Herlinger, E.; Jameson, R. F.; Linert, W.: Spontaneous autoxidation of dopamine. *Journal of the Chemical Society, Perkin Transactions 2* **1995**, 259-263.

(136) Deming, T. J.: Mussel byssus and biomolecular materials. *Current Opinion in Chemical Biology* **1999**, *3*, 100-105.

(137) Karim, M.; Linnell, W.; Sharp, L.: POTENTIAL RESERPINE ANALOGUES: Part II. 3, 4, 5-Trimethoxybenzoic Acid Derivatives. *Journal of Pharmacy and Pharmacology* **1960**, *12*, 82-86.

(138) Jie, Y.; Niskala, J. R.; Johnston-Peck, A. C.; Krommenhoek, P. J.; Tracy, J. B.; Fan, H.; You, W.: Laterally patterned magnetic nanoparticles. *Journal of Materials Chemistry* **2012**, *22*, 1962-1968.

(139) Mattson, K. M.; Latimer, A. A.; McGrath, A. J.; Lynd, N. A.; Lundberg, P.; Hudson, Z. M.; Hawker, C. J.: A facile synthesis of catechol-functionalized poly (ethylene oxide) block and random copolymers. *Journal of Polymer Science Part A: Polymer Chemistry* **2015**, *53*, 2685-2692.

(140) Liu, J.; Cui, L.; Losic, D.: Graphene and graphene oxide as new nanocarriers for drug delivery applications. *Acta biomaterialia* **2013**, *9*, 9243-9257.

(141) Hummers Jr, W. S.; Offeman, R. E.: Preparation of graphitic oxide. *Journal of the american chemical society* **1958**, *80*, 1339-1339.